Exploration of Sleep-Related Oscillatory Abnormalities in Alzheimer's Disease

Paulina Schnur

Nov 2024

A thesis submitted to the University of Strathclyde in accordance with the requirements for award of the degree of Doctor of Philosophy at the Strathclyde Institute of Pharmacy and Biomedical Sciences

Strathclyde Institute of Pharmacy and Biomedical Sciences, University of Strathclyde, Glasgow G4 0RE

Declaration of authenticity and author's rights

This thesis is the result of the author's original research. It has been composed by the author and has not been previously submitted for examination which has led to the award of a degree.

The copyright of this thesis belongs to the author under the terms of the United Kingdom Copyright Acts as qualified by University of Strathclyde Regulation 3.50. Due acknowledgment must always be made of the use of any material contained in, or derived from, this thesis.

Signed:

Date: 15.11.2024

Published Work

This work has been presented in parts at conferences and seminars.

International and national conference poster presentations

Paulina Schnur, Nicole Byron, Tommaso Patriarchi, Shuzo Sakata
Experience-dependent deficits in sharp wave-ripples in 5xFAD mice
FENS, June 2024
CBD seminar, April 2024
ARUK, March 2024
SNG, August 2024

Paulina Schnur, Shuzo Sakata
Sharp wave-ripples and sleep spindles across sleep-wake cycles in 5xFAD mice
ARUK Scotland, August 2023
ARUK, March 2023

Acknowledgments

Foremost, I would like to express my deepest gratitude to my supervisor, Dr Shuzo Sakata, for his guidance and support over the past years. His experience and expertise were of immense value in the conductance of this study. Beyond this study, his great passion for research and high quality standards had a vital impact on me, inspiring and motivating me on my path to becoming a researcher. I could not have wished for a better supervisor and role model.
I would also like to thank our collaborator, Dr Tommaso Patriarchi, for supplying the acetylcholine sensor for this project.

Furthermore, I want to thank the members of the Sakata lab. A special thanks goes to Dr Mirna Merkler for all her help, guidance and encouragement over the past years.

Additionally, I would like to thank the staff of the animal facility for their help and advice in caring for the mice used in this project.

Finally, I would like to thank Ross Hendry and Paula Bauer for their endless emotional support during stressful times. I am beyond grateful for having such a strong support system.

Table of Contents

List of Figures

List of Tables

Abbreviations

Aβ	Amyloid-β
ACh	Acetylcholine
AD	Alzheimer's Disease
AF	Autofluorescence
ANOVA	Analysis of variance
APOE-ε4	apolipoprotein-ε4
APP	Amyloid precursor protein
ATP	Adenosine triphosphate
BBB	Blood-brain barrier
BFCS	Basal forebrain cholinergic system
CDR	Clinical dementia rating
CRISPR	Clustered regular interspaced short palindromic repeats
CSF	Cerebrospinal fluid
CTF-β	C-terminal fragment β
DBS	Deep brain stimulation
EC	Entorhinal cortex
EC_{50}	Half-maximum effective concentration
EEG	Electroencephalogram
EMG	Electromyography
FAD	Familiar Alzheimer's Disease
FDA	US Food and Drug Administration
FDG	Fluorodeoxyglucose
fMRI	Functional magnetic resonance imaging
hBACE1	Human rate-limiting β-site enzyme 1
HC	Hippocampus
hmM3R	Human muscarinic M3 receptor
HSD	Honest significant difference
IL	Interleukin
ISF	Interstitial fluid

LDT	Laterodorsal tegmentum
LED	Light-emitting diode
LFP	Local field potential
MA	Movement artifacts
MCI	Mild cognitive impairment
mPFC	Medial prefrontal cortex
MRI	Magnetic resonance imaging
NMDA	N-methyl-d-aspartate
NOR	Novel object recognition
NREM	Non-rapid eye movement
OF	Open field
OCT	Optical coherence tomography
OCTA	Optical coherence tomography angiopathy
PBS	Phosphate buffered saline
PET	Positron emission tomography
PFC	Prefrontal cortex
PPT	Pedunculopontine nucleus
PSD	Power spectral density
PSEN1	Presenilin1
PSEN2	Presenilin2
PV	Parvalbumin-positive
RAS	Reticular activating system
REM	Rapid eye movement
ROS	Reactive oxygen species
rTMS	Transcranial magnetic stimulation
SAD	Sporadic Alzheimer’s Disease
SO	Slow oscillation
SWR	Sharp-wave ripple
SWS	Slow-wave sleep
TGF-ß	Transforming growth factor ß
TRN	Thalamic reticular nucleus

Abstract

A hallmark of Alzheimer's disease (AD) pathology is amyloid plaques which can lead to neuroinflammation, cellular dysfunction and altered neuronal activity. Both AD patients and mouse models exhibit abnormal neural oscillations, including altered hippocampal sharp-wave ripples (SWRs) and cortical sleep spindles. Although these oscillations play a role in memory formation and consolidation, it remains poorly understood how abnormal oscillations relate to novel experiences. We hypothesised that SWRs and sleep spindles are altered in 5xFAD mice, an AD mouse model, in the context of novelty. We performed in vivo electrophysiological recordings in a freely behaving condition to characterize hippocampal SWRs and cortical sleep spindles across the sleep-wake cycle in 5xFAD mice. Although SWRs during non-rapid eye movement (NREM) sleep increased just after exposure to a novel environment or exploration of a novel object in littermate controls, this increase was absent in AD mice. On the other hand, cortical sleep spindles and their co-occurrence with SWRs did not show an experience-dependent increase and were not altered in AD mice, suggesting that thalamocortical functions are spared from amyloid pathology. To examine if the diminished SWRs are associated with abnormal cholinergic tone in the hippocampus, we performed electrophysiology in a freely behaving condition while optically monitoring hippocampal acetylcholine levels across sleep-wake cycles. Here we found abnormalities in cholinergic dynamics at state transitions in AD mice, potentially contributing to the diminished SWR rate. Our findings highlight the complexity of AD, revealing that hippocampal SWRs are significantly disrupted by amyloid pathology in the context of novelty, potentially as a result of abnormal cholinergic dynamics, while thalamocortical functions remain unaffected.

1 Introduction

1.1 Alzheimer's disease

1.1.1 Pathology

Alzheimer's Disease (AD) is a chronic neurodegenerative disease and the main cause of dementia (Alzheimer's Association, 2018). The World Alzheimer Report 2019 estimated 50 million people being affected worldwide. The number of cases is expected to triple by 2025 (Alzheimer's Disease International, 2019).

1.1.1.1 Brief history of Alzheimer's Disease

Two mayor hallmarks of AD are amyloid plaques and neurofibrillary tangles. These were first described by physician Alois Alzheimer in 1906 when alterations in brain tissue were discovered during post-mortem autopsy of a female patient, the now famous Auguste D, displaying symptoms of memory impairments, aphasia and disorientation prior to her death. The alterations observed included uniform brain atrophy, arteriosclerotic changes in larger cerebral vessels, neurofibrillary changes within neurons, now known as neurofibrillary tangles, and abnormal deposits outside the neurons, now known as amyloid plaques (Maurer, Volk, & Gerbaldo, 1997).
At the time, the scientific community paid little attention to these findings, regarding AD as no more than a very rare pre-senile disorder, unconnected to senile dementia (Jucker, Beyreuther, Haass, Nitsch, & Christen, 2006). It was not until the 1970s when accumulating evidence showed that senile dementia was in fact the disease described by Alzheimer and the leading cause for dementia (Katzman, 1976; Tomlinson, Blessed, & Roth, 1968, 1970). Ever since, the scientific community has given great attention to the disease, allocating great amounts of funding to unravel the underlying causes and progression, identify biomarkers for diagnosis, and forms of treatment (Cupers, Sautter, & Vanvossel, 2006). Although it has been found that dementia can result from a variety of disorders, including cerebrovascular disease,

Lewy body disease and Parkinson's Disease, AD remains to be the leading cause of the majority of dementia cases ("2023 Alzheimer's disease facts and figures," 2023).

1.1.1.2 Epidemionolgy

Age is by far the greatest risk factor for developing AD. While the prevalence is estimated to be just below 5% at the age of 65, it almost doubles with every 5 years after that (Qiu, Liu, Chen, Zhao, & Li, 2015). Multiple age-related changes are thought to contribute to the increased risk of AD, including an upregulated inflammatory profile, damage to the vascular system, mitochondrial dysfunction, accumulation of oxidative stress, and atrophy (Finger, Moreno-Gonzalez, Gutierrez, Moruno-Manchon, & McCullough, 2022).

With life expectancy increasing steadily in western countries, the number of patients diagnosed with age-related diseases, such as AD, also increases.

Several modifiable risk factors for AD have been identified. A higher level of education in early life (< 45 years) has been found to reduce the risk of developing dementia (Larsson et al., 2017; Livingston et al., 2017; Norton, Matthews, Barnes, Yaffe, & Brayne, 2014), although this observation does not allow to distinguish whether this preventative effect stems from the cognitive stimulation or the overall cognitive abilities. Two studies reported people engaging in cognitively demanding activities and social outings showed less decline of cognitive abilities, and had a lower risk of developing dementia, independent of their educational background (Chan et al., 2018; Lee et al., 2018). This is sometimes referred to as the 'use it or lose it' theory. Another risk factor is hearing loss (Golub, Brickman, Ciarleglio, Schupf, & Luchsinger, 2020; Loughrey, Kelly, Kelley, Brennan, & Lawlor, 2018). While the relationship here is not fully understood, it has been found that hearing impairments are associated with a volume loss in the hippocampus (HC) and entorhinal cortex (EC) (Armstrong et al., 2019). The use of hearing aids has been shown to reduce the risk of dementia in hearing-impaired individuals (Amieva, Ouvrard, Meillon, Rullier, & Dartigues, 2018; Uchida et al., 2019). Traumatic brain injury is another factor associated with the risk of dementia and AD (Fann et al., 2018; Nordström & Nordström, 2018). Single incidences of such injuries have been associated with increase hyper-phosphorylated tau (Cao et al., 2017; Zanier et al., 2018). More severe injuries and repeated injuries have been found to have a bigger impact on the risk for dementia (Tolppanen, Taipale, & Hartikainen, 2017).

Another important factor increasing the risk of dementia and AD is exposure to air pollutants. Studies in animal models have suggested that pollutants accelerate neurodegeneration by causing transcriptional changes, leading to increased intracellular amyloid-β (Aβ) and tau (Israel et al., 2023). Nitrogen dioxide, carbon monoxide and fine ambient particulate matter produced by car exhausts or the burning of wood are amongst the pollutants identified to have an impact on the risk to develop dementia (Carey et al., 2018; Oudin et al., 2016; Oudin, Segersson, Adolfsson, & Forsberg, 2018; Peters et al., 2019). Diabetes is another risk factor for AD. Severity and duration of diabetes has been found to be positively correlated with individual risk (Chatterjee et al., 2016). Studies investigating the effect of different diabetes medications on the risk to develop AD or other forms of dementia have reported contradicting outcomes. One study found patients treated with metformin to have a lower risk compared to patients with other or no medication (Sabia et al., 2019), while another study did not observe this protective effect of metformin (McMillan, Mele, Hogan, & Leung, 2018).
Further risk factors include a diet low in vitamin B, C, D, E, and selenium, low social contacts, depression, obesity, cardiovascular diseases, low amounts of exercise, smoking and excessive alcohol consumption (Livingston et al., 2020).

Strikingly, more women develop AD than men. For later ages (80+) this can be explained by the overall longer life expectancy of women. For younger ages (60 - 80) this does not apply, however (Viña & Lloret, 2010). Women with AD also experience greater decline in cognitive capacities than men with AD (Laws, Irvine, & Gale, 2018) and these differences seem to persist, even when taking genetic risk factors of patients into account (Gale, Baxter, & Thompson, 2016; Tensil et al., 2018). Although it is not fully understood why women are more likely to develop AD and why they experience faster cognitive decline, the influence of sex hormones is likely to be contributing to the differences between sexes. Studies suggest a connection between verbal memory decline in the early stages of AD and alterations in hippocampal function caused by a decline in estradiol levels during menopause (Jacobs et al., 2016; Reitz & Mayeux, 2014). The idea of changes in sex hormones during menopause promoting the development of AD in women is further supported by findings showing that estrogen reduces the generation of Aβ peptides, which form amyloid beta plaques (Xu et al., 1998). It is therefore possible that estrogen initially has a protective effect which is lost during menopause as estrogen levels

plummet. Awareness of these sex differences is important when conducting AD research and equal inclusion of both sexes, in both human and animal studies, is essential.
Beyond the despair and suffering AD brings to those affected and their loved ones, the disease effects society as a whole. Although AD is a major reason for nursing home placements (Fratiglioni et al., 2000; Wadman, 2012), many AD patients remain to live at home in the care of family members. These caregivers carry a great burden far beyond the burden of financial cost, providing up to 70 h of unpaid care work per week and chancing their own health and well-being (Stefanacci, 2011). The burden of AD on society are undisputed. In the next subchapters, I will delve deeper into the underlying causes and mechanisms of the disease.

1.1.1.3 Types of Alzheimer's Disease

AD cases are classified in two groups: familiar AD (FAD) and sporadic AD (SAD). FAD cases are rare, only accounting for 1-5% of all AD cases, and an early onset before the age of 65 is one of its defining characteristics (Reitz & Mayeux, 2014). In FAD, a causal mutation is observed in three genes: presenilin1 (PSEN1), presenilin 2 (PSEN2) and amyloid precursor protein (APP), a type of single-pass transmembrane protein (Jarmolowicz, Chen, & Panegyres, 2015). Mutations of these three genes affect the cleavage and processing of APP. Mutations in APP occur in close proximity of the protein's cleavage site, affecting the cleavage by α-, ß- and γ-secretase (Kowalska, 2003). Mutations in PSEN1 and PSEN2 promote the cleavage of APP by γ-secretase (Lee et al., 2002; Martins et al., 1995).
SAD makes up the majority of AD cases, but its causes remain unclear. However, several genes have been found to be associated with SAD, with apolipoprotein-ε4 (APOE-ε4) having the strongest impact (Liu, Liu, Kanekiyo, Xu, & Bu, 2013). Unlike the genes affected in FAD, APOE-ε4 does not impact the cleavage of APP, but the clearance and aggregation of amyloid ß into amyloid plaques (reviewed in (Liu et al., 2013)). Although FAD and SAD seem to have different underlying causes, they share similar cellular mechanism and studying one group may help us understand the other.

1.1.1.4 Amyloid cascade

The amyloid cascade hypothesis has been established to identify the underlying mechanism of amyloid plaques in FAD (Hardy & Higgins, 1992):
In the non-pathological pathway, APP is cleaved by α-secretase and γ-secretase, leading to the production of soluble amyloid peptides which can be easily cleared from the extracellular space.
In the amyloidogenic pathway, APP is cleaved by ß-secretase and γ-secretase. This leads to the production of APP-ß and C-terminal ß, which is consequentially cleaved by γ-secretase into p83 and amyloid-β (Aβ) (Figure 1.1). These Aβ peptides, consisting of 36 to 43 amino acids each, can then aggregate into oligomers and amyloid plaques (Jarrett, Berger, & Lansbury, 1993). Most amyloid plaques are made up of Aβ42, Aβ peptides consisting of 42 amino acids. Aβ42 is most prone to aggregation due to its hydrophobicity due to its expanded C-terminus (Gremer et al., 2017; Jarrett et al., 1993; Teplow, 1998).

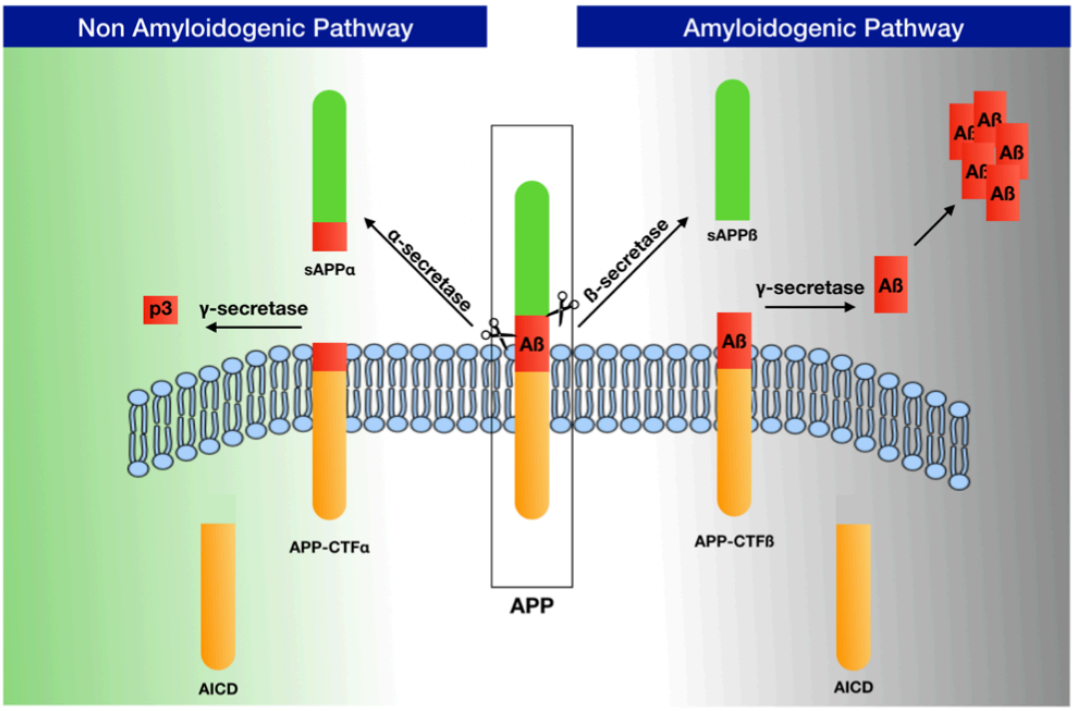

Figure 1.1 Amyloidogenic and non amyloidogenic pathway. *Cleavage of the amyloid precursor protein (APP) by α-secretase (non-amyloidogenic pathway, left) or ß-secretase (amyloidogenic pathway, right).*

Besides Aβ plaques, non-aggregated Aβ monomers and oligomers pose a threat to the brain. They come in insoluble forms, contain high amounts of beta-sheets, organised in either parallel or non-parallel structures (Ahmed et al., 2010; Chen et al., 2017; Yu et al., 2009) and insoluble forms, without this beta-sheet structure (Zhang et al., 2000). The soluble forms of Aβ are particularly dangerous, as they can easily spread throughout the brain. In fact, studies have found that these soluble Aβ oligomers are more toxic than deposited Aβ plaques (Haass & Selkoe, 2007) and that the ratio between soluble Aβ42 and Aβ40 is highly relevant for the severity of the AD pathology (Murray et al., 2012; Nutu et al., 2013; Waragai et al., 2012). Furthermore, soluble Aβ oligomers contribute to so-called seeding of amyloid plaques. Here, soluble oligomers can act as seeds, inducing more Aβ to join and form larger aggregates. Since such soluble Aβ oligomers can travel through the brain, this seeding effect greatly contributes to the spread of the disease (Subedi, Sasidharan, Nag, Saudagar, & Tripathi, 2022)

The presence of Aβ has devastating effects at the cellular level.

Aβ has high affinity binding sites for metals such as iron, zinc and copper, allowing the formation of reactive oxygen species (ROS) (Allsop, Mayes, Moore, Masad, & Tabner, 2008; Butterfield, 2002). When the amount of ROS exceeds the antioxidant defence system, this imbalance is called oxidative stress, which causes oxidation of nucleic acids, oxidation of proteins, peroxidation of lipids and ultimately cell death (Butterfield & Sultana, 2011).

ROS are specifically dangerous to neurons due to low amounts of the antioxidant glutathione (Dringen, Pfeiffer, & Hamprecht, 1999), their membrane structure, which largely consist of polysaturated fatty acids (Hazel & Williams, 1990) and their high demand of oxygen (Smith et al., 1995). Another significant threat of ROS is that the damage they cause can accumulate over time (Benzi & Moretti, 1995).

The brain has several means of clearing Aβ. One of them is drainage through interstitial fluid (ISF). Here, Aβ is diffused from the ISF to cerebrospinal fluid (CSF) and consequently drained into the blood (Yoon & Jo, 2012). Several amyloid-degrading enzymes have been identified to break down the protein to aid this process (Eckman et al., 2006; Tucker et al., 2000; Yoon & Jo, 2012). Unfortunately, this clearance is insufficient in keeping up with the increase of Aβ as the pathology progresses.

Another important mechanism is cell-mediated clearance, which will now be discussed in the context of neuroinflammation.

1.1.1.5 Neuroinflammation

With amyloid plaques posing a considerable threat to the brain, immunological mechanisms are in place to attempt clearance of Aβ and plaques. In the presence of Aβ and amyloid plaques, neuroinflammation is commonly observed. The inflammation response involves a large number of different cell types, mediators and moderators. In this process, pro-inflammatory cytokines are produced, including interleukin (IL)-1β, IL-6, IL-18, as well as small molecule messengers such as nitric oxide, and reactive oxygen species (DiSabato, Quan, & Godbout, 2016). The presence of pro-inflammatory molecules can have devastating effects, including synaptic dysfunction, neuronal death and suppressed neurogenesis (Lyman, Lloyd, Ji, Vizcaychipi, & Ma, 2014). Astrocytes and microglia are the two most important cell types implicated in neuroinflammation. Microglia are constantly probing their environment for pathogens and cellular debris. When detecting Aβ and amyloid plaques, they migrate to the location and bind to Aβ oligomers, causing microglia to enter an activated state (Bamberger, Harris, McDonald, Husemann, & Landreth, 2003). Once activated, microglia secrete proinflammatory cytokines to mobilise more immune cells (El Khoury et al., 2003; Stewart et al., 2010) and initiate phagocytosis of aggregated Aβ (Frackowiak et al., 1992; Paresce, Ghosh, & Maxfield, 1996). This clearance of amyloid plaques is ineffective. Although the exact cause is yet to be fully understood, a number of concepts have been proposed to explain the failure of efficient clearance. Possible explanations are the increased cytokine levels which cause the Aβ phagocytosis receptors of microglia to be downregulated (Hickman, Allison, & El Khoury, 2008), as well as the generation of speck-like protein, caused by signalling pathways of microglia after phagocytosis is initiated, which can leak into the extracellular space and cross-seed amyloid plaques (Venegas et al., 2017) in AD mouse models.

Like microglia, reactive astrocytes cluster in proximity to amyloid plaques. The main function of reactive astrogliosis is the recovery of compromised tissue and neuroprotection. While astrocyte atrophy has been reported in early stages of AD mouse models (Olabarria, Noristani, Verkhratsky, & Rodríguez, 2010), astrocytes become reactive during later stages, releasing interleukins and cytokines and have also a potential role in internalising and degradation of amyloid plaques (Wyss-Coray et al., 2003). However, Aβ causes calcium dysregulation in astrocytes by enhancing calcium signalling. This is believed to alter astrocytic activity and interfere with their function of neuromodulation (Lee, Kosuri, & Arancio, 2014). Furthermore,

astrocytes release cytokines tumour necrosis factor α (TNFα), IL-1ß, IL-6 and transforming growth factor ß (TGF-ß), which have been shown to promote the formation of plaques (Liao, Wang, Cheng, Kuo, & Wolfe, 2004). Neuroinflammation is believed to play an important role in the initiation of AD pathology. Systemic inflammation induced by risk factors such as infections, diabetes or smoking, can cause neuroinflammation through active transport though the blood-brain barrier (BBB) or disruption of the BBB (Calsolaro & Edison, 2016). Inflammation is also observed in cases of traumatic brain injury (Johnson et al., 2013), which increases the risk for AD, further strengthening the proposed link between risk factors, neuroinflammation and AD development.

1.1.1.6 Tau pathology

Apart from Aβ plaques, tau tangles are an important component of AD. These tangles are situated inside neurons and formed when tau, a microtubule stabilisation protein, undergoes hyper-phosphorylation (Ballatore, Lee, & Trojanowski, 2007; Buée, Bussière, Buée-Scherrer, Delacourte, & Hof, 2000). Under non-pathological conditions, tau develops double rings around microtubules, thereby aiding their up-keep and axonal transport (Weingarten, Lockwood, Hwo, & Kirschner, 1975). Its phosphorylated state is under equilibrium, highly regulated by phosphorylation and dephosphorylation mechanisms. In AD, this equilibrium is out of balance. More specifically, a downregulation of phosphatases, responsible for the dephosphorylation of tau, has been reported (Matsuo et al., 1994). When tau reaches a hyperphosphorylated state, as seen in AD, it loses its affinity to microtubules, becoming detached and starts to aggregate. This aggregation can be observed in two steps: pairs of tau filaments form helices, which then cluster together to form tangles (Figure 1.2).

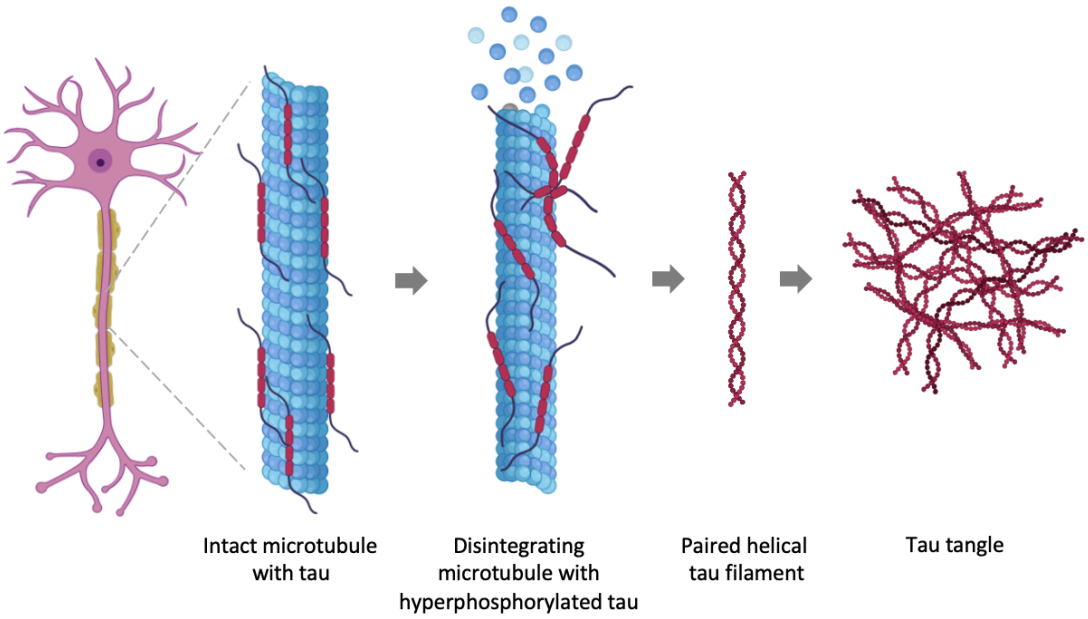

Figure 1.2 Development of tau tangles. *Illustration created with BioRender.com.*

When the stabilisation of microtubules is insufficient, their structure starts to break down and axonal transport is disrupted (Ballatore et al., 2007; Lindwall & Cole, 1984). Here, tau tangles themselves pose as obstacles preventing cargo and vesicle transport by blocking their path. Neurons affected by tau tangles therefore cannot function properly, amplifying the neurodegeneration in AD pathology (Ballatore et al., 2007). Intracellular tau tangles can also cross across synapses; therefore tau pathology has been observed to spread across the brain over time (d'Errico & Meyer-Luehmann, 2020). This spread has been replicated in both in vivo and in vitro studies, where tau aggregates were injected (Ahmed et al., 2014; Clavaguera et al., 2013; Clavaguera et al., 2009; Guo et al., 2016; Lasagna-Reeves et al., 2012). Traditionally, tau tangles and Aβ plaques have been viewed as independent components of AD with little to no interaction. In the past years, however, this view has been questioned and a synergistic effect between the two pathological components has been suggested (Busche & Hyman, 2020). Characterising and understanding such a synergic relationship could help developing more potent therapeutic interventions in the future.

1.1.1.7 Mouse models

The pathology of AD is immensely complex, and a lot of research is being conducted to understand the underlying mechanisms and identify therapeutic targets. Studies in humans are mostly limited to non-invasive methods and post-mortem examination, severely limiting the research questions that can be addressed. Non-animal research is being conducted where possible. However, to investigate mechanisms only observable in living systems, animal models are being used to gain new insights into the disease. Mice are among the most widely used animals for AD research. The first AD mouse model - PDAPP - was created in 1995 by expressing the human APP gene with the Indian V717F gene mutation. PDAPP mice showed development of amyloid plaques, activated microglia and reactive astrocytes, synaptic loss and cognitive impairment (Games et al., 1995). Since then, novel mouse models have been developed to either mimic the amyloid pathology, tau pathology, or a combination of both. For years, modelling the disease in mice has been achieved by the development of transgenic models where genetic mutations discovered in FAD patients are over expressed. More recently, AD mouse models have been developed through knock-in/out or clustered regular interspaced short palindromic repeats (CRISPR) gene editing.

1.1.1.7.1 Transgenic mouse models

Transgenic mouse models have been widely used in AD research for the past decades. They have been developed to either model the amyloid or tau pathology of AD. Initial models harbouring mutations found in FAD patients to overexpress APP showed an increase in Aβ production and aggregation, as well as cognitive decline. Neurodegeneration, however, could not be observed (Chishti et al., 2001; Games et al., 1995; Hsiao et al., 1996). Alternative mouse models were developed to carry PSEN1/2 mutations. This approach failed to show Aβ aggregation (De Strooper et al., 1998). However, the combination of both approaches showed promising results. Today, the most widely used models comprise co-expression of human APP carrying one or multiple FAD-like mutations (Arctic E693G, Austrian T714I, Dutch E693Q, Florida I716V, Iberian I716F, Indian V717F, London V717I and Swedish KM670/671NL) and PSEN1 carrying one or more FAD mutations (M146L, M146V,

L286V and ΔE9). These co-expression models provide a more comprehensive phenotype, but they fail to model the tau pathology of AD.

To overcome this limitation, the 3xTg-AD mouse model was developed. It is a triple transgenic model harbouring APP (Swedish), PSEN1 (M146V) and TauP301L transgenes. While it managed to model both the amyloid and tau pathology, the mutation used to induce tau pathology in this model has not been directly linked to AD pathology in humans and might not depict the mechanisms of the disease accurately (Oddo et al., 2003).

Nevertheless, transgenic mouse models with or without tau pathology are widely used in research.

One AD mouse model frequently used in research is the 5xFAD mouse. This model was developed by co-expression of human APP (carrying the Swedish K670N/M671L, Florida I716V, and London V717I mutations) and PSEN1 (carrying the M146L and L286V mutations) (Oakley et al., 2006). More specifically, site-directed mutagenesis was utilised to introduce the FAD mutations into APP and PSEN1 complementary DNA. This was followed by subcloning onto the Thy-1 promoter and the resulting transgenes were then injected into pronucei of individual embryos, allowing the Thy-1 promoter to facilitate expression of the transgenes (Oakley et al., 2006). The combination of 5 mutations causes a rapid progression of amyloid plaque development. Earliest changes can be observed in the form of intraneural Aβ in subicular and layer V pyramidal neurons at as early as 6 weeks old. At 2 months of age, amyloid plaques can be found in the hippocampus, thalamus and cortex (Richard et al., 2015), which then spread to the frontal, parietal and entorhinal cortices as well as dentate gyrus (Giannoni et al., 2016). Along with Aβ deposition, gliosis increases in these brain areas. As Aβ accumulation becomes more prominent, degeneration of synapses can be observed at 4 month and neuronal loss at 6 months (Eimer & Vassar, 2013; Oakley et al., 2006). The first type of neuronal cells to be lost at 6 months are cholinergic neurons in the basal forebrain (Devi & Ohno, 2010). In male 5xFAD mice, the Aβ pathology seems to reach its maximum at around 10 months, while female mice show an increase up until 14 months, indicating that sex differences do occur in this mouse model (Bhattacharya, Haertel, Maelicke, & Montag, 2014). The onset of memory deficits largely coincides with the onset neuronal loss (Flanigan, Xue, Kishan Rao, Dhanushkodi, & McDonald, 2014; O'Leary, Robertson, Chipman, Rafuse, & Brown,

2018; Xiao et al., 2015) although some deficits have been reported even earlier, at around 4-5 months (Devi & Ohno, 2010; Oakley et al., 2006).

Models carrying multiple mutations tend to have a faster progression of AD-like pathology (Yokoyama, Kobayashi, Tatsumi, & Tomita, 2022). An aggressive progression can be advantageous in research, but it is not suitable for certain research questions. Investigation of cellular, oscillatory or behavioural changes before the deposition of amyloid plaques, for example, is more conveniently studied in a mouse model with slower pathological progression. It is also important to question whether over-engineering of mouse models to display a more aggressive pathology diverges further from human pathology. The overexpression of APP in mouse models can have off-target side effects. Fragments related to APP are usually involved in calcium homeostasis, transcription and functions involved in memory, making it difficult to distinguish if changes observed in these models are due to the AD phenotype or a side effect of increased APP expression (Chang & Suh, 2005; Nicolas & Hassan, 2014). Beyond this, it is important to note that transgenic mouse models are based on the pathology of FAD. While the pathology of FAD and SAD are similar, subtle differences will go undetected when research is done on transgenic mouse models alone. While there are currently no alternative models to mimic the pathology of SAD, there has been progress in the development of mouse models attempting to omit the artifacts of APP overexpression using novel techniques of knock-in/out and gene editing.

1.1.1.7.2 Knock-in mouse models

To create a mouse model that mimics the Aβ pathology without the overexpression of APP, researchers have started to use knock-in strategies. Unlike transgenic mouse models, where the genetic sequences are introduced at random locations and native gene regulation and expression patterns can be disrupted, knock-in mice are generated by introducing genetic mutations directly into the genes original location on the genome, allowing native regulation and expression to be preserved. One of these models, APP^{NL-F} was created by humanising the APP gene and knocking-in the Swedish and Beyreuther/Iberian mutations. This model showed Aβ accumulation, neuroinflammation and memory impairments with limited changes in APP expression (Saito et al., 2014). More of such knock-in models have since been

created, including APP^{NL-G-F}, harbouring the Swedish, Iberian and Arctic mutation, APP^{G-F} mice, harbouring the Beyreuther/Iberian and Arctic mutations (Watamura et al., 2022) and PLB4 mice, expressing the human rate-limiting β-site enzyme 1 (hBACE1), which has been identified to cleave APP in human AD pathology (Plucińska et al., 2014).
Such new mouse models have not only allowed the modelling of a more realistic AD pathology, but characterisation and comparison of these novel mouse models has revealed new insights into the pathology of AD. By combining different mutations in knock-in mouse models, researchers have found that humanised Aβ alone can induce endosomal enlargement. Previously it had been suggested that this enlargement was dependent on C-terminal fragment β (CTF-β) (Jiang et al., 2010; S. Kim et al., 2016; Kwart et al., 2019). The new findings now suggest multiple pathways to be involved: CTF-β-dependent, Aβ-dependent and APP-independent pathways (Knupp et al., 2020; Pensalfini et al., 2020; Watamura et al., 2022).

1.1.1.8 Conventional treatments

Multiple therapeutic approaches have been developed in an attempt to slow or stop the pathology of AD over the years, targeting either Aβ, tau or the immune activation states. One approach was to inhibit Aβ through γ-secretase inhibitors (De Strooper, Vassar, & Golde, 2010; Kretner et al., 2016) or ß-secretase inhibitors (Lo et al., 2021; Sur et al., 2020; Wessels et al., 2020). Unfortunately, both approaches showed low clinical efficacy and were accompanied by serious side effects (McDade et al., 2021; Siemers et al., 2007; Siemers et al., 2006). It is important to note that these studies were conducted on patients who showed clear symptoms of AD. Whether such approaches could potentially have a preventative effect if applied before the onset of AD remains unclear. In any case, the side effects of these approaches remain too severe for approval.
At this point, there are four drugs approved for the treatment of AD in the UK. Three of these drugs (donepezil, galantamine and rivastigmine) are acetylcholinesterase inhibitors. They bind to acetylcholinesterase, prevent it from breaking down acetylcholine (ACh) and thereby increase the amount ACh in the extracellular space and its signalling (Briggs, Kennelly, & O'Neill, 2016; Chu, 2012; Mendiola-Precoma, Berumen, Padilla, & Garcia-Alcocer, 2016). ACh is an excitatory neurotransmitter involved in learning, memory and sleep regulation. In AD,

cholinergic neurons show severe degeneration resulting in a deficiency of ACh (Bowen, Smith, White, & Davison, 1976). By inhibiting acetylcholinesterase, the drugs increase the amount of ACh in the brain and promote ACh signalling. Studies investigating the effectiveness of these drugs indicate that the treatment can delay cognitive decline by 6-12 months. It has also been shown that donepezil can increase cerebral blood flow and reduce atrophy of the cortex, HC and basal forebrain (Hampel et al., 2018). Although these drugs show therapeutic benefits, these benefits have only been observed in 60% of patients (Chu, 2012). It is unclear why a large percentage of patients don't seem to benefit from these treatments.

The fourth drug currently approved for treatment in the UK is memantine, a N-methyl-d-aspartate (NMDA) antagonist. NMDA receptors are activated by glutamate and can be found in pyramidal cells in the cortex and HC. Binding of glutamate to NMDA receptors enhances the long-term potentiation of synapses of these pyramidal neurons, making them important for learning and memory. Excessive stimulation of these receptors, however, leads to excitotoxicity, mediated by excessive influx of Ca^{2+} (Choi, 1987), which causes gradual loss of synaptic function, neuronal cell damage and cell death (Rothman & Olney, 1986). In AD, excessive amounts of glutamate are available to act on NMDA receptors, due to impaired uptake and recycling mechanisms (Arias, Arrieta, & Tapia, 1995; Fernández-Tomé, Brera, Arévalo, & de Ceballos, 2004; Parpura-Gill, Beitz, & Uemura, 1997). Memantine binds to NMDA receptors, thereby blocks glutamate and reduces excitotoxicity (Chu, 2012). In animal models, memantine has also been shown to reduce levels of Aβ and inflammatory markers (Folch et al., 2018). Clinical studies in human AD patients have shown small improvements in cognitive functions in moderate and severe AD cases, but not in mild cases (McShane et al., 2019). Memantine is often chosen as a second-line treatment, for patients who are already taking one of the acetylcholinesterase inhibitor drugs (Arvanitakis, Shah, & Bennett, 2019) as the combination of both treatments showed more effective improvements of cognition than memantine alone (Schmidt et al., 2015).

Although both acetylcholinesterase inhibitors and NMDA antagonists have been shown to delay and ease symptoms of AD, improvements are small, and not all patients benefit from taking them. Furthermore, both options fail to cure the disease or prevent its progression.

1.1.1.9 Emerging treatments

1.1.1.9.1 Anti-amyloid drugs

Novel treatments for AD include so-called anti-amyloid therapies aiming to clear Aβ from the brain. The drug aducanumab was conditionally approved by the US Food and Drug Administration (FDA) in 2021, making it the first treatment targeting not the symptoms but the underlying cause of AD. It is a monoclonal antibody that selectively binds to soluble Aβ oligomers and insoluble Aβ fibrils. By binding to Aβ, aducanumab aims to facilitate the clearance of Aβ by engaging the brains immune system (Budd Haeberlein et al., 2022; Schneider, 2020; Sevigny et al., 2016). The development and approval of aducanumab has caused debate and controversy within the scientific and medical community. Although some patients with early stages of AD showed small cognitive improvements, these were accompanied by severe side effects, including microhaemorrhages and oedema (Budd Haeberlein et al., 2022). Due to safety concerns, lack of data on how patients with later stages of AD might respond to the treatment, and overall small benefits in patients with early AD, the European Medicines Agency has rejected the approval of aducanumab.
Another drug, donanemab, also follows the idea of amyloid-binding antibodies. Donanemab, however, binds specifically to an N-terminal pyroglutamate Aβ epitope which is only found in plaques, but not other Aβ species (Demattos et al., 2012; Lowe, Willis, et al., 2021). Early clinical studies have found a reduction in amyloid plaques after administration of this drug in patients with mild cognitive impairment (MCI), moderate and severe AD (Lowe, Duggan Evans, et al., 2021). A further trial in patients with early symptoms of AD found only small effects on the clearance of plaques and cognitive decline. Side effects in the form of edema and effusions was prominent in 26.7 % of participants (Mintun et al., 2021), a percentage severely questioning the safety of this drug.
In 2023 another anti-amyloid drug, lecanemab, was approved by the FDA. Similar to aducanumab, it is an antibody that aims to clear Aβ from the brain. Clinical trials have shown some clearance of Aβ and small cognitive improvements in early AD patients. Side effects similar to the ones of aducanumab have been reported but seem to occur less frequently in patients treated with lecanemab (Budd Haeberlein et al., 2022; Swanson et al., 2021; van Dyck et al., 2023).

1.1.1.9.2 Drugs for other targets

Besides anti-amyloid drugs, drugs targeting other aspects of AD are being considered. Neuroinflammation is one of these targets. Drugs in development here are mostly anti-inflammatory, although some aim to specifically activate the immune response and thereby enhance clearance of plaques (Cummings, Osse, & Kinney, 2023). Oxidative stress is another target for treatment. Anti-oxidants, B vitamins and poly-saturated fatty acids have been found to be associated with a decreased risk for AD (Hu et al., 2013), leading to clinical trials to test the effect of antioxidants. One of these is currently in phase III (NCT04842552), where the drug hydralazine is tested. It activates an antioxidant pathway, increasing mitochondrial function and autophagy, among others (Wang et al., 2021) which should be beneficial to slow down the AD pathology.
Another approach is the screening of already approved drugs to see whether they can have a positive effect on AD pathology. By screening over 1000 FDA-approved drugs, the drug levosimendan was found to significantly inhibit tau aggregation (Lim et al., 2023). This approach of screening previous drugs has several benefits: it is a faster and more cost-efficient, the drugs have already passed extensive safety testing, and their pharmacokinetics are already known. However, with AD being a highly complex disease, chances of finding a single drug to address all pathways and mechanisms of the disease are low. Therefore, multi-target drugs are another approach, aiming to achieve synergistic effects across multiple processes in AD (Turgutalp & Kizil, 2024).

1.1.1.9.3 Neuromodulation

As the development of treatments targeting the molecular aspects of AD pathology has been proven difficult, scientists are considering new targets for treatment. A new approach revolves around the idea of targeting circuit dysfunctions in AD by neuromodulation, an approach that utilised the manipulation of neuronal activity to reinstate normal circuit function and thereby resolve abnormalities on the molecular, cellular and synaptic level.
Among the invasive techniques of neuromodulation is deep brain stimulation (DBS). Here, electrodes are implanted chronically to deliver electric pulses. Phase I clinical trials used DBS in AD patients and found an increase in hippocampal volume and

lower cognitive decline in patients (Laxton et al., 2010). In phase II, however, it was found that only patients over the age of 65 showed small improvements after DBS, while younger patients showed worsening of cognitive abilities, leading to the termination of the trial (Lozano et al., 2016).

Non-invasive methods of brain stimulation have also been explored. Among them is transcranial magnetic stimulation (rTMS). This tool utilises electromagnetic pulses to stimulate the brain. Studies investigating rTMS as a treatment for AD have reported an improvement in cognitive functions in AD patients (Koch et al., 2018; Traikapi et al., 2023), and maintaining of cognitive abilities in AD patients receiving rTMS, compared to patients who received sham stimulation (Koch et al., 2022).

In recent years, using neuromodulation to target gamma oscillations in AD has been a popular approach (Adaikkan et al., 2019; Bobola et al., 2020; Cimenser et al., 2021; Iaccarino et al., 2016). Gamma oscillations are rhythmic neuronal activities with a frequency range of 30 – 90 Hz. They play an important role in cognitive functions such as attention, learning and memory by facilitating the communication between different brain regions (Buzsáki & Wang, 2012). In AD, gamma oscillations seem to be altered, although studies in human patients showed conflicting evidence. Some studies have reported reduced gamma power in the cortex of AD patients (Başar, Emek-Savaş, Güntekin, & Yener, 2016; Ribary et al., 1991; Stam et al., 2002) while other studies have reported gamma power to be increased in AD patients (Başar, Femir, Emek-Savaş, Güntekin, & Yener, 2017; Rossini et al., 2006; van Deursen, Vuurman, van Kranen-Mastenbroek, Verhey, & Riedel, 2011; Wang et al., 2017). This could be due to different approaches for detecting gamma oscillations (EEG versus MEG) or different cohorts of AD patients (early stages, moderate or severe AD). Despite these conflicting findings in human patients, research on AD mouse models consistently showed reduced gamma power (reviewed in (Byron, Semenova, & Sakata, 2021)), so neuromodulation to reinstate normal gamma oscillations was explored as a therapeutic approach for AD treatment. Initial studies on AD mouse models showed a reduction in Aβ after optogenetic stimulation of hippocampal parvalbumin-positive (PV) interneurons at 40 Hz (Iaccarino et al., 2016), and improved spatial memory performance after optogenetic stimulation at 40 Hz of the medial septum (Etter et al., 2019). These findings lead to the investigation of non-invasive 40 Hz stimulation techniques as a treatment option. Previous work had proven that 40 Hz light flicker can entrain the firing of neurons in the visual cortex in humans (Herrmann, 2001; Jones et al., 2019;

Pastor, Artieda, Arbizu, Valencia, & Masdeu, 2003). Inspired by this, researchers investigated if sensory stimulation by light flicker or auditory stimulation could also entrain neurons in other brain regions. They found entrained gamma oscillation not only in the visual and auditory cortex but also in the CA1 of the hippocampus and in the prefrontal cortex (Lustenberger et al., 2018; Martorell et al., 2019; Pastor et al., 2002). In AD animal models, visual and/or auditory stimulation at 40 Hz showed a reduction in Aβ levels and tau phosphorylation (Adaikkan et al., 2019; Iaccarino et al., 2016; Martorell et al., 2019). Therefore, human studies have been conducted to test the application of non-invasive gamma stimulation on AD patients. These studies used either visual stimulation, or combined auditory and visual stimulation with treatments lasting between several days to several months. They reported small benefits of 40 Hz treatment in the shape of improved functional connectivity of the default mode network, improved circadian rhythm, improved cognition, less ventricular enlargement and less hippocampal atrophy (Chan et al., 2022; Cimenser et al., 2021; Da et al., 2024; He et al., 2021). However, none of these studies have found changes in the molecular and cellular pathologies. Although the benefits of these 40 Hz treatments were small, they indicate that neural oscillations could be a target for non-invasive treatment options for AD. It remains unclear if such interventions could have greater benefits when applied at earlier time points of the disease, ideally in the pre-clinical stage, before the onset of cognitive decline.
In order to test therapeutic approaches in early stages of AD, strategies for identifying patients before the disease manifests in cognitive decline need to be explored. In the following section I will outline the conventional biomarkers used for diagnosis, as well as novel biomarkers.

1.1.1.10 Biomarkers

Biomarkers are measurable indicators of biological and physiological processes, pathological abnormalities or responses to therapeutic interventions. Traditional AD biomarkers are derived from imaging techniques and CSF. Novel approaches investigate biomarkers derived from EEG, blood, urine, saliva and genetic analysis. An overview of current and emerging biomarkers is depicted in Figure 1.3. In the following subchapters these conventional and novel biomarkers will be discussed.

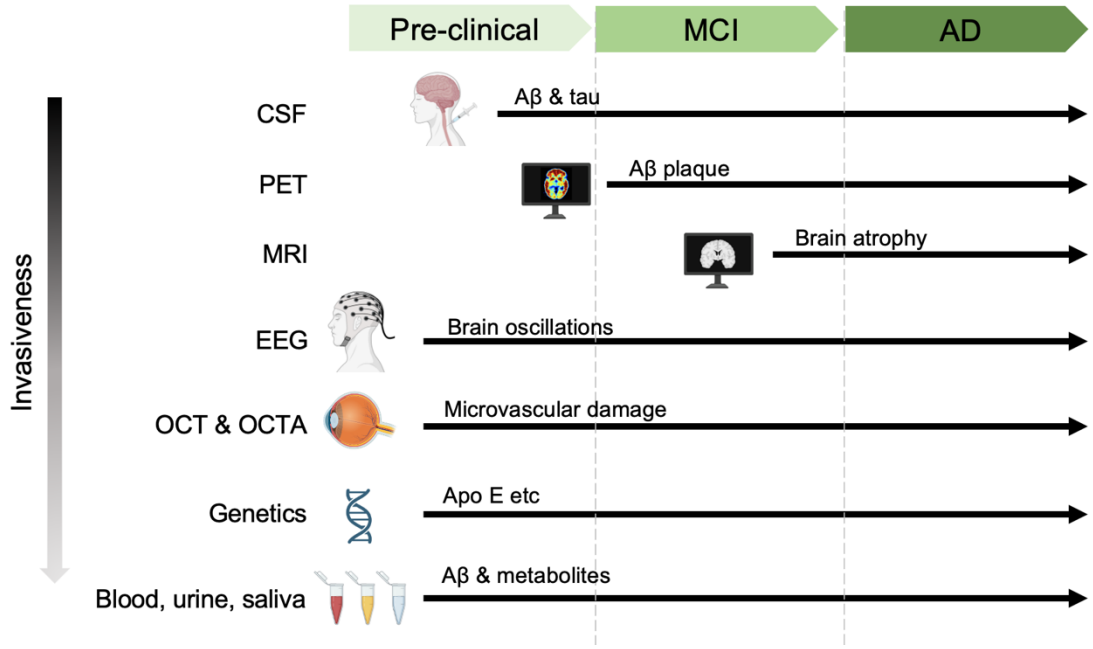

***Figure 1.3 Biomarkers of AD**. Overview of biomarker screening modalities shown in accordance to their invasiveness and reported or proposed time point of diagnosis in the disease progression: cerebrospinal fluid (CSF), positron emission tomography (PET), magnetic resonance imaging (MRI), electroencephalogram (EEG), optical coherence tomography (OCT), optical coherence tomography angiopathy (OCTA), genetics, blood, urine and saliva. Illustration partially created with BioRender.com.*

1.1.1.10.1 Conventional biomarkers

Among the most frequently utilised biomarkers in AD are Aβ and tau. Both can be found in the CSF. For the analysis of Aβ, the amount of Aβ42 is specifically relevant for diagnosis. The level of Aβ42 found in CSF negatively correlates with the amount of Aβ plaques found by positron emission tomography (PET) scans. Analysis of the ratio between Aβ42 and Aβ40 is further used as an indicator for the progression from the pre-clinical stage to MCI and AD (Jack et al., 2016). Tau in the CSF is

analysed in a similar fashion, although higher levels of tau show a positive correlation with the amount of plaques in the brain (Ossenkoppele, van der Kant, & Hansson, 2022).

Functional brain imaging, including magnetic resonance imaging (MRI) and PET, are also frequently used in clinical settings as it allows to determine whether a patient showing symptoms of MCI is likely to develop AD. A meta-analysis covering 24 studies with over 1000 patients reported 89% sensitivity and 85% specificity for PET scans and 73% sensitivity and 81% specificity for MRI in respect to its ability to identify patients with MCI who would later progress to develop AD (Yuan, Gu, & Wei, 2009).

Another study compared the performance of MRI, PET and CSF analysis in patients at different stages of AD. They divided patients according to their scores of clinical dementia rating (CDR). For patients with a low CDR rating of 0.5, classified as ‘questionable’, sensitivity of CSF analysis was 90%, for PET 71.4%, for MRI 81.9%. In patients with a CDR rating of 1, classified as ‘mild’, sensitivity of CSF analysis was 95.5%, for PET 96.7%, and for MRI 76.9%. In patients with the CDR rating of 2, ‘moderate’, sensitivity was highest with 100% for CSF, 100% for PET and 93.3% for MRI (Morinaga et al., 2010). Such comparative studies and meta-analysis highlight the differences in methodologies assessing biomarkers of AD and their reduced sensitivity in early stages of the disease.

1.1.1.10.2 Novel biomarkers

Due to the invasiveness and high costs of conventional biomarker assessments, novel biomarkers are continuously being developed.

One non-invasive biomarker that is currently being investigated for the diagnosis of AD is EEG.

Patients show slowing of EEG, manifesting in decreased spectral power of high frequency oscillations, including alpha, beta and gamma, and increased spectral power of low frequencies, including delta and theta. By assessing the power spectrum and synchronisation characteristics of EEGs, AD patients could be diagnosed in the future (H. Zhang et al., 2021).

Another non-invasive approach is the assessment of microvascular changes in the retina of the eye. The idea here is to utilise optical coherence tomography (OCT) or optical coherence tomography angiopathy (OCTA) to detect damage in the microstructure of the retina. Such changes have been observed in patients in the pre-clinical stage, MCI and AD (Zhang, Wang, Shi, Shen, & Lu, 2021).

Furthermore, biomarkers in bodily fluids other than CSF are being investigated. Among the most promising approaches are the testing of blood, saliva and urine. In blood samples, 19 proteins have been identified to have predictive properties regarding the AD status of a patient (Jiang et al., 2022). Metabolite markers from saliva samples have been reported to distinguish between patients in the pre-clinical stage, MCI and AD (Huan et al., 2018). In urine samples, metabolites were found that could help physicians to distinguish between patients with MCI and AD (Wang et al., 2023).

These novel biomarkers show great potential for faster, more cost-efficient and less invasive methods for diagnosing individuals with AD at early stages of the disease.

1.1.2 Altered brain oscillations

1.1.2.1 Overview of brain oscillations

Brain oscillations are differentiated in terms of their spectral band and functions. Oscillations below 1 Hz are referred to as slow oscillations and oscillations of 1 - 4 Hz are known as delta. They both occur predominantly during NREM sleep and are associated with memory consolidation processes (Adamantidis, Gutierrez Herrera, & Gent, 2019). Oscillations of 4 - 10 Hz are termed theta, and oscillations of 10 - 15 Hz as alpha, which are associated with short-term storage, manipulation and retrieval of information and passive attention (Hsieh & Ranganath, 2014; Roux & Uhlhaas, 2014). Oscillations of 15 - 30 Hz are known as beta oscillations. They are mainly associated with external concentration, but also anxiety and an overall “busy mind” (Abhang, Gawali, & Mehrotra, 2016). Lastly, 30 - 90 Hz oscillations are referred to as gamma. Gamma is linked to concentration, attention selection, working memory and memory encoding (Fries, 2015; Jensen, Kaiser, & Lachaux, 2007; Miller, Lundqvist, & Bastos, 2018; Osipova et al., 2006).

The presence of Aβ, neuroinflammation and neuronal loss in AD have far reaching effects on various brain oscillations. Early EEG studies in AD patients reported three major changes in oscillations: slowing of EEG, reduced complexity of EEG and reduced functional connectivity. EEG slowing is observed in posterior brain regions, along with diffuse slow activity and reduced activity in the alpha and beta band and the extend of these changes correlated with the degree of cognitive impairment (Brenner, Reynolds, & Ulrich, 1988; Gordon & Sim, 1967; Letemendia & Pampiglione, 1958; Weiner & Schuster, 1956). Reports regarding the reduced complexity of AD patient EEGs include reduced complexity of activity across almost the entire brain, assessed as the correlation dimension D2, which corresponds to the amount of independent variables needed to explain brain dynamics (Besthorn, Sattel, Geiger-Kabisch, Zerfass, & Förstl, 1995; Jeong, Kim, & Han, 1998; Woyshville & Calabrese, 1994). Furthermore, functional connectivity has been found to be reduced across cortical areas. Especially the coherence of the alpha and beta band seems to be affected (Besthorn et al., 1994; Locatelli, Cursi, Liberati, Franceschi, & Comi, 1998; Sloan, Fenton, Kennedy, & MacLennan, 1994).

Since these early observations in AD patients, more abnormalities in neural oscillations have been observed in both AD patients (Bakker et al., 2012; Dickerson et al., 2005; Sorg et al., 2007) and AD mouse models, including neurons in the hippocampus exhibiting hyperactivity caused by reduced GABAergic inhibition (Busche & Konnerth, 2016). Such hyperactivity is also induced by direct delivery of exogenous amyloid-β into the brains of healthy mice (Busche et al., 2012). Since the production of amyloid-β is activity-dependant, the increase in neuronal activity also leads to an increase in amyloid-β, leading to a vicious cycle (Bero et al., 2011; Yamamoto et al., 2015). Restoring the balance of excitation and inhibition in AD mice has been shown to restore the functionality of neuronal circuits and prevent behavioural impairments (Busche & Konnerth, 2016).

Such studies indicate that targeting abnormal neural oscillations are a promising approach to find a treatment for AD. When studying AD, it is particularly interesting to focus on brain oscillations and states associated with learning and memory.

In learning and memory, specific oscillations are believed to facilitate the different stages of memory formation. In the encoding phase and retrieval phase, theta and gamma oscillations are particularly important and show an increase in power which is believed to reflect the load of new information that needs to be processed (Bastiaansen & Hagoort, 2003; Griffiths & Jensen, 2023; Howard et al., 2003). The oscillations involved during the memory consolidation phase will be discussed in more detail in the context of sleep in the following section.

1.1.2.2 Sleep

Sleep is a reversible state of quiescence, essential for survival and characterised by immobility and reduced responsiveness (Cirelli & Tononi, 2008; Medori et al., 1992). Although the purpose of sleep is still unclear, the influence of sleep duration and quality on biological functions is undisputed (McEwen, 2006; Mullington, Haack, Toth, Serrador, & Meier-Ewert, 2009; Robles & Carroll, 2011). Sleep consists of two distinct states: rapid eye movement (REM) sleep and non-REM (NREM) sleep. In humans, sleep is further subdivided into stage N1, N2 and N3, with N1 being the lightest and N3 being the deepest stage of NREM sleep. N3 is also referred to as slow-wave sleep (SWS) due to its characteristic slow oscillations and synchronised delta activity. In both humans and mammals, SOs are generated when cortical networks alternate between up-states of membrane depolarisation and down-states

of hyperpolarisation in synchrony. These SOs spread anterior to posterior, as well as to subcortical regions (Massimini, Huber, Ferrarelli, Hill, & Tononi, 2004; Wierzynski, Lubenov, Gu, & Siapas, 2009).

During healthy aging, sleep architecture changes in humans. These changes can be observed in the form of reduced SWS and REM sleep, more N1 and N2 sleep, and an increase in sleep fragmentation (Petit, Gagnon, Fantini, Ferini-Strambi, & Montplaisir, 2004; Van Cauter, Leproult, & Plat, 2000). In patients with AD and MCI, these changes are exaggerated (Bonanni et al., 2005; Prinz et al., 1982). These changes in sleep occur before the onset of cognitive decline, during the so-called pre-clinical stage, when Aβ is beginning to build up in the brain (Ju et al., 2013). Furthermore, the decrease in overall sleep duration in this stage seems to be correlated directly to the amount of Aβ present in the brain (Spira et al., 2013). It is not known what exactly causes the changes in sleep architecture in AD. However, neuronal degeneration in sleep regulating areas are likely to contribute. Brain regions involved in sleep regulation include the basal forebrain, hypothalamus, thalamus, pons and brainstem. All of these areas are affected by AD (Holth, Patel, & Holtzman, 2017). Furthermore, grey matter loss is a likely contributor. A strong association has been found between grey matter loss in the medial prefrontal cortex (mPFC), an area important for the regulation of NREM sleep, along with reduced volume in the cholinergic basal forebrain and REM decrease in MCI (Sanchez-Espinosa, Atienza, & Cantero, 2014; Whitehouse et al., 1982).

Since changes in sleep architecture have been consistently linked to Aβ and AD pathology, the relationship between sleep and Aβ is of great interest.

In healthy humans, wild-type mice and AD mouse models, levels of Aβ fluctuate over the daily 24 h period and strongly correlate with the circadian rhythm: Aβ levels increase during awake times and decrease during sleep (Kang et al., 2009). A possible explanation for these differences between Aβ levels during sleep and wake is the distinct neuronal activity during these states. In the awake state, increased neuronal firing releases Aβ (Cirrito et al., 2005). During SWS, however, neuronal networks show less synaptic activity (Vyazovskiy, Cirelli, Pfister-Genskow, Faraguna, & Tononi, 2008) and therefore likely release less Aβ. Another contributing factor is the facilitation of Aβ clearance through the glymphatic system during sleep (Xie et al., 2013). In human sleep deprivation studies, levels of Aβ42, Aβ40 and Aβ38 have been reported to be increased in the CSF after just one night of sleep deprivation in healthy young adults (Lucey et al., 2018; Ooms et al., 2014). Sleep

deprivation in an APP/PS1 mouse model has shown the same effect of sleep deprivation and also showed that administration of an orexin receptor antagonist to increase sleep duration significantly decreased Aβ pathology (Kang et al., 2009).

Besides the restorative function, sleep plays a vital role in memory consolidation. Earliest studies investigating the effect of sleep on memory performance date back to the 1920s. Here, human subjects were reported to perform better on memory tests when they had slept after the learning procedure (Jenkins & Dallenbach, 1924). Consequently, the memory-enhancing role of sleep has been intensely investigated. Early explanations revolved around a passive involvement of sleep, assuming that sleep protects the learned information from being overwritten by new information. This effect is also referred to as retroactive interference (Ellenbogen, Hulbert, Stickgold, Dinges, & Thompson-Schill, 2006). Since then, the view of sleep has shifted towards a more active role in memory consolidation.
The concept of active systems consolidation accounts for the process of transforming new, labile information, also referred to as engrams, into stable long-term memories (Buzsáki, 1989). Different brain areas are believed to hold different aspects of new information, forming memory networks, which are being integrated into unique memories by the HC (McClelland, McNaughton, & O'Reilly, 1995; Nadel & Moscovitch, 1997). Neuronal representations in the HC are repeatedly reactivated during sleep. Reactivation is mostly observed during SWS, but also occurs during quiet wakefulness (reviewed in(Atherton, Dupret, & Mellor, 2015; O'Neill, Pleydell-Bouverie, Dupret, & Csicsvari, 2010)). This reactivation spreads across the associated memory network, strengthening the memory representation through synaptic strengthening. Studies involving recordings of multiple brain areas simultaneously have shown that hippocampal reactivation co-occurs with neuronal firing in the neocortex, amygdala and striatum, where a temporal delay is observed (Girardeau, Inema, & Buzsáki, 2017; Ji & Wilson, 2007; Lansink, Goltstein, Lankelma, McNaughton, & Pennartz, 2009). This delay indicates that reactivation originates in the HC. However, ensemble reactivation outside the HC has been observed to occur independently of HC activity (O'Neill, Boccara, Stella, Schoenenberger, & Csicsvari, 2017). Although this indicates that the HC is not the sole initiator of memory reactivation, it has also been shown that HC-independent long-term memory consolidation still depends on the activation of HC-dependent mechanism during sleep (Sawangjit et al., 2018).

With the HC being one of the earliest brain regions affected by the pathology of AD, investigating brain oscillations involved in memory consolidation in the HC and associated areas is of great interest. Two brain oscillations in particular – sharp-wave ripples and sleep spindles – will now be described in more detail and their abnormalities in AD will be discussed.

1.1.2.3 Sharp-Wave Ripples

Hippocampal replay is accompanied by sharp-wave ripples (SWRs) (Diba & Buzsáki, 2007; Kudrimoti, Barnes, & McNaughton, 1999). They consist of the sharp wave - a large amplitude deflection corresponding to the synchronous depolarisation of a large population of neurons in the CA1, followed by the ripples - a fast oscillation pattern of 120 - 250 Hz reflecting the activity of pyramidal cell assemblies (Buzsáki, Horváth, Urioste, Hetke, & Wise, 1992; Buzsáki, Leung, & Vanderwolf, 1983; Suzuki & Smith, 1987) (Figure 1.4).

SWRs are believed to arise from the CA3 region of the HC (Buzsáki et al., 1983; Sullivan et al., 2011) and can be observed in all regions of the HC (Figure 1.4). Neuronal activity in the CA3 excites large subsets of CA1 pyramidal cells (Valero et al., 2017), and interneurons (Palop & Mucke, 2016). This coordinated excitation and inhibition of the pyramidal cell ensembles manifests as SWRs in the CA1 region (Buzsáki, 2015). Parvalbumin-expressing fast-spiking inhibitory interneurons have also been reported to be involved in the generation of SWRs in mice, as they propagate signals to the entorhinal cortex (EC) (Roth, Beyer, Both, Draguhn, & Egorov, 2016; Ylinen et al., 1995). The EC shows increased firing activity just before SWRs occur in the CA1 in rats (Oliva, Fernández-Ruiz, Fermino de Oliveira, & Buzsáki, 2018), suggesting that the EC is involved in triggering the occurrence of SWRs. However, the expression of SWRs being ‘triggered’ is somewhat questionable. Early studies in rats showed that during states of elevated arousal, the excitation stemming from the CA3 is suppressed by activation of presynaptic muscarinic and cannabinoid receptors (Hasselmo, 2006; Hounsgaard, 1978; Robbe et al., 2006). During times of quiet rest and NREM sleep, these supressing effects are removed, allowing recurrent excitation from the CA3. This indicated that SWRs are not induced, but ‘released’ when suppressing mechanisms are absent (Buzsáki et al., 1983).

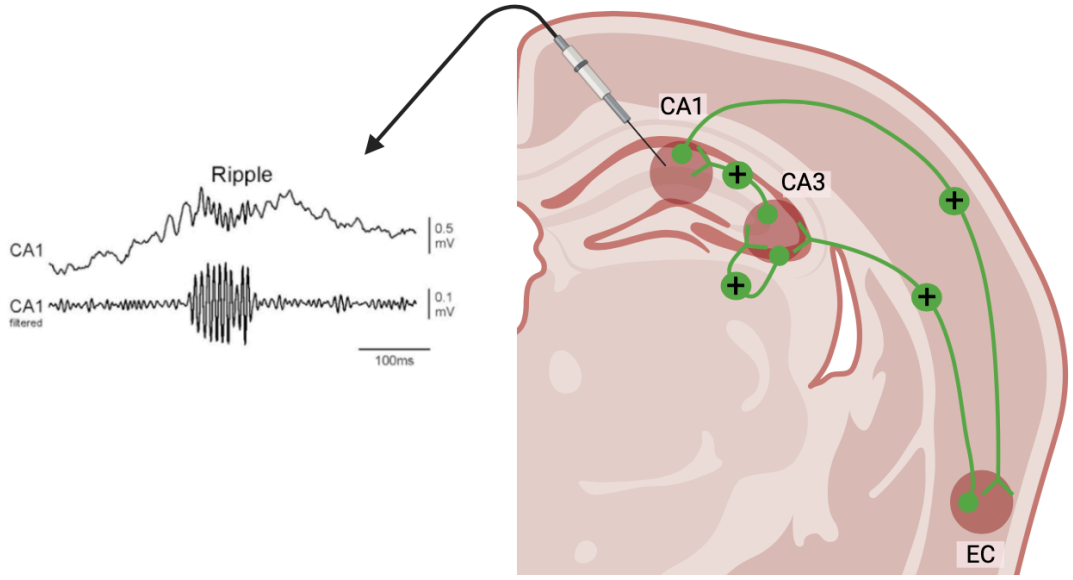

Figure 1.4 Sharp-wave ripple generation. *Left top: representative trace of a SWR in the CA1. Left bottom: 140-250 Hz filtered trace of a SWR in the CA1. Adapted from Nicole et al., 2016. Right: Generation and propagation of SWRs in the HC. Excitatory connections shown in green. Illustration created with BioRender.com.*

SWRs can be observed in both awake and sleep states (Carr, Jadhav, & Frank, 2011; O'Neill et al., 2010) but they predominantly occur during slow-wave sleep where they are believed to be involved in memory consolidation (Buzsáki, 1989; Squire & Alvarez, 1995). Hippocampal SWRs accompany hippocampal replay during NREM sleep (Buzsáki, 2015; Diba & Buzsáki, 2007; Ecker et al., 2022; Kudrimoti et al., 1999) where gamma-band patterns observed during learning are reactivated by SWRs in post-learning sleep (Zhang, Fell, & Axmacher, 2018). Furthermore, reactivation of firing patterns induces long-term potentiation of synapses between the CA1 and CA3 when replay is accompanied by SWRs (Sadowski, Jones, & Mellor, 2016). Since SWRs are highly involved in memory consolidation, it is unsurprising that an increase in SWR occurrence has been repeatedly reported during and just after learning (Cheng & Frank, 2008; Karlsson & Frank, 2008; Nicole et al., 2016; O'Neill, Senior, Allen, Huxter, & Csicsvari, 2008). Multiple studies have investigated the causal relationship of SWR occurrence and memory consolidation by disrupting SWRs during post-learning sleep. Disruption of SWRs by electric stimulation of CA3-CA3 connections, suppression of CA3 input to the CA1, and activation of the median raphe or locus coeruleus, have all been reported to cause impaired learning, evidenced by worse performance in memory tasks (Ego-Stengel & Wilson, 2010; Girardeau, Benchenane, Wiener, Buzsáki, &

Zugaro, 2009; Nakashiba, Buhl, McHugh, & Tonegawa, 2009; Novitskaya, Sara, Logothetis, & Eschenko, 2016; Wang et al., 2015). Interestingly, SWRs have also been observed to increase after such inhibition, indicating the presence of a learning-based homeostatic control mechanism of SWRs (Girardeau, Cei, & Zugaro, 2014).

In AD, the hippocampus shows large amounts of amyloid-β plaques causing progressive degeneration of neurons and memory impairments (Fox et al., 1996; West, Coleman, Flood, & Troncoso, 1994; West, Kawas, Stewart, Rudow, & Troncoso, 2004). As mentioned previously, the CA1, CA3 and EC are all involved in SWR generation and SWRs are crucial for memory consolidation. Interestingly, the EC is the first region in the HC to be affected by amyloid-β accumulation in the pathology of AD (Harris et al., 2010). Since SWRs arise from the HC and are highly involved in memory consolidation, exploring their role in AD is of great interest.
In AD mouse models, SWRs are being recorded to investigate their frequency of occurrence, oscillation frequencies, power and amplitude. In APP/PS1 mice, SWRs have been reported to occur less frequently and reduced in power (Jura, Macrez, Meyrand, & Bem, 2019). In 5xFAD mice, SWRs have been shown to occur less frequently, exhibiting lower gamma power, a lower amplitude and shorter duration (Iaccarino et al., 2016; Prince et al., 2021). The underlying mechanisms of these disturbances of SWRs in AD are yet to be understood. In 5xFAD mice, a reduced excitatory synaptic drive to parvalbumin basket cells has been observed, suggesting a disruption of the coupling between interneurons and pyramidal cells in the HC-EC (Caccavano et al., 2020). In a mouse model of tauopathy, excitatory pyramidal neurons were found to fire more frequently during SWRs while inhibitory interneurons did not (Witton et al., 2016).
Although only few studies have aimed to identify the cause of SWR disruption in AD, its link to memory deficits has been investigated more frequently in recent years. Studies have reported deficits in spatial memory co-occurring with altered SWRs in 5xFAD mice (Caccavano et al., 2020), that the injection of amyloid-β oligomers induces a reduction of SWRs as well as spatial memory deficits in WT mice (Nicole et al., 2016) and that impaired SWRs correlate with long-term, but not short-term, memory deficits in fear conditioning of APP/PS1 mice (Hyunwoo Yang & Yong Jeong, 2021).

Furthermore, optogenetic stimulation extending the duration of spontaneous SWRs has been shown to improve spatial memory performance in WT mice, indicating a causal relationship between the duration of SWRs and their efficiency in memory consolidation (Fernández-Ruiz et al., 2019).

There are, however, reports contradicting this assumption. Inhibiting the generation of SWRs using optogenetic stimulation in WT mice has been reported to not interfere with the formation of spatial memory (Kovács et al., 2016) and APP/PS1 mice have been reported to have intact spatial memory despite their deficit in SWRs (Jura et al., 2019). These findings suggest that the lack of SWRs in AD mouse models could be compensated to some extent, although it remains unclear how. Nevertheless, SWRs seem to play a crucial role in memory consolidation. Previous studies have shown that the SWRs in the HC do not occur independently, but in synchronisation with slow wave activity and sleep spindles in the cortex (Siapas & Wilson, 1998; Staresina et al., 2015). The characteristic of sleep spindles, their functional roles and coupling to SWRs will now be discussed in the following sections.

1.1.2.4 Sleep Spindles

Sleep spindles were one of the first electrophysiological features to be discovered during sleep in humans (Loomis, Harvey, & Hobart, 1935). They are surface manifestations of bursts of synchronised neural activity of 11 – 15 Hz with a duration of 0.5 - 3 s, occurring during NREM sleep in the cortex in mammals (Tamminen, Payne, Stickgold, Wamsley, & Gaskell, 2010). They are believed to arise from activity in the thalamocortical loop, which consist of the thalamic reticular nucleus and thalamocortical neurons (Steriade, 2006). Their generation relies on coordinated, reciprocal interactions between the excitatory neurons in the thalamus and neocortex and inhibitory neurons in the thalamic reticular nucleus (TRN). The TRN appears to serve as a pacemaker, by exhibiting burst-like rhythmic firing patterns, which initiate the cycle of inhibitory and excitatory processes between the thalamus, neocortex and TRN, leading to the generation of sleep spindles (Fernandez & Lüthi, 2020). A schematic of the generation of sleep spindles is depicted in Figure 1.5.

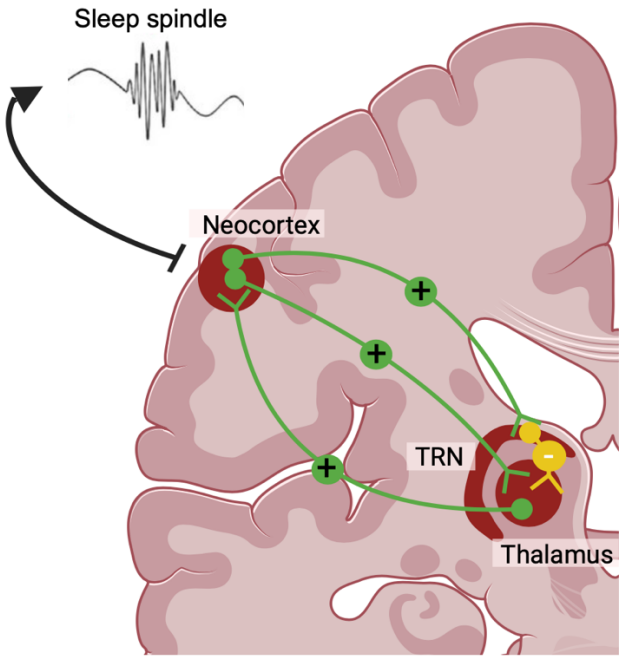

Figure 1.5 Sleep spindle generation. *Excitatory (green) and inhibitory (yellow) connections between the neocortex, thalamus and thalamic reticular nucleus (TRN) contributing to cortical sleep spindles. Illustration created with BioRender.com.*

Sleep spindles possess two functional roles. Firstly, they preserve the state of sleeping. Based on human studies, it has been theorised that sleep spindles inhibit non-threatening sensory input (Claude et al., 2015; Wei, Hunter, & Ross, 2017), as

the activation of TRN neurons inhibits the transmission of signals to the cerebral cortex (Ferrarelli & Tononi, 2011). Evidence for the sleep-stabilising effect of spindles comes from studies in humans, rats and mice, where the stimulation or suppression of sleep spindles lead to longer or shorter duration of NREM sleep, respectively (Aston-Jones & Bloom, 1981; Colonnese et al., 2010; Wimmer et al., 2012).

Secondly, they facilitate memory consolidation.

As described in chapter 1.1.2.2, the HC, and particularly hippocampal SWRs, play a major role in the storage and reactivation of memory traces. Sleep spindles are believed to represent the cortical component of the hippocampal-neocortical communication for long-term memory storage (Sirota, Csicsvari, Buhl, & Buzsáki, 2003). Studies in humans investigating the correlation of learning and sleep spindles have found an increase in the number of sleep spindles during sleep following learning conditions compared to non-learning conditions, and found the increase in sleep spindle number to be positively correlated with better memory performance on the following day (Fogel & Smith, 2006; Gais, Mölle, Helms, & Born, 2002).

It has further been shown that induction of slow wave activity via transcranial magnetic stimulation can increase the number of sleep spindles and enhance memory performance in humans (Marshall, Helgadóttir, Mölle, & Born, 2006). Since slow wave activity and sleep spindles are temporally linked, it is currently not known whether the sleep spindles, the slow oscillations, or the combined effect of both oscillations is the driving force of the cortical component of hippocampal-neocortical communication necessary for memory consolidation during sleep. It is generally assumed that sleep spindles, like SWRs, occur during the up-state of cortical slow waves. However, sleep spindles show an inverse relationship with slow wave activity: their occurrence tends to increase with the duration of sleep, while slow wave activity is highest at the beginning of sleep in humans (Aeschbach & Borbély, 1993). Estimates for how many sleep spindles are temporally coupled to slow waves range between 50 - 70% in humans and mice (Fernandez et al., 2018; Kim, Hwang, Lee, Sung, & Choi, 2015; Mölle, Bergmann, Marshall, & Born, 2011; Nir et al., 2011), indicating that a considerable amount of spindles occur independently from slow waves.

Like SWRs, sleep spindles have previously been investigated in the context of Alzheimer's Disease and since they can be easily recorded via non-invasive EEG, multiple studies come from research in human AD patient. Healthy aging itself has been previously reported to negatively affect the density, amplitude and duration of sleep spindles (Crowley, Trinder, Kim, Carrington, & Colrain, 2002) and changes in sleep spindles are believed to be accelerated in AD. Sleep spindle density was found to be decreased in AD patients compared to age-matched healthy participants (Kam et al., 2019; Latreille et al., 2015). Analysis of individual differences between participants have also shown a correlation between lower spindle density and cognitive performance (Gorgoni et al., 2016; Kam et al., 2019; S. Liu et al., 2020) and a negative correlation between lower spindle density and Aβ42 levels in the cerebrospinal fluid (Kam et al., 2019). The duration of spindles has also been found to be abnormal in AD, with patients exhibiting shorter spindles, which correlated negatively with cognitive performance (Kam et al., 2019; S. Liu et al., 2020). Lastly, the amplitude of sleep spindles has been found to be lower in AD patients (Latreille et al., 2015; S. Liu et al., 2020; Taillard et al., 2019), but this decrease is less pronounced and was found to be a less reliable indicator for identifying individuals with AD or MCI compared to spindle density and duration (S. Liu et al., 2020).

Interestingly, a recent study found that amyloid-positive individuals with no cognitive impairments show lower precision in the coupling of slow waves and sleep spindles compared to healthy, age-matched controls (Pulver et al., 2024), indicating that sleep spindles and/or slow waves start to show abnormalities before the onset of cognitive decline. Another study, using positron emission tomography, found that abnormalities in spindle-slow oscillation coupling could predict future tau accumulation, but not amyloid burden, in the brain (Winer et al., 2019). Tau levels have further been reported to explain up to 45% of variance in sleep spindle duration (Kam et al., 2019), indicating tau pathology to have an impact on sleep spindles in particular.

1.1.2.5 Coupling of sleep spindles and sharp-wave ripples

According to the hypothesis of active systems consolidation, time-locked rhythms in the thalamus, hippocampus and cortex create a time window of favourable neuronal circumstances for the consolidation of memory traces during sleep. As described in the previous sections, hippocampal SWRs are believed to initiate the replay of memory traces. When coupled to cortical sleep spindles and slow oscillations, memory consolidation is believed to be facilitated. Studies in support of this have reported an increase in coupling of SWRs and spindles in post-learning sleep in humans, mice and rats (Maingret, Girardeau, Todorova, Goutierre, & Zugaro, 2016; Mölle, Eschenko, Gais, Sara, & Born, 2009; Steadman et al., 2020). Further, artificially increasing the number of SWR-coupled spindles through closed-loop feedback stimulation of the prefrontal cortex has shown to improve memory performance (Maingret et al., 2016).

During NREM sleep, hippocampal discharge is temporally coupled to the occurrence of individual sleep spindles (Sirota et al., 2003). This time locking implies a pathway through which circuits involved in sleep spindle generation also recruit hippocampal units. Support for this idea comes from studies reporting sinks during SWRs in the hippocampus related to spindles (Staresina et al., 2015; Sullivan, Mizuseki, Sorgi, & Buzsáki, 2014) but the exact mechanism is yet to be fully understood.

A recent study investigating the temporal coupling of SWRs and sleep spindles in an amyloid over-expressing AD mouse model, has found reduced numbers of SWRs occurring together with sleep spindles (Zhou et al., 2022), indicating that the presence of Aβ disrupts the coordination of sleep spindles and SWRs.

1.1.3 The cholinergic system

Acetylcholine is an effective modulator synthesised from acetyl coenzyme A and choline through the enzyme choline acetyltransferase (Stedman & Stedman, 1937). ACh production and signalling is carefully regulated through components such as acetylcholinesterase, an enzyme degrading ACh by hydrolysation it (Davis et al., 1992). The two major cholinergic receptors are muscarinic and nicotinic ACh receptors, named according to their responsiveness to the agonist nicotine and muscarine. Nicotinic ACh receptors are ligand-gated ion channels, which produce a fast response by opening. They are found in the central nervous system, where they play a role in learning and reward, and at the neuromuscular junction. Muscarinic ACh receptors, in contrast, are G-protein-coupled receptors, which trigger slower and long-lasting intracellular signalling pathways. They are abundant in the central nervous system, where they are involved in regulating memory, attention and arousal, and in the peripheral nervous system, where they mediate the innervation of visceral organs (Carlson & Kraus, 2024).

An intact cholinergic system is crucial for the regulation of neurogenesis, neuroprotection and synaptic plasticity (Frinchi, Scaduto, Cappello, Belluardo, & Mudò, 2018).
The brain comprises a complex cholinergic system playing a crucial role in the regulation of various cognitive and physiological processes. In the brainstem, the pedunculopontine nucleus and laterodorsal tegmental nucleus are involved in the regulation of arousal, wakefulness and REM sleep. The reticular activating system (RAS) is part of the brain stem and involved in the regulation of the overall excitability and EEG patterns. It promotes wakefulness and attention through modulation of thalamic and cortical activity. In the basal forebrain, the nucleus basalis of Meynert projects to the neocortex and regulates attention and learning, while projections from the medial septum reach to the HC, regulating memory formation and spatial navigation. A simplified illustration of the cholinergic system and the main regions involved is depicted in Figure 1.6.
In the following sections, the cholinergic system will be discussed in the context of the sleep-wake cycle, memory and cognition and the pathology of Alzheimer's Disease.

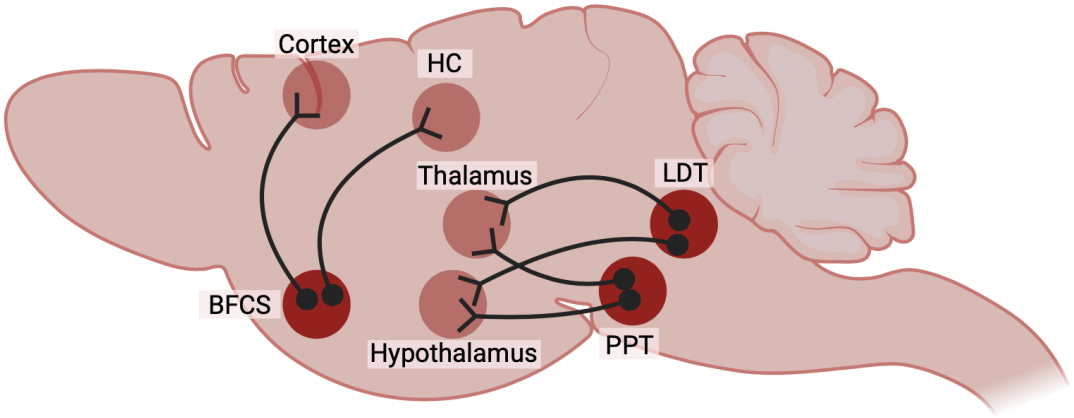

Figure 1.6 Schematic of the cholinergic system. *Cholinergic projections from the basal forebrain cholinergic system (BFCS) to the cortex and hippocampus (HC), from the laterodorsal tegmentum (LDT) and pedunculopontine nucleus (PPT) in the brain stem to the thalamus and hypothalamus. Illustration created with BioRender.com.*

1.1.3.1 Role of the cholinergic system in sleep-wake regulation

Acetylcholine shows characteristic changes across the sleep-wake cycle where cholinergic activity is highest during wakefulness and REM sleep and lowest during NREM sleep. Since high cholinergic activity had been believed to be associated with high arousal early on, the significant difference in cholinergic activity between NREM and REM sleep, which are both states of low arousal, intrigued scientist. Many studies investigating acetylcholine across the sleep-wake cycle therefore focused on the role of cholinergic signalling during REM sleep. Early studies in cats indicated cholinergic signalling to play an important role in the generation of REM sleep (Jouvet, 1972; Szymusiak & McGinty, 1986). Studies investigating the underlying mechanisms, identified the cholinergic signalling in the brain stem as the key component for the generation of REM sleep (Baghdoyan, Rodrigo-Angulo, McCarley, & Hobson, 1984; Shouse & Siegel, 1992; Webster & Jones, 1988). Since then, research has revealed more details of the involvement of the cholinergic system in driving brain oscillations across the sleep-wake cycle. The cholinergic system enhances the responsiveness of neurons with cholinergic activity from the nucleus basalis projecting to the neocortex, from the septum to the HC, and from the RAS to the thalamus. The cholinergic pathways stemming from the RAS are highly active during wakefulness and REM sleep and its projections extend throughout the reticular formation reaching the substantia nigra, basal forebrain, thalamus and cerebellum. Stimulation of the RAS promotes gamma oscillations, supresses slow

and delta oscillations, thereby causing cortical desynchronisation characteristic for wakefulness and REM sleep. When cholinergic activity is absent, slow oscillations occur, characteristic for NREM sleep (Platt & Riedel, 2011). The importance of the cholinergic system in sleep-wake regulation has further been highlighted by causal links between cholinergic abnormalities and sleep disorders. An extreme form of sleep disorder is narcolepsy, where individuals experience frequent, sudden periods of involuntary sleep. Here, down-regulation of the RAS output is believed to play a causal role and lesions in the RAS following traumatic injury have been reported to induce sudden sleep (Jang, Seo, & Kwon, 2016). In AD patients, abnormalities in REM sleep in particular have been proposed to be caused by dysfunction of the cholinergic signalling of the brainstem and basal forebrain cholinergic system (BFCS) (Montplaisir, Petit, Gauthier, Gaudreau, & Décary, 1998). As previously described in chapter 1.1.1.7, cholinesterase inhibitors are among the current treatment options for AD. Although there are some discrepancies, studies investigating the effect of these drugs on sleep dysfunctions indicate a REM sleep promoting effect (Markowitz, Gutterman, Lilienfeld, & Papadopoulos, 2003; Moraes Wdos et al., 2006). Donezepil, for example, has been found to increase the percentage of time spent in REM sleep, a shorter latency to REM and higher REM density in AD patients (Kanbayashi et al., 2002). Other studies have found a positive effect of donezepil on NREM sleep in AD patients with obstructive sleep apnea. Here, light sleep (stage 2) and overall sleep time was increased (Cooke et al., 2006; Moraes, Poyares, Sukys-Claudino, Guilleminault, & Tufik, 2008). Since normal cholinergic activity varies across the sleep-wake cycle, the timing of administration of cholinesterase inhibitors is crucial. Administration of the drug in the early hours of the morning should allow the natural decrease of ACh necessary for NREM sleep to occur (Nieoullon, Bentué-Ferrer, Bordet, Tsolaki, & Förstl, 2008). This decrease in ACh during NREM sleep is particularly important for memory consolidation, which I will now discuss in the following chapter in the context of learning and memory mechanisms across the sleep-wake cycle.

1.1.3.2 Role in learning and memory

ACh has been proposed to play a role in memory and cognition almost 40 years ago (Davies, 1985) as studies in humans and animals have reported memory impairments caused by anticholinergic treatments (Deutsch, 1971; Drachman & Leavitt, 1974) and loss of cholinergic cells in the basal forebrain (BF) has been identified as a consistent feature of the pathology of AD (Schliebs & Arendt, 2006). The BFCS has therefore been particularly under investigation in the research of sleep, memory, cognition and Alzheimer's Disease. It projects from the basal forebrain, a deep structure consisting of multiple small nuclei, to the PFC, HC, EC and amygdala. More specifically, the PFC and amygdala receive inputs from the nucleus basalis of Meynert and substantia innominate, while the HC and EC receive input from the medial septum and vertical diagonal band nuclei (Frotscher & Léránth, 1985; Gaykema, Luiten, Nyakas, & Traber, 1990; Kondo & Zaborszky, 2016; Mesulam, Mufson, Levey, & Wainer, 1983; Woolf, 1991). In return, the PFC, HC, EC and amygdala send reciprocal signals to the BFCS for modulation (Krettek & Price, 1978; Mesulam & Mufson, 1984; Russchen, Amaral, & Price, 1985). To achieve precise spatial and temporal signalling, the projections of the BSCF are spatially-specifically mapped comprising multiple signalling modes (Obermayer, Verhoog, Luchicchi, & Mansvelder, 2017; Parikh, Kozak, Martinez, & Sarter, 2007) allowing either phasic or tonic transmission of acetylcholine (Sarter & Lustig, 2020). The early findings of the BFCS being compromised in AD have led to the development of the cholinergic hypothesis of geriatric memory dysfunction. This theory posits that impaired cholinergic transmission contributes to a big extent to cognitive decline in elderly people and especially AD patients (Bartus, Dean, Beer, & Lippa, 1982). Since then, our understanding of ACh and its involvement in memory and cognition has improved considerably. Research in this area has particularly investigated ACh in the HC. Studies investigating extracellular ACh levels in the HC of freely behaving animals have reported an increase in hippocampal ACh during HC-dependent learning tasks. The duration and magnitude of this increase has been found to differ between tasks and is believed to reflect the degree to which the HC is engaged in the learning activity (Calandreau et al., 2006; Chang & Gold, 2003; McIntyre, Marriott, & Gold, 2003; Nail-Boucherie, Dourmap, Jaffard, & Costentin, 2000; Ragozzino, Pal, Unick, Stefani, & Gold, 1998). Depleting cholinergic transmission to the HC has been found to prevent the creation of place

representations of novel environments, while firing patterns of place cells in familiar environments did not seem to be affected (Ikonen, McMahan, Gallagher, Eichenbaum, & Tanila, 2002), indicating a role of hippocampal ACh in the encoding of new information, but not the reactivation of previous memories. Building up on these findings, the biphasic cholinergic activation hypothesis was developed. This hypothesis assumes two distinct roles of hippocampal cholinergic activity: an initial phase of activation followed by a phase of inhibition. The activation phase is characterised by an increase in ACh signalling in the HC, facilitating on-line processing of novel information, as observed during learning tasks. The inhibition phase is believed to occur after learning, characterised by a decrease in cholinergic activity, aiding the consolidation of new memories. Evidence for this theory stems from studies reporting an increase in ACh in the HC during a learning task followed by a decrease where the amplitude of both increase and decrease correlated with learning rate (Marighetto, Micheau, & Jaffard, 1993, 1994). Furthermore, it has been found that cholinergic activity enhances the flow of new information from the cortex to the HC through the EC and dentate gyrus. Here, cholinergic activity selectively suppressed the synaptic transmission within the CA1 and CA3. It is believed that by reducing the excitatory signals in the CA1 and CA3, ACh minimises interference from previously stored memories, therefore allowing the prioritisation of the encoding of new information (Hasselmo & Schnell, 1994; Hasselmo, Schnell, & Barkai, 1995; Klink & Alonso, 1997). When levels of ACh in the HC decrease, the inhibition of excitatory feedback within the CA1 and CA3 decreases, thereby promoting hippocampal output to the EC and consolidation of memory (Girardeau et al., 2009; Hasselmo & McGaughy, 2004).

1.1.3.3 Association with brain oscillations

Since the cholinergic pathways reach a wide variety of areas throughout the brain, it is not surprising that cholinergic signalling has a direct impact on a range of brain oscillations, including those involved in learning and memory. In the previous chapters, the impact of cholinergic systems on oscillations has been mentioned to some extent. I will now summarise and build up on the findings previously discussed, highlighting oscillation patterns enhanced by or disrupted by cholinergic activity.

1.1.3.3.1 Oscillations enhanced by cholinergic activity

Theta rhythm, which is important for memory formation and particularly strong during REM sleep, has been reported to be directly influenced by cholinergic activity. More specifically, cholinergic agonists, have been found to induce theta oscillations in the HC (Huerta & Lisman, 1993; Konopacki, MacIver, Bland, & Roth, 1987) while cholinergic antagonists disrupt the generation and tuning of theta oscillations (Asaka, Seager, Griffin, & Berry, 2000; Monmaur, Collet, Puma, Frankel-Kohn, & Sharif, 1997; Teitelbaum, Lee, & Johannessen, 1975). Interestingly, it is slow theta that is affected by the disruption of cholinergic activity, but not fast theta (Kramis, Vanderwolf, & Bland, 1975), indicating specific frequencies to be more ACh-sensitive.

Gamma oscillations are also associated with higher cognitive functions such as attention, working memory and perception. Administration of cholinergic agonists have been reported to induce gamma oscillations (Fisahn, Pike, Buhl, & Paulsen, 1998; Pálhalmi, Paulsen, Freund, & Hájos, 2004). Administration of the acetylcholinesterase inhibitor donepezil has been reported to cause the same effect (Spencer, Middleton, & Davies, 2010). A further study investigating the impact of ACh on gamma oscillations revealed that ACh regulates the power of gamma, but not its frequency. This effect was found to be dose-dependent (Betterton, Broad, Tsaneva-Atanasova, & Mellor, 2017).

Gamma oscillations are commonly fixed to the phase of theta (Lisman & Jensen, 2013). The coupling of theta and gamma has also been found to be dependent on cholinergic activity. More specifically, spatially constrained cholinergic stimulation

has been reported to induce gamma oscillations modulated by theta where ACh modulates the excitability of neuronal networks (Yang et al., 2021).

1.1.3.3.2 Oscillations supressed by cholinergic activity

Among the oscillations that are likely to be supressed by cholinergic activity are the oscillations patterns associated with NREM sleep: slow oscillations, delta oscillations, SWRs and sleep spindles. They have been found to occur when ACh levels are low (Kametani & Kawamura, 1990; Marrosu et al., 1995). The drop in cholinergic signalling is believed to lift the cholinergic suppression of glutamatergic synapses, resulting in the excitatory feedback necessary for these NREM sleep-related oscillation patterns (Buzsáki, 1986, 1989). While observations of the effect of ACh on slow oscillations, delta and sleep spindles are mostly correlative, the impact on ACh on SWRs has been studied in more detail. Here, multiple studies have shown that cholinergic activity in the HC reaches a minimum during SWRs and that stimulation of cholinergic neurons suppresses the occurrence of SWRs (Vandecasteele et al., 2014; Y. Zhang, L. Cao, et al., 2021). In the context of AD, these findings are particularly interesting, since disruptions in the cholinergic signalling are well documented and observed along with memory impairments.

1.1.4 Techniques for investigation of brain activity

Methods for measuring brain activity have been developed to measure different aspects of brain activity. They can be invasive or non-invasive, measure activity on cellular or population level, and be based on electrophysical or imaging approaches. In the next chapters I will discuss some of the most frequently used methods and their benefits and limitation in research.

1.1.4.1 Non-invasive techniques

Non-invasive methods are used for research and diagnosis of neural disorders and brain damage in humans. Magnetic resonance imaging (MRI), positron emission tomography (PET) and electroencephalography (EEG) are popular non-invasive techniques in the biomedical field. While they allow rapid and precise monitoring of brain activity, their spatial resolution is weaker compared to invasive methods.

1.1.4.1.1 Magnetic resonance imaging

MRI utilises magnetic fields to align hydrogen atom nuclei in the brain and scans signals of the nuclei returning to their original state. These signals can then be converted into an image. Based on this principle, functional MRI (fMRI) measures brain activity indirectly, by detecting changes in blood flow coinciding with neural activity: when neuronal firing is increased, the demand for energy in the form of adenosine triphosphate (ATP) increases. ATP is produced through glycolytic oxygenation of glucose by the mitochondria. To deliver the additional oxygen required, blood flow increases locally and delivers oxygen in the form of oxygenated haemoglobin. These local changes in the oxygenation of haemoglobin can be detected by fMRI, as deoxyhemoglobin is paramagnetic, causing magnetic field distortions influencing the fMRI signal (Glover, 2011; Ogawa, Lee, Kay, & Tank, 1990). fMRI has a good spatial resolution, although it does not allow to investigate activity of individual cells. Temporal resolution of this technique is not great, with a delay of 5-6 seconds between the stimulus onset and the peak of the detected signal. Therefore, fast changes in neural firing cannot be detected (Glover, 2011).

1.1.4.1.2 Positron emission tomography

PET is a nuclear medicine technique used to investigate physiological processes. Here, radioactive substances are administrated as a tracer. These radiotracers can be designed to target a wide range of metabolic and physiological processes in the brain, depending on the research question. Once administrated, radiotracers emit positrons as they undergo radioactive decay. When these positrons collide with electrons, photons are generated forming gamma rays. These rays can be detected by a scanner. Specific radiotracers can be used in PET to visualise changes in cerebral blood flow, glucose metabolism and the activity of neurotransmitters. Fluorodeoxyglucose (FDG) is a tracer commonly used for PET in brain research. FDG is taken up by cells in proportion to their current demand of glucose, thereby reflecting their firing activity. An increase in glucose metabolism can be observed as an increase in the gamma ray signal detected (Heurling et al., 2017). While PET allows a wider variety of applications by choosing different tracers, its spatial resolution is lower compared to fMRI. Furthermore, PET relies on indirect measurement of brain activity, with slow kinetics of the uptake of the tracer and image acquisition ranging from 30 s to several minutes (Phelps & Mazziotta, 1985), greatly limiting its applications. It is, however, a good tool for the diagnosis of AD patients. FDG-PET can distinguish between healthy brains and AD brains. As loss of neuropil and synapses and neuronal functional impairments are reflected by hypo-metabolism, this can be detected in AD patients (Ou et al., 2019; Shivamurthy, Tahari, Marcus, & Subramaniam, 2015). Other tracers that directly bind to Aβ fibrils or tau can be used in PET to determine the amyloid or tau status of patients or to evaluate the efficacy of treatments (Jack et al., 2018; Lagarde et al., 2019; Okamura et al., 2018; Rowe et al., 2008).

Although fMRI and PET can be useful method for investigating large changes in brain activity, diagnosis and treatment efficacy evaluation, their poor temporal resolution does not allow the observation of fast changes in neuronal activity. Furthermore, both techniques are expensive to conduct. These limitations can be overcome by replacing or pairing it with other methods such as EEG.

1.1.4.1.3 Electroencephalogram

EEG is an inexpensive tool for recording brain activity. Unlike PET and fMRI, which measure brain activity indirectly, EEG measure the activity of neurons directly by recording electric current changes on the scalp stemming from the summation of excitatory and inhibitory post-synaptic potentials in cortical neurons (Matsumoto & Marsan, 1964). With an average size of 10 mm in diameter, a single EEG electrode records electric signals from a pool of approximately 250,000 neurons (Feyissa & Tatum, 2019). Synchronised activity of such a pool of neurons is referred to as local field potential (LFP). EEG has a poor spatial resolution and the signal strength weakens as it passes through the meninges, skull and skin, but it does have a good temporal resolution and allows for the detection of fast events. EEG can be used as a diagnostic tool for AD, as it can detect the absence of alpha rhythms in posterior brain regions, associated with AD (Brenner et al., 1988; Gordon & Sim, 1967), along with overall decrease in alpha (8-15 Hz) and beta (16-31 Hz) power with simultaneous increase in delta (0.5-4 Hz) and theta (4-8 Hz) power (Bennys, Rondouin, Vergnes, & Touchon, 2001; Malek, Baker, Mann, & Greene, 2017). Analysis of theta power in particular has been shown to distinguish AD patients from healthy controls with an accuracy of 86%, which is comparable to the accuracy achieved by PET scans assessing glucose metabolism (Szelies et al., 1992; Szelies, Mielke, Herholz, & Heiss, 1994). Application of EEG is less restrictive compared to fMRI and PET scans, as the method is not only less expensive but allows the recording of brain activity over longer periods as it allows patients to move more freely. This is particularly useful in the context of sleep research. Participants can wear EEGs throughout the night and provide valuable insight into brain activity during sleep stages. With sleep playing an important role in AD, EGG sleep studies are therefore a powerful tool to identify new biomarkers of the disease. However, since EEG recordings only allow the investigation of superficial layers of the brain, more invasive methods are needed to investigate deeper regions.

1.1.4.2 Invasive techniques

Invasive techniques allow the investigation of a wide variety of brain activities at population and cellular level. Their application, however, is mostly restricted to animal research and, in some cases, to epilepsy patients undergoing surgery. Invasive techniques can be classified in two categories: electrophysiological and optical approaches.

1.1.4.2.1 Electrophysiological approaches

Electrophysiological approaches aim to record the electric current generated by neuronal activity. The most commonly used techniques here are intracranial EEG, patch-clamp and extracellular electrophysiological recordings using electrodes.

1.1.4.2.1.1 Electrocorticography

Electrocorticography is a type of intracranial EEG, measuring neural activity at the surface of the brain, unlike non-invasive EEG where recordings are taken at the scalp. This technique provides stronger signals, better spatial resolution and fewer artefacts (Hill et al., 2012). It can, however, still only record superficial layers of the brain. For access deeper regions, electrocorticography can be combined with other recording methods. Like non-invasive EEG, electrocorticography measures the summation of excitatory and inhibitory post-synaptic potentials in cortical neurons and does not allow for recordings of activity at single cell level.

1.1.4.2.1.2 Whole-cell recording

To record activity of single cells, whole-cell recordings can be conducted using the patch-clamp technique. In this method, micropipettes are used to puncture individual neurons. Suction is applied to rupture the membrane of the neuron to establish an electrical connection between the pipette and intracellular compartment of the neuron. This connection has a low resistance and allows the detection of electric signals, generated by the flow of ion currents within the cell (Furue, Katafuchi, & Yoshimura, 2007; Jordan, 2021). Such single cell recordings can be done in both

brain slices and in vivo. For in vivo recordings, head-fixed conditions are common to minimise movement of the animal. The technique allows the direct measurement of neural spiking activity and membrane potential dynamics. This allows the investigation of functioning of individual neurons, neural circuits and synaptic communication. However, since cells have to be recorded one at a time, each recording session provides data of a small number of individual cells (Furue et al., 2007). The technique is difficult to master, as one can easily hit blood vessels or glia cells instead of neurons. Recording sites are limited to superficial layers of the brain, with most recordings being conducted around 500 µm. Some recordings have been reported to be conducted up to 1000 µm deep (Tao, Zhang, Xiong, & Zhou, 2015).

1.1.4.2.1.3 Extracellular electrophysiological recordings

To assess brain activity in brain regions deeper than transcranial EEG and patch-clamp allow, electrodes are frequently used. Such electrodes come in various shapes and sizes. The simplest form of electrodes are wire electrodes, often composed of tungsten. They are a simple and cost-efficient way to monitor extracellular voltage fluctuations in the surrounding of the electrode tip. While wire electrodes are often used in the form of bipolar electrodes, consisting of two wires, they have been developed to contain as many as 48 microwires, allowing to record from multiple regions simultaneously (Nicolelis, Ghazanfar, Faggin, Votaw, & Oliveira, 1997). One mayor limitation of wire electrode is that they can only record activity at one depth as a time, at the tip of the wire.

To achieve depth-resolved recordings, silicon probes can be used. These probes comprise multiple microarrays along the shank allowing the recording of activity at different depths. Depending on the desired spatial resolution, such silicon probes can consist of more than 32 channels and come in the form of single-shank probes or multi-shank probes (Buzsáki, 2004; Csicsvari et al., 2003).

Recently, new microarrays have been developed. They are called Neuropixels and come in a range of configurations. Neuropixels 1.0, comprised of a single shank with 394 recording channels, was first introduced (Jun et al., 2017), followed by Neuropixels 2.0, containing 4 shanks with over 5000 channels (Steinmetz et al., 2021). These probes allow high-resolution recordings of neural activity across multiple sites, allowing detailed investigation of brain functions and circuits.

Some drawbacks of electrodes and silicon probes are artefacts and tissue damage and although these methods allow for recording of multiunit activity, specific cell types can only be targeted when combined with optotagging techniques. To observe activity from specific cell types, a range of optical approaches can be used.

1.1.4.2.2 Optical approaches

The two most common optical approaches are two-photon imaging and fibre photometry. These optic approaches have gained popularity over the past decades.

1.1.4.2.2.1 Two-photon imaging

Invented in 1990, two-photon excited fluorescence laser scanning microscopy proposes an optical method for studying the morphology and function of brain cells (Denk, 1994; Denk, Strickler, & Webb, 1990). In this method, laser beams are focused through microscope objectives to excite fluorescent molecules and fluorescent light resulting from the excitation is collected. By moving the laser beam within the tissue, a 2D or 3D image is created (Helmchen, 2009). Cell-type specific recordings can be conducted by choosing different genetically encoded fluorescent proteins which are expressed under cell-type specific promotors. The development of calcium indicators, such as GCaMP (Nakai, Ohkura, & Imoto, 2001), genetically encoded voltage indicators and indicators for neurotransmitter or enzymatic activity allows a wide range of brain activities to be monitored with two-photon imaging. The imaging depth is usually restricted to $\sim$ 500 μm (Cheng et al., 2020), making this method unsuitable for the investigation of deeper brain regions. Novel two-photon microscopes, however, have been developed to increase the scanning range along the z-axis, allowing imaging of deeper regions and 3D functional imaging of over 1000 cells simultaneously (Zong et al., 2022). Novel techniques are also emerging to increase the imaging speed to achieve a higher temporal resolution (Wu, Ji, & Tsia, 2021). While this technique provides excellent spatial resolution, its field of view is restricted. Furthermore, the setups necessary for this technique are complex and expensive.

1.1.4.2.2.2 Fibre photometry

Another optical method is fibre photometry. Here, genetically encoded proteins are also used, but instead of utilising a microscope to direct the excitation light and collect resulting fluorescent light emission, an implantable fibre is used (Figure 1.7). These fibres come in the form of flat fibres or tapered fibres. Flat fibres are commonly used with a 200 - 400 μm diameter and deliver and collect light at a single depth, while tapered fibres have a narrow tip of several nm and allow depth-resolved measurements by manipulation of the angle of light entering the fibre (Pisanello et al., 2017). Regardless of the fibre chosen, non-specific signals need to be accounted for. Such non-specific signals stem from movement artifacts (MA) and autofluorescence (AF). MAs are artificial changes in the fluorescent signal, caused by movements of the fibre. This can occur due to movement of the animal, loose connection, external disturbance or tension of the optic cable. To account for MAs, isosbestic illumination can be applied. This additional illumination is of a wavelength outside the range the sensor is sensitive to. This illumination provides a control, as it should be unaffected by the indicators binding state and any change in signal reflects MAs. By rapidly alternating between the isosbestic and sensor-sensitive illumination, an isosbestic control signal and a sensor-specific signal is acquired (Figure 1.7, right). Using the isosbestic signal, movement artifacts can then be subtracted from the sensor-specific signal (Byron & Sakata, 2023; C. K. Kim et al., 2016; Patel, McAlinden, Mathieson, & Sakata, 2020).

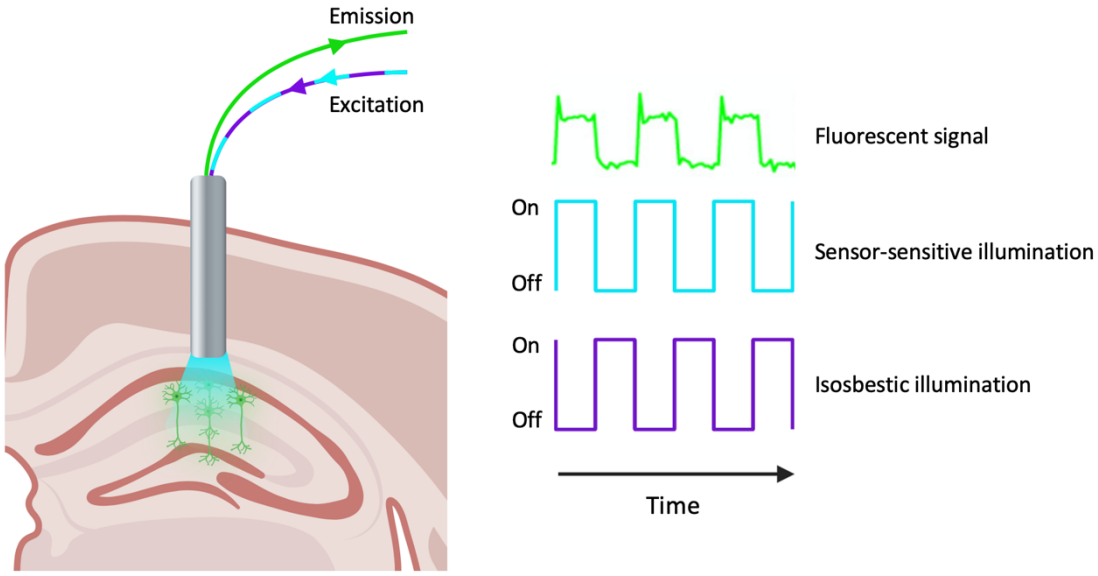

Figure 1.7 Schematic of fibre photometry. *Left: Principle of fibre photometry. Excitation light passes through the optic fibre to illuminate sensor-expressing cells. Emission is collected through the same fibre. Right: sensor-sensitive (blue) and isosbestic (purple) illumination pattern and resulting fluorescent signal (green). Partially adapted from Patel et al., 2020. Illustrations created with BioRender.com.*

AF has to be accounted for as well. The recording system itself is a source of AF, particularly the patch cable and fibre itself (Bianco et al., 2021; Byron & Sakata, 2023). This is caused by internal reflection due to differing refractive indices of the fibre glass and polymer. At each of these reflection point, part of the light energy is emitted into the cladding of the patch cable. This energy can be converted into fluorescence by an unknown component. The resulting AF can vary in intensity and shows changes over time. By turning the light source on prior to experimental procedures, the system can be photobleached to reduce the AF (Byron & Sakata, 2023; Simpson et al., 2024).

Fibre photometry has a lower spatial resolution compared to two-photon imaging, as it records activity from multiple cells simultaneously. However, fibre photometry setups are more affordable and therefore an excellent option for research question that do not require data at cellular or subcellular level. Lastly, fibre photometry has a high temporal resolution, allowing the observation of fast dynamic changes, although the temporal resolution is ultimately limited by the temporal dynamic performance of the sensor used.

1.1.4.2.2.3 Optical indicators

When using fibre optical approaches, it is important to choose an appropriate indicator based on the research question. Indicators vary in terms of selectivity, sensitivity and the cells they are can be expressed in. What all indicators have in common is that they consist of two components. The first component is the sensing domain, which a ligand binds to and which undergoes a conformational change in response to the binding. Instead of binding of a ligand, such a conformational change is caused by changes in membrane potential in some indicators. The second component is the fluorescent reporter domain, in which the conformational change is converted into a fluorescent signal which can be detected by fibre photometry. While the type of sensing domain determines the specificity, affinity and kinetics of the indicator, the type of reporter domain determines the intensity and wavelength of the output signal (Simpson et al., 2024). To further illustrate the function and characteristics of indicators, the recently reported AchLightG sensor will now be described in detail (Figure 1.8).

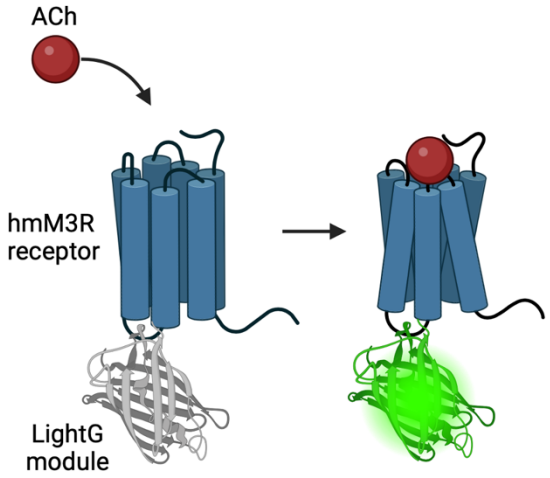

Figure 1.8 Schematic of AchLightG. *Binding of ACh causes a confirmational change in the hmM3R receptor, thereby activating the LightG module which produces fluorescence. Illustrations created with BioRender.com.*

The sensing domain of AchLightG is the human muscarinic M3 receptor (hmM3R) single graft which is a G protein-coupled receptor activated by the neurotransmitter acetylcholine. The binding of acetylcholine induces a conformational change in the receptor, involving shifts in the position of transmembrane helices and associated domains of the receptor. This conformational change is transmitted to the attached fluorescent reporter module. The reporter domain of this sensor is the so-called

LightG module. This module responds to the conformational change by altering its fluorescent properties (Kagiampaki et al., 2023) (Figure 1.8). This change in fluorescence is detected by fibre photometry. AchLightG has a half-maximal effective concentration (EC_{50}) of 203 nM. Compared to previous acetylcholine sensors e.g. ACh2.0 and ACh3.0 which have a EC_{50} of approximately 2 μM (Jing et al., 2020), AchLightG shows better sensitivity for acetylcholine, making it well suited for the detection of low levels of ACh (Kagiampaki et al., 2023).

1.2 Hypothesis and aims

Alzheimer's disease is a highly complex, progressive disease. Conventional biomarkers such as Aβ are currently assessed for diagnosis using expensive and invasive methods. Among the emerging alternative biomarkers are brain waves in the form of EEG measurements. We hypothesise that brain oscillations can be a biomarker for AD. More specifically, we hypothesise that abnormalities in oscillation patterns during sleep can give valuable insights into the pathology of AD. We therefore wanted to identify abnormalities in sleep oscillations believed to be important for memory consolidation in particular. Two promising candidates – SWRs and sleep spindles – were chosen as oscillations of interest. We hypothesised that SWRs and sleep spindles are abnormal in AD. We further hypothesised that abnormalities in SWRs are due to abnormalities in the cholinergic signalling in the HC. To further broaden our understanding of SWRs and sleep spindles, we wanted to characterise them in the context of novelty and learning.

In summary, the aims of this project were the following:

1. Investigate abnormalities in sleep architecture in the context of novelty and learning in 5xFAD mice.
2. Investigate abnormalities in SWRs in the context of novelty and learning in 5xFAD mice.
3. Investigate abnormalities in sleep spindles in the context of novelty and learning in 5xFAD mice.
4. Investigate abnormalities in cholinergic activity in the HC as an underlying mechanism for abnormalities in SWRs in 5xFAD mice.

5xFAD mice, a well-established mouse model which rapidly develops Aβ plaques, was chosen for this project. In vivo electrophysiological recordings in freely behaving condition were performed using intercranial EEG and LFP recordings via bipolar electrodes, which provide an inexpensive, reliable method for the recording of brain activity. Fibre photometry was chosen for the recording of cholinergic activity, as this method can be easily combined with electrophysiological recordings. Here, we utilised a novel sensor (AchLightG) with excellent sensitivity and kinetic properties.

2 Methods

2.1 Animals

Female and male 5xFAD+ (FAD+) and 5xFAD- (WT) mice on a C57BL/6J genetic background (JAX006554, The Jackson Laboratory) (Oakley et al., 2006; Oblak et al., 2021) were housed in a 12 h light/dark cycle in pairs of litter mates. Genotypes were ensured by real-time polymerase chain reaction (conducted by Transnetyx), using a tissue sample obtained during ear-tagging.

For electrophysiological recordings, 12 mice were used between the ages of 3.5 and 7.5 months. For fibre photometry recordings, 16 mice were used between the ages of 4.5 and 9 months. A comprehensive overview of all mice used in this study, including animals for training, optimisation and hypothesis development, is shown in Figure 2.1. Although the genotype of the mice was known during the experiments, all data analysis was performed in MATLAB using the same codes for the data of all mice, ensuring unbiased analysis of the data.

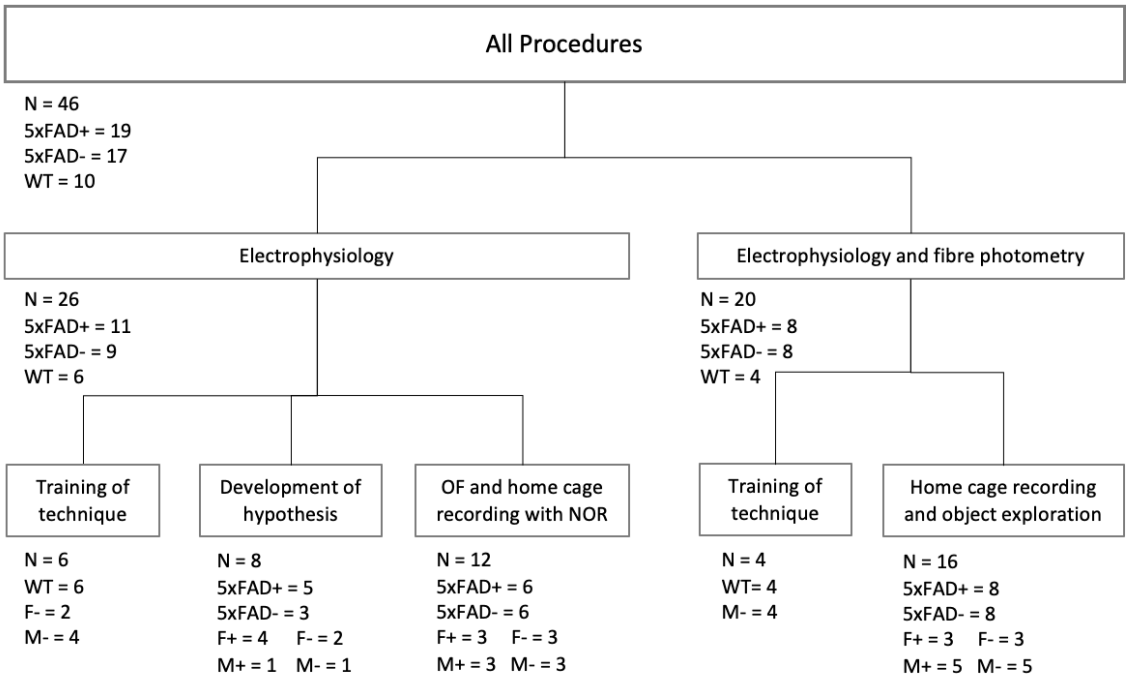

Figure 2.1 Flow chart of all animals used for experiments. *Number of animals used for each experiment are shown along with numbers of genotypes and sex.*

All animal experiments and procedures were performed in accordance with the United Kingdom Animals (Scientific Procedures) Act of 1986 Home Office regulations and approved by the Home Office (PP0688944) and the University of Strathclyde's Ethical Committee.

2.2 In vivo electrophysiology

2.2.1 Fabrication of implants

2.2.1.1 EEG and EMG connectors

Three 2-row connectors (SDL-112-T-12, Semtec) were used to make a connector. Two copper wires (1,5 cm, ⌀ 0.2 mm, 357-918, RS PRO) for cortical EEG, two copper wires for grounding (1,5 cm & 1 cm, ⌀ 0.2 mm, RS PRO), where one ground was used and one was prepared as a back-up in case of a faulty connection, and two 32 (7/40) AWG SPC wires for EMG (1,5 cm, 2840/7, ALPHA WIRE) were stripped of their insulation at either end (0.3 cm) and soldered to one connector pin each (Figure 2.2 C). Connections were covered with dental cement for protection and stability (Simplex rapid liquid and power, Kemdent).

2.2.1.2 Bipolar electrode fabrication

Two stainless steel wires (AISI 302, 0.1mm diameter, FE205850/2, GoodFellow) were cut to 1.5 cm. Wires were stripped of their insulation on one end each (0.3 cm). The bare end of each wire was wrapped around one pin of two 1-row connectors (SS-132-T-2-N, Semtec) and covered with silver conductive paint (186-3593, RS PRO). The connection was secured with dental cement (Simplex rapid liquid and power, Kemdent). The wires were twisted together, straightened and a small amount of super glue (918-6872, RS PRO) was applied along the twisted wire bundle, leaving the tips free. One wire tip was trimmed to create a 0.1 cm offset between the two tips (Figure 2.2 A-B). Impedance was measured prior to insertion and electrodes with an impedance between 20 – 200 kOhm were used for insertion.

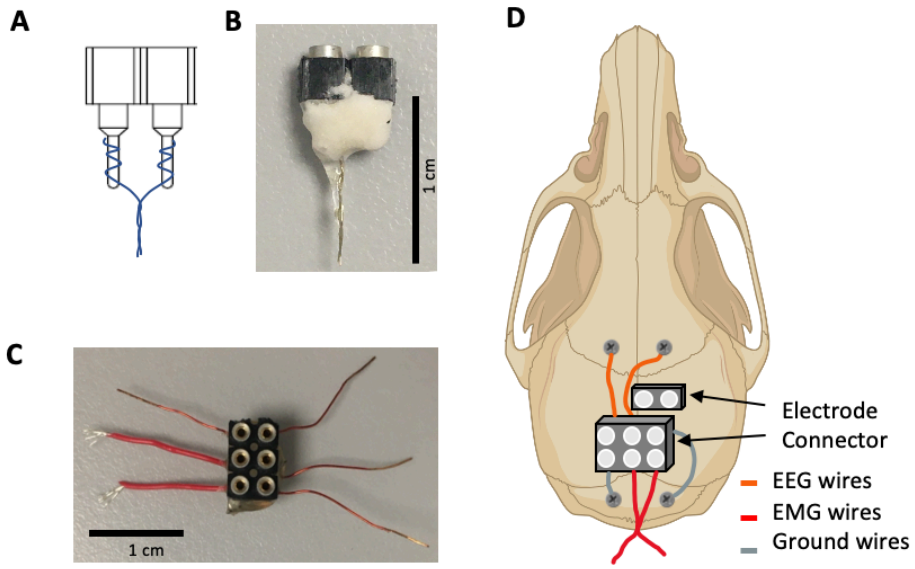

***Figure 2.2 Schematic of surgical implants**. **A)** Design of bipolar electrodes for electrophysiological recordings. **B)** Image of bipolar electrode. **C)** Image of connector for electrophysiological recordings. **D)** Schematic of the position of bipolar electrode, connector, skull screws and wires on the skull. Illustrations partially created with BiroRender.com.*

2.2.2 Implantation surgery

Mice were anesthetised with 1-1.5% isoflurane (3-5% for induction) delivered with 0.8 L/min air flow and placed on a stereotaxic frame (SR-5M-HT, Narishige) with an incisor bar and ear bars, where their body temperature was maintained at 37 °C using a feedback temperature controller (50-7221-F, Harvard Bioscience). Breathing was monitored throughout the procedure and anaesthetic was adjusted accordingly. The heads of mice were shaved using electric clippers and skin was cleaned with ethanol (70%) and iodopovidone. Hylo Night eye ointment was applied to the eyes to protect them from exposure to surgical lights. Analgesia was provided by administration of Naropin (0.2%, 0.08 ml) subcutaneously at the side of incision and Rimadyl (0.01%, 20 mg/kg diluted in injecting saline) subcutaneously in the back. An incision was made along the midline using a sterile surgical blade to expose the skull. 3% H_2O_2 was applied to dissolve connective tissue on the skull surface. Bregma and lambda were marked and the relative hight of the two landmarks was measured to estimate the tilt of the skull. Adjustments were made to achieve a height difference of less than 100 µm.

Two skull screws (418-7123, RS Components) were implanted in the front (AP +1.5 mm from bregma, ML ±1 mm) for cortical electroencephalogram (EEG) and two skull screws in the back (AP -2 mm from lambda, ML +2 mm) as a ground and backup ground. The corresponding wires of the connector were wrapped around the skull screws and the connection was secured with dental cement. Two wires were inserted into the neck muscles for electromyography (EMG). Craniotomy (AP -2 mm, ML +1.5 mm from bregma) was performed for insertion into the HC. A bipolar electrode was inserted into the CA1 (-1.5 mm DV) and the site was sealed with biocompatible gel (Kwik-Sil, World Precision Instruments) (Figure 2.2 D). Dental cement was used to secure the electrode and connector, and to cover the skull surface and screws. After surgery, mice were kept in their home cage on a heat map for 1 h to aid recovery. 24 h after surgery, additional analgesia was provided orally in the form of Rimadyl (20 mg/kg, 0.01% diluted in injecting saline). Mice were single housed in a high-roofed cage with *ad libitum* access to water and food. Their recovery was assessed daily for 4 days.

2.2.3 *In vivo* electrophysiological recordings across sleep-wake cycle

Mice were habituated for 5 days to handling until they sat calmly in the cupped hands of the experimenter without signs of stress. Electrophysiological signals were recorded by connecting the head-cap of mice to a male 18-pin nano dual row connector (Omnetics) and a head-stage amplifier (HST/32V- G20 and PBX3, Plexon). The signal was passed through a preamplifier (PBX3, Plexon) and to an amplifier interface board (BNC-16B, Plexon) through rainbow cables. Finally, signals were digitalised at 1 kHz at a DAQ (NI USB-6211 DAQ, National Instruments) and recorded using a custom-written programme (LabVIEW, National Instruments). Top-view videos were recorded at 20 Hz with another custom-written programme (LabVIEW, National Instruments).

In week 1, mice were recorded in a white open field box (30 cm width x 30 cm depth x 40 cm height) for 2.5 hours on 4 consecutive days (Figure 2.3 A top). In week 2, mice were recorded for 1.5 hours in their home cage to be habituated to being tethered in their familiar environment. After the recording, mice were place in the open field box from week 1, which now contained landmarks on the northern and southern wall (A4 paper with black stripes and A4 paper with black dots) and there were allowed to freely explore for 10 min. On day 1 – 4, mice underwent two recording sessions in their home cage. They first underwent a baseline recording in the home cage for 1 h. Then, they were re-introduced to the open field box, which now contained two identical objects (Figure 2.3 B). After 10 minutes of exploration, mice underwent a second recording in their home cage for 1.5 h (post-learning session). The procedure was repeated for 4 days with the same objects in the open field box. On day 4, two additional steps were introduced. After the post-learning session, mice were reintroduced to the open field box, which now contained one familiar and one novel object, for 10 min. After this novel experience, mice were recorded again in their home cage for 1.5 h (Figure 2.3 A bottom left). The procedure was repeated 4 weeks later with new objects (Figure 2.3 A bottom, C).

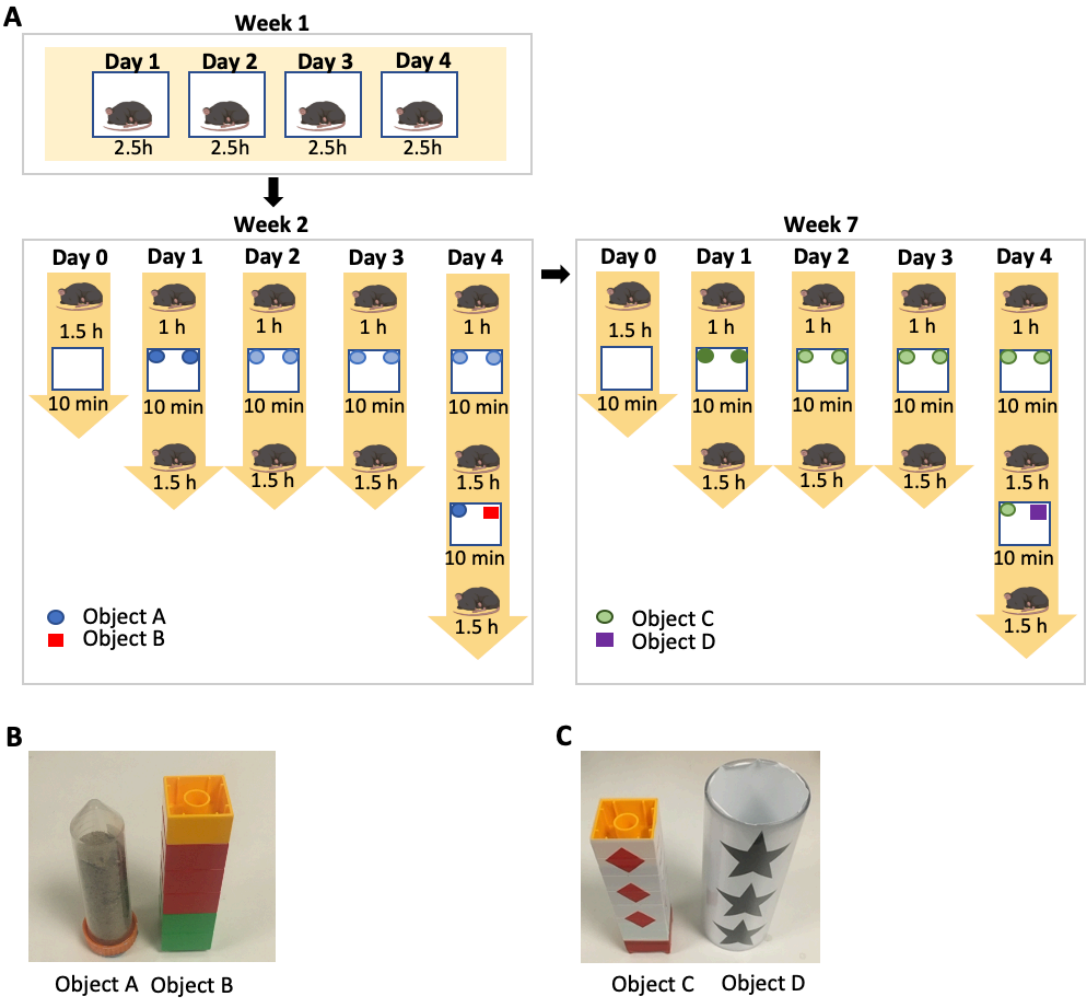

Figure 2.3 Experimental design of electrophysiological recordings. A) *Workflow of experiments. Top: In week 1, mice were recorded in an OF box for 2.5 h for 4 consecutive days. Bottom left: home cage recordings with NOR test. On day 0 of week 2, mice first underwent a 1.5 h recording in their home cage to habituate them to the tethered condition and then explore the empty OF box with landmarks on the walls for 10 min. On day 1-4 mice were recorded in their home cage for 1 h, then explored two identical objects in the OF box for 10 min (Learning sessions), then were recorded in their home cage for another 1.5 h. On day 4, mice underwent an additional 10 min in the OF box with one object being replaced by a new one (Test session), and an additional 1.5 h recording in their home cage. Bottom right: After 4 a week break, experiments were repeated following the same procedure as in week 2. Two new objects were used.* ***B)*** *Images of objects used for the NOR test in week 2.* ***C)*** *Images of objects used for the NOR test in week 7.*

2.3 Simultaneous electrophysiology and fibre photometry

2.3.1 Fabrication of implants

2.3.1.1 EEG and EMG connectors

Connectors were fabricated as previously described in section 2.2.1.1.

2.3.1.2 Bipolar electrode fabrication

Bipolar electrodes were fabricated as previously described in section 2.2.1.2. To allow bending of the electrodes to combine them with optic fibres, wires were cut to 2 cm, creating a slightly longer electrode than used in previous experiments.

2.3.1.3 Optic fibre fabrication

Insulation was stripped of an optic fibre (FP400URT, Thorlabs). A ruby scribe (S90R, Thorlabs) was used to create a small indent at 1.6 cm of the fibre. The fibre was then carefully pulled apart, creating a flat tip. Next, Hi-temp epoxy (353NDPK, Thorlabs) was added to the flat side of a ceramic ferrule (CF440-10, Thorlabs) and the fibre was pushed inside. The fibre was cut to the desired length at the round side of the ferrule and a drop of epoxy was added into it. Epoxy was then heated to 200 °C to harden. Lastly, the fibre was polished in circular motion using fibre polishing sheets (LF30D, LF6D, LF3D, LF1D, LFCF, Thorlabs). Light output of the fibre was measured by connecting the fibre to the systems patch cable (Ø400 µm Core, MAF3L1, Thorlabs), while driving the 405 nm LED and 470 nm LED separately at 5 V and measuring the light power at the respective wave length using an optical power meter kit (PM120VA, Thorlabs). Measurements of the fibre output were then compared to the optical power signal of the patch cable alone and the light coupling efficiency of the fibre was calculated. Lastly, a custom written LabView code was used to measure the light output power of the fibre at different voltages for both LEDs. Before implantation, optic fibres were combined with bipolar electrodes to create optrodes: The tip of the bipolar electrode was aligned with the tip of the fibre, lowered by 1 mm and secured with super glue (Figure 2.4 A-B).

2.3.2 Viral injections

Mice were anesthetised with 1-1.5% isoflurane (3-5% for induction) delivered with 0.8 L/min air flow and placed on a stereotaxic frame (SR-5M-HT, Narishige) with an incisor bar and ear bars, where their body temperature was maintained at 37 °C using a feedback temperature controller (50-7221-F, Harvard Bioscience). Breathing was monitored throughout the procedure and anaesthetic was adjusted accordingly. The heads of mice were shaved using electric clippers and skin was cleaned with ethanol (70%) and iodopovidone. Hylo Night eye ointment was applied to the eyes to protect them from exposure to surgical lights. Analgesia was provided by administration of Naropin (0.2%, 0.08 ml) subcutaneously at the side of incision and Rimadyl (0.01%, 20 mg/kg diluted in injecting saline) subcutaneously in the back. An incision was made along the midline using a sterile surgical blade to expose the skull. 3% H_2O_2 was applied to dissolve connective tissue on the skull surface. Bregma and lambda were marked and the relative hight of the two landmarks was measured to estimate the tilt of the skull. Adjustments were made to achieve a height difference of less than 100 µm.

A small burr hole was created to at AP -2 mm, ML +1.5 mm from bregma for viral injection at two different depths. A glass micropipette, mounted on a motorised injector (Nanoliter2010, WPI), was slowly inserted into to brain to the first injection site at a depth of -1.7 mm DV and then retracted to -1.65 mm DV, where 250 nL of viral vector (AAV2/9-hSyn-AchLightG, gifted by Professor Tomasso Patriarchi, University of Zürich; titer 1.0 x 10^{13} vg/mL) (Kagiampaki et al., 2023) was injected at a rate of 25 nL/min (Figure 2.4 C). After the first injection, and an additional 10 min of waiting, the micropipette was retracted to the second injection site at -1.4 mm DV, where an additional 250 nL of the viral vector was injected at a rate of 25 nL/min. After the second injection, the micropipette was left for an additional 10 minutes, before being slowly retracted from the brain. The exposed brain surface was sealed with biocompatible gel (Kwik-Sil, World Precision Instruments) and the skull and skin were dampened with sterile PBS. Finally, sutures were performed to close the incision site. After surgery, mice were left on a heat map for 1 h to aid recovery before being group housed with their litter mates with *ad libitum* access to water and food. 24 h after surgery, additional analgesia was provided orally in the form of Rimadyl (20 mg/kg, 0.01% diluted in injecting saline). The recovery was assessed daily for 4 days.

2.3.3 Implantation surgery

2 weeks after viral injection, implantation surgery was conducted as described in section 2.2.2. After insertion of EEG skull screws and EMG wires, an optrode was inserted (AP -2 mm, ML +1.5 mm from bregma) for the tip of the optic fibre to be at -1.4 mm DV, placing the tip of the bipolar electrode at -1.5 mm DV (Figure 2.4 C-D). Dental cement was used to secure the electrode and cover the skull surface and screws. After surgery, mice were kept in their home cage on a heat map for 1 h to aid recovery. 24 h after surgery, additional analgesia was provided orally in the form of Rimadyl (20 mg/kg, 0.01% diluted in injecting saline). Mice were single housed in a high-roofed cage with *ad libitum* access to water and food. Their recovery was assessed daily for 4 days.

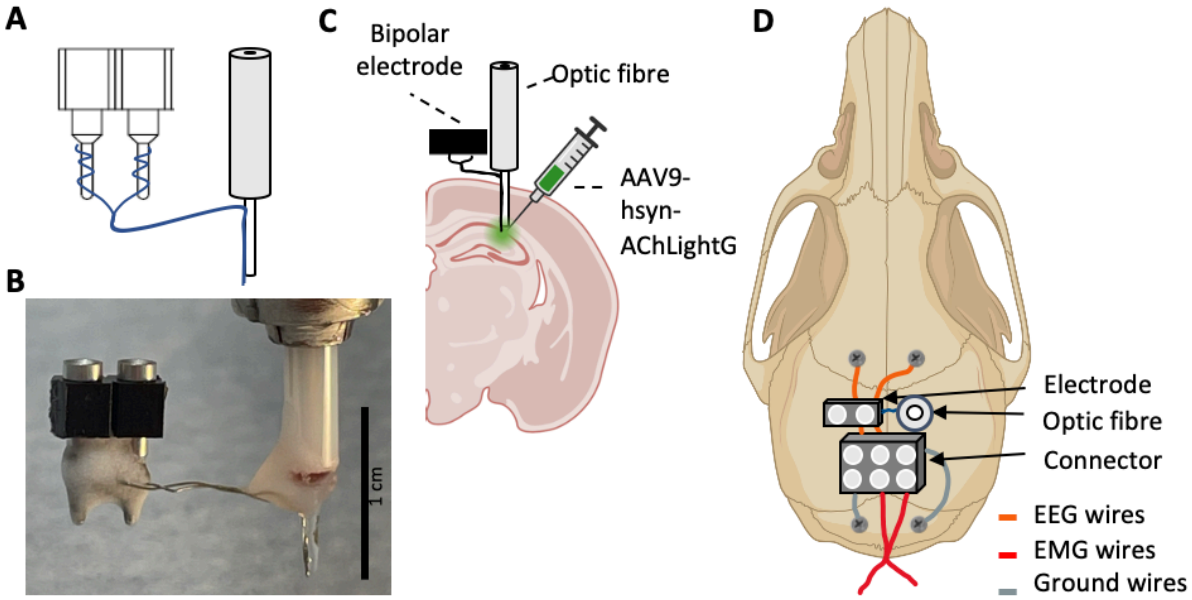

Figure 2.4 Schematic of surgical implants. A) *Design of optrodes composed of a bipolar electrode and optic fibre.* ***B)*** *Image of an optrode.* ***C)*** *Schematic of injection site and optical implant.* ***D)*** *Schematic of the position of optrode, connector, skull screws and wires on the skull. Illustrations partially created with BioRender.com.*

2.3.4 Setup

The fibre photometry setup was designed and calibrated as previously described (Patel et al., 2020) with the help of Dr Nicole Byron and Dr Niall McAlinden to allow illumination with two different wavelengths and simultaneous recording of light emission from AchLightG-expressing neurons. The first wavelength was applied for optical excitation of AchLightG (470 nm LED, M470L3, Thorlabs) to capture acetylcholine-dependent changes in fluorescent signal. The second wavelength was used to obtain acetylcholine-independent isosbestic signals (405 nm LED; M405L3, Thorlabs). The LEDs were driven by one LED driver each (LEDD1B), controlled individually through a DAQ (USB-6211, National Instruments) (Figure 2.5 A-B). Light stimulation was applied through a custom written LabView code, at a pulse frequency of 400 Hz with a 50% duty cycle. Synchronisation pulses were created to later reconstruct which LED was turned on at any given time. The voltage for each LED was adjusted for each recording according to the light output measurements for each fibre (1.1363-1.4845 V for 405 nm LED, 0.8705-1.2487 V for 470 nm LED) to achieve a target power of 35 µW. Light from the LEDs passed through an aspheric lens (AL2520M-A, Thorlabs), excitation filter (FB470-10 and FB405-10, Thorlabs) and dichroic mirror (DMLP425R, Thorlabs) into a fibre launch system (KT110/M, Thorlabs) connected to a multimode patch cable connected to the implanted fibre via a ceramic mating sleeve (ADAF1, Thorlabs). Light emitted from Ach-LightG expressing neurons was passed through the optic fibre, a dichroic mirror (MD498, Thorlabs) and into the photodetector (NewFocus 2151, Newport) connected to the DAQ. Light emission was recorded simultaneously with electrophysiology signals (as described in 2.4) at 5 kHz. For a full list of all components see Table 1.

2.3.5 In vivo Recordings

After a 5 day recovery period following surgeries, mice were habituated to handling for 5 days prior to recording. More specifically, mice were habituated to sitting in the experimenters cupped hand until calmly allowing their head cap implant to be touched with no signs of stress. On day 0, their head-cap implant was connected, as previously described in 2.4. The dust cap was removed from the implanted fibre and the fibre was additionally cleaned with isopropanol before being connected to the fibre patch cable via a ceramic mating sleeve. Mice were recorded in their home cage positioned in a cabinet lined with copper wire, serving as a Faraday cage, for 2 h to habituate them to the tethered condition. To avoid photobleaching, the fibre photometry system remained turned off on the habituation day. On day 1, mice were recorded in their home cage for 1 h as a baseline recording. Then, all cables were removed from the mice and they were placed in the 30 cm x 30 cm open field box containing landmarks and two identical objects, as described in 2.4, and allowed to explore freely for 10 min. Then, mice were immediately recorded again in their home cage for 1.5 h (Figure 2.5 C).

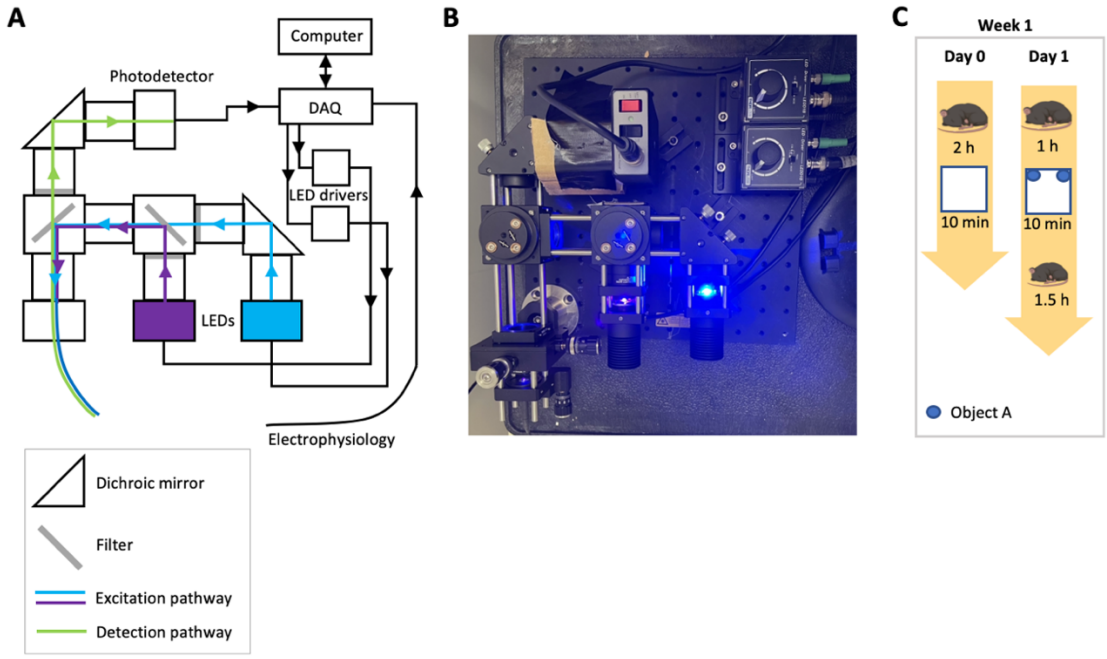

Figure 2.5 Fibre photometry setup and recording protocol. A) *Schematic of fibre photometry setup.* ***B)*** *Image of fibre photometry setup.* ***C)*** *Recording procedure of simultaneous fibre photometry and electrophysiological recording. On habituation day 0, no fibre photometry was recorded to avoid photobleaching.*

Table 1. List of components for fibre photometry system.

Component	Supplier	Product Code	Quantity
Photodetector	Newport	NewFocus 2151	1
470 nm LED	Thorlabs	M470L3	1
405 nm LED	Thorlabs	M405L3	1
LED driver	Thorlabs	LEDD1B	2
LED power source	Thorlabs	KSP101	2
LED holder	Thorlabs	CP12	2
Dichroic mirror	Thorlabs	DMLP425R	1
Dichroic mirror	Thorlabs	MD498	1
Excitation filter	Thorlabs	FB470-10	1
Excitation filter	Thorlabs	FB405-10	1
Bandpass filter	Thorlabs	MF525-39	1
Broadband dielectric mirror	Thorlabs	BB1-E02	2
Mirror mount	Thorlabs	KCB1C/M	2
Aspheric lens	Thorlabs	AL2520M-A	4
Cage plate for lens	Thorlabs	CP08/m	4
Lens tubes	Thorlabs	SM103-P5	5
Filter holder	Thorlabs	C4W	2
Filter holder	Thorlabs	B4C/M	2
Filter holder	Thorlabs	FFM1	2
Fibre launch	Thorlabs	KT110/M	1
Patch cable	Thorlabs	M82L01	1

The setup was designed by Dr Amisha Patel (Patel et al., 2020).

2.4 Histology

To verify the electrode position and plaques after recordings, mice were deeply anesthetised with a pentobarbital and lidocaine and perfused transcardially with phosphate buffered saline (PBS) followed by 4% paraformaldehyde/0.1 M phosphate buffer, pH 7.4. Brains were removed and kept in the same fixative overnight at 4°C before then being stored in 30% sucrose PBS for at least 2 days. Immunohistochemical staining was performed by Symeon Gerasimou and Jacques Ferreira. Brains were cut into 50 µm coronal sections using a sliding microtome (SM2010R, Leica) and stained with DAPI (1:500, Sigma-Aldrich) and Thioflavin-S (0.01%, T1892, Sigma-Aldrich).
Brain slices of mice that underwent viral injections were stained with DAPI (1:1000, Sigma-Aldrich), monoclonal mouse anti-eYFP/GFP (1:2000, ab1218, Abcam), Goat anti-Mouse IgG (H+L) Cross-Adsorbed Secondary Antibody (1:1000, Alexa Fluor™ 488, Thermo Fisher Scientific) and Thiazine Red (0.05%, VWR Chemicals). The sections were cover-slipped with fluoromount-G (Thermo Fisher Scientific) and imaged under the epifluorescent microscope (Eclipse E600, Nikon) using a custom-written image acquisition program (LabVIEW, National Instruments).

2.5 Data analysis

2.5.1 Plaque quantification

Plaque burden in the HC was assessed using ImageJ software. A colour threshold (~100 – 137) was applied to only capture the green plaques. A second threshold was applied to exclude green signals of low brightness. This second threshold was set individually for each image, depending on the intensity of the background fluorescence. Using the build-in function in ImageJ, particles were analysed with a minimum size of 1 pixel and maximum size of 150 pixels to exclude artefacts, and the % of area covered by plaques in the HC was calculated.

2.5.2 Electrophysiology

Electrophysiological signals were analysed in MATLAB at 1 kHz sampling rate. Recordings conducted at 5 kHz sampling rate were downsampled to 1 kHz prior to further analysis.

2.5.2.1 Arousal state analysis

Behavioural states were classified offline as awake, NREM sleep and REM sleep in 4 s intervals based on EEG and EMG signals using a custom-written MATLAB GUI (Figure 2.6 A). Episodes of high EMG power were scored as awake, episodes with low EMG signal and high delta or sigma power were scored as NREM sleep, and episodes of low EMG signal with high theta power were scored as REM sleep (Figure 2.6 B).

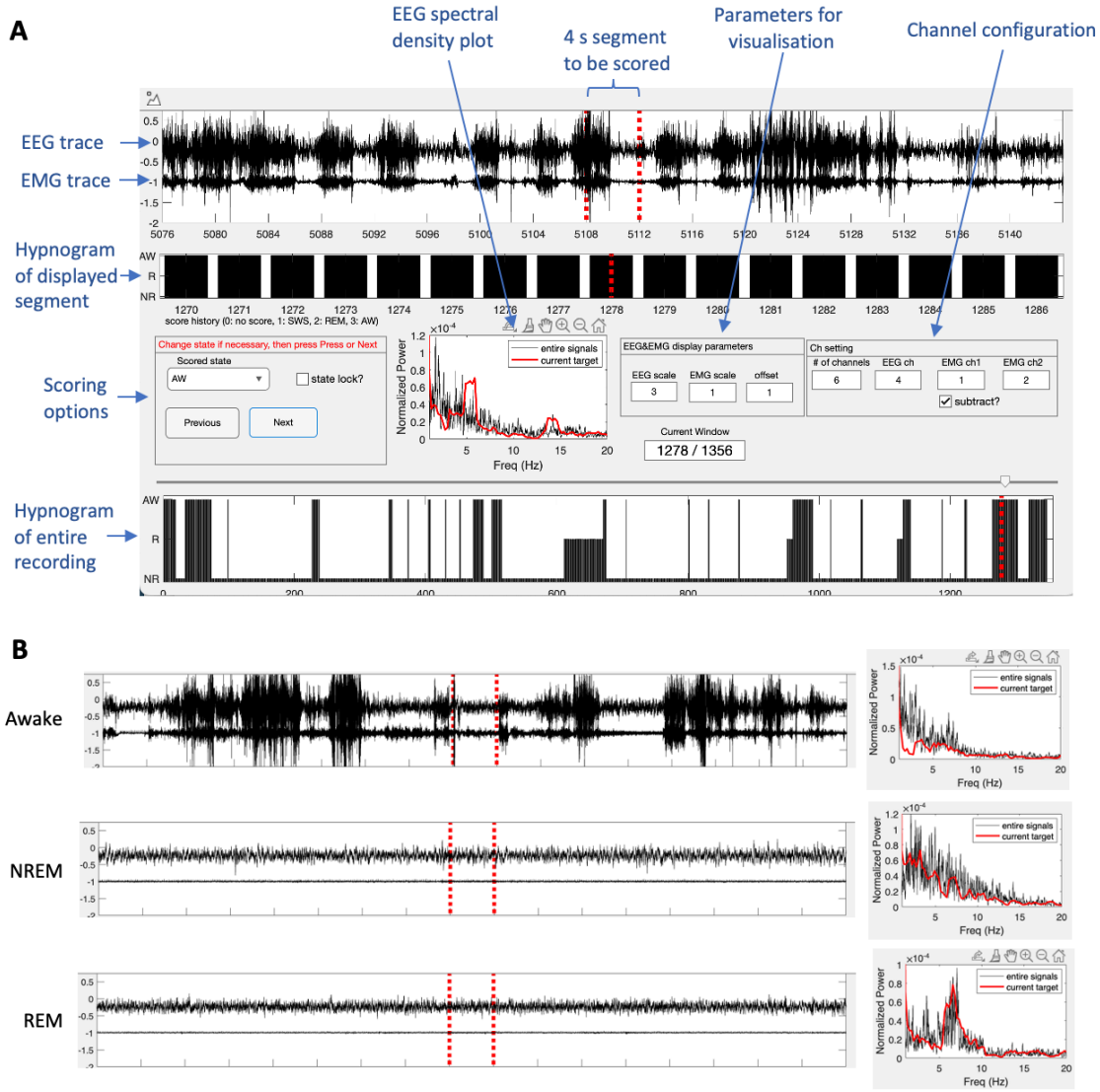

Figure 2.6 Manual sleep scoring. A) *Graphical user interface for sleep scoring.* ***B)*** *Examples of EEG and EMG traces (left) for awake (top), NREM (middle) and REM (bottom). Dotted red lines indicate the start and end point of the 4 s window used to calculate the EEG density plots shown on the right.*

2.5.2.2 Analysis of sleep architecture

Sleep architecture was assessed by calculating the percentage of time spent in each arousal state, the number of episodes per hour of each arousal state, the average duration of episodes in each arousal state, and the latency to the first sleep episode for each animal in each recording. Potential differences between genotypes and along recording sessions were assessed using repeated measures ANOVA, followed by Tukey HSD post-hoc test.

2.5.2.3 Sharp-wave ripple detection

Episodes of NREM sleep were analysed to detect sharp-wave ripples. LFP signals recorded from the bipolar electrode were band-pass filtered at 140-250 Hz with a 3rd-order Butterworth filter and the envelope of the filtered signal was calculated by calculating the root-mean-square over a sliding window of 20 ms. Signals during REM episodes were used to compute two thresholds: the higher threshold was calculated as mean signal + 5 x SD and the lower threshold was calculated as mean signal + 2 x SD. For recordings without REM episodes, a 12-30 s section of noise-free NREM, occurring at the end of a NREM episode, was manually selected. To detect SWRs, events where the signal power exceeded the higher threshold were detected as SWR candidates. The onset and offset was determined as the time points where the signal power crossed the lower threshold (Figure 2.7). SWRs with overlapping onsets and offsets were merged into one SWR event. Events with a duration below 20 ms and above 300 ms were excluded. To exclude artefacts caused by short, abrupt muscle movements during sleep, root-mean-square EMG signal during each SWR event was calculated and compared to the EMG threshold, calculated as 2 x root-mean-square of the EMG signal of REM episodes or noise-free NREM section. SWR events with EMG power higher than the EMG threshold were classified as artifacts and excluded from further analysis.

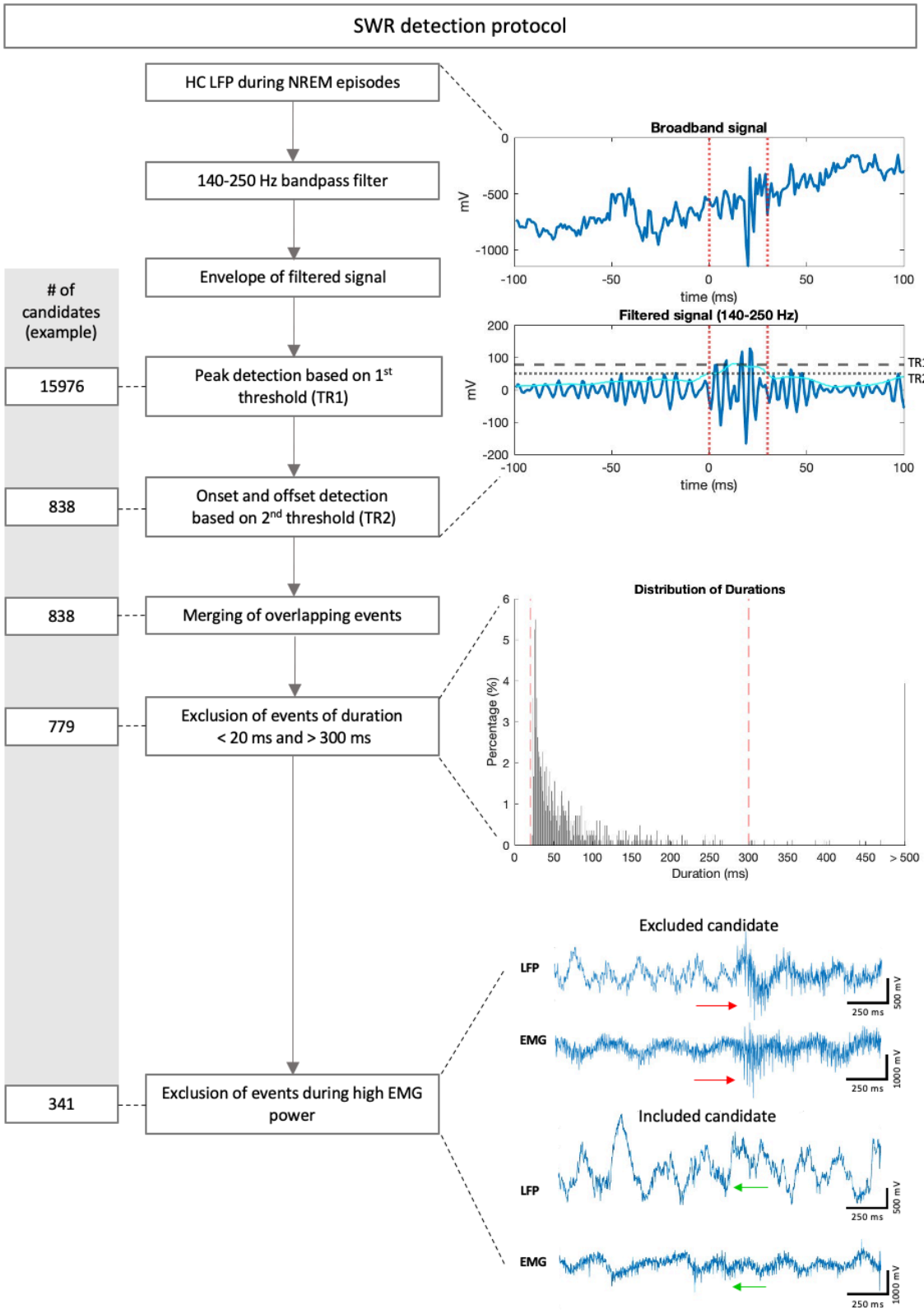

Figure 2.7 Sharp wave-ripple detection. *Left: example of SWR candidate numbers for each step in a 1 h recording of a WT mice. Middle: steps of SWR candidate identification and exclusion. Right: Visualisation of crucial steps. Right, top: Example wide-band hippocampal signal (blue) around the SWR onset +- 100 ms and hippocampal signal around SWR onset*

filtered in 140-250 Hz frequency band (blue) and envelope of filtered signal (cyan). SWRs are detected when the envelope of the filtered signal exceeds the 5th standard deviation (threshold 1, black dashed line) and onset and offset (red dotted lines) of each SWR are determined by the time points of the 2nd standard deviation being crossed (threshold 2, black dotted line). Right, middle: distribution of durations of detected candidates with lower and upper cut-off at 20 ms and 300 ms (red dashed lines). Right, bottom: visualisation of a SWR candidate excluded due to high EMG power (red arrows) and an included candidate without increase EMG power (green arrows)

2.5.2.4 Sleep spindle detection

Episodes of NREM sleep were analysed to detect sleep spindles. EEG signals from both hemispheres were band-pass filtered using a custom designed Butterworth filter applying a first stopband frequency at 3 Hz, first passband frequency at 10 Hz, second passband frequency at 15 Hz, second stopband frequency 22 Hz and a stopband attenuation level at 24 dB. The envelope of the filtered signal was calculated by calculating the root-mean-square over a sliding window of 750 ms. Signals during NREM sleep were used to compute two thresholds: the higher threshold was calculated as the mean signal x 3.5 and the lower threshold was calculated as mean signal x 2. To detect sleep spindles, events where the signal power exceeded the higher threshold were detected as spindle candidates. The onset and offset was determined as the time points where the signal power crossed the lower threshold (Figure 2.8). Spindle events with overlapping onsets and offsets were merged into one spindle event. Events with a duration below 500 ms and above 10000 ms were excluded. To exclude artefacts caused by muscle movements during sleep, root-mean-square EMG signal during each sleep spindle event was calculated and compared to the EMG threshold, calculated as 2 x root-mean-square of the EMG signal across all NREM sleep. Sleep spindle events with EMG power higher than the EMG threshold were classified as artifacts and excluded from further analysis.

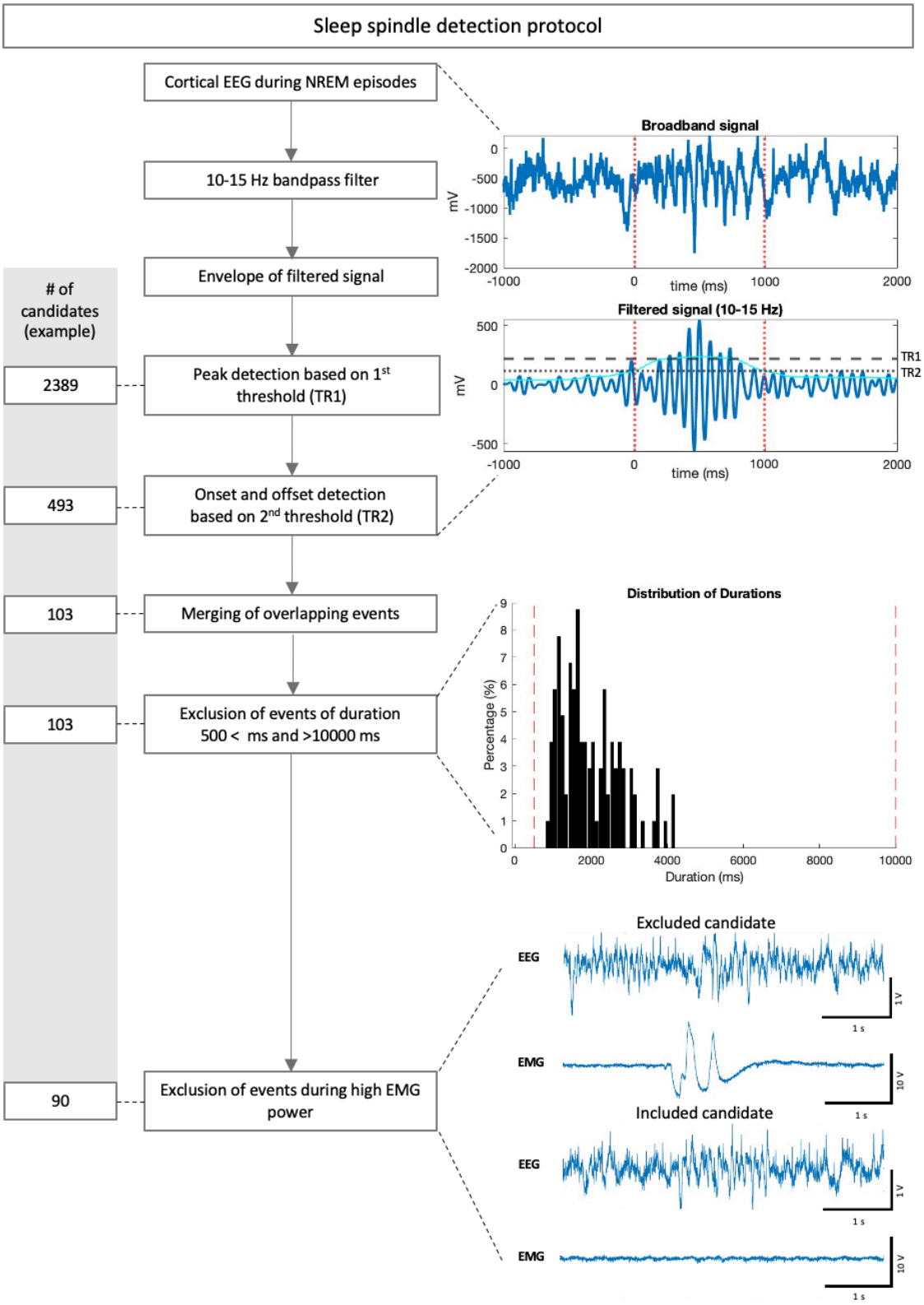

Figure 2.8 Sleep spindle detection. *Left: example of sleep spindle candidate numbers for each step in a 1 h recording of a WT mice. Middle: steps of sleep spindle candidate identification and exclusion. Right: Visualisation of crucial steps. Right, top: Example wide-band cortical signal (blue) around the sleep spindle onset (-1000 ms – + 2000 ms) and signal*

filtered in 10-15 Hz frequency band with envelope (cyan). Sleep spindles are detected when the envelope of the filtered signal exceeds the upper threshold of 3.5 x mean signal during NREM sleep (threshold 1, black dashed line) and onset and offset (red dotted lines) of each event are determined by the time points where the second threshold of 2 x mean signal during NREM sleep is crossed (threshold 2, black dotted line). Right, middle: distribution of durations of detected candidates with lower and upper cut-off at 500 ms and 10000 ms (red dashed lines). Right, bottom: visualisation of a sleep spindle candidate excluded due to high EMG power and an included candidate without increase EMG power.

2.5.2.5 Sharp-wave ripple and sleep spindle quantification

After detection of SWR and sleep spindle events, the average occurrence of SWRs/s and sleep spindles/min were calculated for individual NREM sleep episodes and across all NREM sleep episodes for each animal in each recording session. To assess the duration of the events, the average durations were calculated for each NREM sleep episode and across all NREM sleep episodes for each animal for each recording. Averages were then compared between WT and FAD+ mice across sleep episodes and across recordings. For recordings conducted in combination with the NOR test, the relative change in SWR and sleep spindle rates were additionally assessed by subtracting the average rate during baseline recordings from the average rate during post-learning recordings.

2.5.2.6 SWR - sleep spindle coupling

To assess the co-occurrence of SWRs and sleep spindles, LFP signals from the CA1 were band-pass filtered at 140-250 Hz with a 3rd-order Butterworth filter and the envelope of the filtered signal was calculated by calculating the root-mean-square over a sliding window of 20 ms. The timing of sleep spindle onsets detected in the ipsilateral cortex were used to create a 4 s time window from 2 s before the onset of spindles until 2 s after the onset. The enveloped signal of the CA1 within these time windows was z-scored based on -2 to -1 s signal before the spindle onset and the mean for each recording was calculated. Z-scoring is a process of standardisation where values are converted into z-scores, which represent the number of standard deviations the value is above or below the mean of the dataset. The z-score is calculated as follows: $z = \frac{(x-\mu)}{\sigma}$ where x is the variable, μ is the mean and σ is the standard deviation.

2.5.2.7 Spectral analysis

To analyse the power of different frequency band during sleep, Welch's power spectral density (PSD) estimate was calculated for the following frequencies: SWR range (140 – 250 Hz), high gamma (53 – 80 Hz), low gamma (30 – 47 Hz), alpha (10 -15 Hz), theta (4 – 10 Hz) and delta (1 – 4 Hz). The frequency band between 47 – 53 Hz was excluded from analysis to avoid contamination caused by 50 Hz noise in some recordings. The PSD was calculated for each sleep episode, the total power was calculated for each frequency band of interest and then normalised by dividing it by the total power of the 0 – 40 Hz frequency range.

2.5.3 Fibre photometry

2.5.3.1 Signal reconstruction

Fluorescent signals were reconstructed using an approach previously reported (Patel et al., 2020): According to the synchronisation pulses of the two LEDs, the median signal during each illumination period was calculated for excitation at 405 nm and 470 nm. Then, a 3rd-order 1 Hz lowpass Butterworth filter was applied to eliminate high-frequency noise. Double exponential fitting was applied to account for photobleaching (Figure 2.9 A, B) and linear scaling was performed on the 405 nm signal to account for moving artefacts. To estimate dF signals, the linearly scaled 405 nm signal was then subtracted from the 470 nm signal (Figure 2.9 C). Finally, dF signals were z-scored.

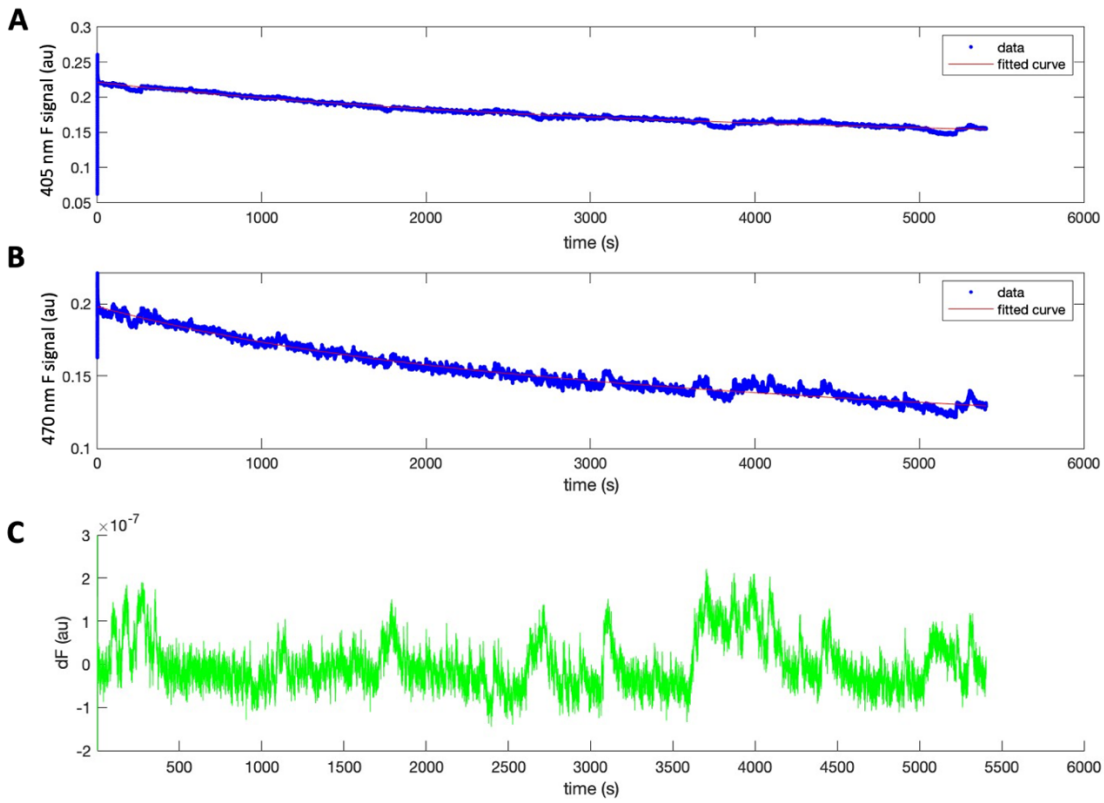

Figure 2.9 Fluorescent signal reconstruction. A) *405 nm signal trace (blue) and exponential fitting curve (red).* ***B)*** *470 nm signal trace (blue) and exponential fitting curve (red).* ***C)*** *Scaled and z-scored fluorescent signal.*

2.5.3.2 Analysis of cholinergic signal across tone across arousal states

The average fluorescent signal was calculated for each arousal state for each recording session of each animal. Differences between genotypes were assessed, as well as across recording sessions, using t-tests.

Changes in the fluorescent signal were further analysed at state transitions from NREM to REM sleep, NREM sleep to wakefulness, wakefulness to NREM sleep and REM sleep to wakefulness. Here a time window of -20 s to +20 s around the time of transition was chosen by progressively increasing the window size until the signal stabilised both before and after the transition time 0. Fluorescent signals in this time window were z-scored and the average signal was computed for all transitions of WT and FAD+ mice. The Change in fluorescent signal was then calculated by subtracting the average of each pre-transition signal from the average post-transition signal for each transition. Averages were then compared between WT and FAD+ mice using t-tests.

2.5.3.3 Analysis of cholinergic signal at SWR timing

Changes in fluorescent signal around SWR timing was assessed by z-scoring the signal across a -100 to +100 s time window around the peak of each SWR event. The average signal in this time window was then calculated along with the standard error of mean for each animal for each recording.

To investigate transient increases of fluorescent signal at SWR timing, EMG signals were assessed around SWR timing following the same computations as used for the fluorescent signal. The EMG power and fluorescent signal at the peak of each SWR event were then compared and their correlation was assessed by calculating Pearson's correlation coefficient.

2.6 Behaviour analysis

Videos of mice exploring objects in the open field box were analysed using DeepLabCut, a deep neural network for markerless pose estimation (Mathis et al., 2018). First, body parts where manually marked on 300 randomly selected frames: nose, left ear, right ear, neck, left shoulder, right shoulder, left hip, right hip, and tail base. Next, the algorithm was trained for 500,000 iterations. Videos with markers for all body parts were created to inspect the accuracy of pose estimation. The coordinates of body parts throughout the recording where then analysed in MATLAB. In a custom written script, the distance from the nose of each animal to the objects in the open field box at any given time was computed. When the nose coordinates moved withing a certain radius of an object, the time spent within this radius was counted as exploration of objects. To calculate the discrimination index, two parameters were explored: the distance from the object (0 – 15 cm in 1 cm intervals) and time cut-offs (1 – 10 min in 1 min intervals).

The discrimination index was computed as the time spent exploring object A minus the time spent exploring object B divided by the total time of exploration of either object.

$$Discrimination\ index = \frac{object\ A\ time - object\ B\ time}{object\ A\ time + object\ B\ time}$$

For group statistics, discrimination indices were computed with 6 different combinations of parameters (2 or 5 cm exploration radius and 2, 5 or 10 min time cut-offs).

2.7 Statistical analysis

All statistical analysis was performed offline using custom-written scripts (MATLAB R2022b, MathWorks). A significance level of $p < 0.05$ was chosen for all analysis. Kolmogorov-Smirnov test for normality and Bartlett's test for homogeneity of variance were performed to assess data distribution and to choose appropriate statistic tests. T-tests were performed to assess differences between genotypes in regards to SWR and sleep spindle rate, discrimination index and average cholinergic tone in each state. Repeated measures analysis of variance (ANOVA) was performed to investigate differences in sleep architecture. 2-way ANOVA was performed to assess SWR rate and sleep spindle rate differences along genotypes, sexes, and recording sessions. Tukey honest significant difference (HSD) was chosen as post-hoc test for all ANOVAs.

To assess the correlation between plaque burden and SWR rate, Pearson's correlation coefficient was calculated and statistical significance was assessed. Cochran–Mantel–Haenszel test was conducted to assess the occurrence of cholinergic peaks among recording sessions and genotypes.

All data is shown as mean ± standard error of mean, unless stated otherwise.

3 Results

The aim of this project was to investigate brain oscillations during sleep that are involved in memory consolidation and to explore potential abnormalities in our mouse model – the 5xFAD mice. To do so, we conducted electrophysiological recordings measuring EEG in the cortex, local field potentials in the HC and EMG from the neck muscle across the sleep-wake cycle. We explored the frequency and duration SWRs and sleep spindles in WT and FAD+ mice in the context of a novel versus familiar environment (chapter 3.1), before learning versus after learning (chapter 3.2) and investigated acetylcholine in the HC as a possible cause for oscillatory abnormalities (chapter 3.3).

3.1 Sharp-wave ripples and sleep spindles during sleep in a novel environment

Since both SWRs and sleep spindles have previously been associated with memory consolidation, we wanted to assess how these brain oscillation events change in situations of increased memory consolidation demand – novel situations – compared to situations with low memory consolidation demand – familiar situations. To do so, we conducted in vivo recordings over the span of 4 consecutive days in an open field box for 2.5 h each. Mice were not habituated to the open field box prior to the first recording session. Therefore, the first recording in this novel environment should present a novel situation with an increased demand of memory consolidation. Over the following days, mice would be expected to become familiar with the environment and the demand for memory consolidation should decline. The recording protocol (Figure 3.1.1 A) was conducted with a total of 12 mice: 6 WT and 6 FAD+ mice, 3 males and 3 females in each group. For the first 3 days, data of all 12 mice was included in the analysis. On day 4, one male WT mouse was excluded due to no sleep and one male WT and one male FAD+ mice were excluded due to excessive noise caused by construction work above the recording

room. These differences in sample size on day 4 were accounted for with appropriate statistical analysis. Histology images were processed to verify genotypes (Figure 3.1.1 B) and to assess the electrode position in each mouse. A summary of the electrode tip position of each mouse is depicted in Figure 3.1.1 C.

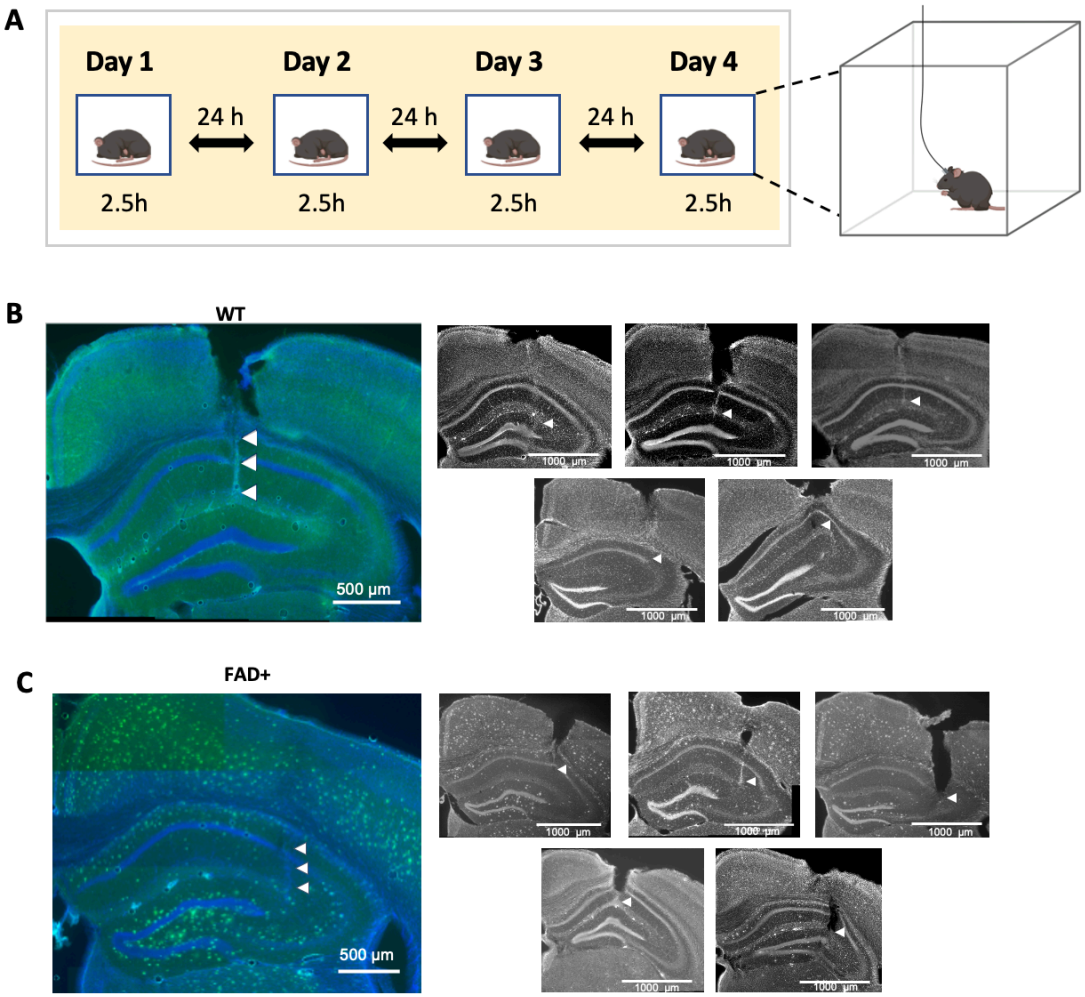

Figure continued on the next page.

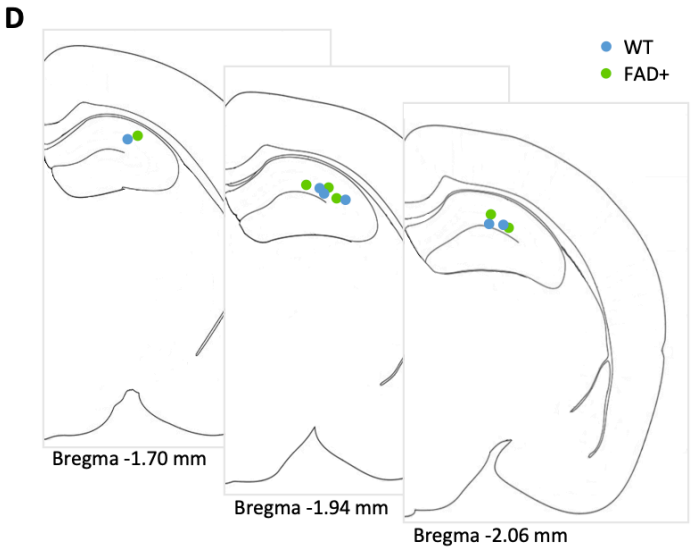

Figure 3.1.1 Recording protocol of open field recordings and electrode positions. A) *Recording protocol in week 1. Recordings were conducted for 4 consecutive days in freely-behaving condition in a white box (30 cm x 30 cm) for 2.5 h per day. No habituation to the box was conducted prior to recordings.* ***B)*** *Histology images of WT mice confirming electrode position in the HC. Slices stained with TS (green) and DAPI (blue). White triangles indicate position of the electrode shank. Scale bars 500 and 1000 µm.* ***C)*** *Histology images of FAD+ mice confirming electrode position and plaque pathology. Slices stained with TS (green) and DAPI (blue). White triangles indicate position of the electrode shank. Scale bars 500 and 1000 µm.* ***D)*** *Summary of electrode position based on histological images. Tips of electrodes are indicated as dots in blue for WT mice and green for FAD+ mice. Illustrations partially created with BioRender.com*

3.1.1 Sleep architecture in a novel environment

Since studies in humans have reported changes in sleep to occur in AD patients (Bonanni et al., 2005; Ju et al., 2013), we first investigated differences in sleep architecture between our FAD+ and WT mice by comparing the fraction of time spent in each state, mean duration of state episodes, mean number of state episodes per hour and latency to sleep across all days (Figure 3.1.2).

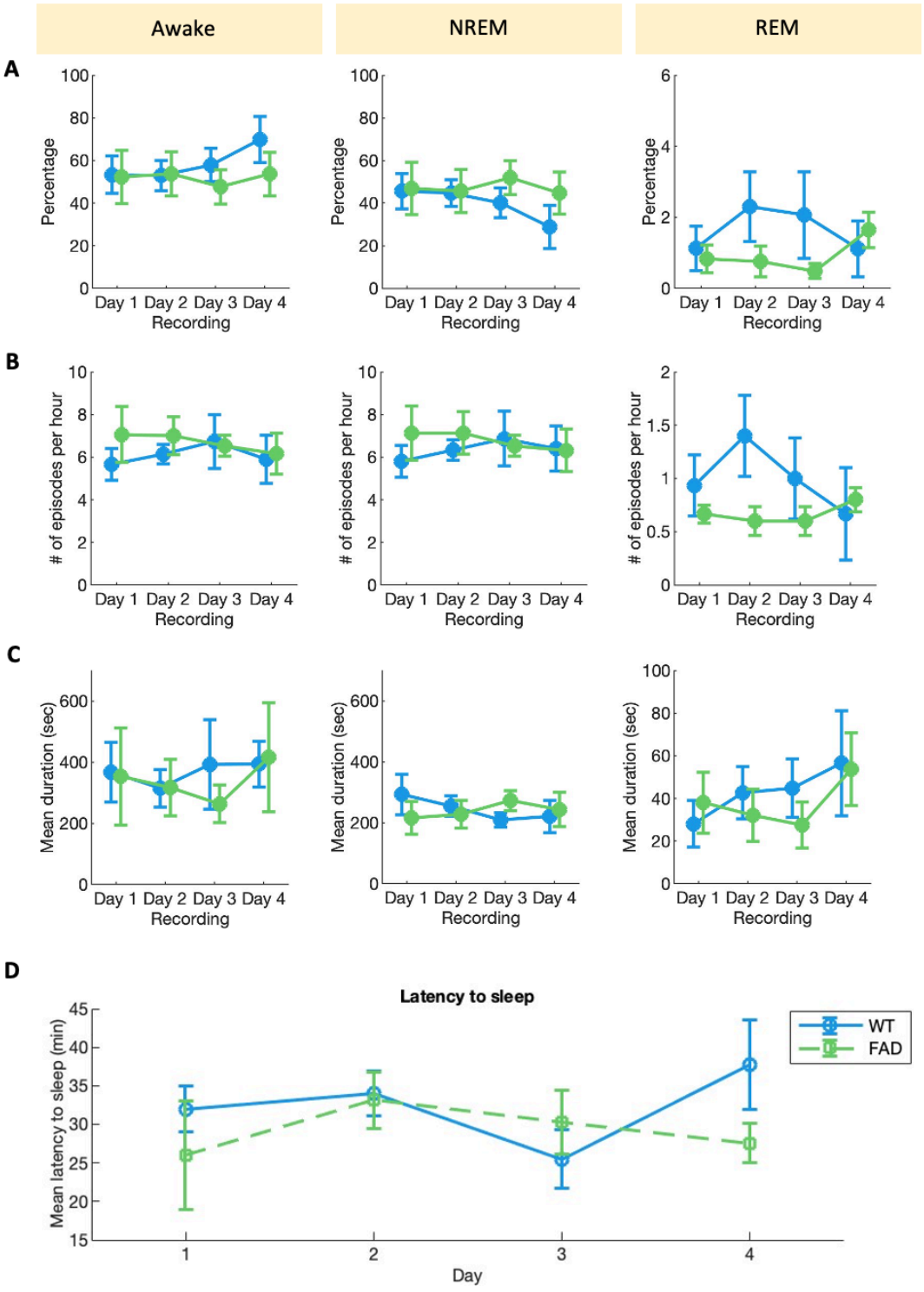

Figure 3.1.2 Sleep architecture of WT and FAD+ mice across recordings. A) *Percentage of time spent in each state: awake (AW, left), non-REM (NREM, middle) and REM (right) for WT (n = 6, blue) and FAD+ mice (n = 6, green) across recording days.* ***B)*** *Mean number of awake episodes (left), NREM episodes (middle) and REM episodes (right) per hour of recording of WT (n = 6, blue) and FAD+ mice (n = 6) across recording days.* ***C)*** *Mean duration of awake episodes (left), NREM episodes (middle) and REM episodes (right) for WT (n = 6, blue) and FAD+ mice (n = 6, green) across recording days.* ***D)*** *Latency to first sleep episode of WT (n = 6, blue) and FAD+ mice (n = 6, green) across recording days. Error bars: standard error of mean.*

Repeated measures analysis of variance (ANOVA) was conducted to investigate differences in the percentage of time spent in each state across recording days and between genotypes. ANOVA for the awake percentage of WT and FAD+ mice across the 4 recording days revealed no significant main effect along recording days ($F(3, 30) = 0.02$, $p = 0.99$) and no significant interaction effect between genotype and day ($F(3, 30) = 0.46$, $p = 0.72$) (Figure 3.1.2 A, left). ANOVA for NREM percentage also showed no significant main effect of recording day ($F(3, 30) = 1.27$, $p = 0.30$) an no significant interaction between genotype and day ($F(3, 30) = 0.23$, $p = 0.88$) (Figure 3.1.2 A, middle). Similarly, no significant effect of recording day was found for the percentages of REM ($F(3, 30) = 0.37$, $p = 0.77$) and no significant interaction between genotype and day ($F(3, 30) = 2.52$, $p = 0.23$) (Figure 3.1.2 A, right). These finding indicate that the overall amount of time spent in each state did not change across recording days and that the percentage of time spent in each state does not differ between FAD+ and WT.

To investigate potential differences in sleep fragmentation between genotypes and along recording days, the number of awake, NREM and REM episodes per hour was next assessed and repeated measures ANOVAs were conducted for each state across the four days of recording. No significant main effect of days was found for the number of awake episodes per hour ($F(3, 24) = 0.65$, $p = 0.59$) and no significant interaction effect of genotype and day ($F(3, 24) = 0.25$, $p = 0.86$) (Figure 3.1.2 B, left). For the number of NREM episodes per hour, no significant main effect of day was found ($F(3, 24) = 0.48$, $p = 0.7$) and no significant interaction between genotype and day ($F(3, 24) = 0.25$, $p = 0.86$) (Figure 3.1.2 B, middle). Analysis of the number of REM episodes per hour also revealed no significant main effect of day ($F(3, 24) = 0.4$, $p = 0.75$) and no significant interaction between genotype and day ($F(3, 24) = 0.69$, $p = 0.57$) (Figure 3.1.2 B, right). These findings indicate no significant differences in the number of episodes of each state between genotypes and among recording days.

As an additional indicator for sleep fragmentation, the average duration of episodes of each state was assessed and potential differences among days and between genotypes were analysed. Repeated measures ANOVA of awake episode durations revealed no significant main effect of recording day ($F(3, 21) = 0.77$, $p = 0.53$) and no significant interaction between genotype and day ($F(3, 21) = 0.01$, $p = 1$) (Figure 3.1.2 C, left). Analysis of NREM episode durations revealed no significant main effect of day ($F(3, 21) = 0.11$, $p = 0.96$) and no significant interaction between

genotype and day ($F(3, 21) = 0.88$, $p = 0.47$) (Figure 3.1.2 C, middle). Similarly, there was no significant main effect of day on the durations of REM episodes ($F(3, 21) = 2.2$, $p = 0.12$) and no significant interactions of genotype and day ($3, 21) = 0.11$, $p = 0.95$) (Figure 3.1.2 C, right). These findings indicate no differences in average state episode durations between genotypes and among recording days. Finally, the latency to the first NREM episode was compared between FAD+ and WT mice for each recording day. Repeated measures ANOVA revealed no significant main effect of days ($F(3, 21) = 0.71$, $p = 0.56$) and no significant interaction between genotype and days ($F(3, 21) = 0.9$, $p = 0.46$) (Figure 3.1.2 D). These results indicate no change in sleep latency across recording days and no difference in sleep latency between WT and FAD+ mice.

Together, the analysis of percentage of time spent in each state, the numbers of episodes in each state per hour, the average duration of episodes and the latency to the first sleep episode indicated no abnormalities in sleep architecture in FAD+ mice. There were also no significant changes across recording days, indicating no effect of novelty of the environment on the sleep architecture of mice.

3.1.2 High frequency of sharp-wave ripple occurrence during sleep in a novel environment is absent in FAD+ mice

We wanted to investigate the occurrence of SWRs in FAD+ and WT animals and how they might change when mice slept in a novel versus familiar environment. SWRs were detected during NREM sleep episodes using the 2-threshold detection method (see chapter 2.5.1.2). Inspection of the raw trace of a single SWR event (Figure 3.1.3 A, top), 140-250 Hz filtered traces of the event (Figure 3.1.3 A, middle) and current wavelet transform of the event (Figure 3.1.3 A, bottom) showed the characteristic sharp-wave component, ripple, and increase in 140-250 Hz frequency power just after the detected onset of the SWR event. The sharp-wave component was preserved across the mean of 1233 raw traces of SWR events (Figure 3.1.3 B, top), while the ripple was preserved across the mean of 1233 filtered traces of SWR events (Figure 3.1.3 B, middle). The average current wavelet transform of 1233 SWR events showed an increase in the 140 – 250 Hz frequency range just after the SWR onset as well a decrease in this range just before the onset (Figure 3.1.3 B, bottom). The raw trace, filtered trace and current wavelet transform all illustrate the characteristic features of SWRs, indicating that the 2-threshold detection method reliably identifies SWR events.

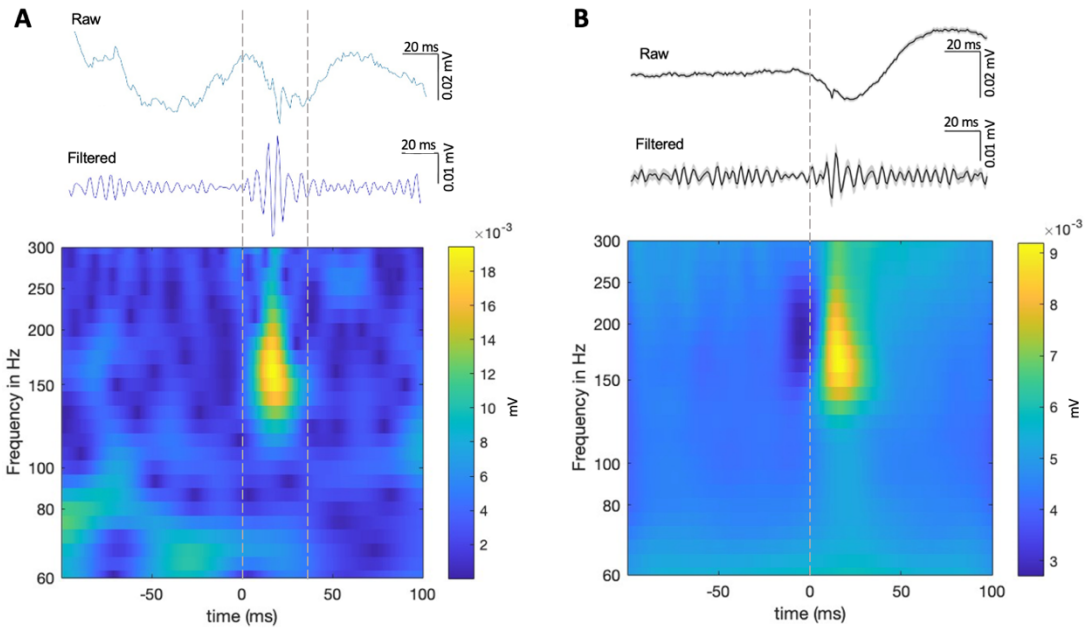

Figure 3.1.3 Time-frequency profile of SWRs. A) *Top: raw trace of a single SWR event. Middle: event filtered in 140-250 Hz frequency band. Bottom: time frequency representation (current wavelet transform) of single SWR event. Dashed lines represents SWR onset and offset.* ***B)*** *Top: mean of n = 1233 raw SWR traces. Shaded area indicates standard error of mean. Middle: mean of n = 1233 SWR traces, filtered in 140-250 Hz frequency band. Shaded area indicates standard error of mean. Bottom: mean time-frequency representation (current wavelet transform) of 1233 SWRs. Dashed line represents SWR onset.*

To test the hypothesis that SWRs are abnormal in AD, the average SWR occurrence and durations were assessed for each of the 4 recording days. As SWR occurrence is associated with increased memory consolidation, the frequency of SWR occurrence was assessed as the average number of SWRs per second during NREM sleep and compared between WT and FAD+ mice, along with the distribution of SWR durations, for each recording day, allowing observations of changes in SWRs as mice become familiar with the environment.

First, the average occurrence of SWRs for WT and 5xFAD mice was compared across recording days using repeated measures ANOVA (Figure 3.1.4 A).

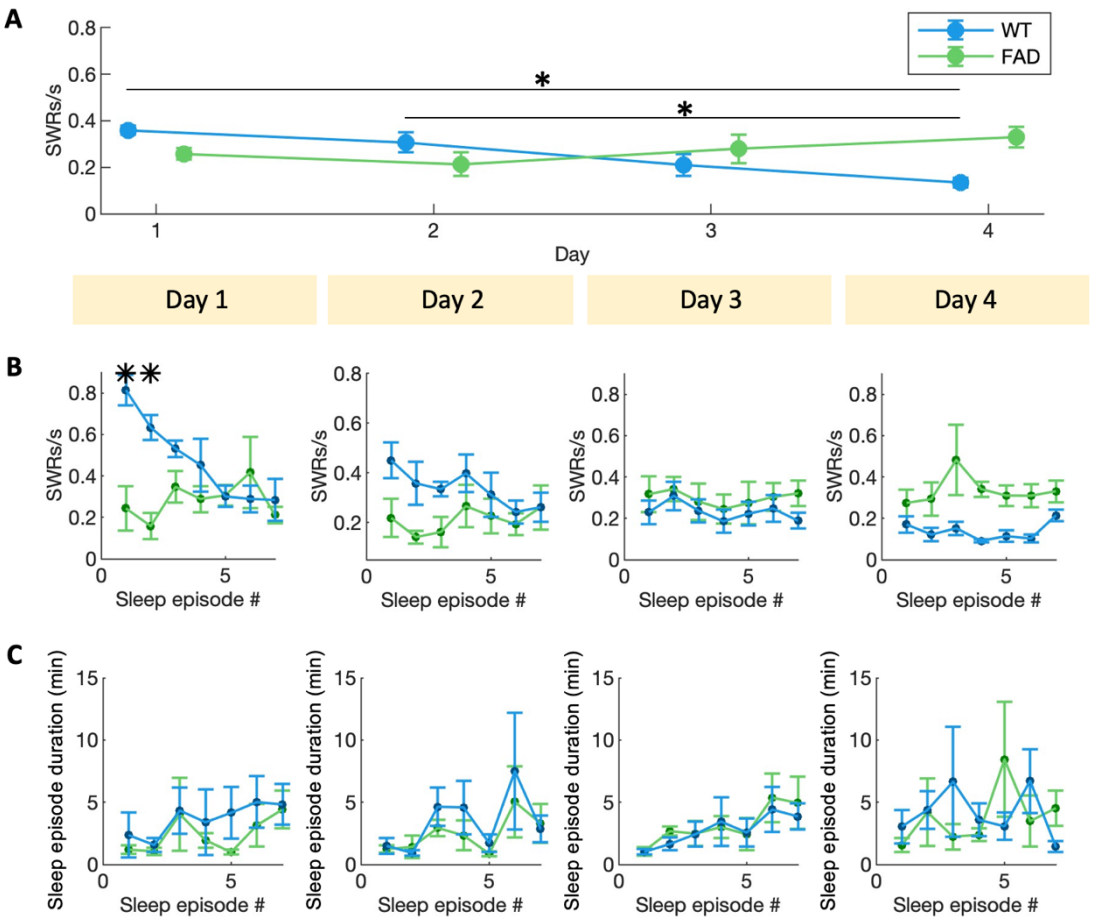

Figure 3.1.4 Occurrence of SWRs across recordings and NREM episodes. A) *Average SWRs/s of WT (n = 6, blue) and FAD+ (n = 6, green) mice across recording days. Post-hoc Tukey HSD test, * p < 0.05.* ***B)*** *Average SWRs/s across NREM episodes of WT (n = 6, blue) and FAD+ (n = 6, green) mice across recording days. Post-hoc Tukey HSD test, * p < 0.05.* ***C)*** *Average duration of sleep episodes in minutes of WT (n = 6, blue) and FAD+ (n = 6, green) mice across recording days.*

Repeated measures ANOVA revealed a significant effect of the recording day ($F(3, 21) = 3.1$, $p = 0.049$) and a significant interaction between recording day and genotype ($F(3, 21) = 5.77$, $p = 0.005$). Post-hoc comparison using Tukey honest significant difference (HSD) test revealed significant differences in SWR frequency for WT mice, where the SWR frequencies on day 1 ($p = 0.038$) and day 2 ($p = 0.004$) were significantly lower than on day 4. No significant differences were found in FAD+ mice across recording days (Figure 3.1.4 A).

These findings indicate that WT mice exhibit a higher number of SWRs than FAD+ mice when sleeping in a novel environment with the numbers of SWRs decreasing over the following days as the environment becomes familiar, while the number of SWRs in FAD+ mice is unchanged in the context of novelty and familiarisation.

To investigate whether SWR frequency changes within recordings, i.e. across NREM episodes, and if such changes are consistent between WT and FAD+ mice, 2-way ANOVAs were conducted for each recording day (Figure 3.1.4 B). As the total number of NREM episodes varied between recording days and mice, the first 7 episodes were analysed to keep the sample number consistent across groups and recording days.

A significant effect of genotype on SWR frequency was found in the day 1 recording ($F(1, 70) = 17.44$, $p < 0.001$), indicating that WT mice showed significantly more SWR than FAD+ mice across sleep episodes. Additionally, a significant main effect of sleep episode number was found ($F(8, 70) = 2.29$, $p = 0.04$) as well as a significant interaction effect between genotype and sleep episode number ($F(8, 70) = 4.34$, $p < 0.001$). Post-hoc comparison using HSD test revealed significant differences in SWR frequency between WT and FAD+ mice during sleep episode 1 ($p < 0.001$) and sleep episode 2 ($p = 0.01$).

On day 2, a significant effect of genotype on SWR frequency was found ($F(1, 70) = 12.05$, $p < 0.001$). No significant main effect of sleep episode number was found ($F(6, 70) = 0.83$, $p = 0.55$) and no significant interaction effect between genotype and sleep episode number ($F(6, 70) = 0.08$, $p = 0.57$). Post-hoc comparison using Tukey HSD test revealed no significant differences in SWR frequency between WT and FAD+ mice among sleep episodes.

On day 3, no significant effect of genotype ($F(1, 70) = 3.25$, $p = 0.08$) or sleep episode number ($F(6, 70) = 0.48$, $p = 0.82$) was found as well as no significant interaction ($F(6, 70) = 0.12$, $p = 0.99$). On day 4, a significant effect of genotype on SWR frequency was found ($F(1, 42) = 15.96$, $p < 0.001$). No significant main effect of sleep episode number was found ($F(6, 42) = 0.92$, $p = 0.49$) and no significant interaction effect between genotype and sleep episode number ($F(6, 42) = 0.76$, $p = 0.60$). Post-hoc comparison using Tukey HSD test revealed no significant differences in SWR frequency between WT and FAD+ mice among sleep episodes (Figure 3.1.4 B).

Since SWR frequency was found to change among sleep episodes with a significant interaction with the genotype on day 1, the durations of sleep episodes were compared between WT and FAD+ mice for each recording day. This analysis was performed to rule out significant differences between genotypes in early sleep episodes undiscovered in the previous investigation of sleep architecture.

To test if sleep episode duration changes within recordings and if such changes are consistent between WT and FAD+ mice, 2-way ANOVAs were conducted for each recording day (Figure 3.1.4 C).
No significant effect of genotype on the duration of NREM episodes was found on day 1 ($F(1, 70) = 1.97$, $p = 0.17$). There was also no significant effect of sleep episode number ($F(6, 70) = 1.15$, $p = 0.34$) and no significant interaction between genotype and sleep episode number ($F(6, 70) = 0.18$, $p = 0.98$).
On day 2, no significant effect of genotype ($F(1, 70) = 0.99$, $p = 0.32$), sleep episode number ($F(6, 70) = 2.14$, $p = 0.06$) or interaction ($F(6, 70) = 0.24$, $p = 0.96$) was found.
Similarly, no significant effect of genotype ($F(1, 70) = 0.29$, $p = 0.59$), sleep episode number ($F(6, 70) = 2.18$, $p = 0.06$) and interaction ($F(6, 70) = 0.12$, $p = 0.99$) was found on day 3.
Lastly, no significant effect of genotype ($F(1, 70) = 0.17$, $p = 0.68$), sleep episode number ($F(6, 70) = 0.48$, $p = 0.82$) and interaction ($F(6, 70) = 0.88$, $p = 0.52$) was found on day 4 (Figure 3.1.4 C).
These results indicate that sleep episode durations are not significantly different between FAD+ and WT mice and that duration of these NREM episodes do not significantly differ among sleep episode numbers. It can be concluded that increases in SWRs in early sleep episodes observed in WT mice are unlikely to be due to differences in NREM episode durations.

Since sex differences in regard to AD pathology progression and sleep changes are known to be present in human AD patients (Johnson, Duncan, & Murphy, 2024), potential sex differences in SWR occurrence in WT and FAD+ mice were investigated by performing t-tests for each day and 2-way ANOVAs along sleep episodes for each day separately for each genotype group.

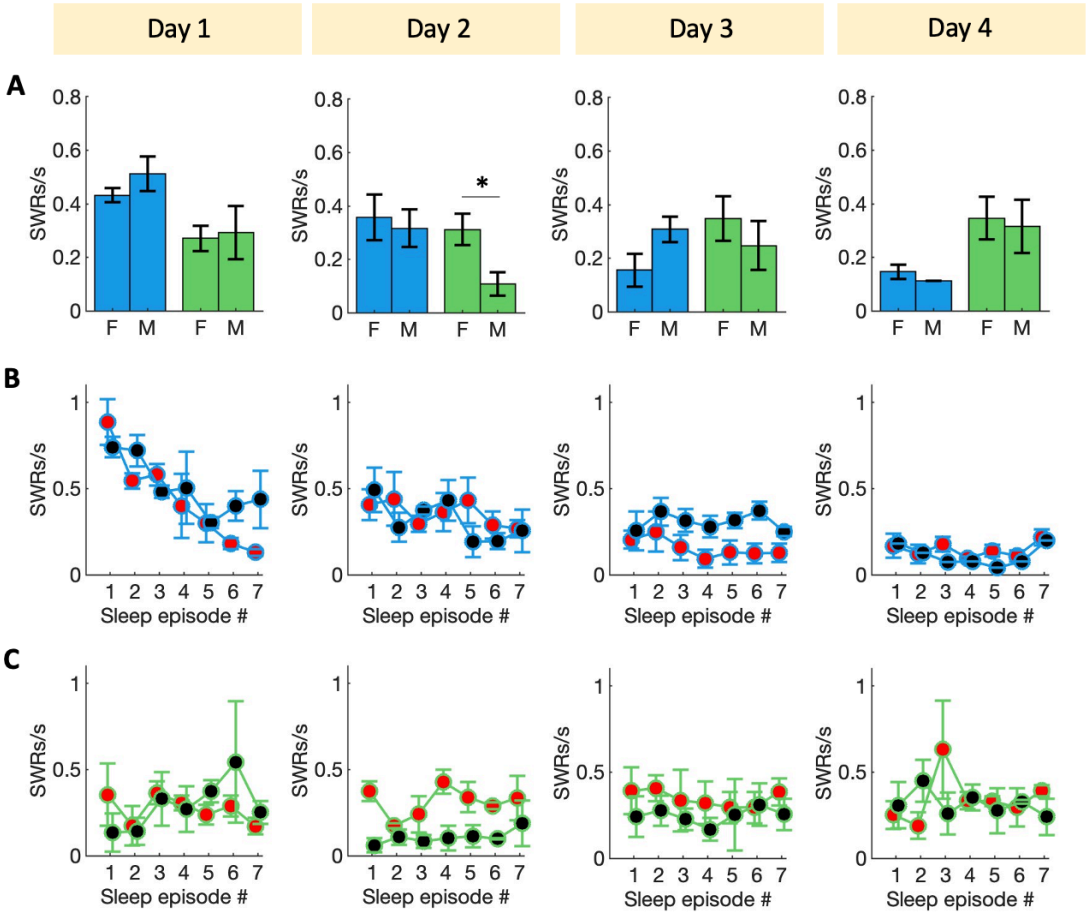

Figure 3.1.5 Sex differences in SWR occurrence. A) *Average SWRs/s of female WT (n = 3, blue), male WT (n = 3, blue), female FAD+ (n = 3, green) and male FAD+ (n = 3, green) mice across recording days. T-test, * p < 0.05.* ***B)*** *Average SWRs/s across NREM episodes of female WT (n = 3, red) and male WT (n = 3, black) mice across recording days.* ***C)*** *Average SWRs/s across NREM episodes of female FAD+ (n = 3, red) and male FAD+ (n = 3, black) mice across recording days.*

The average number of SWRs/s on each recording day was assessed for female and male mice separately to investigate potential sex differences. T-test between sexes in both groups of genotypes revealed no significant differences on day 1 (WT p = 0.32, FAD+ p = 0.85), day 3 (WT p = 0.12, FAD+ p = 0.46) and day 4 (WT p = 0.58, FAD+ p = 0.84). On day 2, however, a significant difference was found in FAD+ mice where females exhibited more SWRs than male mice (p = 0.049). No significant difference was found between female and male WT mice on day 2 (p = 0.73) (Figure 3.1.5 B-C).

Next, we investigated potential sex differences in SWR occurrence along sleep episodes, performing 2-way ANOVAs.

In WT mice, no significant main effect of sex was found on day 1 ($F(1, 28) = 1.93$, $p = 0.18$), day 2 ($F(1, 28) = 0.57$, $p = 0.45$), on day 4 ($F(1, 14) = 0.24$, $p = 0.64$) and no significant interaction between sex and sleep episode on day 1 ($F(6, 28) = 1.22$, $p = 0.33$), day 2 ($F(6, 28) = 0.86$, $p = 0.54$) and day 4 ($F(6, 14) = 0.23$, $p = 0.96$). On day 3, however, a significant main effect of sex was found ($F(1, 28) = 16.65$, $p < 0.001$) with no significant interaction between sex and sleep episode ($F(6, 28) = 0.41$, $p = 0.87$). HSD post-hoc test revealed no significant difference between male and female WT mice across sleep episodes (Figure 3.1.5 B).
In FAD+ mice, no significant main effect of sex was found on day 1 ($F(1, 28) = 0.09$, $p = 0.77$), on day 3 ($F(1, 28) = 2.59$, $p = 0.12$), day 4 ($F(1, 21) = 0.35$, $p = 0.56$) and no significant interaction between sex and sleep episode on day 1 ($F(6, 28) = 0.64$, $p = 0.69$), day 3 ($F(6, 28) = 0.15$, $p = 0.99$) and day 4 ($F(6, 21) = 0.69$, $p = 0.66$). On day 2, a significant main effect of sex was found ($F(1, 28) = 26.87$, $p < 0.001$) with no significant interaction between sex and sleep episode number ($F(6, 28) = 0.81$, $p = 0.57$). Tukey HSD post-hoc tests showed no significant difference between male and female FAD+ mice among sleep episodes (Figure 3.1.5 C).

Together, these results indicate a higher frequency of SWR occurrence during early sleep episodes in WT mice when sleeping in a novel environment. In WT mice, this higher number of SWRs seems to diminish over days as the environment becomes familiar. In FAD+ mice, SWR numbers did not change across recording days, indicating abnormalities in SWR occurrence in the AD mouse model.

To assess a potential correlation between the low number of SWR in FAD+ mice and the amount of plaque in the hippocampus, we compared the plaque load of each mouse to the SWR rate during the first sleep episode on the first recording day, since this was the sleep episode that showed the biggest difference between genotypes in regards to SWR occurrence (Figure 3.1.6).

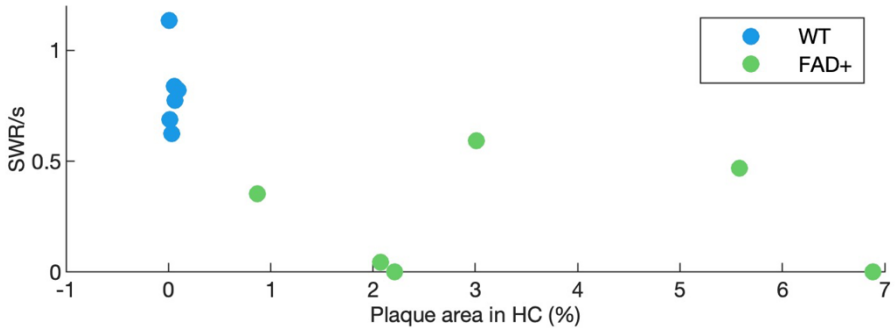

Figure 3.1.6 Correlation between plaque load and SWR frequency in a novel environment. *Percentage of HC area covered in plaque and SWR rate of WT mice (n = 6, blue) and FAD+ mice (n = 6, green) in the first sleep episode in a novel environment.*

Pearson's correlation coefficient was computed and statistical correlation was assessed. No significant correlation was found for WT mice (r = -0.17, p = 0.74) and FAD mice (r = -0.0724, p = 0.89). These findings indicate no correlation between the plaque burden in the HC and SWR occurrence in response to novelty.

Since a previous study has indicated a connection between long-duration SWRs and increased memory demand in rats (Fernández-Ruiz et al., 2019), we wanted to investigate the durations of SWR and potential changes over the 4 recording days, as well as potential differences between WT and FAD+ mice. First, the average duration of SWRs of WT mice and FAD+ mice were analysed for each recording day (Figure 3.1.7 A).

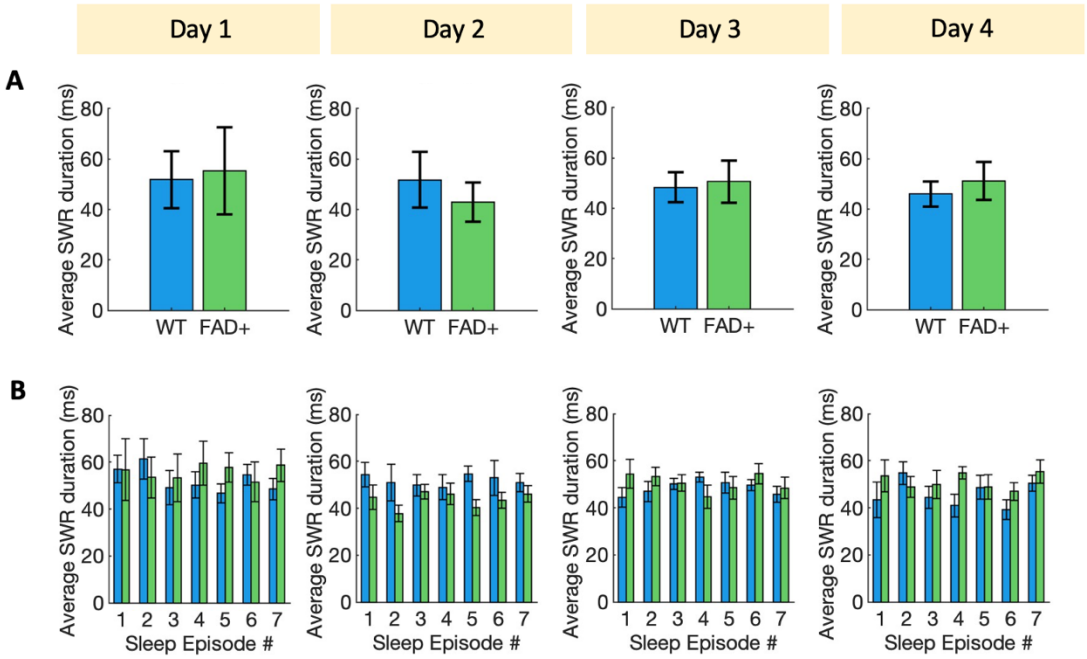

Figure 3.1.7 Average duration of SWRs across recordings and NREM episodes. A) *Average duration of SWR events in ms on each recording day (WT n = 6, blue. FAD+ n = 6, green).* ***B)*** *Average duration of SWR events in ms across sleep episodes (WT n = 6, blue. FAD+ n = 6, green). Post-hoc Tukey HSD test, * p < 0.05.*

T-tests revealed no significant differences between the average duration of SWRs of WT and FAD+ mice on day 1 (p = 0.67), day 2 (p = 0.14), day 3 (p = 0.59) and day 4 (p = 0.25). Since an increase of SWRs was observed during the early sleep episodes in the WT mice on the first recording day, the average duration of SWR was also investigated for each sleep episode on each day to examine differences between WT and FAD+ mice (Figure 3.1.7 B). Repeated measures ANOVA revealed no significant main effect of genotype on day 1 ($F(1, 6) = 0.62$, $p = 0.46$), on day 2 ($F(1, 10) = 2.37$, $p = 0.15$), on day 3 ($F(1, 9) = 0.11$, $p = 0.75$) and day 4 ($F(1, 7) = 1.41$, $p = 0.27$). Furthermore, no significant interaction of genotype and sleep episode was found on day 1 ($F(1, 6) = 1.28$, $p = 0.3$), on day 2 ($F(1, 10) = 2.18$, $p = 0.17$), on day 3 ($F(1, 9) = 0.03$, $p = 0.86$), and on day 4 (1, 7) = 2.09, p = 0.19). (Figure 3.1.7 B).

These findings indicate no differences between WT and FAD+ mice in regard to their average SWR durations.

3.1.3 Sleep spindles are unchanged during NREM sleep in a novel environment

Since we found FAD+ mice to show a lack of novelty-modulated high number of SWRs, we next wanted to investigate whether sleep spindle occurrence is also novelty-modulated and whether their occurrence is reduced in FAD+ mice. Therefore, sleep spindles were detected during NREM sleep episodes using a 2-threshold detection method (see chapter 2.5.1.3). Inspection of the raw trace of a single sleep spindle event (Figure 3.1.8 A, top), 10 - 15 Hz filtered trace of the event (Figure 3.1.8 A, middle) and current wavelet transform (Figure 3.1.4 8, bottom) showed the characteristic spindle waveform and increase in 10 - 20 Hz frequency power shortly after the detected onset of the sleep spindle event. The characteristic spindle waveform was preserved across the mean of 57 raw traces of sleep spindle events from a single recording session of a WT mouse (Figure 3.1.8 B, top), as well as across the mean of 57 filtered traces (Figure 3.1.8 B, middle). The average current wavelet transform of these 57 sleep spindle events showed a strong increase in the 12 - 15 Hz frequency range just after the sleep spindle onset which diminished roughly 1000 ms after the onset. A smaller increase in this frequency range is found between 1000 - 2000 ms after the detected onset, indicating a fraction of sleep spindles of a duration longer than 1000 ms (Figure 3.1.8 B, bottom).

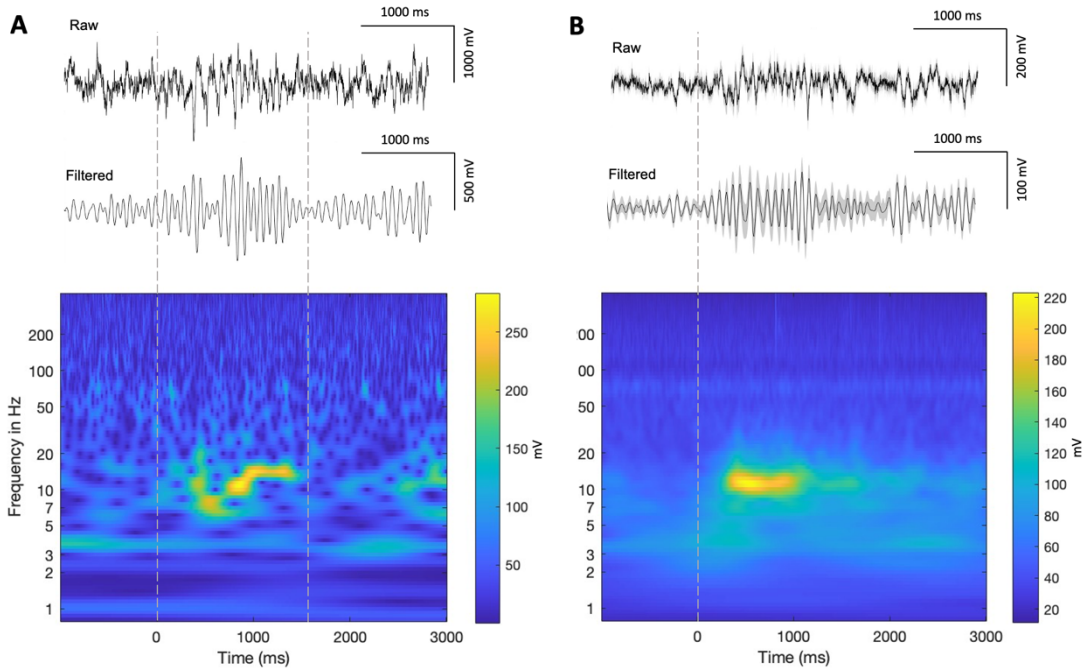

Figure 3.1.8 Time-frequency profile of sleep spindles. A) *Top: raw trace of a single sleep spindle event. Middle: event filtered in 10 – 15 Hz passband with 3 – 22 Hz stopband. Bottom: time frequency representation (current wavelet transform) of single sleep spindle event. Dashed lines represent sleep spindle onset and offset.* ***B)*** *Top: mean of n = 57 raw sleep spindle traces. Shaded area indicates standard error of mean. Middle: mean of n = 57 sleep spindle traces, filtered in 10 – 15 Hz passband with 3 – 22 Hz stopband. Shaded area indicates standard error of mean. Bottom: mean time-frequency representation (current wavelet transform) of 57 sleep spindles. Dashed line represents sleep spindle onsets.*

To test the hypothesis that sleep spindles are abnormal in AD, we assessed the average sleep spindle occurrence and durations across the 4 recording days. First, the average occurrence of sleep spindles for WT and 5xFAD mice was compared across recording day and statistical significance was assessed using repeated measures ANOVA (Figure 3.1.9 A).

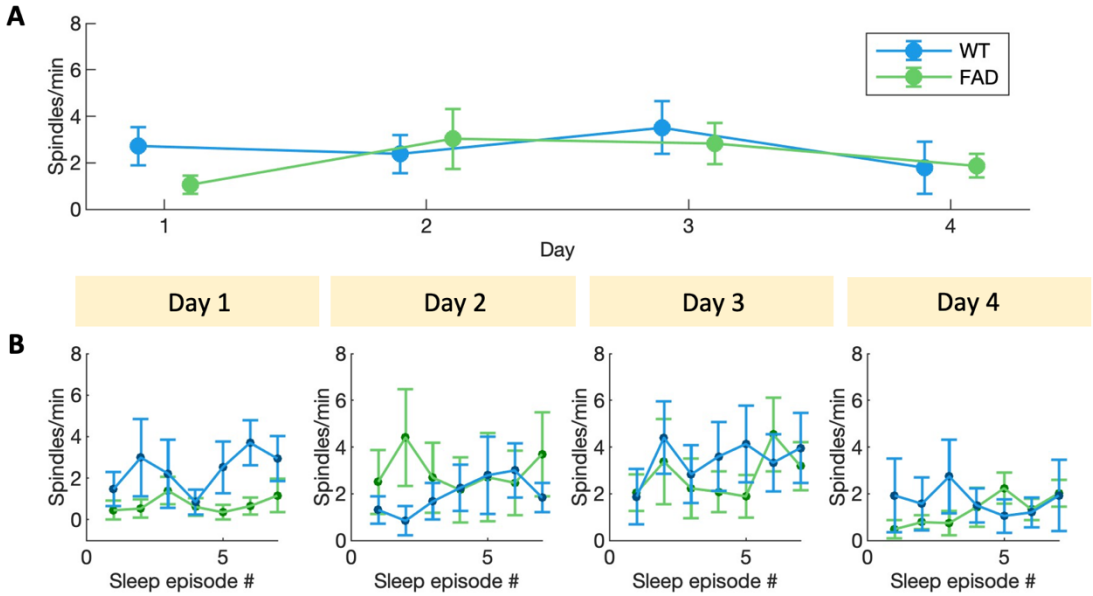

Figure 3.1.9 Occurrence of sleep spindles across recordings and NREM episodes. A) *Average sleep spindles/min of WT (n = 6, blue) and FAD+ (n = 6, green) mice across recording days.* ***B)*** *Average sleep spindles/min across NREM episodes of WT (n = 6, blue) and FAD+ (n = 6, green) mice across recording days.*

Repeated measures ANOVA revealed no significant main effect of recording day ($F(3, 21) = 1.01$, $p = 0.38$) and no significant interaction of recording day and genotype ($F(3, 21) = 0.49$, $p = 0.69$) (Figure 3.1.9 A). These results indicate that sleep spindle occurrence is not modulated by novel experience and not abnormal in FAD+ mice.

However, since we had previously found differences in SWRs across sleep episodes, we wanted to examine the occurrence of sleep spindles across sleep episodes to look for subtle differences undetected by the mean frequency taken across the whole recording days.

Using 2-way ANOVA, the influence of sleep episode number and genotype on sleep spindle frequency was investigated.

A significant effect of genotype on sleep spindle frequency was found in the day 1 recording ($F(1, 70) = 10.12$, $p = 0.002$), indicating a significant difference in sleep spindle frequency between FAD+ and WT mice. However, no significant effect of sleep episode number was found ($F(6, 70) = 0.63$, $p = 0.71$) and no significant interaction effect between genotype and sleep episode number ($F(6, 70) = 0.53$, $p = 0.78$). Post-hoc comparison using Tukey HSD test revealed no significant differences in sleep spindle frequency between WT and FAD+ mice among sleep episodes. On day 2, no significant effect of genotype on sleep spindle frequency

was found (F(1, 70) = 1.86, p = 0.18), as well as no significant effect of sleep episode number (F(6, 70) = 0.13, p = 0.99) and no significant interaction effect between genotype and sleep episode number (F(6, 70) = 0.55, p = 0.77). Similarly, no significant effect of genotype on sleep spindle frequency was found on day 3 (F(1, 70) = 0.93, p = 0.34), as well as no significant effect of sleep episode number (F(6, 70) = 0.61, p = 0.72) and no significant interaction effect between genotype and sleep episode number (F(6, 70) = 0.36, p = 0.9). No significant effect of genotype on sleep spindle frequency was found on day 4 (F(1, 70) = 0.02, p = 0.89), as well as no significant effect of sleep episode number (F(6, 70) = 0.19, p = 0.98) and no significant interaction effect between genotype and sleep episode number (F(6, 70) = 0.54, p = 0.77) (Figure 3.1.9 B).

Next, potential sex differences within each genotype group were investigated using n-way ANOVA for each recording day. In WT mice, no main effect of sex on the sleep spindle occurrence was found on day 1 (F(1, 28) = 2.8, p = 0.11), on day 2 (F(1, 28) = 1.26, p = 0.27), day 3 (F(1, 28) = 0.61, p = 0.44) and day 4 (1, 28) = 0.1, p = 0.76). Further, no significant interaction between sex and sleep episode number was found on day 1 (F(6, 28) = 1.74, p = 0.15), day 2 (F(6, 28) = 0.96, p = 0.47), day 3 (F(6, 28) = 93, p = 0.49) and day 4 (F(1, 28) = 1.1, p = 0.41). In FAD+ mice, there was also no significant main effect of sex on the sleep spindle occurrence on day 1 (F(1, 28) = 0.88, p = 0.36), day 2 (F(1, 28) = 0, p = 0.96), day 3 (F(1, 28) = 1.16, p = 0.29) and day 4 (F(1, 21) = 0.65, p = 0.43). Further, no significant interaction between sex and sleep episode number was found on day 1 (F(6, 28) = 0.65, p = 0.69), day 2 (F(6, 28) = 1.08, p = 0.4), day 3 (F(6, 28) = 0.44, p = 0.85) and day 4 (F(6, 21) = 2.16, p = 0.09) in FAD+ mice.

These findings indicate that there are no abnormalities in sleep spindle frequency in FAD+ mice and that sleep spindles do not change across recording days or sleep episodes in WT mice as they become familiar with the novel environment.

Next, the duration of all sleep spindle events of WT mice and FAD+ mice were analysed for each recording day (Figure 3.1.10 A).

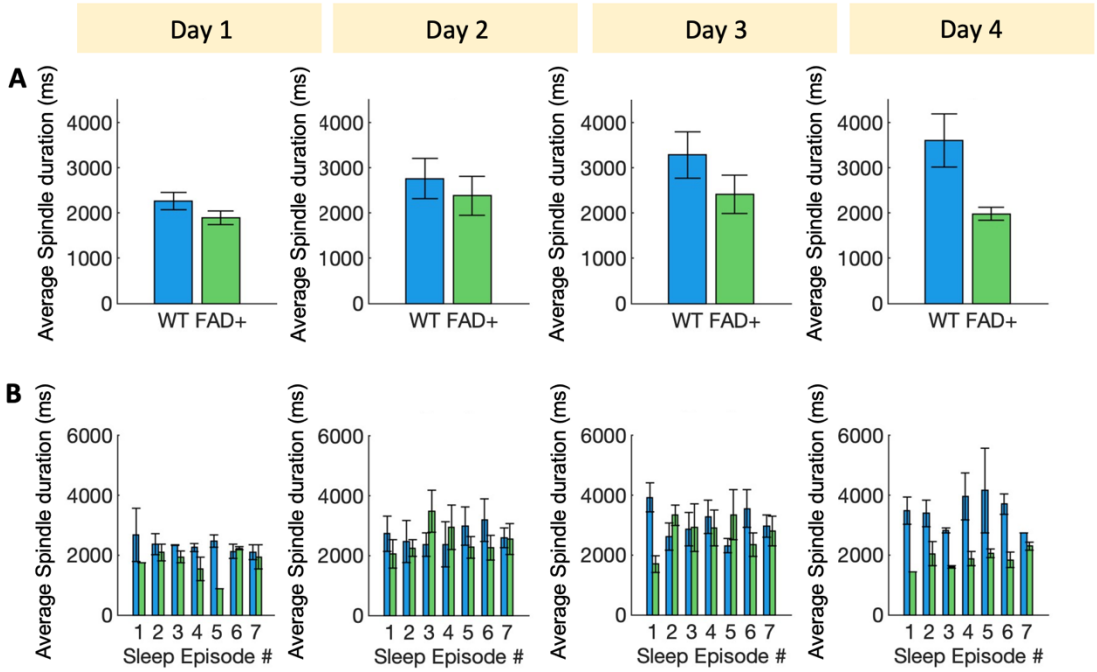

Figure 3.1.10 Average duration of sleep spindles across recordings and NREM sleep episodes. A) *Average duration of sleep spindle events of WT(n = 6, blue) and FAD+ mice (n = 6, green).* ***B)*** *Average duration of sleep spindle events of WT(n = 6, blue) and FAD+ mice (n = 6, green) across sleep episode on each recording day.*

No significant differences between the average duration of sleep spindles of WT and FAD+ mice were found on day 1 ($p = 0.25$), day 2 ($p = 0.6$), day 3 ($p = 0.26$) and day 4 ($p = 0.15$) (Figure 3.1.10 A).

To investigate potential differences across sleep episodes, the average sleep spindle durations for each sleep episode on each day were assessed. Since some sleep episode did not have enough sleep spindle events, repeated measures ANOVA could not be conducted. Therefore, multiple t-tests with Bonferroni correction were performed. No significant differences were found between genotypes across sleep episodes on all recording days (Figure 3.1.10 B).

Overall, our findings suggest that sleep spindle occurrence is unaffected by the experience of sleeping in a novel environment. Further, the occurrence and average duration of sleep spindles does not appear to be abnormal in FAD+ mice.

3.1.4 Spectral analysis of EEG and hippocampal LFP during NREM sleep

Next, we examined the spectral power in the HC and cortex during sleep of 6 frequency bands: SWR range (140 – 250 Hz), high gamma (53 – 80 Hz), low gamma (30 – 47 Hz), alpha (10 -15 Hz), theta (4 – 10 Hz) and delta (1 – 4 Hz). Frequencies around 50 Hz were excluded from analysis to avoid contamination caused by 50 Hz noise in some recordings. Analysis was performed for each recording day (Figure 3.1.11 A, Figure 3.1.12 A) and for each individual sleep episode for each day (Figure 3.1.11 B, Figure 3.1.12 B).

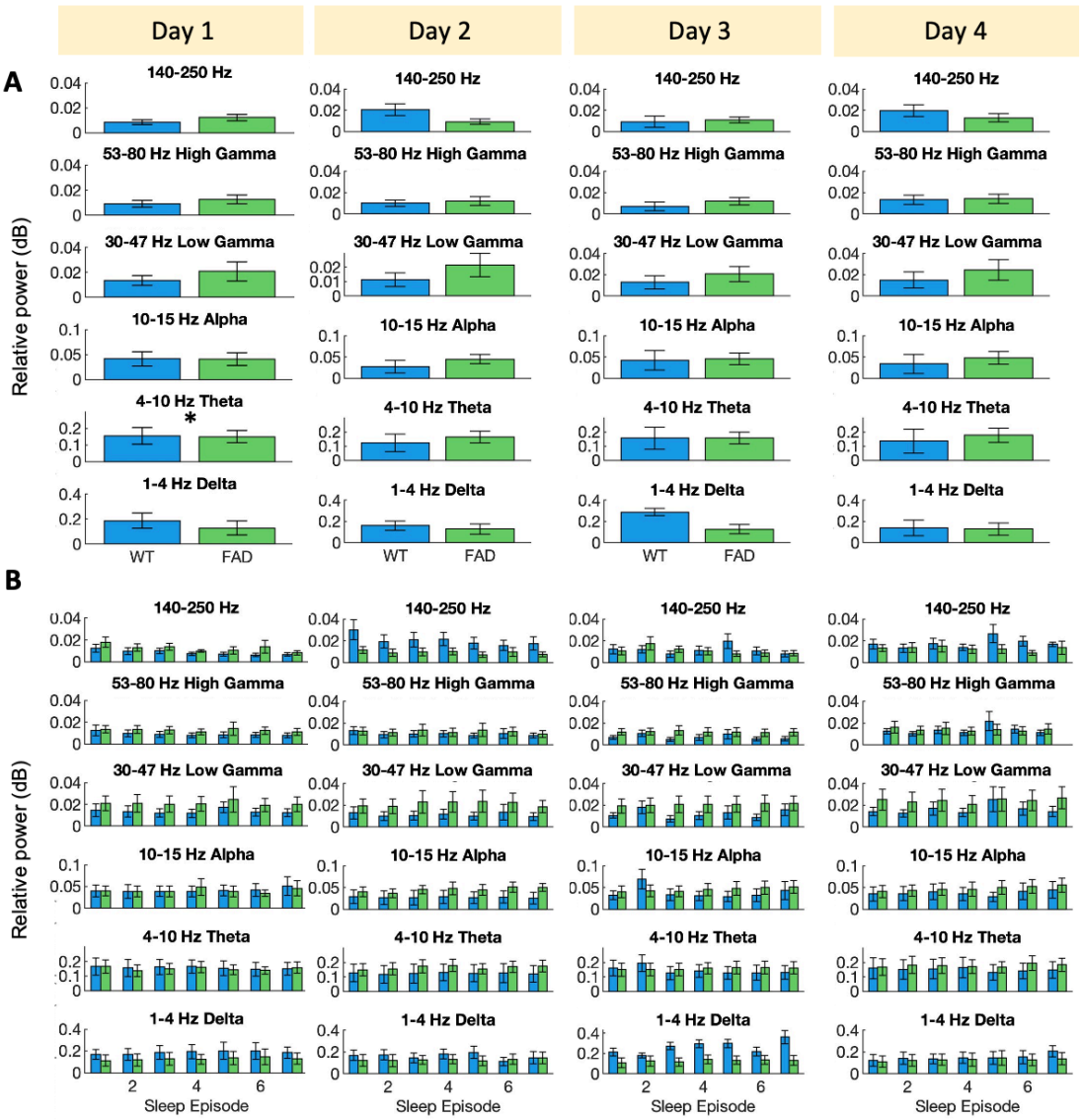

Figure 3.1.11 Relative power of EEG frequency bands during NREM sleep. A) *Average power of frequency bands normalised by the average power of 1 – 40 Hz across recording days of WT (n = 6, blue) and FAD+ mice (n = 6).* ***B)*** *Average power of frequency bands normalised by the average power of 1 – 40 Hz across sleep episodes on all recording days of WT (n = 6, blue) and FAD+ mice (n = 6).*

To examine differences between WT and FAD+ mice, t-tests were conducted for each frequency band on each recording day. A significant difference was found on day 1 in the theta band ($p = 0.045$) where WT mice showed a higher theta power during NREM sleep compared to FAD+ mice (Figure 3.1.11 A). No significant difference was found among the other frequency bands or among the other recording days. Next, differences among individual sleep episodes were examined using repeated measures ANOVA (Figure 3.1.11 B). For the delta range, a significant main effect of genotype was found on day 3 ($F(1, 13) = 6.66$, $p = 0.023$)

and a significant interaction between genotype and sleep episode ($F(1, 13) = 7.65$, $p = 0.016$). No significant difference was found between genotypes on any other day or among any other frequency range.

Next, the same analysis was performed for frequencies in the HC during NREM sleep (figure 3.1.12).

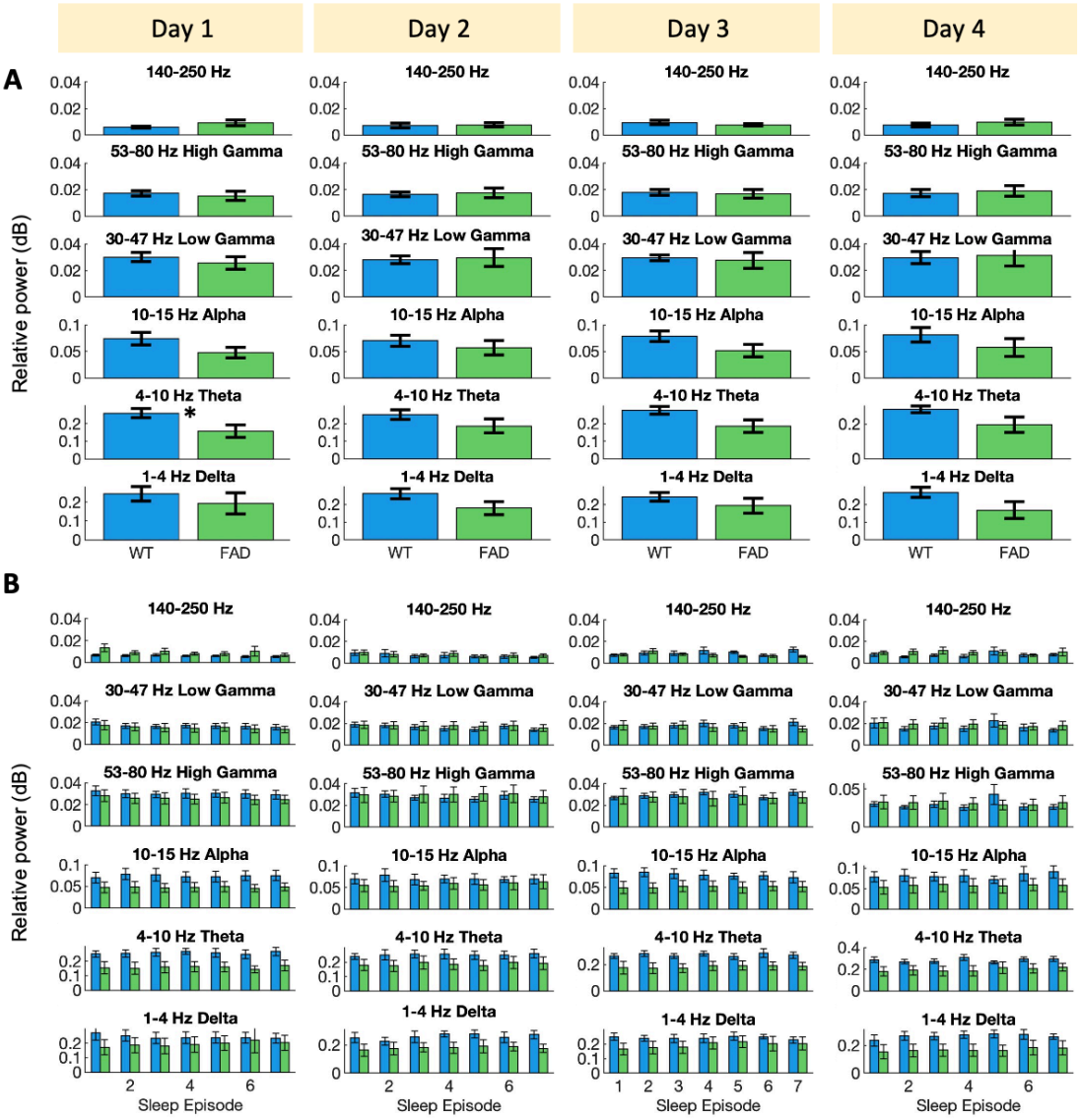

Figure 3.1.12 Relative power of hippocampal frequency bands during NREM sleep. A) *Average power of frequency bands normalised by the average power of 1 – 40 Hz across recording days of WT (n = 6, blue) and FAD+ mice (n = 6).* ***B)*** *Average power of frequency bands normalised by the average power of 1 – 40 Hz across sleep episodes on all recording days of WT (n = 6, blue) and FAD+ mice (n = 6).*

To examine differences between WT and FAD+ mice, t-tests were conducted for each frequency band on each recording day. Like in the EEG, a significant difference was found in the HC only on day 1 in the theta band ($p = 0.045$) where WT mice showed a higher theta power during NREM sleep compared to FAD+ mice (Figure 3.1.12 A). No significant difference was found among the other frequency bands or among the other recording days. Next, differences among individual sleep episodes were examined using repeated measures ANOVA (Figure 3.1.12 B). For the theta range, a significant main effect of genotype was found on day 1 ($F(1, 13) = 5.36$, $p = 0.043$) and on day 3 ($F(1, 13) = 5.53$, $p = 0.035$), as well as a significant interaction between genotype and sleep episode on day 1 ($F(1, 13) = 5.61$, $p = 0.035$) and day 3 ($F(1, 13) = 5.23$, $p = 0.039$). No significant difference was found between genotypes on any other day or among any other frequency range.

3.1.5 Summary

In this chapter we explored SWRs, sleep spindles and the power of various frequency bands in the context of sleeping in a novel environment and how they change as the environment becomes familiar.

We found that WT mice show a high number of SWRs when sleeping in a novel environment which diminished as the environment becomes familiar. We found that this high number in SWRs is absent in FAD+ mice. Similarly, we found a higher theta power during NREM sleep on the first recording day only in WT but not FAD+ mice. Since FAD+ mice showed no abnormalities in sleep architecture, the absence of more SWR and higher theta power is unlikely to be due to fundamental differences in overall sleep time or fragmentation. We found no changes in sleep spindles in the context of novelty or familiarity and no abnormalities in FAD+ mice.

3.2 Sharp-wave ripples and sleep spindles before and after novel object recognition test

Our findings described in section 3.1 indicated a novelty-modulated high number of SWRs to occur in WT mice while sleeping in a novel environment. This increase was absent in FAD+ mice. A reduction of SWRs across days was found in WT mice, suggesting a familiarisation process to the environment accompanied by a reduced need for memory consolidation. However, there is no proof that the initial increase in SWRs in WT mice lead to the consolidation of memories of the novel environment and that WT mice remember the environment on the following days while FAD+ mice do not. To overcome this considerable limitation, we decided to investigate changes in SWRs and sleep spindles in the context of the novel object recognition test in week 2. Unlike week 1, brain activity during sleep was now recorded in the home cage – a more natural and familiar setting – instead of the open field box.

On day 0, a 1.5 h habituation recording was conducted. Even though mice were sleeping in their home cage, being in the tethered condition and differences in smells, noises and lighting condition in the experimental room compared to the familiar holding room, could still present a novel experience. On the following 4 days, mice underwent 1h baseline recordings (B1 - B4) in their home cage each day. After the baseline recording, mice were introduced to the open field box containing two identical objects and were allowed to explore for 10 minutes (TR1 - TR4). After these training sessions, mice were placed back in their home cage for a 1.5 h post-exploration recording (P1 - P4). On the last recording day, this recording session was followed by another exploration session in the open field box, in which one of the objects was replaced by a novel object. This session was the test session, in which each mouses ability to distinguish the novel object from the familiar object was assessed by analysing the time spent exploring the novel object. This test is based on the assumption that natural curiosity towards a new object indicates intact memory of – and reduced interest in – the familiar object. After the test session, mice were placed back into their home cage for a final 1.5 h recording (P5). The experimental flow is depicted in Figure 3.2.1. After a 4 week break the protocol was repeated with new objects.

A total of 12 mice underwent recordings in the first round (week 2). In the second round (week 7), one male WT, one male FAD+ and one female WT mouse were excluded due to bad signal quality.

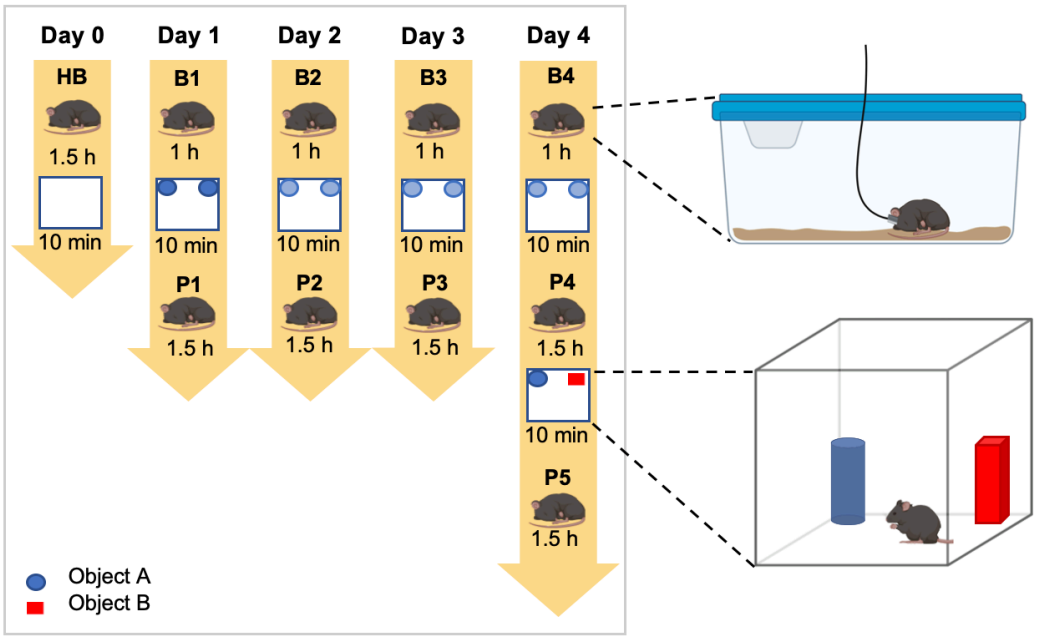

Figure 3.2.1 Recording protocol of home cage recordings and novel object recognition test (NOR) in week 2. *After a habituation recording (HB) in tethered condition in the home cage on day 0, each day started with a 1h baseline recording (B1-B4) in tethered condition in the home cage, followed by 10 min of exploration of 2 identical objects in the open field box in untethered condition and post-exploration recording (P1-P4) in the home cage in tethered condition. On day 4, the post-exploration recording (P4) was followed by another 10 min exploration session in the open field box, now containing a novel object, and another post-exploration recording (P5) in the home cage. Illustrations partially created with BioRender.com*

3.2.1 Sleep architecture across novel object recognition test trials

As a first step, sleep architecture of WT and FAD+ mice was analysed and compared among recordings and between genotypes to investigate potential abnormalities in FAD+ mice. The mean time spent in each state was analysed, along with the average number of episodes per hour and the latency to the first NREM sleep episode.

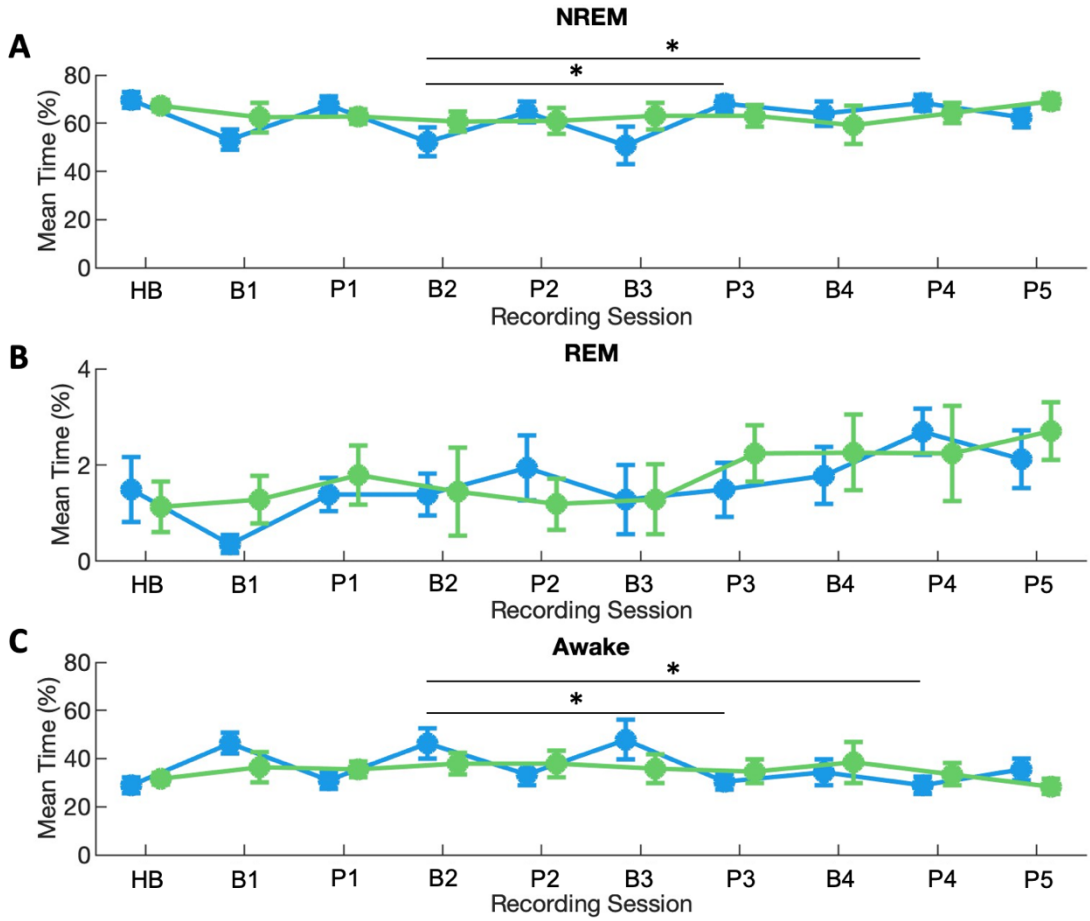

Figure 3.2.2 Sleep architecture assessed as the percentage of time spent in each state of WT and FAD+ mice across habituation (HB), baseline (B) and post-exploration (P) home cage recordings. A) *Percentage of time spent in non-REM (NREM) sleep of WT (n = 10, blue) and FAD+ mice (n = 11, green) across all home cage recording sessions.* ***B)*** *Percentage of time spent in REM sleep of WT (n = 10, blue) and FAD+ mice (n = 11, green) across all home cage recording sessions.* ***C)*** *Percentage of time spent awake for WT (n = 10, blue) and FAD+ mice (n = 11, green) across all home cage recording sessions. Error bars: standard error of mean.*

First, the percentage of time spent in NREM sleep was investigated using repeated measures ANOVA. A significant effect of recording session was found ($F(9, 171) = 2.45$, $p = 0.01$) but no significant interaction of genotype and recording session ($F(9, 171) = 1.6$, $p = 0.12$). Post-hoc comparison using Tukey HSD test revealed significant differences in the percentage of time spent in NREM sleep in WT mice between the baseline 2 recording (B2) and the post exploration recording 3 (P3) ($p = 0.02$) and between the B2 and the post exploration recording 4 (P4) ($p = 0.004$). No significant differences were found in FAD+ mice (Figure 3.2.2 A). Analysis of the percentage of REM sleep showed a significant effect of recording session ($F(9, 171) = 2.07$, $p = 0.03$) but no significant interaction of genotype and recording session ($F(9, 171) = 0.5$, $p = 0.81$) (Figure 3.2.2 B). Post-hoc comparison using Tukey HSD test revealed no significant difference between the percentage of REM sleep across recordings. Analysis of the percentage of awake time showed a significant effect of recording session ($F(9, 171) = 2.52$, $p = 0.01$) but no significant interaction of genotype and recording session ($F(9, 171) = 1.5$, $p = 0.15$). Post-hoc comparison using Tukey HSD test revealed significant differences in the percentage of time spent in NREM sleep in WT mice between the baseline 2 recording (B2) and the post exploration recording 3 (P3) ($p = 0.02$) and between the B2 and the post exploration recording 4 (P4) ($p = 0.003$). No significant differences were found in FAD+ mice (Figure 3.2.2 C).

To further investigate sleep architecture, the average numbers of state episodes per hour were analysed as an indicator for sleep fragmentation among recording sessions and between genotypes.

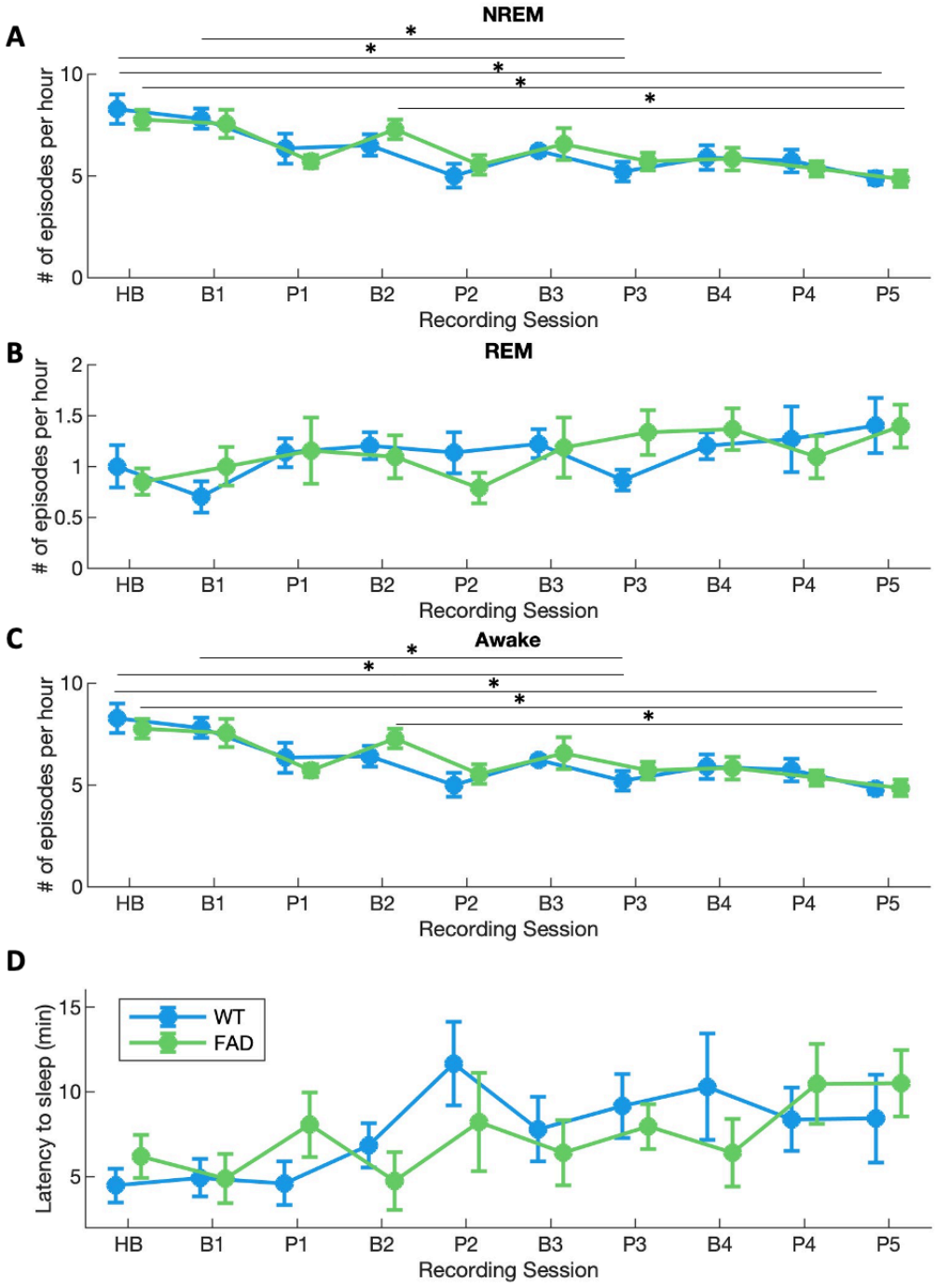

Figure 3.2.3 Sleep architecture assessed as average number of episodes in each state and sleep latency of WT and FAD+ mice across habituation (HB), baseline (B) and post-exploration (P) home cage recordings. A) *Mean number of NREM episodes per hour of WT (n = 10, blue) and FAD+ mice (n = 11, green) across all home cage recording sessions.* ***B)*** *Mean number of REM episodes per hour of WT (n = 10, blue) and FAD+ mice (n = 11, green) across all home cage recording sessions.* ***C)*** *Mean number of awake episodes per hour of WT (n = 10, blue) and FAD+ mice (n = 11, green) across all home cage recording sessions.* ***D)*** *Latency to first NREM sleep episode of WT (n = 10, blue) and FAD+ mice (n = 11, green) across home cage recording sessions. Error bars: standard error of mean.*

A significant effect of recording session on the number of NREM episodes per hour was found ($F(9, 162) = 7.58$, $p < .0001$) but no significant interaction with the genotype ($F(9, 162) = 0.38$, $p = 0.94$). Post-hoc comparison using Tukey HSD test revealed a significant difference for WT mice between the HB recording and P3 recording ($p = 0.01$), between HB and P5 recording ($p = 0.03$) and between B1 and P3 ($p = 0.02$). For FAD+ mice, significant differences were found between the HB and P5 recording ($p = 0.02$), and between B4 and P5 ($p = 0.01$) (Figure 3.2.3 A). The analysis of number of REM episodes per hour showed no effect of recording session ($F(9, 162) = 1.68$, $p = 0.1$) and no interaction with genotype ($F(9, 162) = 0.89$, $p = 0.53$) (Figure 3.2.3 B). Analysis of the number of awake episodes per hour showed a significant recording session effect ($F(9, 162) = 7.64$, $p < 0.001$) and no significant interaction with genotype ($F(9, 162) = 0.41$, $p = 0.93$). Post-hoc comparison using Tukey HSD test revealed significant differences between the HB and P3 recording ($p = 0.01$), between HB and P5 ($p = 0.02$), and between B1 and P3 ($p = 0.02$) for WT mice. In FAD+ mice, significant differences occurred between HB and P5 recording ($p = 0.02$) and between B2 and P5 ($p = 0.005$) (Figure 3.2.3 C).

Finally, the latency to the first NREM episode was compared between FAD+ and WT mice along recording sessions. Repeated measures ANOVA revealed a significant main effect of recording session ($F(9, 162) = 2.6$, $p = 0.01$) and no significant interaction between genotype and recording session ($F(9, 162) = 1.06$, $p = 0.4$). Post-hoc analysis using Tukey HSD, however, revealed no significant differences between recording sessions (Figure 3.2.3 D).

Together, these results indicate subtle differences in sleep architecture in mice along some recording session but no significant difference between WT and FAD+ mice.

3.2.2 Novelty-induced increase in sharp-wave ripples is absent in FAD+ mice

The aim of this experiment was to investigate how the exploration of either novel or familiar objects affects the occurrence of SWRs and sleep spindles in WT and FAD+ mice. First, the number of SWRs/s was compared along recording session and between genotypes, followed by assessment of the change in SWR rate between baseline recordings and post-exploration recordings and finally the average duration of SWR events across recording sessions (Figure 3.2.4).

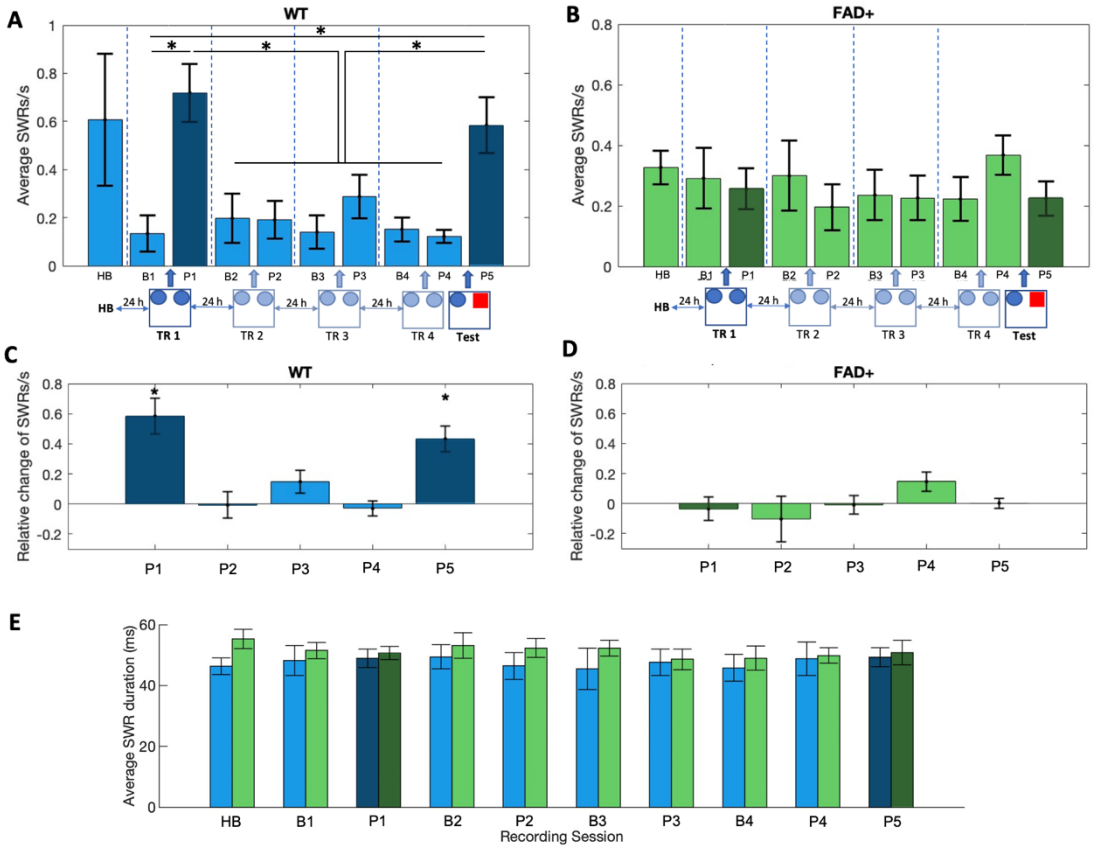

Figure 3.2.4 Occurrence and durations of SWRs in WT and FAD+ mice across habituation (HB), baseline (B) and post-exploration (P) home cage recordings. A) *Average numbers of SWRs/s of WT mice (n = 10) across HB, B and P recording sessions. Bars of darker colour indicate P recordings after a novel exploration experience. Dashed vertical lines are shown to indicate the 5 recording days. Illustrations below the plot indicate the sessions of the NOR test between the B and P recordings with novel experience sessions shown in darker colours. Post-hoc Tukey HSD test, * p < 0.05.* ***B)*** *Average numbers of SWRs/s of FAD+ mice (n = 11) across HB, B and P recording sessions. Bars of darker colour indicate P recordings after a novel exploration experience. Dashed vertical lines are shown to indicate the 5 recording days. Illustrations below the plot indicate the sessions of the NOR test between the B and P recordings with novel experience sessions shown in darker colours.* ***C)*** *Change in SWR/s in P1-P5 recordings relative to respective B1-*

*B4 recording in WT mice (n = 10). T-tests against 0 with Bonferroni correction, * p < 0.05.* ***D)*** *Change in SWR/s in P1-P5 recordings relative to respective B1-B4 recording in FAD+ mice (n = 11).* ***E)*** *Average SWR durations of WT (n = 10, blue) and FAD+ (n = 11, green) mice across HB, B and P recordings.*

An ANOVA investigating the effect of recording session and genotype on the numbers of SWRs/s revealed a significant main effect of recording session ($F(8, 162) = 6.02$, $p < 0.001$), no significant main effect of genotype ($F(1, 162) = 1.77$, $p = 0.19$) and a significant interaction between recording session and genotype ($F(8, 162) = 6.9$, $p < 0.001$). To further assess the differences between recordings and the interaction between recording session and genotype, 1-way ANOVAs were conducted for each genotype group individually. Analysis of the WT group showed a significant main effect of recording session ($F(8, 81) = 9.7$, $p = < 0.001$), but the FAD+ group did not ($F(8, 90) = 1.3$, $p = 0.25$). Post-hoc Tukey HSD test revealed the numbers of SWRs/s in WT mice to be significantly higher in the P1 recording compared to B1 ($p < 0.001$), B2 ($p < 0.001$), P2 ($p < 0.001$) B3($p < 0.001$) , P3 ($p = 0.003$), B4 ($p < 0.001$), and P4 ($p < 0.001$). SWRs were also significantly higher in P5 compared to B1 ($p < 0.001$), B2 ($p = 0.003$), P2 ($p < 0.001$), B3 ($p = 0.001$), P3 ($p = 0.02$), B4 ($p < 0.001$), P4 ($p < 0.001$) (Figure 3.2.4 A). No differences were found among recordings of FAD+ mice (Figure 3.2.4 B). To investigate possible sex differences, 2-way ANOVAs were conducted for WT and FAD+ mice separately to investigate the effect of sex along recordings. A significant main effect of sex was found for WT mice ($F(1, 72) = 11.49$, $p = 0.001$) with no significant interaction between sex and recording session ($F(8, 71) = 0.74$, $p = 0.66$). Post-hoc t-test comparing number of SWRs/s of all recordings combined between WT and FAD+ mice found male WT mice to have significantly more SWRs/s ($p = 0.04$), however multiple t-tests for each recording revealed no significant difference between female and male WT mice. For FAD+ mice, no significant effect of sex ($F(1, 81) = 0.67$, $p = 0.41$) and no significant interaction between sex and recording session ($F(8, 81) = 0.53$, $p = 0.83$) was found. To further quantify how the exploration of objects affects the occurrence of SWRs, the change in SWR rates – relative to the respective baseline session of each day – was computed and t-tests against 0 with Bonferroni correction were conducted to identify post-experience sessions with a significant change in SWR rate. In WT mice, significant increase in SWRs were found in P1 ($p = 0.002$) and P5 ($p < 0.001$) (Figure 3.2.4 C). No significant changes were found in FAD+ mice (Figure 3.2.4 D). We investigated potential sex differences in the relative change in SWRs using Mann-Whitney U tests, since the Shapiro-Wilk test indicated

no normal distribution in some recordings. This analysis revealed no significant differences between sexes in both WT and FAD+ mice.

Our results indicate an increase in the number of SWRs in WT mice only after exploration of objects for the first time. Repeated exploration did not lead to an increase in SWRs. No increase in SWRs was observed in FAD+ mice, indicating abnormalities in SWR occurrence.

The average duration of SWRs was next compare between genotypes for each recording. Repeated measures ANOVA revealed no significant main effect of genotype ($F(1, 19) = 0.66$, $p = 0.43$) and no significant interaction between genotype and recording session ($F(1, 19) = 0.37$, $p = 0.55$) (Figure 3.2.4 E).

These findings indicate that the average duration of SWRs was not abnormal in FAD+ mice and did not change across recording sessions.

3.2.3 No novelty-induced changes in sleep spindles

Since a novelty-induced increase in SWRs was found in WT mice and we found this increase to be absent in FAD+ mice, the occurrence of sleep spindles along recording sessions and between genotypes was investigated in the same fashion. First, the number of sleep spindles per minute was compared along recordings and between genotypes. Then, changes in sleep spindle occurrence after object exploration compared to baseline recordings were determined and compared between recordings and genotypes. Lastly, the average duration of sleep spindles was assessed across recordings and between genotypes.

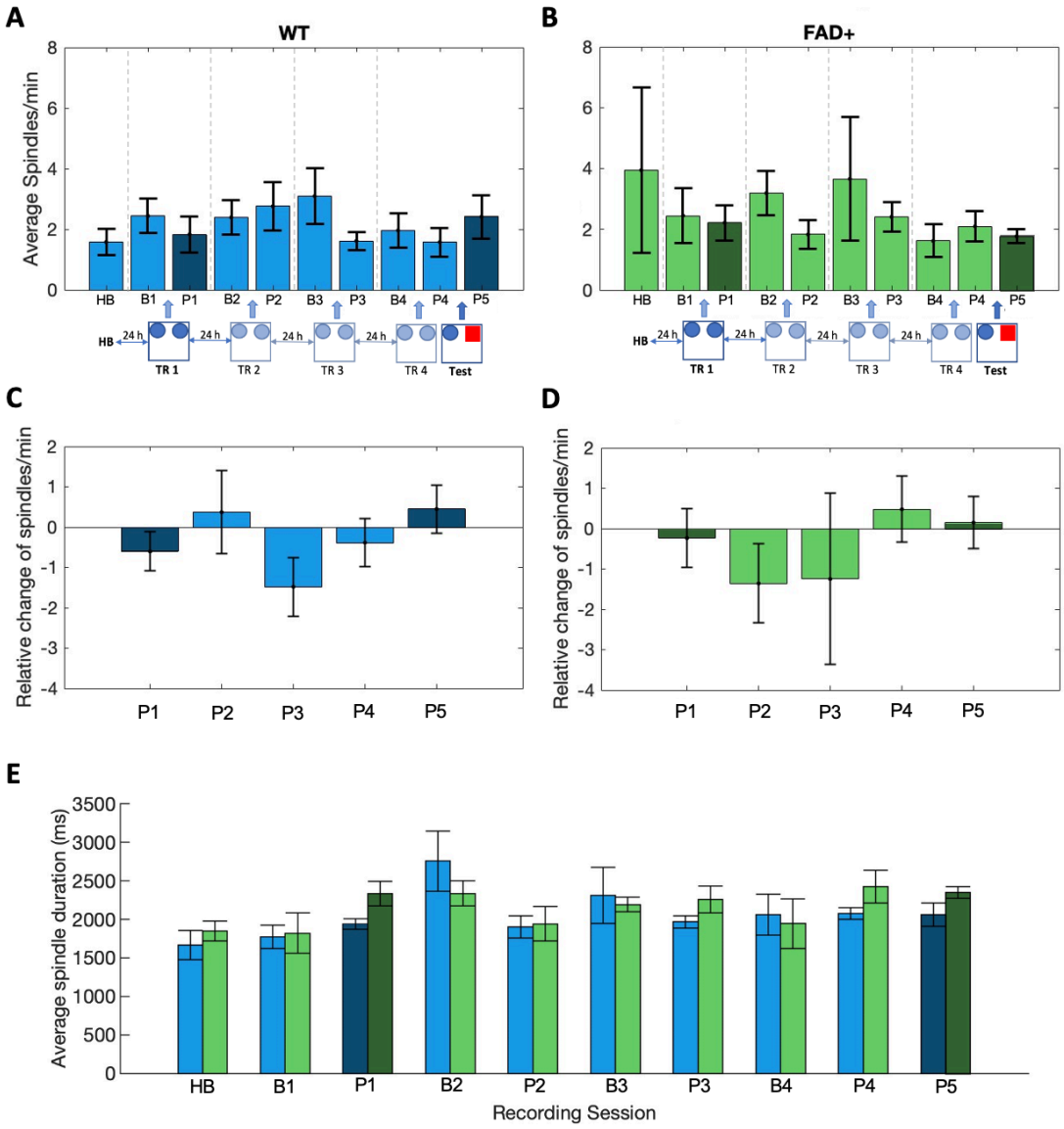

Figure 3.2.5 Occurrence and durations of sleep spindles in WT and FAD+ mice across habituation (HB), baseline (B) and post-exploration (P) home cage recordings. A) *Average numbers of sleep spindles/min of WT mice (n = 10) across HB, B and P recording sessions. Bars of darker colour indicate P recordings after a novel exploration experience. Dashed vertical lines are shown to indicate the 5 recording days. Illustrations below the plot indicate the sessions of the NOR test between the B and P recordings with novel experience sessions shown in darker colours.* ***B)*** *Average numbers of sleep spindles/min of FAD+ mice (n = 11) across HB, B and P recording sessions. Bars of darker colour indicate P recordings after a novel exploration experience. Dashed vertical lines are shown to indicate the 5 recording days. Illustrations below the plot indicate the sessions of the NOR test between the B and P recordings with novel experience sessions shown in darker colours.* ***C)*** *Change in sleep spindles/min in P1-P5 recordings relative to respective B1-B4 recording in WT mice (n = 10).* ***D)*** *Change in sleep spindles/min in P1-P5 recordings relative to respective B1-B4 recording in FAD+ mice (n = 11).* ***E)*** *Average duration of sleep spindles of WT (n = 10, blue) and FAD+ (n = 11, green) mice across HB, B and P recordings. Mann-Whitney U tests, * p < 0.05.*

To investigate differences in sleep spindle occurrence between genotypes and recording sessions, a 2-way ANOVA was conducted. No significant effect of genotype was found ($F(1, 162) = 0.28$, $p = 0.6$), no significant main effect of recording session ($F(8, 162) = 0.9$, $p = 0.52$) and not significant interaction between genotype and recording session ($F(8, 162) = 0.33$, $p = 0.95$). Additional ANOVA for each genotype separately confirmed that there were no differences in sleep spindles along recordings in WT ($F(8, 81) = 0.67$, $p = 0.72$) (Figure 3.2.5 A) or in FAD+ mice ($F(8, 90) = 0.6$, $p = 0.77$) (Figure 3.2.5 B). Next, potential sex differences were investigated. Since the Shapiro-Wilk test indicated no normal distribution of our data in some recording sessions, Mann-Whitney U tests were conducted for WT and FAD+ mice for each recording session. No significant differences between sexes were found.

To further quantify how exploration of objects affects the occurrence of sleep spindles, the change in sleep spindle rates - relative to the respective baseline recording of each day – was computed and t-tests against 0 with Bonferroni correction were conducted to identify post-experience recordings with a significant change in sleep spindle rate. In both WT and FAD+ mice, no significant changes in sleep spindle rate relative to baseline were found (Figure 3.2.5 C-D). Potential sex differences in the change in sleep spindle rate were investigated using Mann-Whitney U tests. No significant differences between sexes were found along recording sessions.

These findings indicate no abnormalities in sleep spindle occurrence in FAD+ mice and no experience-dependent changes in sleep spindle occurrence in either group.

Finally, the average duration of sleep spindles was analysed for each recording session to investigate differences between genotypes. Repeated measures ANOVA revealed no significant main effect of genotype ($F(1, 19) = 0.65$, $p = 0.46$) and no significant interaction of genotype and recording session ($F(1, 19) = 0.92$, $p = 0.35$). These findings indicate no differences in sleep spindle durations between genotypes and across recording sessions. (Figure 3.2.5 E).

Overall, our findings indicate that sleep spindle occurrence is not experience-dependent and that FAD+ mice do not show abnormalities in spindle occurrence.

3.2.4 No novelty-induced changes in sharp-wave ripple – sleep spindle coupling

Since a previous study has reported a sequential coupling of sleep spindles and SWRs and its link to systems consolidation (Staresina, Niediek, Borger, Surges, & Mormann, 2023), the co-occurrence of sleep spindles and SWRs was next assessed to investigate novelty-induced changes in the coupling as well as differences between genotypes. To do so, the time of sleep spindle onsets was set as time 0 and a time window of 2 s before and 2 s after the onsets was chosen to investigate changes in hippocampal activity.

As a first step, changes in hippocampal signal in the SWR frequency range were analysed as the mean of all recording sessions for WT and FAD+ mice. Signals in the SWR frequency range increased after the sleep spindle onset in both WT and FAD+ mice, reaching a maximum peak around 400 ms after the sleep spindle onset (Figure 3.2.6 A). To examine potential differences in these peaks between genotypes, the amplitude of the peaks in SWR frequency signal was assessed for each mouse in each recording (Figure 3.2.6 B). T-test revealed no significant difference between WT and FAD+ mice ($p = 0.5$). However, since experience-dependent differences in SWRs were found in previous analysis between WT and FAD+ mice (chapter 3.2.2), potential experience-dependent effects on the SWR-spindle coupling were investigated by separately examining changes in the SWR frequency signals in B1 and B4 recordings (Figure 3.2.6 C), where no significant differences in SWR and spindle occurrence had previously been found between genotypes, and changes in SWR frequency signals in P1 and P5 (Figure 3.2.6 E), which previously had shown significant differences in SWR occurrence between FAD+ and WT mice. The increase in SWR frequency signal was present in both baseline and post-learning recording. T-tests investigating differences between the genotypes found no significant difference in the peaks in baseline sessions ($p = 0.94$) (Figure 3.2.6 D) and neither in post-learning sessions ($p = 0.53$) (Figure 3.2.6 F). Together, these findings indicate that the coupling of spindles and SWRs is not experience-dependent and that FAD+ mice do not show abnormalities in coupling.

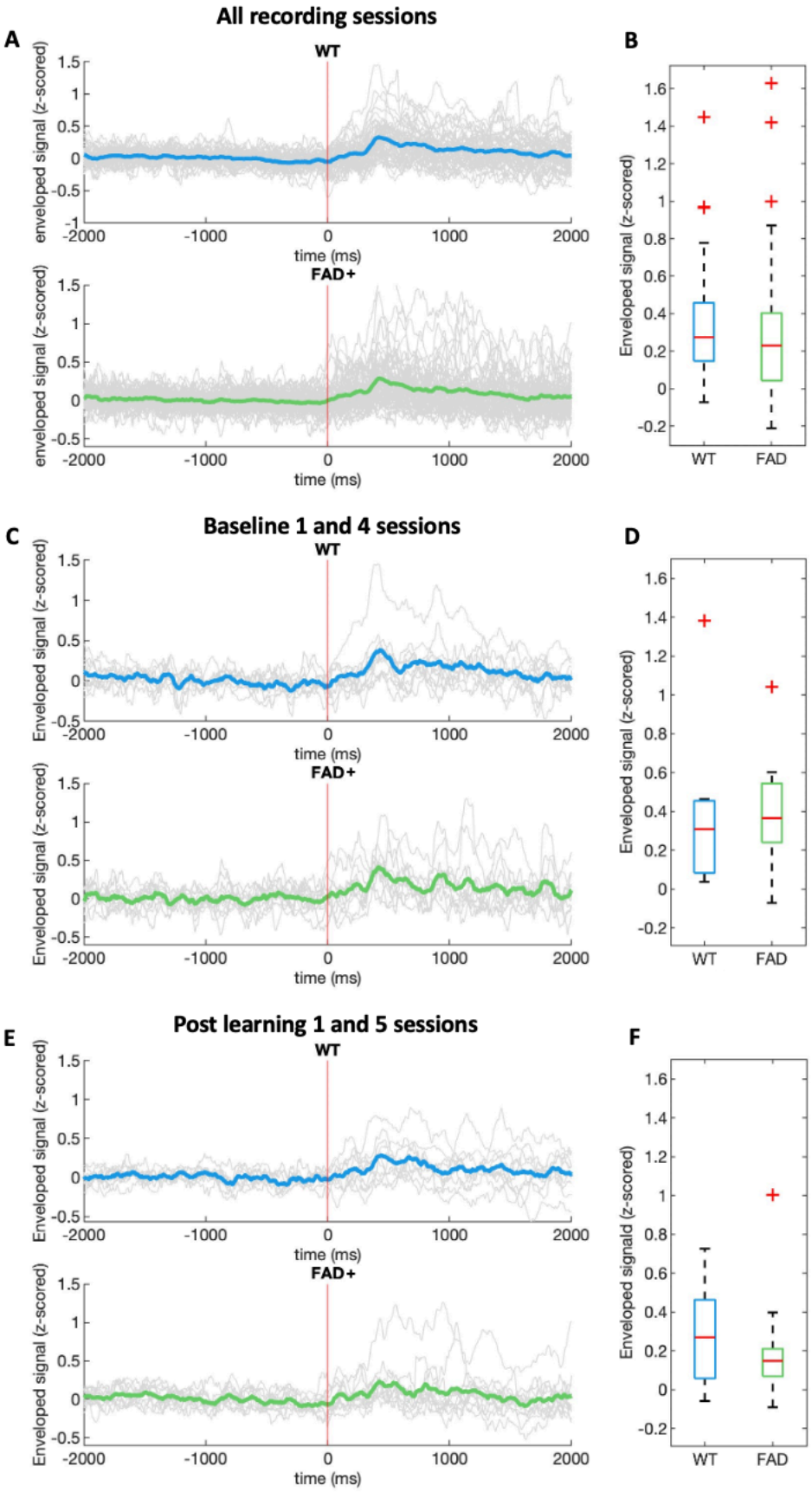
All recording sessions
A
WT
FAD+
enveloped signal (z-scored)
time (ms)
B
Enveloped signal (z-scored)
WT
FAD
Baseline 1 and 4 sessions
C
D
Post learning 1 and 5 sessions
E
F
Enveloped signald (z-scored)

Figure 3.2.6 Co-occurrence of sleep spindles and SWRs in WT and FAD+ mice. A) *Mean trace of hippocampal signal around sleep spindles onset of WT mice (top, blue) and FAD+ mice (bottom, green) along all recording sessions. Hippocampal signals were filtered in 140 – 250 Hz range and the envelope was z-scored based on the first 1000 ms. Individual traces of each recording session of each mouse (WT n = 10, FAD+ n = 11) are shown in grey. Red vertical lines indicate the onset of sleep spindle events.* ***B)*** *Comparison of peak amplitude of individual traces of hippocampal signal of WT (n = 10, blue) and FAD+ (n = 11, green) mice across all recording sessions. Boxplots show 25th and 75th percentile with medians in red and whiskers indicating maximum and minimum values. Outlier shown as red crosses.* ***C)*** *Same as A, but showing the mean and individual traces of B1 and B4 recordings only.* ***D)*** *Same as B, but only comparing peak amplitudes of B1 and B4 recordings.* ***E)*** *Same as A, but showing the mean and individual traces of P1 and P5 recordings only.* ***F)*** *Same as B, but only comparing peak amplitudes of P1 and P4 recordings.*

3.2.5 Results of the novel object recognition test

The overall idea of the experiment described in this chapter so far, was to combine our sleep recordings with the novel object recognition test (NOR) to observe changes in SWRs and sleep spindles in the context of learning and memory. Our aim was to identify differences in SWR and sleep spindle occurrence between genotypes and investigate how these differences affect memory performance.

Our NOR test consistent of 4 training sessions (TR1 - TR4), where mice explored two identical objects on 4 consecutive days, and one test session (Test) where one object was replaced by a novel object. Since a significant increase in SWRs was found after WT mice explored the identical objects for the first time (TR1) and after one object was replaced by a novel one (Test), and this increase was absent in FAD+ mice, exploration of objects during the test session in WT and FAD+ mice was analysed to investigate whether the absence of SWR increase in FAD+ mice leads to memory deficits. The NOR test assumes that mice express a curiosity for novelty, therefore exploring novel objects more than familiar objects. Therefore, mice with intact memory should show a preference for exploring a novel object, while mice with memory impairments should explore novel and familiar objects equally. The so-called discrimination index is used as a measurement for memory performance in the NOR test. It is calculated as the time spent with the new object minus the time spent with the old object divided by the combined exploration time of both objects. A positive discrimination index is usually interpreted as a preference for the novel object, a negative index is interpreted as a preference for the familiar object and a discrimination index close to 0 indicates no preference. When performing this test, two major parameters need to be considered: what distance

from the objects is considered as exploration and for how long exploration is assessed. In literature, a range of different combinations of parameters have been reported. In terms of test duration, reports range from 3 minutes (Szczepańska, Bojarski, Popik, & Malikowska-Racia, 2023) over 5 min (Zhang et al., 2012) to 10 min (Lueptow, 2017), while the distance from the object counted as exploration is often set at 2 or 3 cm (Lueptow, 2017; Shimoda, Ozawa, Ichitani, & Yamada, 2021). As a first step, different combinations of parameters were analysed to investigate the robustness of the discrimination index.

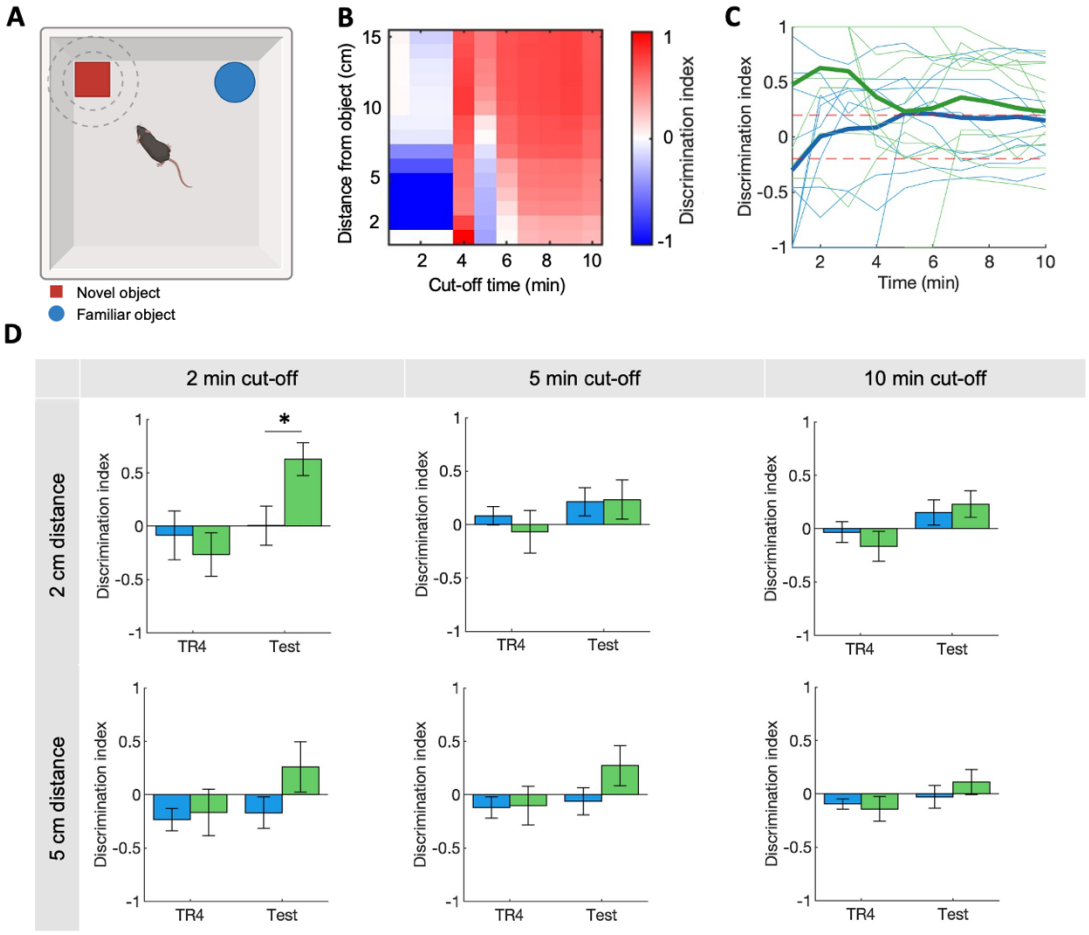

Figure 3.2.7 Analysis of the novel object recognition test. A) *Schematic of top-view video visuals of the NOR test. Dashed and dotted circles represent exploration zones of 5 cm and 2 cm distance from the object, respectively. Novel object shown in red, familiar object shown in blue.* ***B)*** *Representative heatmap of parameter investigation showcasing how definition of cut-off time and exploration radius affects the discrimination index. Preference of the familiar object (negative discrimination index) shown in blue, preference for the novel object (positive discrimination index) shown in red.* ***C)*** *Representative change in mean of the D-index across time of during the test session with a 2 cm exploration radius. Thick lines show mean discrimination index of WT (blue) and FAD+ (green). Individual traces of each animal are shown in thinner lines of the respective colour according to genotype.*

Red dashed lines represent the ± 0.2 cut-off for preference indication ***D)*** *Discrimination Index of WT (blue) and FAD+ mice (green) across TR1-TR4 and test session using 6 combinations of parameter combinations. T-test, * p < 0.05. Illustrations partially created with BioRender.com*

The distance from the object (Figure 3.2.7 A) was explored ranging from 1 cm to 15 cm. Cut-off times were explored ranging from 1 minute up to 10 minutes. A representative heatmap of discrimination index for each parameter combination for a single WT mouse during the test session is shown in Figure 3.2.7 B. Different combinations of parameters lead to drastically different discrimination indices. For example, choosing a 2 cm exploration radius with a 3 min cut-off time lead to a discrimination index close to -1, indicated the mouse preferred the familiar object, while setting the cut-off time just one minute later lead to a discrimination indices close to +1, indicating a preference for the novel object (Figure 3.2.7 B). To further look into how cut-off time influences the discrimination index, indices were calculated for each cut-off time from 1 to 10 minutes and changes in individual mice, as well as the mean across genotypes, were assessed for the exploration radius of 2 cm (Figure 3.2.7 C). Results showed strong preferences for one object in individual mice at early cut-off times which gradually disappeared at later cut-off times. The mean discrimination index of the two genotypes also varied accordingly across cut-off times (Figure 3.2.7 C). Finally, 6 combinations of parameters were chosen to explore memory performance of all WT and FAD+ mice during the last training session and the test session. Average discrimination index of WT and FAD+ mice for these sessions varied based on the combination of parameters (Figure 3.2.7 D). T-test between FAD+ and WT were conducted for the training and test session for each combination of parameters. A significant difference between genotypes was only found in the test session using the 2 min cut-off and 2 cm exploration radius combination ($p = 0.02$) where FAD+ mice had a significantly higher discrimination index at 0.63, indicating preference for the novel object, compared to WT mice at 0.01. Such a low discrimination index as found in the mean of the WT mice is usually interpreted as mice showing no preference. As shown in Figure 3.2.7 C, however, individual WT mice did show preference for either the new or old object. This effect seems to be abolished when assessing the mean discrimination index of the group of mice, so that in all 6 combinations of parameters, no preference for either the novel or familiar object was found in WT mice in the test session.

Our findings indicate great variability in the outcome of the NOR test, i.e. the discrimination index, as it is highly dependent on the chosen parameters. Significant differences between genotypes were sparse and only found with certain parameter combinations. The expected positive discrimination index in WT mice in the test session was not found with any combination of parameters, indicating no clear preference for the novel object. FAD+ mice, however, showed a preference for the novel object in the test session when data was analysed with specific parameter combinations.

3.2.6 Summary

In this chapter we explored SWRs and sleep spindles in the context of the NOR test. We found that SWRs are novelty-modulated: they increase in WT mice after a novel exploration experience, compared to baseline recordings. We found that this novelty-induced increase is absent in FAD+ mice. Since FAD+ mice showed no abnormalities in sleep architecture, the absence of SWR increase is unlikely to be due to fundamental differences in overall sleep time or fragmentation. We found no novelty-induced changes in sleep spindles and no changes in SWR-spindle coupling. FAD+ mice showed no evidence for abnormalities in sleep spindle or SWR-spindle coupling. The increase in SWRs in WT mice did not lead to better performance during the NOR task. The absence of SWRs increases in FAD+ mice did not lead to poorer performance in the NOR test compared to WT mice. We found considerable variability in the outcome of the NOR test, depending on what parameters were chosen to investigate object exploration preferences, indicating low robustness of the discrimination index in our data.

3.3 Investigation of acetylcholine across the sleep-wake cycle

Since we found the novelty-dependent modulation of SWRs to be absent in FAD+ mice, we wanted to investigate the underlying mechanism of this lack in SWRs. Previous studies suggest that SWRs are generated when the CA3 excites large subsets of CA1 pyramidal cells and interneurons (Buzsáki, 2015; Palop & Mucke, 2016; Valero et al., 2017). The excitation stemming from the CA3 is believed to only occur when supressing effects caused by the activation of cholinergic and cannabinoid receptors in the CA3 are absent (Buzsáki et al., 1983; Hasselmo, 2006; Hounsgaard, 1978; Robbe et al., 2006). Since cholinergic neurons are amongst the first types of neurons to degenerate in AD and dysregulation of the cholinergic system is a prominent factor of AD (reviewed in (Chen, Huang, Yang, & Hong, 2022)), we hypothesise that abnormalities in ACh activity in our AD mouse model contribute to the absence of SWRs.

To test this hypothesis, we investigated abnormalities in ACh activity in the HC across the sleep-wake cycle. Here, we performed simultaneous electrophysiology and fibre photometry recordings to measure cholinergic tone in the HC in 8 FAD+ and 8 WT mice before and after a novel experience.

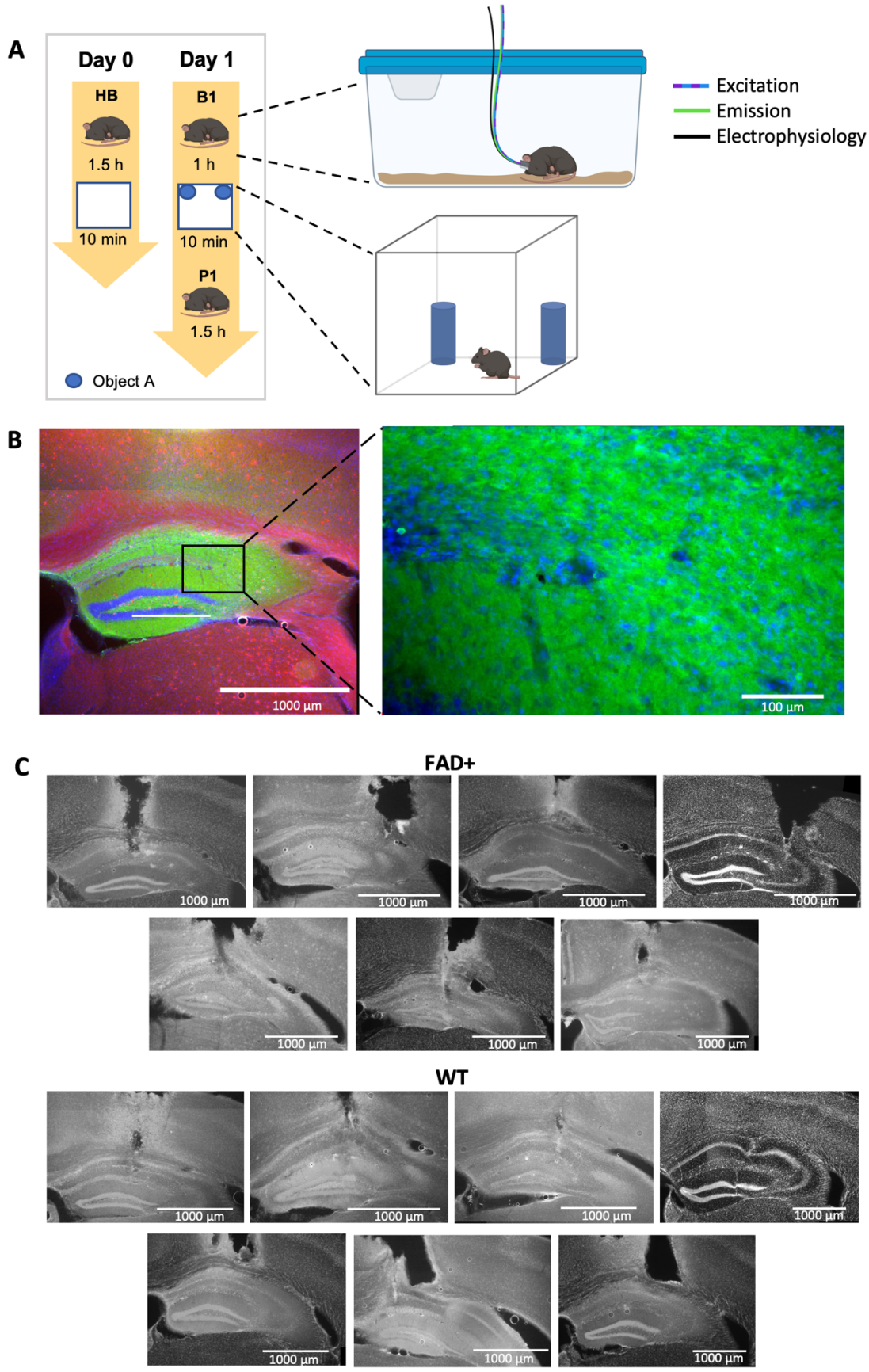

Figure continued on next page.

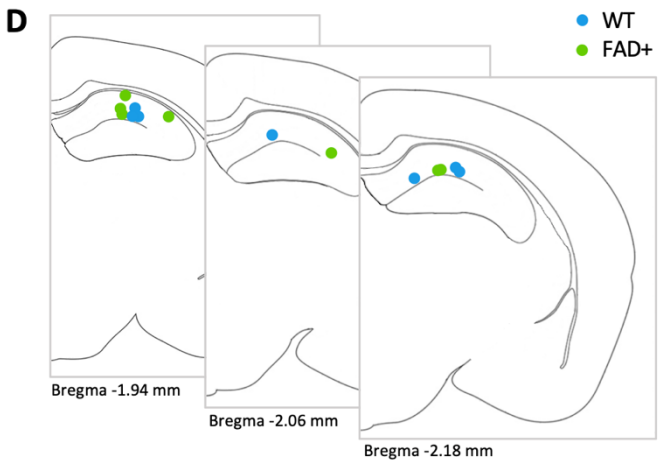

Figure 3.3.1 Recording protocol, viral expression and electrode positions of simultaneous electrophysiology and fibre photometry recordings. *After a habituation mock-recording (HB) in tethered condition in the home cage on day 0, mice underwent a 1 h baseline recording (B1) in the home cage on day 1, followed by 10 min of exploration of 2 identical objects in the open field box and a post-exploration recording (P1) in their home cage.* ***B)*** *Representative histology images of a FAD+ mouse showing viral expression (GFP, green), amyloid plaques (Alexa Fluor, red) and DAPI (blue). Scale bar 1000 µm (left) and 100 µm (right).* ***C)*** *Electrode and/or fibre position of each mouse. Top: FAD+ mice, Bottom: WT mice.* ***D)*** *Schematic of electrode position based on histological images. Tips of electrodes are indicated as dots in blue for WT mice and green for FAD+ mice. Illustrations partially created with BioRender.com*

Our prior test recordings in 4 test mice indicated a significant loss of fluorescent signal due to photobleaching when recording for more than 3 hours. We therefore conducted a shortened version of the previous experimental design described in chapter 3.2. We performed a mock-recording on day 0 to habituate the mice to the procedure. Mice were fully tethered in their home cage but the recording system remained turned off. On day 1, mice underwent a 1 h baseline recording (B1) followed by exploration of 2 identical objects in the open field box, followed by a 1.5 h post-exploration recording (P1) (Figure 3.3.1 A). Data of one male WT mouse was excluded due to an unstable fibre implant and one female FAD+ mouse was excluded due to poor quality of the fluorescent signal. Viral expression and electrode position was confirmed in the remaining 7 FAD+ and 7 WT mice in histological analysis (Figure 3.3.1 B-C). We first analysed the sleep architecture, SWR and sleep spindle occurrence based on the electrophysiological signals. Then, we investigated the cholinergic signalling in the HC across the sleep-wake cycle, at state transitions, and around the timing of SWR events in FAD+ mice and WT mice.

3.3.1 Sleep architecture of WT and FAD+ mice along recording sessions

As a first step we assessed the percentage of time spent in each state, the numbers of episodes per hour and latency to the first sleep episode as measurements of sleep architecture of both genotypes in B1 and P1 recordings.

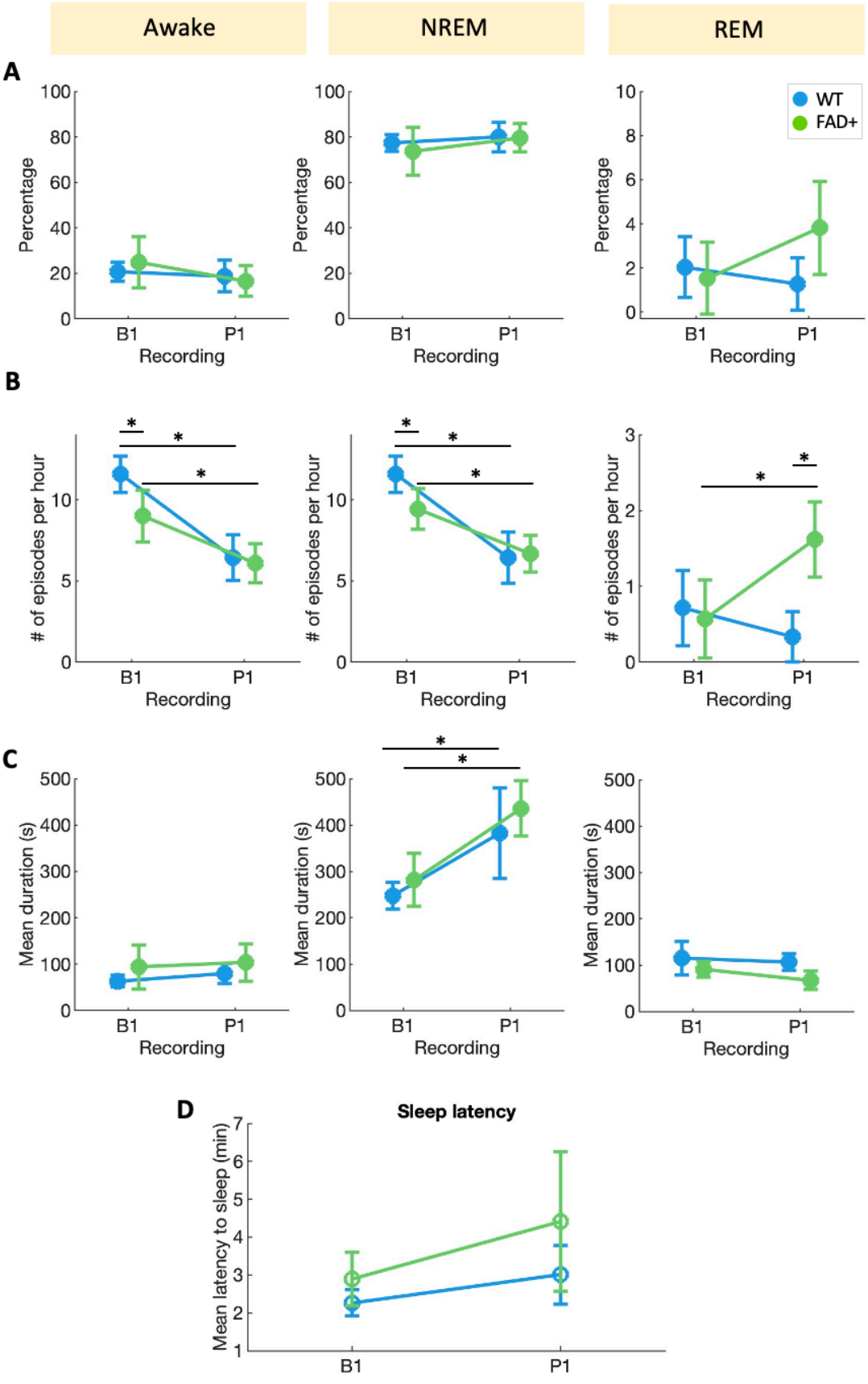
Awake
NREM
REM
A
Percentage
Recording
B1
P1
WT
FAD+
B
# of episodes per hour
C
Mean duration (s)
D
Sleep latency
Mean latency to sleep (min)

Figure 3.3.2 Sleep architecture of WT and FAD+ mice across fibre photometry recordings. A) *Percentage of time spent in each state: awake (AW, left), non-REM (NREM, middle) and REM (right) for WT (n = 7, blue) and FAD+ mice (n = 7, green) across baseline (B1) and post-exploration (P1) recording.* ***B)*** *Mean number of awake episodes (left), NREM episodes (middle) and REM episodes (right) per hour of B1 and P1 recordings of WT (n = 7, blue) and FAD+ mice (n = 7, green). Post-hoc multiple comparison with Bonferroni correction, * p < 0.05.* ***C)*** *Mean duration in seconds of awake episodes (left), NREM episodes (middle) and REM episodes (right) per hour of B1 and P1 recordings of WT (n = 7, blue) and FAD+ mice (n = 7, green). Post-hoc multiple comparison with Bonferroni correction, * p < 0.05.* ***D)*** *Latency to first sleep episode of WT (n = 7, blue) and FAD+ mice (n = 7, green) in B1 and P1 recordings. Error bars: standard error of mean.*

Repeated measures ANOVA was conducted for the percentage of time spent in each state in the B1 and P1 recording session. We found no significant effect of recording session ($F(1, 12) = 2.07$, $p = 0.18$) and no significant interaction between recording session and genotype ($F(1, 12) = 0.81$, $p = 0.39$) on the percentage of time spent awake (Figure 3.3.2 A, left). There was also no significant effect of recording session on the percentage of time spent in NREM sleep ($F(1, 12) = 1.68$, $p = 0.22$), no significant interaction between recording session and genotype ($F(1, 12) = 0.24$, $p = 0.63$) (Figure 3.3.2 A, middle) and no significant effect of recording session ($F(1, 12) = 0.68$, $p = 0.43$) and no significant interaction ($F(1, 12) = 2.77$, $p = 0.12$) on the percentage of time spent in REM sleep (Figure 3.3.1 A, right). We next assessed the number of episodes of each state using repeated measures ANOVA. We found a significant main effect of recording session ($F(1, 12) = 33.13$, $p < 0.001$) with no interaction of genotype and session ($F(1, 12) = 1.87$, $p = 0.20$) of awake episodes. Post-hoc multiple comparison using Tukey's HSD test revealed a significant difference between WT and FAD+ mice in B1 recordings ($p = 0.04$), a significant difference in WT mice between B1 and P1 recordings ($p <0.001$) and a significant difference in FAD+ mice between B1 and P1 recordings ($p = 0.02$) (Figure 3.3.2 B, left). Repeated measures ANOVA revealed a significant main effect of recording session ($F(1, 12) = 38.1$, $p < 0.001$) on the number of NREM episodes but no interaction between group and recording session ($F(1, 12) = 2.51$, $p = 0.14$). Post-hoc multiple comparison using Tukey's HSD test revealed a significant difference between WT and FAD+ mice in B1 recordings ($p = 0.047$), a significant difference in WT mice between B1 and P1 recordings ($p <0.001$) and a significant difference in FAD+ mice between B1 and P1 recordings ($p = 0.025$) (Figure 3.3.2 B, middle). When investigating the number of REM episodes, repeated measures ANOVA revealed no significant main effect of recording session ($F(1, 12) = 2.39$, $p = 0.15$) but a significant interaction between genotype and recording session ($F(1, 12)$

= 8.92, p = 0.01). Post-hoc multiple comparison using Tukey's HSD test revealed a significant difference between WT and FAD+ mice in P1 recordings (p = 0.003) and a significant difference in FAD+ mice between B1 and P1 (p = 0.008) (Figure 3.3.2 B, right).

We further investigated the average duration of episodes of wakefulness, NREM and REM sleep. Repeated measures ANOVA showed no significant main effect of recording session (F(1, 12) = 1.14, p = 0.31) and no significant interaction between genotype and recording session (F(1, 12) = 0.07, p = 0.79) (Figure 3.3.2.C, left). For the mean duration of NREM episodes, repeated measures ANOVA revealed a significant main effect of recording session (F(1, 12) = 14,87, p = 0.002) but no interaction between genotype and recording session (F(1, 12) = 0.07, p = 0.79). Post-hoc multiple comparison using Tukey's HSD test revealed that WT mice showed significantly longer NREM episode durations in the P1 recording compared to the B1 recording (p = 0.013). The same effect was found among FAD+ mice (p = 0.026) (Figure 3.3.2 C, middle). For REM episodes, repeated measures ANOVA revealed no significant main effect of recording session on the mean duration of episodes (F(1, 12) = 2.61, p = 0.18) and no significant interaction between genotype and recording session (F(1, 12) = 0.3, p = 0.61) (Figure 3.3.2.C, right).

Lastly, sleep latency was compared between genotypes and recording sessions. Repeated measures ANOVA revealed no significant main effect of recording session (F(1, 12) = 1.33, p = 0.27) and no significant interaction between genotype and session (F(1, 12) = 0.38, p = 0.55) (Figure 3.3.2 D).

Together, our findings suggest less sleep fragmentation in the P1 recording as indicated by the lower numbers and longer durations of NREM episodes in both groups of mice. Differences between genotypes were found in the B1 recording, where WT mice showed slightly more sleep fragmentation than FAD+ mice, and in the P1 recording where FAD+ mice showed more REM episodes than WT mice. No differences were found in the overall percentage of time spent in each state or in sleep latency. Overall, the time spent awake was very low in both recordings compared to our previous experiments. This is likely due to the fibre photometry cable used in these experiments, which adds weight and is less flexible than the electrophysiology cable, making it more difficult and tiring for mice to move.

3.3.2 Confirmation of our previous SWR and sleep spindle findings

After assessing sleep architecture, we wanted to replicate our previous finding of SWRs occurring more frequently in WT, but not FAD+, mice after exploring objects for the first time, and that sleep spindles are not novelty-modulated and not diminished in FAD+ mice.

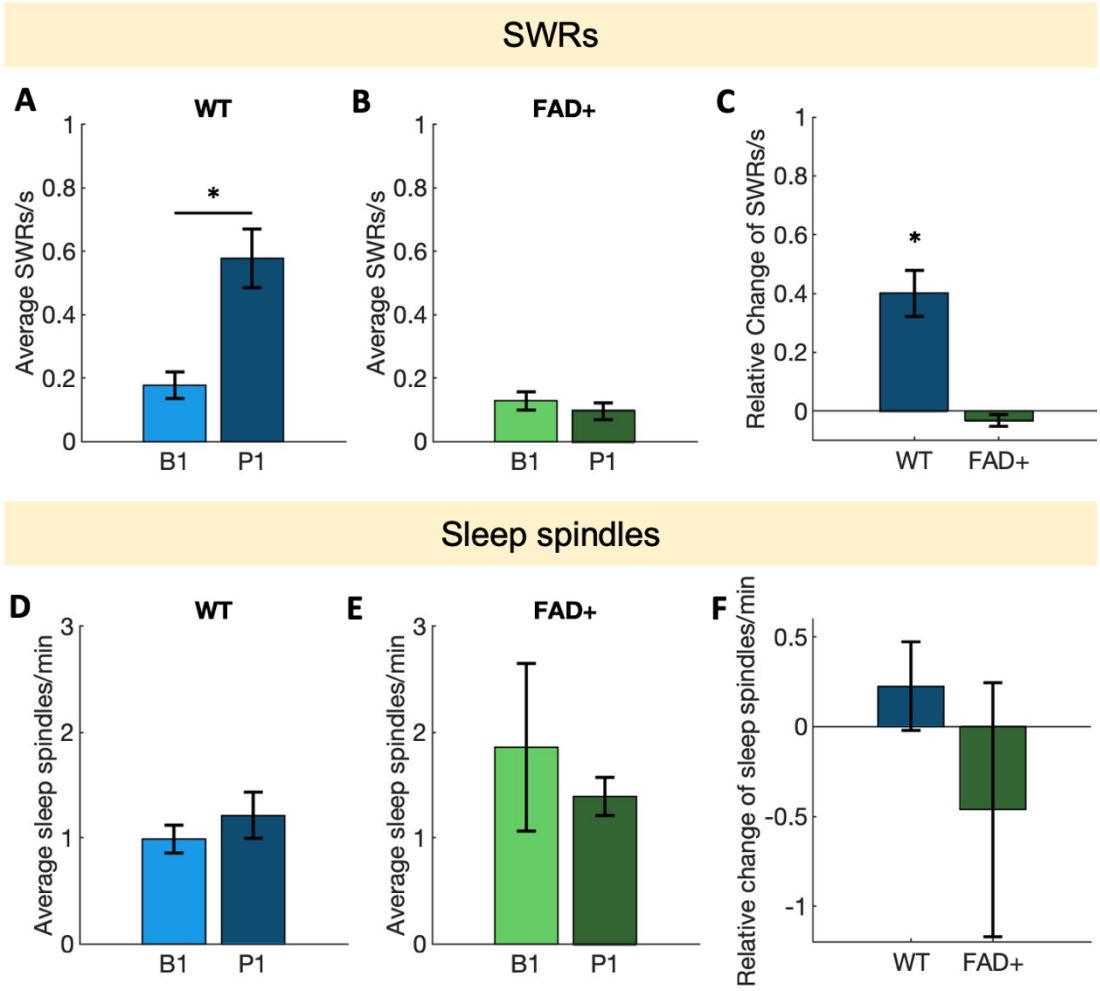

Figure 3.3.3 SWR and sleep spindle occurrence in WT and FAD+ mice before and after object exploration. A) *Average number of SWRs/s of n = 7 WT mice in baseline recording (B1) and post-exploration recording (P1). T-test, * p < 0.05.* ***B)*** *Average number of SWRs/s of n = 7 FAD+ mice in B1 and P1.* ***C)*** *Change in the number of SWRs/s in P1 relative to B1 for WT (n = 7, blue) and FAD+ (n = 7, green) mice. T-test against 0, * p < 0.05.* ***D)*** *Average number of sleep spindles/min of n = 7 WT mice in B1 and P1 recording.* ***E)*** *Average number of sleep spindles/min of n = 7 FAD+ mice in B1 and P1 recording.* ***F)*** *Change in the number of sleep spindles/min in P1 relative to B1 for WT (n = 7, blue) and FAD+ (n = 7, green) mice.*

We performed t-tests to compare the SWR rate in the B1 and P2 recording for WT and FAD+ mice separately. In WT mice, we found a significantly higher rate of SWRs in the P1 recording ($p = 0.002$) (Figure 3.3.3 A). In FAD+ mice, SWR rates did not differ between the B1 and P1 recording ($p = 0.15$) (Figure 3.3.3 B). Comparison of the P1 SWR rate relative to baseline recording showed only a significant increase in WT mice ($p = 0.002$) but not in FAD+ mice ($p = 0.15$) (Figure 3.3.3 C).

Next, t-tests were performed to compare the rate of sleep spindles in the B1 and P2 recording in WT and FAD+ mice. No significant difference was found in WT mice ($p = 0.4$) (Figure 3.3.3 D) and in FAD+ mice ($p = 0.53$) (Figure 3.3.3 E). The relative change in sleep spindles compared to baseline recordings was also not significant in either group (WT: $p = 0.4$, FAD+: $p = 0.53$).

This analysis shows that we successfully replicated our previous findings in a new cohort of mice: SWRs are novelty-modulated in WT mice, this novelty-induced increase in SWRs is absent in FAD+ mice. Sleep spindles do not increase after a novel experience and FAD+ mice do not show abnormalities in sleep spindle occurrence.

3.3.3 Cholinergic tone in the hippocampus across the sleep-wake cycle in WT and FAD+ mice

After confirming that the WT mice in this cohort showed a novelty-induced increase in SWRs after object exploration which was absent in FAD+ mice, we wanted to investigate the cholinergic tone in the HC across the sleep-wake cycle and investigate potential differences between genotypes.

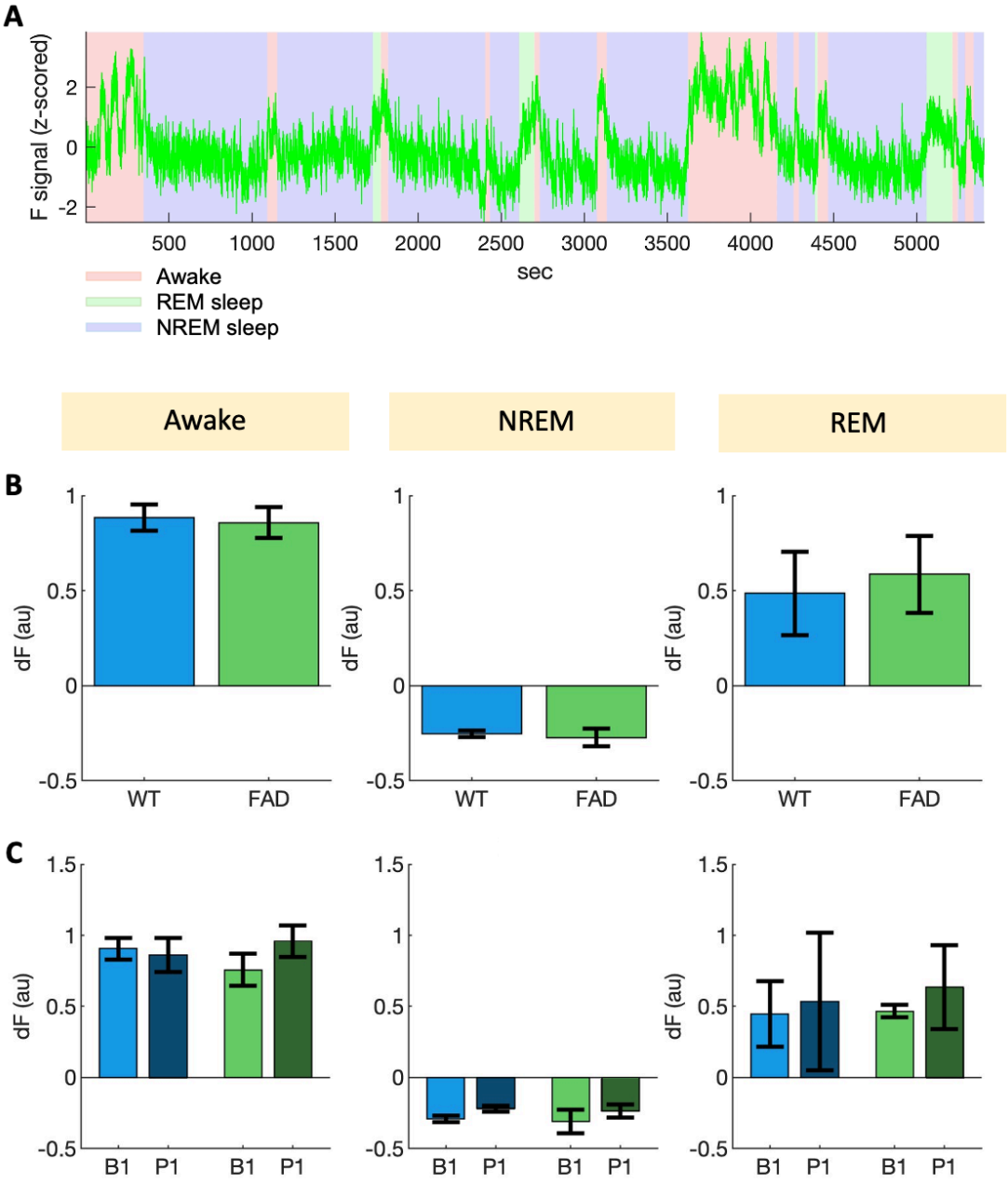

Figure 3.3.4 Cholinergic tone across the sleep-wake cycle. A) *Representative trace of fluorescent signal across awake (red), REM (green) and NREM (blue) episodes of a WT*

mouse. ***B)*** *Average fluorescent signal in all recordings of WT mice (n = 7, blue) and FAD+ mice (n = 7, green) during awake state (left), NREM sleep (middle) and REM sleep (right).* ***C)*** *Comparison of average fluorescent signal in B1 and P1 recording of WT (n = 7, blue) and FAD+ mice (n = 7, green) during awake (left), NREM (middle) and REM sleep (right). Post-exploration recordings are indicated in darker colours.*

We found cholinergic activity to vary greatly across the sleep-wake cycle (Figure 3.3.4 A). During wakefulness, the cholinergic tone was highest with fluctuations across time. During NREM sleep, the cholinergic activity was lowest with little fluctuations. Cholinergic activity also showed low fluctuation during REM sleep and was elevated here, but lower compared to the activity during awake times (Figure 3.3.4 A).

To investigate abnormalities in cholinergic tone in the FAD+ mice, we compared the average signal in each state between FAD+ and WT mice. T-tests revealed no significant difference between the cholinergic signal of WT and FAD+ mice during awake state ($p = 0.8$), NREM sleep ($p = 0.75$) or REM sleep ($p = 0.72$) (Figure 3.3.4 B).

Since we had found SWR occurrence to only be different between genotypes in the P1 recording, but not the B1 recording, we next wanted to investigate differences in cholinergic tone across the two recordings for each state. 2-way ANOVA revealed no significant main effect of genotype ($F(1, 24) = 0.05$, $p = 0.86$), of recording session ($F(1, 24) = 0.41$, $p = 0.64$) or interaction between genotype and recording session ($F(1, 24) = 1.3$, $p = 0.26$) on the cholinergic tone during awake times (Figure 3.3.4 C, left). Analysis of the cholinergic signal during NREM sleep revealed a trend but no significant main effect of genotype ($F(1, 24) = 124.25$, $p = 0.057$), a significant main effect of recording session ($F(1, 24) = 1895.85$, $p = 0.02$) and no significant interaction between genotype and recording session ($F(1, 24) = 0$, $p = 0.97$). Post-hoc analysis using Tukey's HSD revealed no significant differences amongst recording sessions of genotypes (Figure 3.3.4 C, middle). During REM episodes, no significant main effect of genotype ($F(1, 13) = 2$, $p = 0.39$), of recording session ($F(1, 13) = 8.85$, $p = 0.21$) or interaction between genotype and recording session ($F(1, 13) = 0.02$, $p = 0.9$) was found (Figure 3.3.4 C, right).

Together, these findings indicate no significant differences in the overall cholinergic tone among all states between WT and FAD+ mice.

3.3.4 Change in cholinergic tone at state transitions

Although we did not find any significant differences between genotypes when assessing the mean cholinergic activity in each state, we wanted to assess potential differences at a smaller time scale, as averaging the cholinergic tone across several minutes could mask subtle differences. We therefore assessed the change in cholinergic signal at transition times, i.e. when mice transitioned from NREM to REM sleep, from NREM to awake, from awake to NREM and from REM to awake. A time window of -20 s to +20 s around the transition was chosen by progressively increasing the window size until the signal stabilised in both the initial and final few seconds before and after the transition.

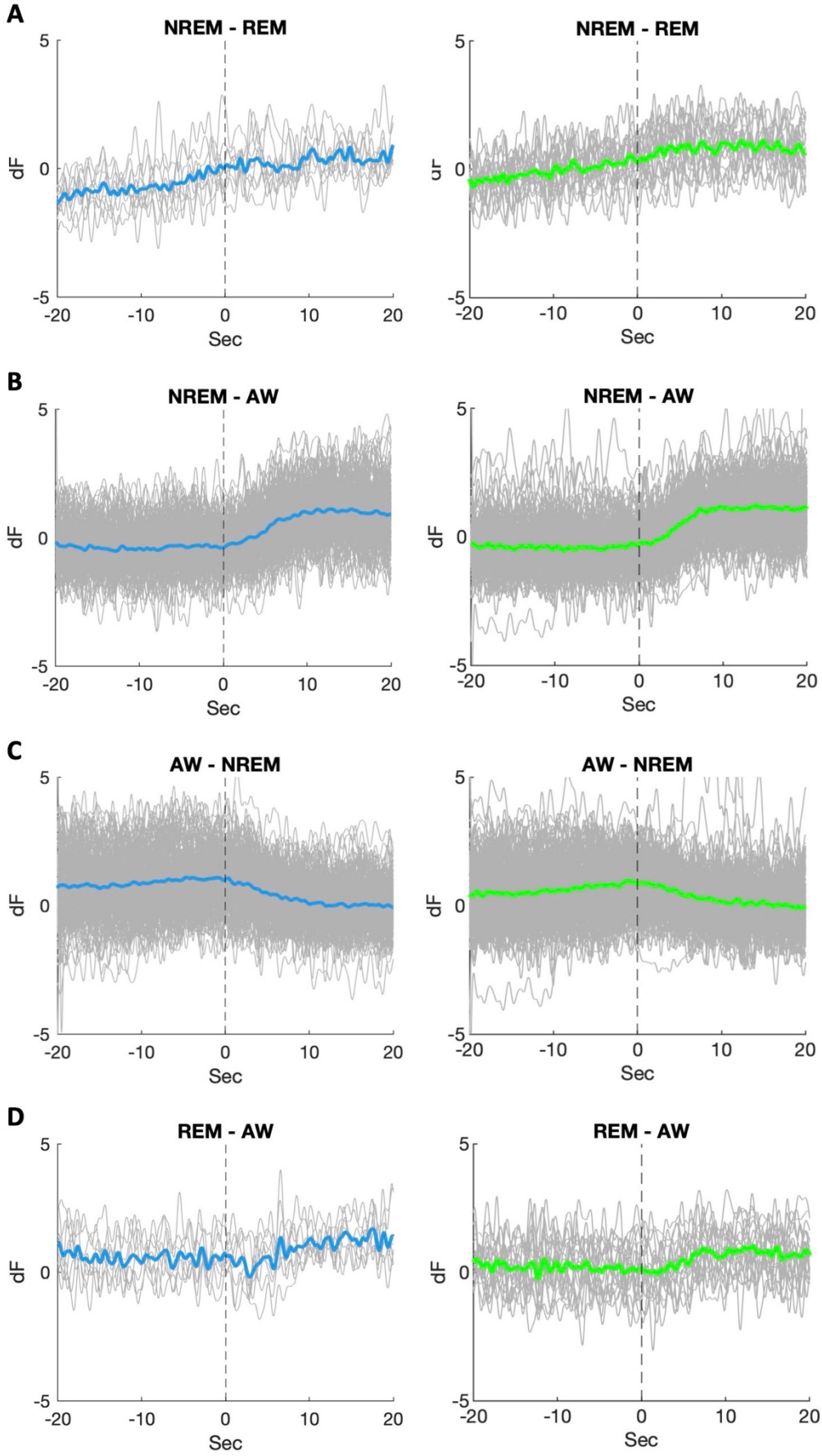
A
NREM - REM
NREM - REM
B
NREM - AW
NREM - AW
C
AW - NREM
AW - NREM
D
REM - AW
REM - AW
dF
Sec
5
0
-5
-20
-10
0
10
20

Figure 3.3.5 Dynamics of cholinergic tone at state transitions. A) *Individual traces (grey) and mean (colour) of cholinergic signal at transitions from NREM to REM sleep of WT mice (left, blue) and FAD+ mice (right, green).* ***B)*** *Individual traces (grey) and mean (colour) of cholinergic signal at transitions from NREM to awake of WT mice (left, blue) and FAD+ mice (right, green).* ***C)*** *Individual traces (grey) and mean (colour) of cholinergic signal at transitions from awake to NREM sleep of WT mice (left, blue) and FAD+ mice (right, green).* ***D)*** *Individual traces (grey) and mean (colour) of cholinergic signal at transitions from REM to awake of WT mice (left, blue) and FAD+ mice (right, green).*

In both WT and FAD+ mice, we saw distinct patterns of changes in fluorescent signal for the 4 types of state transitions.

When transitioning from NREM to REM sleep we observed a slow increase in cholinergic tone starting before the onset of REM sleep (Figure 3.3.5 A). When transitioning from NREM sleep to wakefulness, we saw a sharp increase of cholinergic tone which occurred delayed after the awakening of the mice (Figure 3.3.5 B). When transitioning from awake to NREM sleep, however, the cholinergic tone decreased without a delay and more slowly (Figure 3.3.5 C). Transitions from REM to wakefulness showed a small increase in cholinergic tone which occurred slightly delayed after awakening (Figure 3.3.5 D).

We further investigated the change in cholinergic tone across transitions in WT and FAD+ mice, using t-tests. Here, we assessed the difference between the pre-transition signal and post-transition signal for each transition type by computing the mean signal before the transition and subtracting it from the mean signal after the transition.

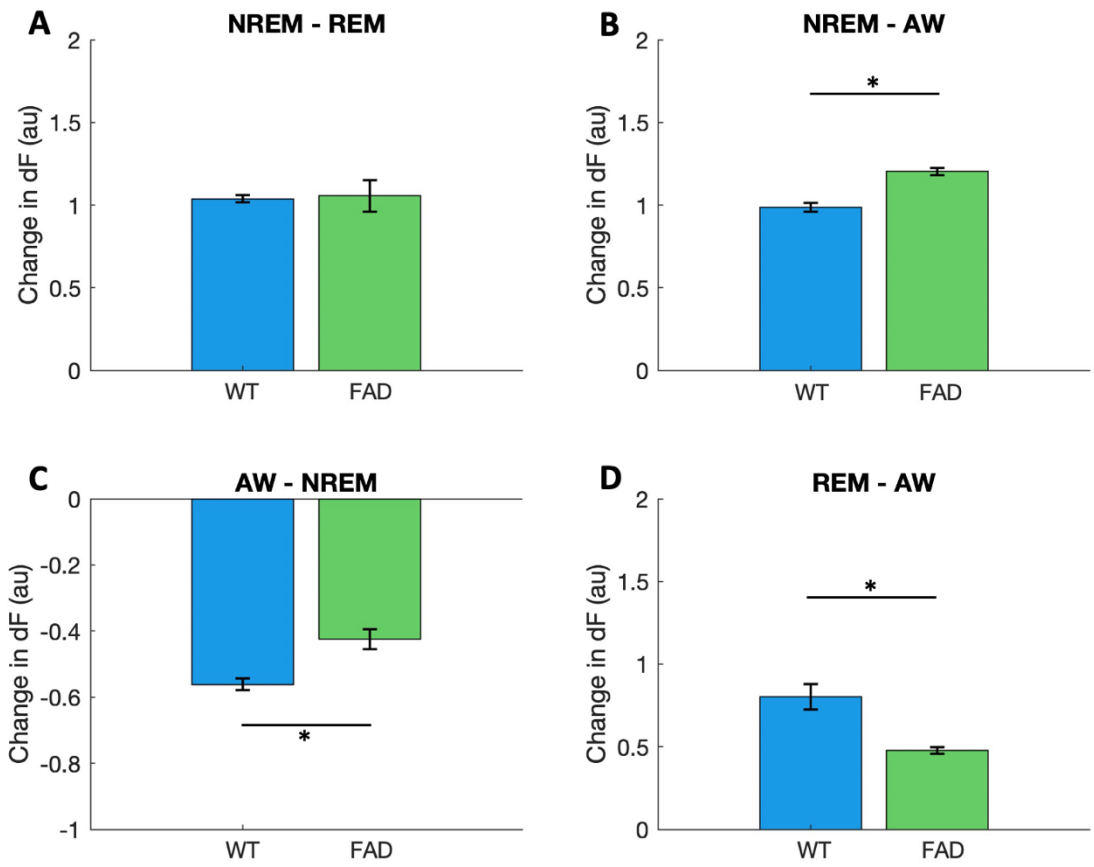

Figure 3.3.6 Change in cholinergic tone at state transitions. A) *Increase in cholinergic tone after REM onset compared to pre-transition NREM signal of WT (n = 7, blue) and FAD+ mice (n = 7, green).* ***B)*** *Increase in cholinergic tone after awakening compared to pre-transition NREM signal of WT (n = 7, blue) and FAD+ mice (n = 7, green). T-test, *p < 0.05.* ***C)*** *Decrease in cholinergic tone after NREM onset compared to pre-transition wakefulness signal of WT (n = 7, blue) and FAD+ mice (n = 7, green). T-test, *p < 0.05.* ***D)*** *Increase in cholinergic tone after awakening compared to pre-transition REM signal of WT (n = 7, blue) and FAD+ mice (n = 7, green). T-test, *p < 0.05.*

We found no significant differences between genotypes in the increase of cholinergic signal at NREM to REM transition ($p = 0.86$) (Figure 3.3.6 A). We did, however, find a significant difference between genotypes in the increase in cholinergic signal at NREM to wakefulness transition ($p < 0.001$) and in the transition from REM to awake ($p = 0.002$) (Figure 3.3.6 D). We further found a significant difference between genotypes in the decrease of cholinergic signal at wakefulness to NREM transition ($p < 0.001$) (Figure 3.3.6 C).

Our data shows that FAD+ mice exhibit a stronger increase in cholinergic signal when transitioning from NREM sleep to awake than WT mice, but show a lower

increase when transitioning from REM sleep to awake. Furthermore, FAD+ show a lower decrease in cholinergic signal when transitioning from wakefulness to NREM sleep. Since this analysis is based on z-scored fluorescent signals, this analysis cannot determine whether these differences in the change of signal are due to differences in signal in the pre-transition state or due to differences in the post-transition state.

Nonetheless, this analysis indicates that there are differences in the dynamics of acetylcholine in the HC between FAD+ and WT mice, which have gone undetected in our previous analysis in chapter 3.3.3.

3.3.5 Dynamics of cholinergic tone around SWRs

Finally, we wanted to assess cholinergic tone around the occurrence of SWRs. Since a previous study has shown that SWRs occur during transient decreases of cholinergic activity (Y. Zhang, L. Cao, et al., 2021), we assessed the dynamics of cholinergic tone at the SWR peak $\pm$ 100 s in WT and FAD+ mice.

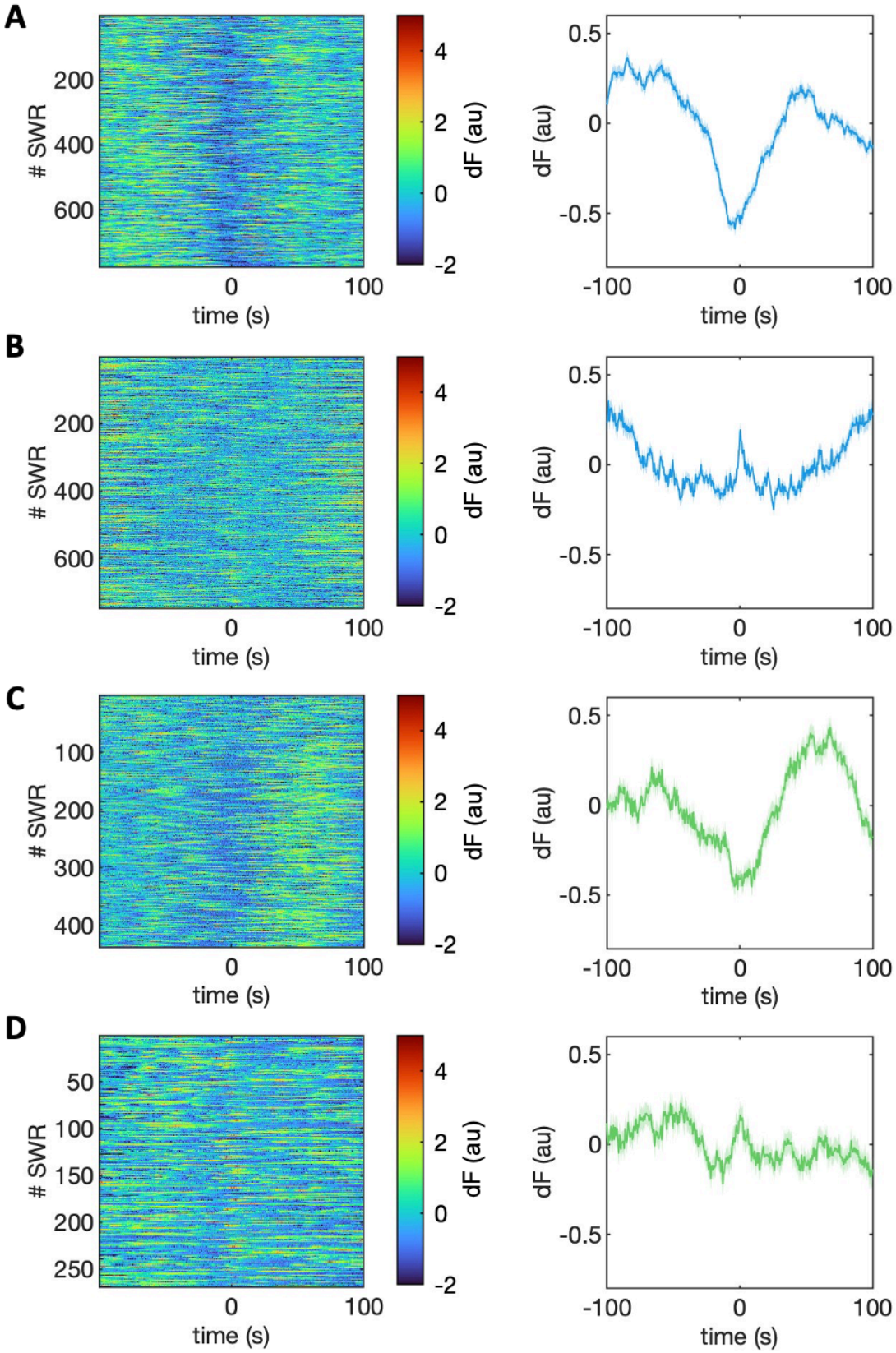

Figure 3.3.7 Transient changes in cholinergic tone around SWRs. A) *Normalised change in AchLightG signal around SWRs (left) and mean change in AchLightG signal centred on SWR peaks (right) of WT1 mouse in B1.* ***B)*** *Normalised change in AchLightG*

signal around SWRs (left) and mean change in AchLightG signal centred on SWR peaks (right) of WT2 mouse in P1. ***C)*** *Normalised change in AchLightG signal around SWRs (left) and mean change in AchLightG signal centred on SWR peaks (right) of FAD+1 mouse in B1.* ***D)*** *Normalised change in AchLightG signal around SWRs (left) and mean change in AchLightG signal centred on SWR peaks (right) of FAD+1 mouse in P1.*

We observed the cholinergic signal to decrease and reach a minimum at the time of SWR occurrence in some of the recordings of both WT and FAD+ mice (Figure 3.3.7 A & C). However, this pattern of cholinergic decline around SWRs was not observed in all recording sessions. In some recordings, in both WT and FAD+ mice, we observed a trend of decline in the mean cholinergic signal, followed by a peak of signal at the timing of SWRs (Figure 3.3.7 B & D, right). Such "peaky" signals were found amongst both the B1 and P1 recording sessions and in both WT and FAD+ mice, indicating that these differences are not due to the novel experience of object exploration or due to differences between genotypes. A summary of the numbers of recordings where peaks were absent or present is depicted in table 2. Here, peaks were defined as any temporary increase in the mean cholinergic signal at the time of SWR occurrence.

Table 2. Overview of recordings containing peaks in cholinergic tone at SWR timing.

Recording session	Genotype	No peak	Peak
B1	WT	4	3
	FAD+	4	3
P1	WT	3	4
	FAD+	2	5

To statistically examine the association between the recording session and genotype with respect to the presence of peaks, we performed the Cochran-Mantel-Haenszel test. This test assesses the association between two categorical variables, recording session and genotype in our case, on a third variable, the presence or absence of peaks. The test revealed no significant association between recording session and genotype with respect to the observation of peaks ($X^2(1) = 0.14$, $p = 0.71$). This indicates that there is no significant difference in the occurrence of peaks between genotypes or recording sessions.

Inspection of the changes in cholinergic signal around individual SWR events (Figure 3.3.7 B & C, left) suggested a fraction of SWR events to be accompanied by an increase in cholinergic activity, instead of a decrease.

We wanted to explore these peaks in cholinergic activity further to investigate the cause of these inconsistencies of cholinergic tone across SWR events. Since high cholinergic activity is usually associated with states of high arousal, we wondered whether these peaks could represent micro-arousals during sleep. We therefore compared the cholinergic tone during SWRs with the EMG signal during SWRs, hypothesising that and increase in arousal could show as an increase in muscle tone.

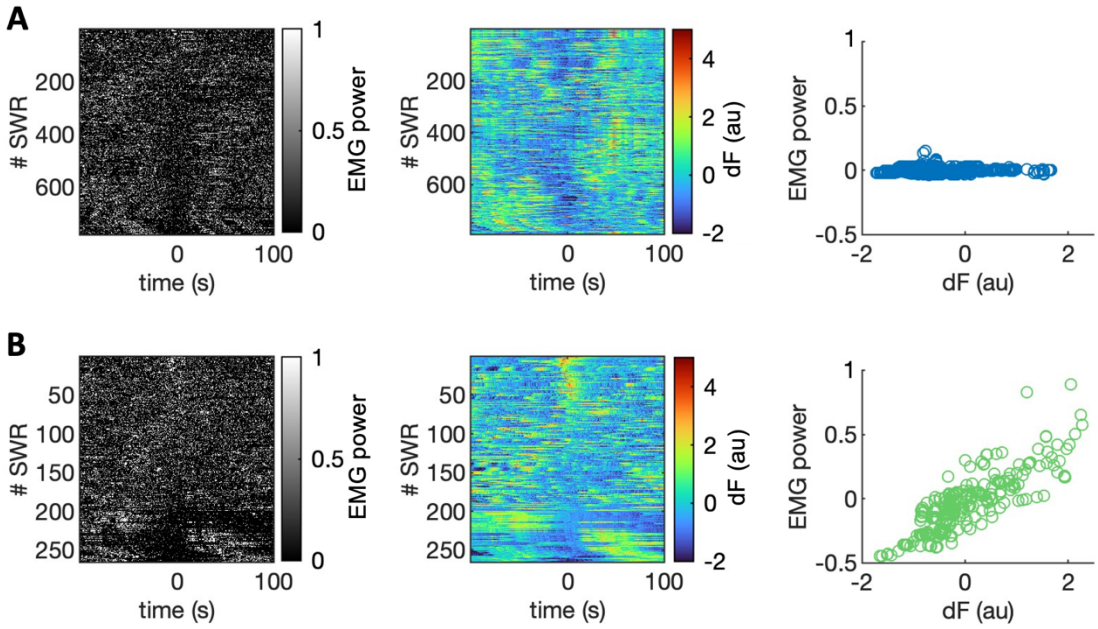

Figure 3.3.8 Inspection and correlation of EMG power and cholinergic tone around SWRs. A) *EMG power around SWR events sorted in descending order (left), corresponding AchLightG signal around SWRs (middle) and correlation of EMG power and AchLightG signal for each SWR event (right) of WT1 in B1.* ***B)*** *EMG power around SWR events sorted in descending order (left), corresponding AchLightG signal around SWRs (middle) and correlation of EMG power and AchLightG signal for each SWR event (right) of FAD+1 in B2.*

We sorted SWRs events according to their EMG power and compared changes in EMG to changes in cholinergic activity across the 200 s time window. Figure 3.3.8 shows two examples of this analysis. In recordings with no peak in cholinergic activity at SWR occurrence, few SWR events showed an increase in EMG power at the time of SWRs (Figure 3.3.8 A, left) and likewise, little SWR events showed an

increase in cholinergic activity (Figure 3.3.8 A, middle). The correlation between EMG power and cholinergic activity, quantified by the correlation coefficient, was low here (r = 0.087) (Figure 3.3.8 A, right). In datasets where a peak in cholinergic activity was found at the time of SWR occurrence, however, EMG power at the time of SWRs was increase in a considerable fraction of SWR events (Figure 3.3.8 B, left), and the cholinergic tone in these SWR events was found to be increased (Figure 3.3.8 B, middle). The correlation between EMG power and cholinergic activity, quantified by the correlation coefficient, was high here (r = 0.824) (Figure 3.3.8 B, right). These findings indicate that the peaks observed in some recordings are due a fraction of SWR events with higher cholinergic activity which coincide with higher EMG power.

We cannot say with absolute certainty whether these peaks are artefacts or not. Therefore, further analysis regarding differences in cholinergic activity around SWRs between genotypes, or across recordings, is challenging.

3.3.6 Summary

Here we investigated cholinergic activity in the HC across the sleep-wake cycle in WT and FAD+ mice before and after exploration of novel objects.

We observed changes in the sleep architecture in both WT and FAD+ mice across recordings, where mice showed less sleep fragmentation in the second recording session. In the first recording, WT mice showed more NREM sleep fragmentation than FAD+ mice. In the second recording, FAD+ mice showed more fragmented REM sleep. The overall time spent in each state and latency to sleep did not differ significantly between genotypes or recording sessions.

As in our previous experiments, we observed an increase in SWRs in WT mice during NREM sleep after novel object exploration compared to baseline sleep. This increase was absent in FAD+ mice. Sleep spindles did not change after object exploration and we found no evidence of abnormalities in sleep spindle occurrence in FAD+ mice.

We showed that levels of cholinergic activity in the HC are distinctively different between wakefulness, NREM and REM sleep. We found no differences in the overall level of cholinergic activity in these states between WT and FAD+ mice or between recording sessions.

We found distinct patterns of changes in cholinergic activity at state transitions, where cholinergic tone increased just before transitioning from NREM to REM sleep occurred, increased with a small delay when waking up, and decreased when transitioning to NREM sleep without a delay. Here we observed differences between genotypes at transitions of mice waking up. FAD+ mice showed a stronger increase in cholinergic activity when waking up from NREM sleep, while WT mice showed a stronger increase in cholinergic tone when waking up from REM sleep. Furthermore, we found cholinergic tone to decrease less when transitioning from wakefulness to NREM sleep in FAD+ mice compared to WT mice.

Lastly, we observed a tendency for cholinergic activity to decrease around the occurrence of SWRs, although cholinergic activity increased during some events in both WT and FAD+ mice.

4 Discussion

4.1 Summary of main findings

The aim of this project was to investigate abnormalities in sleep architecture, SWRs and sleep spindles in 5xFAD mice in the context of novelty and learning, as well as abnormalities in cholinergic activity as an underlying mechanism of SWR abnormalities. To do so, we performed in vivo EEG, EMG, hippocampal LFP and fibre photometry recordings in freely behaving condition across the sleep-wake cycle when mice were in a novel or familiar environment and before and after mice explored novel or familiar objects.

We found no consistent abnormalities in sleep architecture or abnormalities in sleep spindle occurrence in FAD+ mice.

We did, however, observe significant abnormalities in SWRs in FAD+ mice. More specifically, we found a novelty-induced modulation of SWRs in the context of exploration of a novel environment or novel objects in WT mice, which was absent in FAD+ mice. We are the first to report this lack of novelty-induced modulation of SWRs in the 5xFAD mouse model. We further investigated abnormalities in cholinergic activity in the HC as an underlying cause for the absence of this high frequency of SWR occurrence. We found no significant differences in the average cholinergic tone across the sleep-wake cycle between FAD+ and WT mice, but significant differences in the change of cholinergic tone at state transitions. This suggests that even though the overall cholinergic tone was similar between genotypes, impaired cholinergic dynamics at state transitions might underlie the observed differences in SWRs, which in turn could contribute to the cognitive deficits associated with AD.

4.2 No abnormalities in sleep architecture in 5xFAD mice

We found no consistent differences between FAD+ and WT mice in regard to their sleep architecture. Significant differences between genotypes were only observed in the average number of NREM and awake episodes in the B1 session and the number of REM episodes in the P1 session of simultaneous fibre photometry and electrophysiology (Figure 3.3.2 B). WT mice showed a slightly higher number of wake and NREM episodes here, indicating more sleep fragmentation. The average duration of episodes, however, did not differ significantly between genotypes in this recording session (Figure 3.3.2 C) and no indication of a difference in sleep fragmentation between genotypes was found in our other experiments (Figure 3.2.1, Figure 3.2.2, Figure 3.2.3).

These findings were unexpected, since changes in sleep architecture have repeatedly been reported in AD patients (Bonanni et al., 2005; Ju et al., 2013; Prinz et al., 1982; Spira et al., 2013) as well as in multiple AD mouse models (Maezono et al., 2020; Platt et al., 2011; Zhang et al., 2019).

Previous studies investigating sleep in 5xFAD mice have reported contradicting findings. While some studies report no sleep disturbances in this mouse model at 4, 6 and 12 month of age (Oblak et al., 2021; Schneider, Baldauf, Wetzel, & Reymann, 2014), one study reported reduced sleep time and increased sleep fragmentation in 5xFAD mice at 4 - 6.5 month (Sethi et al., 2015). It is important to note, however, that this study used a piezoelectric system to detect and analyse sleep. Although this method is believed to be around 90% accurate (Donohue, Medonza, Crane, & O'Hara, 2008), the use of this method instead of EEG-based sleep scoring could explain discrepancies of their reported results with other literature.

The fact that we did not observe abnormalities in sleep architecture has two major implications for this study. Firstly, any abnormalities in oscillations patterns or ACh signalling in FAD+ mice reported in this study are unlikely to be due abnormalities in sleep architecture. Secondly, since changes in sleep architecture are an important component of AD, abnormalities in oscillations or ACh signalling arising from, or contributing to, sleep disturbances will not be detectable in this mouse model.

4.3 No abnormalities in sleep spindles in 5xFAD mice

We found no significant difference in the rate of sleep spindles between FAD+ and WT mice (Figure 3.1.8, Figure 3.2.5 A - D, Figure 3.3.3 D - F). Under the assumption that sleep spindles have a functional role of preserving the state of sleep (Aston-Jones & Bloom, 1981; Colonnese et al., 2010; Wimmer et al., 2012), these findings align with our findings of no abnormalities in NREM duration in FAD+ mice. Under the assumption that sleep spindles facilitate memory formation, however, it is surprising that we did not only not find any deficits in sleep spindle rates in FAD+ mice, but also that we did not find an increase in sleep spindles in the context of novelty and learning in WT mice. Previous studies have reported an increase in sleep spindles in healthy human subjects after learning tasks (Fogel & Smith, 2006; Gais et al., 2002) and sleep spindle rates have been reported to be reduced in AD patients (Kam et al., 2019; Latreille et al., 2015). One study in particular reported reduced memory consolidation during the night in AD patients, who showed less sleep spindles an performed significantly worse on a verbal task, but not on a spatial task (Hanert et al., 2024), indicating sleep spindles increase might dependent on verbal memory only.

All of the aforementioned studies in human patients are based on recordings of a full night of sleep. In our study, we recorded sleep spindles over the span of 1, 1.5 or 2.5 hours at a time. Since spindle density is known to increase over the course of the night (De Gennaro, Ferrara, Vecchio, Curcio, & Bertini, 2005), this raises the question whether our recording sessions were too short to capture an increase in sleep spindles after learning and differences between genotypes. One study in a different AD mouse model, however, has reported a reduced sleep spindle rate within 50 min recording sessions (Benthem et al., 2020). Therefore, differences between genotypes should be observable in our experimental design. It is important to note here that the mouse model used in the study of Benthem et al., 3xTgAD, is known to show abnormalities in sleep architecture in the form of increased durations of NREM episodes (Benthem et al., 2020; Cushing et al., 2020).

Furthermore Benthem et al. reported no increase in sleep spindles after a learning task in WT mice, which matches our observations. In both humans and rodents, it is believed that motor memory is dependent on sleep spindle activity, while declarative memory is dependent on SWRs and slow-wave activity (Miyamoto, Hirai, & Murayama, 2017). This could explain why our learning task was not followed by an

increase of sleep spindles, but contradicts the findings of Gais et al., who reported an increase in sleep spindles in human subjects after a word-association task, which was not related to motor memory.
Beyond sleep spindle rate, we also assessed the durations of sleep spindles. Here, we found no significant differences between genotypes. A previous study has reported shortening of sleep spindle duration to be associated with an increased risk for AD (Orlando et al., 2024). We did not observe this trend in our mouse model. According to the studies conducted by Kam at al. and Winer et al., abnormalities in sleep spindles in AD are closely linked to the tau pathology, as tau levels in patients explained a large portion in variance in sleep spindle abnormalities and such abnormalities can predict further accumulation of tau in the future (Kam et al., 2019; Winer et al., 2019). Our findings that there are no abnormalities in sleep spindles in our amyloid-based AD mouse model therefore supports the hypothesis that sleep spindle abnormalities in AD arise from tau pathology.

4.4 Lack of novelty-induced modulation of SWRs in a novel environment in 5xFAD mice

Like previous studies (Booth et al., 2016; Ciupek, Cheng, Ali, Lu, & Ji, 2015; Iaccarino et al., 2016), we found a reduced rate of SWRs in our AD mouse model. Since we recorded mice in a novel environment for four consecutive days, we were able to observe changes in SWR rates as mice became familiar with the environment. We found SWR rates to be highest in WT mice on the first day of recording, particularly during the early sleep episodes. The SWR rate decreased within recordings and across days in WT mice, indicating that the need for memory consolidation was highest when mice were first exposed to the novel environment and diminished as exposure was prolonged and repeated. In FAD+ mice, this trend was absent: SWR did not occur more frequently on the first recording day, or in the early sleep episodes and no decrease was observed within recordings or across days (Figure 3.1.3 A – B). Since sleep architecture (Figure 3.1.2), and specifically the duration of NREM episodes, did not differ significantly between genotypes (Figure 3.1.4 C), the difference in SWR rates observed is unlikely to be due to abnormalities in sleep architecture. An unexpected finding is that SWRs in WT mice steadily decreased across days, reaching a level significantly lower than FAD+ mice

on day 4. The SWR rate in FAD+ mice remained consistent throughout all days. These differences in trends between genotypes could reflect differences in need for memory consolidation: Both groups of mice have an increased demand for memory consolidation when they are first exposed to the novel environment. In WT mice, this causes SWRs to occur more frequently, aiding memory consolidation. Due to the successful memory consolidation, the need to consolidate new memories diminished over the following days. In FAD+ mice, however, the high number of SWRs necessary for memory consolidation might not be achieved when exposed to the novel environment. Therefore, the need to consolidate memories on the following days does not dimmish and the SWR rate does therefore not diminish. Previous studies have reported shorter SWRs in AD (Caccavano et al., 2020; Funane et al., 2022; Prince et al., 2021) and a previous study indicating a causal relationship between long-duration SWRs and memory performance (Fernández-Ruiz et al., 2019). However, we did not observe significant differences in the average durations of SWRs in our recordings. Since we assessed the average duration of SWRs, subtle differences might be missed in our analysis. Furthermore, we did not observe a significant correlation between the amount of amyloid plaque in the HC and the frequency of SWRs in our FAD+ mice. This could indicate that a minimum amount of plaques necessary for SWR impairments was already reached in all of our transgenic mice. However, it is questionable whether plaques are a robust measurement to assess AD pathology. Multiple studies in human AD patients have reported a low correlation between plaque burden and the severity of cognitive decline, as well as older, cognitively healthy individuals showing neuropathology levels to a similar extend as AD patients, indicating plaque burden not to be a reliable indicator of cognitive health and some form of resilience being present in unimpaired individuals (Ahangari, Fischer, Schweizer, & Munoz, 2023; Blessed, Tomlinson, & Roth, 1968; Gómez-Isla et al., 1997; Zhang et al., 2023).

This is the first study reporting SWRs to occur more frequently in a novel environment in WT mice and a decrease in SWRs as the environment becomes familiar. Furthermore, it is the first to show a lack of this novelty-induced modulation of SWRs in an AD mouse model.

4.5 Lower theta power during NREM sleep in 5xFAD mice when sleeping in a novel environment

We observed lower theta power in FAD+ mice when they slept in the novel environment for the first time compared to WT mice. This difference was present both in the EEG and hippocampal LFP. On the following recording days, no difference was found between genotypes, indicating that the difference reflects differences in the consolidation of new information. Little studies have explored theta during NREM sleep, as it is most strongly associated with REM sleep and attention during wakefulness. One study in healthy human subjects reported cortical theta bursts to precede hippocampal SWRs during NREM sleep, potentially triggering hippocampal activity and aiding memory consolidation (Jiang, Gonzalez-Martinez, & Halgren, 2019). Our findings suggest that a similar connection might exists between SWRs and theta in mice, as we found both stronger theta power and more SWRs in WT mice compared to FAD+ mice during NREM sleep on the first recording day. In another study, theta bursts in humans during NREM sleep have also been reported to be linked to sleep spindles (Gonzalez et al., 2018). Although we did not see a novelty-induced difference in sleep spindles in our study, the study of Gonzalez and colleagues further indicates that theta during NREM sleep is involved in memory consolidation processes. One study has previously investigated theta power during NREM sleep in AD mouse models. Kent et al. reported a no significant abnormalities in theta power during NREM sleep in the APP/PS1, Tg2576 and 3xTgAD mouse model (Kent, Strittmatter, & Nygaard, 2018), which matches our observations on day 2, 3 and 4. To our knowledge, our study is the first to indicate a novelty-dependent abnormality in theta power in an AD mouse model during NREM sleep.

4.6 Lack of novelty-induced SWR increase after exploration of novel objects in 5xFAD mice

Building up on our findings that WT mice, but not FAD+ mice, show an increase in SWRs when sleeping in a novel environment, we wanted to observe changes in SWRs before and after exploring novel or familiar objects. We found that WT mice showed an increase in post-exploration sleep after exploring objects for the 1st time, but not after exploring the same objects for the 2nd, 3rd and 4th time (Figure 3.2.4 A, C). When a novel object was presented at the end of the recording week, WT mice showed an increase in SWRs again, proving that a decrease in SWR rate is not due to a deterioration of the implanted electrodes and consequent decrease of signal quality. Interestingly, WT mice also showed an increase in SWRs during the habituation recording. Here, mice slept in their home cage in tethered condition for the first time. Although the environment was familiar, the experience of being in this tethered condition, along with different lighting conditions, noises and smells in the experimental room, compared to the holding room, seems to provoke an increase in SWRs to consolidate memories of this novel experience, similar to sleeping in a completely novel environment. In FAD+ mice, we found no change in SWRs across all recordings. The SWR rate did not increase after exploring objects, nor in the habituation or baseline recording (Figure 3.2.4 B, D).

Our findings align with the reports of a previous study where mice showed an increase in SWRs following a spatial recognition test and where this increase was diminished when mice were injected with Aβ0, serving as a model of AD pathology (Nicole et al., 2016). Unlike the aforementioned study, our study did not target spatial memory, but novel object recognition. As of now, the SWR increase induced by novel object exploration has been unreported. Furthermore, we are the first to report the absence of this exploration-dependent increase in a transgenic mouse model for AD.

To assess the impact of this lack in SWR increase on memory performance, we computed the discrimination index as a measurement for object preference. The NOR test assumes that mice with intact memory will spend more time exploring a novel object compared to a familiar object. Initial literature review on the conductance and interpretation of this test revealed a variety of parameter combinations reported (Lueptow, 2017; Shimoda et al., 2021; Szczepańska et al., 2023; Zhang et al., 2012). We therefore calculated the discrimination index with a

range of parameter combinations exploring how the definition of object exploration, i.e. the distance from objects counted as exploration, and the cut-off time of analysis affected the outcome. We observed huge variations in the resulting discrimination index within tests of individual mice (Figure 3.2.7 B) and in group averages (Figure 3.2.7 D). Especially the cut-off time greatly affected the resulting discrimination index (Figure 3.2.7 C). Across the parameter combinations explored, we found a significant difference between genotypes only when considering a 2 cm distance from the object and with a time cut-off at 2 min. FAD+ mice showed a preference for exploring the novel object here, while WT mice did not. A previous study has reported that lower numbers of SWRs in the APP/PS1 mouse model does not impair the consolidation of spatial memory (Jura et al., 2019). Although we did not test spatial memory, it is possible that object recognition memory can also be intact in our mouse model, despite the lack of SWRs.

In no parameter combination did we observe a preference for the novel object in WT mice. This is unexpected, as unimpaired mice are assumed to show curiosity for novelty. The delay interval in our experiment is unlikely to contribute to the neutral discrimination index in WT mice, as there was a 1.5 h delay between the last training session and test session. A previous study has indicated that a range of mouse strains, including C57BL, show a strong preference for novel objects after a delay of 1 h, a less pronounced preference after a 4 h delay and no preference after 24 h (Lueptow, 2017). An important factor in our study that could significantly impact the performance of mice in the NOR test is that mice were single-housed to allow undisturbed recordings in their individual home cage. A previous study has reported that both male and female single-housed mice show signs of depression-like behaviour and do not show a preference for novel objects in the NOR test as group-housed mice do (N. Liu et al., 2020). The assumption that behaviour of mice changes under single-housing conditions therefore might explain why we did not observe preferences for the novel object, as expected in this memory test.

4.7 No abnormalities in sleep spindle – SWR coupling in 5xFAD mice

We found no abnormalities in the coupling of SWRs and sleep spindles in FAD+ mice (Figure 3.2.6). Both WT and FAD+ mice showed an increase in HC ripple power after the onset of sleep spindles. These findings contradict previous studies where a decrease in coupling between sleep spindles and SWRs has been reported (H. Yang & Y. Jeong, 2021; Zhurakovskaya et al., 2019). It is, however, important to note that the aforementioned studies used different analytical approaches to measure coupling, quantifying the cortical spindle-band power during SWRs or the ratio of spindle-nested SWRs to total SWR number. These SWR-centred analysis revealed abnormalities in AD mouse models, while our spindle-centred analysis did not.

Furthermore, we found no changes in coupling between baseline and post-learning sleep. Previous studies have reported an increase in coupling induced by learning (Maingret et al., 2016) and the positive affect of coupling on memory has been shown repeatedly (Maingret et al., 2016; Peyrache, Khamassi, Benchenane, Wiener, & Battaglia, 2009; Siapas & Wilson, 1998; Xia et al., 2017). The fact that we did not observe an increase in coupling further indicates that our spindle-centred approach might not portrait coupling of sleep spindles and SWRs appropriately.

4.8 Abnormalities in acetylcholine dynamics at state transitions in 5xFAD mice

We observed the characteristic changes of ACh across the sleep wake cycle (Figure 3.3.4 A). Our analysis of the average cholinergic signal in each state did not show significant differences between genotypes (Figure 3.3.4 B) which is surprising considering the large body of studies reporting the BFCS to degenerate early on in the AD pathology, leading to reduced cholinergic activity (Bartus et al., 1982; Bekdash, 2021; Chen et al., 2022; Drachman & Leavitt, 1974; Hampel et al., 2018; Schliebs & Arendt, 2006). However, since our analysis is based on z-scored signals, instead of absolute measurements, differences between genotypes might be masked. When assessing differences in the change of cholinergic tone, we did find significant differences between genotypes (Figure 3.3.6). Most interestingly, we found that cholinergic tone decreased less strongly during the transition from wakefulness to NREM sleep in FAD+ mice. Knowing that cholinergic inhibition needs to be absent for SWRs to occur, a slower or less pronounced decrease in ACh in FAD+ mice could therefore be a starting point to explain the reduced number of SWRs observed in our study. However, since our analysis is based on z-scored fluorescent signals, it is not possible to say whether this smaller decrease in cholinergic tone reflects higher cholinergic signalling prior to transitioning or higher signalling after transitioning. Since reduced cholinergic signalling during wakefulness has repeatedly been reported in AD mouse models and patients, the later option seems more likely. Our analysis was based on a rather short time window of 20 s before and after state transition, it is therefore questionable to what degree this difference in ACh at the start of NREM sleep can explain the reduced number of SWRs in FAD+ mice. Further analysis of cholinergic signalling at transition with an extended the time window and analysis of the timing of SWRs withing sleep episodes, i.e. whether they occur predominantly around the onset of sleep in WT mice, would help to investigate this matter further.

4.9 Cholinergic tone at SWR timing

We observed cholinergic tone reaching a minimum at SWR timing (Figure 3.3.7 A, C), as previously reported (Y. Zhang, L. Cao, et al., 2021). However, we also found instanced where SWR events co-occurred with an increase in cholinergic signal, observed as peaks in the average cholinergic signal (Figure 3.3.7 B, D). This increase was observed in both genotypes and both recording sessions (baseline and post-learning sleep), making it unlikely to be linked to genotype or previous experience (Table 2). We further found that in the instances where increases in cholinergic tone were observed, there was a strong correlation between the fluorescent signal and EMG power (Figure 3.3.8). Since elevated levels of ACh and increase in muscle activity are both indicators for increased arousal, it is possible that what we observed here were events of micro arousals during sleep. Such micro arousals have previously reported in NREM sleep, including changes in hippocampal LFP (dos Santos Lima et al., 2019), but our knowledge on such changes is restricted to low frequencies. It remains unclear whether micro arousals coincide with SWRs, or whether they are accompanied by an increase in the SWR frequency band, thereby being falsely identified as SWRs in our study. No previous study has reported an increase in cholinergic tone coinciding with SWRs. In the publication of Zhang et al, it is mentioned that SWR events were manually selected after automated detection based on the signals of neighbouring channels of the electrode. Since we used bipolar electrodes instead of linear electrode arrays, and therefore only had two channels, this extra step for identifying SWRs is not possible in our data. Peaks in cholinergic tone have been previously found in NREM sleep in the presence of fast gamma (Y. Zhang, L. Cao, et al., 2021). However, these finding were based on the analysis of a 80 – 120 Hz frequency band. Since our SWR detection is based on the analysis of the 140 – 250 Hz range, there is no overlap with this particular fast gamma frequency band. Nonetheless, fast gamma could still be coinciding with SWRs in our data or with candidates falsely identified as SWRs. Further analysis would be necessary to characterise the peaks in cholinergic tone observed, before potential differences between genotypes can be explored.

4.10 Limitations

One major limitation of our study is that although we observe experience-dependent increases in SWRs in the context of novelty in WT mice which is absent in FAD+ mice, we do not have a convincing behavioural readout to prove that the increase in SWRs lead to memory consolidation in WT mice and that the lack of SWR increase prevented memory consolidation in FAD+ mice. More specifically, we cannot prove that WT animals became familiar with the novel experimental box across recording days and that FAD+ mice did not. Processing behavioural data is long and slow process since each mouse underwent 4 recordings of 2.5 hours each. Analysis is further complicated by obstructed camera view due to the electrophysiology tether. Nonetheless, a behavioural readout is essential for establishing a link between SWRs and habituation to a novel environment. To address this limitation, we currently analyse behavioural data which will be incorporated in the forthcoming publication of this project.

We also did not we see a preference for the novel object, indicating intact memory, in the NOR test in WT mice. The NOR test itself has considerable limitations. Firstly, the test relies on the natural curiosity of animals which should show in a preference for exploring novel objects. However, the internal state of the animal, such as anxiousness, can greatly impact the behaviour of individual animals. Secondly, the NOR test only assesses a very simple form of recognition memory. It does not reflect the complexity of human memory well, specifically higher-order cognitive processes such as episodic memory, which is highly relevant for AD patients. To date there is no “gold standard” for the conducting the NOR test. Our literature review found a variety of different parameter combinations, including test duration and definition of exploration. When we explored different combinations of parameters in our data, we got widely different outcomes in regard to the discrimination index in individual mice, indicating that the robustness of the discrimination index as an estimate of recognition memory is questionable. Alternative memory tasks with higher complexity, and a higher motivation to perform well in the task, such as labyrinth tasks with a reward, could have been a more robust choice to assess memory performance.

Furthermore, our hippocampal LFP recordings are based on bipolar electrodes. While this is a cost-efficient method, it does not have ideal spatial resolution, as LFPs are recorded from large population of neurons. It is also less reliable for the detection of SWRs compared to the use of linear electrode arrays, where comparison of signals across recording channels aids the separation of SWR events from artefacts (Liu et al., 2022). According to our histological analysis, some of the implanted electrodes were close to the dentate gyrus. Hippocampal dentate spikes are short spikes of large amplitude which have been reported to occur between SWRs and are also involved in memory consolidation processes (Farrell, Hwaun, Dudok, & Soltesz, 2024). These events can be distinguished from SWRs by comparison of LFPs across neighbouring channels of linear electrode arrays, but not in recordings of bipolar electrodes. It is therefore not possible for us to be absolutely sure that none of our detected SWR events are dentate spikes.

Although we did not see any deterioration in the signal of the bipolar electrodes, signals from EMG wires deteriorated over time, possibly due to the slightly acidic environment of the muscle tissue. Lower signal quality could therefore interfere with the SWR and sleep spindle detection, where the exclusion of artefacts relies on the EMG signal.

Furthermore, there are some limitations in our approach to examine cholinergic activity. Fibre photometry records bulk fluorescent signals of a large population of neurons, therefore having a poor spatial resolution. It measures relative changes of acetylcholine, not allowing absolute quantification of the neurotransmitter. This limits our ability to identify differences between recording session and animals.

The fibres we implanted were Ø 400 µm in diameter, which allows to pick up greater fluorescent signal, but also causes considerable tissue damage which can result in inflammation and alteration of normal brain functioning, thereby affecting the data collected in this study.

Lastly, our chosen AD mouse model, 5xFAD, has some limitations. This model is amyloid-based, not expressing tau pathology. While this is helpful in differentiating whether abnormalities are solely caused by amyloid pathology, it prevents us from observing the full spectrum of abnormalities in AD. Under the assumption that abnormalities in sleep spindles in AD are due to tau pathology, for example, we miss this crucial component. 5xFAD is a transgenic mouse model expressing 5 mutations. These mutations are driven by non-physiological, high levels or

transgenic expressing, leading to a fast and aggressive progression of amyloid pathology, which is more severe than what is usually observed in AD patients. This makes it difficult to apply findings in 5xFAD mice to human AD pathology, as it does not reflect the decades-long development of the pathology seen in AD patients. Furthermore, the fast progression makes it very difficult to investigate the pre-clinical stage in this mouse model. Identifying the time at which SWRs start to be impaired in this mouse model, for example, would be very difficult, as 5xFAD mice show amyloid plaques at as early as 2 months old. We therefore do not know whether 5xFAD have a baseline at which they can show SWRs as frequently as WT mice do. The overexpression of APP can also have off-target side effects, as fragments related to APP, such as carboxy-terminal fragments, are involved in calcium homeostasis, transcription and functions involved in memory (Chang & Suh, 2005; Nicolas & Hassan, 2014; Saito et al., 2014). It is therefore difficult to differentiate if observed abnormalities are due to the AD phenotype or side effects caused by the overexpression of APP. Furthermore, this mouse model is based on the genetic mutations found in FAD cases, which only make up a small percentage of all AD cases. This further limits the degree to which findings from 5xFAD studies can be translated to human AD pathology.

4.11 Future work

To overcome the limitation of not having a behavioural readout connecting the absence of the increase in SWRs in FAD+ mice to memory deficits, investigating explorative behaviour of mice in the novel environment could be considered. If mice show increased explorative behaviour, such as increased locomotion, when first introduced to a novel environment, and if this behaviour diminishes as the environment becomes familiar, this could be used as an indicator for intact memory. More sophisticated analysis of differences in the SWR events accompanied by a decrease or increase of cholinergic tone could help to gain insight into why this increase in cholinergic tone is observed in some cases. It would also be very interesting to extend the time window when analysing the change in cholinergic tone at transitions from wakefulness to NREM sleep. Observing how ACh levels differ in the early NREM sleep, and whether SWRs occur specifically in the early minutes of NREM sleep in WT mice, could help to better understand if abnormalities in cholinergic signalling in the HC is an underlying mechanism for the reduced number of SWRs observed in AD.

Future studies should aim to explore the underlying mechanism of the lack of SWRs in AD, ideally using a mouse model expressing both amyloid and tau pathology at a slower rate, allowing the observation of changes from the pre-clinical stage on. Pharmacological or optogenetic approaches could be explored to lower the cholinergic tone during sleep in an AD mouse model, to observe whether a lower cholinergic tone in NREM sleep allows SWRs to occur more frequently. It would also be interesting to test the effect of cholinesterase inhibitors on SWRs in AD. Here, investigating different times of administration and its effect on NREM sleep, SWRs and memory performance could provide valuable insights into why this drug treatment only shows moderate effects. Elongating the duration of SWRs using optogenetic approaches would also be highly interesting, to see if prolonged durations of SWRs can make up for the lower number of events to restore memory consolidation processes.

It would further be interesting to investigate the mechanisms leading to the increase in SWRs in the context of novelty in WT mice. This will not only help us understand the mechanisms of memory consolidation processes during sleep better, but also give us new insights into how such mechanisms might be impaired in AD.

References

2023 Alzheimer's disease facts and figures. (2023). *Alzheimer's & Dementia, 19*(4), 1598-1695. doi:https://doi.org/10.1002/alz.13016

Abhang, P. A., Gawali, B. W., & Mehrotra, S. C. (2016). Chapter 1 - Introduction to Emotion, Electroencephalography, and Speech Processing. In P. A. Abhang, B. W. Gawali, & S. C. Mehrotra (Eds.), *Introduction to EEG- and Speech-Based Emotion Recognition* (pp. 1-17): Academic Press.

Adaikkan, C., Middleton, S. J., Marco, A., Pao, P. C., Mathys, H., Kim, D. N., . . . Tsai, L. H. (2019). Gamma Entrainment Binds Higher-Order Brain Regions and Offers Neuroprotection. *Neuron, 102*(5), 929-943.e928. doi:10.1016/j.neuron.2019.04.011

Adamantidis, A. R., Gutierrez Herrera, C., & Gent, T. C. (2019). Oscillating circuitries in the sleeping brain. *Nature Reviews Neuroscience, 20*(12), 746-762. doi:10.1038/s41583-019-0223-4

Aeschbach, D., & Borbély, A. A. (1993). All-night dynamics of the human sleep EEG. *J Sleep Res, 2*(2), 70-81. doi:10.1111/j.1365-2869.1993.tb00065.x

Ahangari, N., Fischer, C. E., Schweizer, T. A., & Munoz, D. G. (2023). Cognitive resilience and severe Alzheimer's disease neuropathology. *Aging Brain, 3*, 100065. doi:10.1016/j.nbas.2023.100065

Ahmed, M., Davis, J., Aucoin, D., Sato, T., Ahuja, S., Aimoto, S., . . . Smith, S. O. (2010). Structural conversion of neurotoxic amyloid-beta(1-42) oligomers to fibrils. *Nat Struct Mol Biol, 17*(5), 561-567. doi:10.1038/nsmb.1799

Ahmed, Z., Cooper, J., Murray, T. K., Garn, K., McNaughton, E., Clarke, H., . . . O'Neill, M. J. (2014). A novel in vivo model of tau propagation with rapid and progressive neurofibrillary tangle pathology: the pattern of spread is determined by connectivity, not proximity. *Acta Neuropathol, 127*(5), 667-683. doi:10.1007/s00401-014-1254-6

Allsop, D., Mayes, J., Moore, S., Masad, A., & Tabner, B. J. (2008). Metal-dependent generation of reactive oxygen species from amyloid proteins implicated in neurodegenerative disease. *Biochem Soc Trans, 36*(Pt 6), 1293-1298. doi:10.1042/bst0361293

Alzheimer's Disease International. (2019). *World Alzheimer Report 2019*. Retrieved from London: https://www.alzint.org/u/WorldAlzheimerReport2019.pdf

Alzheimer’s Association. (2018). 2018 Alzheimer's disease facts and figures. *Alzheimer's & Dementia, 14*(3), 367-429. doi:https://doi.org/10.1016/j.jalz.2018.02.001

Amieva, H., Ouvrard, C., Meillon, C., Rullier, L., & Dartigues, J. F. (2018). Death, Depression, Disability, and Dementia Associated With Self-reported Hearing Problems: A 25-Year Study. *J Gerontol A Biol Sci Med Sci, 73*(10), 1383-1389. doi:10.1093/gerona/glx250

Arias, C., Arrieta, I., & Tapia, R. (1995). beta-Amyloid peptide fragment 25-35 potentiates the calcium-dependent release of excitatory amino acids from depolarized hippocampal slices. *J Neurosci Res, 41*(4), 561-566. doi:10.1002/jnr.490410416

Armstrong, N. M., An, Y., Doshi, J., Erus, G., Ferrucci, L., Davatzikos, C., . . . Resnick, S. M. (2019). Association of Midlife Hearing Impairment With Late-Life Temporal Lobe Volume Loss. *JAMA Otolaryngol Head Neck Surg, 145*(9), 794-802. doi:10.1001/jamaoto.2019.1610

Arvanitakis, Z., Shah, R. C., & Bennett, D. A. (2019). Diagnosis and Management of Dementia: Review. *Jama, 322*(16), 1589-1599. doi:10.1001/jama.2019.4782

Asaka, Y., Seager, M. A., Griffin, A. L., & Berry, S. D. (2000). Medial septal microinfusion of scopolamine disrupts hippocampal activity and trace jaw movement conditioning. *Behav Neurosci, 114*(6), 1068-1077. doi:10.1037//0735-7044.114.6.1068

Aston-Jones, G., & Bloom, F. E. (1981). Activity of norepinephrine-containing locus coeruleus neurons in behaving rats anticipates fluctuations in the sleep-waking cycle. *J Neurosci, 1*(8), 876-886. doi:10.1523/jneurosci.01-08-00876.1981

Atherton, L. A., Dupret, D., & Mellor, J. R. (2015). Memory trace replay: the shaping of memory consolidation by neuromodulation. *Trends Neurosci, 38*(9), 560-570. doi:10.1016/j.tins.2015.07.004

Baghdoyan, H. A., Rodrigo-Angulo, M. L., McCarley, R. W., & Hobson, J. A. (1984). Site-specific enhancement and suppression of desynchronized sleep signs following cholinergic stimulation of three brainstem regions. *Brain Res, 306*(1-2), 39-52. doi:10.1016/0006-8993(84)90354-8

Bakker, A., Krauss, Gregory L., Albert, Marilyn S., Speck, Caroline L., Jones, Lauren R., Stark, Craig E., . . . Gallagher, M. (2012). Reduction of Hippocampal Hyperactivity Improves Cognition in Amnestic Mild Cognitive Impairment. *Neuron, 74*(3), 467-474. doi:10.1016/j.neuron.2012.03.023

Ballatore, C., Lee, V. M., & Trojanowski, J. Q. (2007). Tau-mediated neurodegeneration in Alzheimer's disease and related disorders. *Nat Rev Neurosci, 8*(9), 663-672. doi:10.1038/nrn2194

Bamberger, M. E., Harris, M. E., McDonald, D. R., Husemann, J., & Landreth, G. E. (2003). A cell surface receptor complex for fibrillar beta-amyloid mediates microglial activation. *J Neurosci, 23*(7), 2665-2674. doi:10.1523/jneurosci.23-07-02665.2003

Bartus, R. T., Dean, R. L., 3rd, Beer, B., & Lippa, A. S. (1982). The cholinergic hypothesis of geriatric memory dysfunction. *Science, 217*(4558), 408-414. doi:10.1126/science.7046051

Başar, E., Emek-Savaş, D. D., Güntekin, B., & Yener, G. G. (2016). Delay of cognitive gamma responses in Alzheimer's disease. *Neuroimage Clin, 11*, 106-115. doi:10.1016/j.nicl.2016.01.015

Başar, E., Femir, B., Emek-Savaş, D. D., Güntekin, B., & Yener, G. G. (2017). Increased long distance event-related gamma band connectivity in Alzheimer's disease. *Neuroimage Clin, 14*, 580-590. doi:10.1016/j.nicl.2017.02.021

Bastiaansen, M., & Hagoort, P. (2003). Event-induced theta responses as a window on the dynamics of memory. *Cortex, 39*(4-5), 967-992. doi:10.1016/s0010-9452(08)70873-6

Bekdash, R. A. (2021). The Cholinergic System, the Adrenergic System and the Neuropathology of Alzheimer's Disease. *Int J Mol Sci, 22*(3). doi:10.3390/ijms22031273

Bennys, K., Rondouin, G., Vergnes, C., & Touchon, J. (2001). Diagnostic value of quantitative EEG in Alzheimer's disease. *Neurophysiol Clin, 31*(3), 153-160. doi:10.1016/s0987-7053(01)00254-4

Benthem, S. D., Skelin, I., Moseley, S. C., Stimmell, A. C., Dixon, J. R., Melilli, A. S., . . . Wilber, A. A. (2020). Impaired Hippocampal-Cortical Interactions during Sleep in a Mouse Model of Alzheimer's Disease. *Curr Biol, 30*(13), 2588-2601.e2585. doi:10.1016/j.cub.2020.04.087

Benzi, G., & Moretti, A. (1995). Are reactive oxygen species involved in Alzheimer's disease? *Neurobiol Aging, 16*(4), 661-674. doi:10.1016/0197-4580(95)00066-n

Bero, A. W., Yan, P., Roh, J. H., Cirrito, J. R., Stewart, F. R., Raichle, M. E., . . . Holtzman, D. M. (2011). Neuronal activity regulates the regional vulnerability to amyloid-β deposition. *Nature Neuroscience, 14*(6), 750-756. doi:10.1038/nn.2801

Besthorn, C., Förstl, H., Geiger-Kabisch, C., Sattel, H., Gasser, T., & Schreiter-Gasser, U. (1994). EEG coherence in Alzheimer disease. *Electroencephalogr Clin Neurophysiol, 90*(3), 242-245. doi:10.1016/0013-4694(94)90095-7

Besthorn, C., Sattel, H., Geiger-Kabisch, C., Zerfass, R., & Förstl, H. (1995). Parameters of EEG dimensional complexity in Alzheimer's disease. *Electroencephalogr Clin Neurophysiol, 95*(2), 84-89. doi:10.1016/0013-4694(95)00050-9

Betterton, R. T., Broad, L. M., Tsaneva-Atanasova, K., & Mellor, J. R. (2017). Acetylcholine modulates gamma frequency oscillations in the hippocampus by activation of muscarinic M1 receptors. *Eur J Neurosci, 45*(12), 1570-1585. doi:10.1111/ejn.13582

Bhattacharya, S., Haertel, C., Maelicke, A., & Montag, D. (2014). Galantamine slows down plaque formation and behavioral decline in the 5XFAD mouse model of Alzheimer's disease. *PLoS One, 9*(2), e89454. doi:10.1371/journal.pone.0089454

Bianco, M., Balena, A., Pisanello, M., Pisano, F., Sileo, L., Spagnolo, B., . . . Pisanello, F. (2021). Comparative study of autofluorescence in flat and tapered optical fibers towards application in depth-resolved fluorescence lifetime photometry in brain tissue. *Biomed Opt Express, 12*(2), 993-1010. doi:10.1364/boe.410244

Blessed, G., Tomlinson, B. E., & Roth, M. (1968). The association between quantitative measures of dementia and of senile change in the cerebral grey matter of elderly subjects. *Br J Psychiatry, 114*(512), 797-811. doi:10.1192/bjp.114.512.797

Bobola, M. S., Chen, L., Ezeokeke, C. K., Olmstead, T. A., Nguyen, C., Sahota, A., . . . Mourad, P. D. (2020). Transcranial focused ultrasound, pulsed at 40 Hz, activates microglia acutely and reduces Aβ load chronically, as demonstrated in vivo. *Brain Stimul, 13*(4), 1014-1023. doi:10.1016/j.brs.2020.03.016

Bonanni, E., Maestri, M., Tognoni, G., Fabbrini, M., Nucciarone, B., Manca, M. L., . . . Murri, L. (2005). Daytime sleepiness in mild and moderate Alzheimer's disease and its relationship with cognitive impairment. *J Sleep Res, 14*(3), 311-317. doi:10.1111/j.1365-2869.2005.00462.x

Booth, C. A., Witton, J., Nowacki, J., Tsaneva-Atanasova, K., Jones, M. W., Randall, A. D., & Brown, J. T. (2016). Altered Intrinsic Pyramidal Neuron Properties and Pathway-Specific Synaptic Dysfunction Underlie Aberrant Hippocampal Network Function in a Mouse Model of Tauopathy. *J Neurosci, 36*(2), 350-363. doi:10.1523/jneurosci.2151-15.2016

Bowen, D. M., Smith, C. B., White, P., & Davison, A. N. (1976). Neurotransmitter-related enzymes and indices of hypoxia in senile dementia and other abiotrophies. *Brain, 99*(3), 459-496. doi:10.1093/brain/99.3.459

Brenner, R. P., Reynolds, C. F., 3rd, & Ulrich, R. F. (1988). Diagnostic efficacy of computerized spectral versus visual EEG analysis in elderly normal, demented and depressed subjects. *Electroencephalogr Clin Neurophysiol, 69*(2), 110-117. doi:10.1016/0013-4694(88)90206-4

Briggs, R., Kennelly, S. P., & O'Neill, D. (2016). Drug treatments in Alzheimer's disease. *Clin Med (Lond), 16*(3), 247-253. doi:10.7861/clinmedicine.16-3-247

Budd Haeberlein, S., Aisen, P. S., Barkhof, F., Chalkias, S., Chen, T., Cohen, S., . . . Sandrock, A. (2022). Two Randomized Phase 3 Studies of Aducanumab in Early Alzheimer's Disease. *J Prev Alzheimers Dis, 9*(2), 197-210. doi:10.14283/jpad.2022.30

Buée, L., Bussière, T., Buée-Scherrer, V., Delacourte, A., & Hof, P. R. (2000). Tau protein isoforms, phosphorylation and role in neurodegenerative disorders. *Brain Res Brain Res Rev, 33*(1), 95-130. doi:10.1016/s0165-0173(00)00019-9

Busche, M. A., Chen, X., Henning, H. A., Reichwald, J., Staufenbiel, M., Sakmann, B., & Konnerth, A. (2012). Critical role of soluble amyloid-β for early hippocampal hyperactivity in a mouse model of Alzheimer’s disease. *Proceedings of the National Academy of Sciences, 109*(22), 8740-8745. doi:10.1073/pnas.1206171109

Busche, M. A., & Hyman, B. T. (2020). Synergy between amyloid-β and tau in Alzheimer's disease. *Nat Neurosci, 23*(10), 1183-1193. doi:10.1038/s41593-020-0687-6

Busche, M. A., & Konnerth, A. (2016). Impairments of neural circuit function in Alzheimer's disease. *Philosophical Transactions of the Royal Society B: Biological Sciences, 371*(1700), 20150429. doi:doi:10.1098/rstb.2015.0429

Butterfield, D. A. (2002). Amyloid beta-peptide (1-42)-induced oxidative stress and neurotoxicity: implications for neurodegeneration in Alzheimer's disease brain. A review. *Free Radic Res, 36*(12), 1307-1313. doi:10.1080/1071576021000049890

Butterfield, D. A., & Sultana, R. (2011). Methionine-35 of aβ(1-42): importance for oxidative stress in Alzheimer disease. *J Amino Acids, 2011*, 198430. doi:10.4061/2011/198430

Buzsáki, G. (1986). Hippocampal sharp waves: their origin and significance. *Brain Res, 398*(2), 242-252. doi:10.1016/0006-8993(86)91483-6

Buzsáki, G. (1989). Two-stage model of memory trace formation: A role for “noisy” brain states. *Neuroscience, 31*(3), 551-570. doi:https://doi.org/10.1016/0306-4522(89)90423-5
Buzsáki, G. (2004). Large-scale recording of neuronal ensembles. *Nat Neurosci, 7*(5), 446-451. doi:10.1038/nn1233
Buzsáki, G. (2015). Hippocampal sharp wave-ripple: A cognitive biomarker for episodic memory and planning. *Hippocampus, 25*(10), 1073-1188. doi:10.1002/hipo.22488
Buzsáki, G., Horváth, Z., Urioste, R., Hetke, J., & Wise, K. (1992). High-frequency network oscillation in the hippocampus. *Science, 256*(5059), 1025-1027. doi:10.1126/science.1589772
Buzsáki, G., Leung, L. W., & Vanderwolf, C. H. (1983). Cellular bases of hippocampal EEG in the behaving rat. *Brain Res, 287*(2), 139-171. doi:10.1016/0165-0173(83)90037-1
Buzsáki, G., & Wang, X. J. (2012). Mechanisms of gamma oscillations. *Annual review of neuroscience, 35*, 203-225. doi:10.1146/annurev-neuro-062111-150444
Byron, N., & Sakata, S. (2023). Fiber photometry-based investigation of brain function and dysfunction. *Neurophotonics, 11*(S1), S11502. Retrieved from https://doi.org/10.1117/1.NPh.11.S1.S11502
Byron, N., Semenova, A., & Sakata, S. (2021). Mutual Interactions between Brain States and Alzheimer's Disease Pathology: A Focus on Gamma and Slow Oscillations. *Biology (Basel), 10*(8). doi:10.3390/biology10080707
Caccavano, A., Bozzelli, P. L., Forcelli, P. A., Pak, D. T. S., Wu, J.-Y., Conant, K., & Vicini, S. (2020). Inhibitory Parvalbumin Basket Cell Activity is Selectively Reduced during Hippocampal Sharp Wave Ripples in a Mouse Model of Familial Alzheimer's Disease. *The Journal of Neuroscience, 40*(26), 5116-5136. doi:10.1523/jneurosci.0425-20.2020
Calandreau, L., Trifilieff, P., Mons, N., Costes, L., Marien, M., Marighetto, A., . . . Desmedt, A. (2006). Extracellular hippocampal acetylcholine level controls amygdala function and promotes adaptive conditioned emotional response. *J Neurosci, 26*(52), 13556-13566. doi:10.1523/jneurosci.3713-06.2006
Calsolaro, V., & Edison, P. (2016). Neuroinflammation in Alzheimer's disease: Current evidence and future directions. *Alzheimers Dement, 12*(6), 719-732. doi:10.1016/j.jalz.2016.02.010
Cao, J., Gaamouch, F. E., Meabon, J. S., Meeker, K. D., Zhu, L., Zhong, M. B., . . . Cai, D. (2017). ApoE4-associated phospholipid dysregulation contributes to development of Tau hyper-phosphorylation after traumatic brain injury. *Sci Rep, 7*(1), 11372. doi:10.1038/s41598-017-11654-7
Carey, I. M., Anderson, H. R., Atkinson, R. W., Beevers, S. D., Cook, D. G., Strachan, D. P., . . . Kelly, F. J. (2018). Are noise and air pollution related to the incidence of dementia? A cohort study in London, England. *BMJ Open, 8*(9), e022404. doi:10.1136/bmjopen-2018-022404
Carlson, A. B., & Kraus, G. P. (2024). Physiology, Cholinergic Receptors. In *StatPearls*. Treasure Island (FL) ineligible companies. Disclosure: Gregory Kraus declares no relevant financial relationships with ineligible companies.: StatPearls Publishing
Copyright © 2024, StatPearls Publishing LLC.
Carr, M. F., Jadhav, S. P., & Frank, L. M. (2011). Hippocampal replay in the awake state: a potential substrate for memory consolidation and retrieval. *Nature Neuroscience, 14*(2), 147-153. doi:10.1038/nn.2732
Chan, D., Shafto, M., Kievit, R., Matthews, F., Spink, M., Valenzuela, M., & Henson, R. N. (2018). Lifestyle activities in mid-life contribute to cognitive reserve in late-life, independent of education, occupation, and late-life activities. *Neurobiol Aging, 70*, 180-183. doi:10.1016/j.neurobiolaging.2018.06.012
Chan, D., Suk, H. J., Jackson, B. L., Milman, N. P., Stark, D., Klerman, E. B., . . . Tsai, L. H. (2022). Gamma frequency sensory stimulation in mild probable Alzheimer's dementia patients: Results of feasibility and pilot studies. *PLoS One, 17*(12), e0278412. doi:10.1371/journal.pone.0278412
Chang, K. A., & Suh, Y. H. (2005). Pathophysiological roles of amyloidogenic carboxy-terminal fragments of the beta-amyloid precursor protein in Alzheimer's disease. *J Pharmacol Sci, 97*(4), 461-471. doi:10.1254/jphs.cr0050014

Chang, Q., & Gold, P. E. (2003). Switching memory systems during learning: changes in patterns of brain acetylcholine release in the hippocampus and striatum in rats. *J Neurosci, 23*(7), 3001-3005. doi:10.1523/jneurosci.23-07-03001.2003
Chatterjee, S., Peters, S. A., Woodward, M., Mejia Arango, S., Batty, G. D., Beckett, N., . . . Huxley, R. R. (2016). Type 2 Diabetes as a Risk Factor for Dementia in Women Compared With Men: A Pooled Analysis of 2.3 Million People Comprising More Than 100,000 Cases of Dementia. *Diabetes Care, 39*(2), 300-307. doi:10.2337/dc15-1588
Chen, G. F., Xu, T. H., Yan, Y., Zhou, Y. R., Jiang, Y., Melcher, K., & Xu, H. E. (2017). Amyloid beta: structure, biology and structure-based therapeutic development. *Acta Pharmacol Sin, 38*(9), 1205-1235. doi:10.1038/aps.2017.28
Chen, Z. R., Huang, J. B., Yang, S. L., & Hong, F. F. (2022). Role of Cholinergic Signaling in Alzheimer's Disease. *Molecules, 27*(6). doi:10.3390/molecules27061816
Cheng, S., & Frank, L. M. (2008). New experiences enhance coordinated neural activity in the hippocampus. *Neuron, 57*(2), 303-313. doi:10.1016/j.neuron.2007.11.035
Cheng, X., Sadegh, S., Zilpelwar, S., Devor, A., Tian, L., & Boas, D. A. (2020). Comparing the fundamental imaging depth limit of two-photon, three-photon, and non-degenerate two-photon microscopy. *Opt Lett, 45*(10), 2934-2937. doi:10.1364/ol.392724
Chishti, M. A., Yang, D. S., Janus, C., Phinney, A. L., Horne, P., Pearson, J., . . . Westaway, D. (2001). Early-onset amyloid deposition and cognitive deficits in transgenic mice expressing a double mutant form of amyloid precursor protein 695. *J Biol Chem, 276*(24), 21562-21570. doi:10.1074/jbc.M100710200
Choi, D. W. (1987). Ionic dependence of glutamate neurotoxicity. *J Neurosci, 7*(2), 369-379. doi:10.1523/jneurosci.07-02-00369.1987
Chu, L. W. (2012). Alzheimer's disease: early diagnosis and treatment. *Hong Kong Med J, 18*(3), 228-237.
Cimenser, A., Hempel, E., Travers, T., Strozewski, N., Martin, K., Malchano, Z., & Hajós, M. (2021). Sensory-Evoked 40-Hz Gamma Oscillation Improves Sleep and Daily Living Activities in Alzheimer's Disease Patients. *Front Syst Neurosci, 15*, 746859. doi:10.3389/fnsys.2021.746859
Cirelli, C., & Tononi, G. (2008). Is sleep essential? *PLoS Biol, 6*(8), e216. doi:10.1371/journal.pbio.0060216
Cirrito, J. R., Yamada, K. A., Finn, M. B., Sloviter, R. S., Bales, K. R., May, P. C., . . . Holtzman, D. M. (2005). Synaptic activity regulates interstitial fluid amyloid-beta levels in vivo. *Neuron, 48*(6), 913-922. doi:10.1016/j.neuron.2005.10.028
Ciupek, S. M., Cheng, J., Ali, Y. O., Lu, H. C., & Ji, D. (2015). Progressive functional impairments of hippocampal neurons in a tauopathy mouse model. *J Neurosci, 35*(21), 8118-8131. doi:10.1523/jneurosci.3130-14.2015
Claude, L., Chouchou, F., Prados, G., Castro, M., De Blay, B., Perchet, C., . . . Bastuji, H. (2015). Sleep spindles and human cortical nociception: a surface and intracerebral electrophysiological study. *J Physiol, 593*(22), 4995-5008. doi:10.1113/jp270941
Clavaguera, F., Akatsu, H., Fraser, G., Crowther, R. A., Frank, S., Hench, J., . . . Tolnay, M. (2013). Brain homogenates from human tauopathies induce tau inclusions in mouse brain. *Proc Natl Acad Sci U S A, 110*(23), 9535-9540. doi:10.1073/pnas.1301175110
Clavaguera, F., Bolmont, T., Crowther, R. A., Abramowski, D., Frank, S., Probst, A., . . . Tolnay, M. (2009). Transmission and spreading of tauopathy in transgenic mouse brain. *Nat Cell Biol, 11*(7), 909-913. doi:10.1038/ncb1901
Colonnese, M. T., Kaminska, A., Minlebaev, M., Milh, M., Bloem, B., Lescure, S., . . . Khazipov, R. (2010). A conserved switch in sensory processing prepares developing neocortex for vision. *Neuron, 67*(3), 480-498. doi:10.1016/j.neuron.2010.07.015
Cooke, J. R., Liu, L., Natarajan, L., He, F., Marler, M., Loredo, J. S., . . . Ancoli-Israel, S. (2006). The effect of sleep-disordered breathing on stages of sleep in patients with Alzheimer's disease. *Behav Sleep Med, 4*(4), 219-227. doi:10.1207/s15402010bsm0404_2
Crowley, K., Trinder, J., Kim, Y., Carrington, M., & Colrain, I. M. (2002). The effects of normal aging on sleep spindle and K-complex production. *Clinical Neurophysiology, 113*(10), 1615-1622. doi:https://doi.org/10.1016/S1388-2457(02)00237-7

Csicsvari, J., Henze, D. A., Jamieson, B., Harris, K. D., Sirota, A., Barthó, P., . . . Buzsáki, G. (2003). Massively parallel recording of unit and local field potentials with silicon-based electrodes. *J Neurophysiol, 90*(2), 1314-1323. doi:10.1152/jn.00116.2003
Cummings, J. L., Osse, A. M. L., & Kinney, J. W. (2023). Alzheimer's Disease: Novel Targets and Investigational Drugs for Disease Modification. *Drugs, 83*(15), 1387-1408. doi:10.1007/s40265-023-01938-w
Cupers, P., Sautter, J., & Vanvossel, A. (2006). European Union research policy and funding for Alzheimer disease. *Nat Med, 12*(7), 774-775. doi:10.1038/nm0706-774
Cushing, S. D., Skelin, I., Moseley, S. C., Stimmell, A. C., Dixon, J. R., Melilli, A. S., . . . Wilber, A. A. (2020). Impaired Hippocampal-Cortical Interactions during Sleep in a Mouse Model of Alzheimer's Disease. *Current Biology, 30*(13), 2588-2601.e2585. doi:https://doi.org/10.1016/j.cub.2020.04.087
d'Errico, P., & Meyer-Luehmann, M. (2020). Mechanisms of Pathogenic Tau and Aβ Protein Spreading in Alzheimer's Disease. *Front Aging Neurosci, 12*, 265. doi:10.3389/fnagi.2020.00265
Da, X., Hempel, E., Ou, Y., Rowe, O. E., Malchano, Z., Hajós, M., . . . Cimenser, A. (2024). Noninvasive Gamma Sensory Stimulation May Reduce White Matter and Myelin Loss in Alzheimer's Disease. *J Alzheimers Dis, 97*(1), 359-372. doi:10.3233/jad-230506
Davies, P. (1985). A critical review of the role of the cholinergic system in human memory and cognition. *Ann N Y Acad Sci, 444*, 212-217. doi:10.1111/j.1749-6632.1985.tb37591.x
Davis, K. L., Thal, L. J., Gamzu, E. R., Davis, C. S., Woolson, R. F., Gracon, S. I., . . . et al. (1992). A double-blind, placebo-controlled multicenter study of tacrine for Alzheimer's disease. The Tacrine Collaborative Study Group. *N Engl J Med, 327*(18), 1253-1259. doi:10.1056/nejm199210293271801
De Gennaro, L., Ferrara, M., Vecchio, F., Curcio, G., & Bertini, M. (2005). An electroencephalographic fingerprint of human sleep. *Neuroimage, 26*(1), 114-122. doi:10.1016/j.neuroimage.2005.01.020
De Strooper, B., Saftig, P., Craessaerts, K., Vanderstichele, H., Guhde, G., Annaert, W., . . . Van Leuven, F. (1998). Deficiency of presenilin-1 inhibits the normal cleavage of amyloid precursor protein. *Nature, 391*(6665), 387-390. doi:10.1038/34910
De Strooper, B., Vassar, R., & Golde, T. (2010). The secretases: enzymes with therapeutic potential in Alzheimer disease. *Nat Rev Neurol, 6*(2), 99-107. doi:10.1038/nrneurol.2009.218
Demattos, R. B., Lu, J., Tang, Y., Racke, M. M., Delong, C. A., Tzaferis, J. A., . . . Hutton, M. L. (2012). A plaque-specific antibody clears existing β-amyloid plaques in Alzheimer's disease mice. *Neuron, 76*(5), 908-920. doi:10.1016/j.neuron.2012.10.029
Denk, W. (1994). Two-photon scanning photochemical microscopy: mapping ligand-gated ion channel distributions. *Proc Natl Acad Sci U S A, 91*(14), 6629-6633. doi:10.1073/pnas.91.14.6629
Denk, W., Strickler, J. H., & Webb, W. W. (1990). Two-photon laser scanning fluorescence microscopy. *Science, 248*(4951), 73-76. doi:10.1126/science.2321027
Deutsch, J. A. (1971). The cholinergic synapse and the site of memory. *Science, 174*(4011), 788-794. doi:10.1126/science.174.4011.788
Devi, L., & Ohno, M. (2010). Phospho-eIF2α level is important for determining abilities of BACE1 reduction to rescue cholinergic neurodegeneration and memory defects in 5XFAD mice. *PLoS One, 5*(9), e12974. doi:10.1371/journal.pone.0012974
Diba, K., & Buzsáki, G. (2007). Forward and reverse hippocampal place-cell sequences during ripples. *Nat Neurosci, 10*(10), 1241-1242. doi:10.1038/nn1961
Dickerson, B. C., Salat, D. H., Greve, D. N., Chua, E. F., Rand-Giovannetti, E., Rentz, D. M., . . . Sperling, R. A. (2005). Increased hippocampal activation in mild cognitive impairment compared to normal aging and AD. *Neurology, 65*(3), 404-411. doi:10.1212/01.wnl.0000171450.97464.49
DiSabato, D. J., Quan, N., & Godbout, J. P. (2016). Neuroinflammation: the devil is in the details. *J Neurochem, 139 Suppl 2*(Suppl 2), 136-153. doi:10.1111/jnc.13607

Donohue, K. D., Medonza, D. C., Crane, E. R., & O'Hara, B. F. (2008). Assessment of a non-invasive high-throughput classifier for behaviours associated with sleep and wake in mice. *Biomed Eng Online, 7*, 14. doi:10.1186/1475-925x-7-14

dos Santos Lima, G. Z., Lobao-Soares, B., Corso, G., Belchior, H., Lopes, S. R., de Lima Prado, T., . . . Ivanov, P. C. (2019). Hippocampal and cortical communication around micro-arousals in slow-wave sleep. *Scientific Reports, 9*(1), 5876. doi:10.1038/s41598-019-42100-5

Drachman, D. A., & Leavitt, J. (1974). Human memory and the cholinergic system. A relationship to aging? *Arch Neurol, 30*(2), 113-121. doi:10.1001/archneur.1974.00490320001001

Dringen, R., Pfeiffer, B., & Hamprecht, B. (1999). Synthesis of the antioxidant glutathione in neurons: supply by astrocytes of CysGly as precursor for neuronal glutathione. *J Neurosci, 19*(2), 562-569. doi:10.1523/jneurosci.19-02-00562.1999

Ecker, A., Bagi, B., Vértes, E., Steinbach-Németh, O., Karlócai, M. R., Papp, O. I., . . . Káli, S. (2022). Hippocampal sharp wave-ripples and the associated sequence replay emerge from structured synaptic interactions in a network model of area CA3. *eLife, 11*, e71850. doi:10.7554/eLife.71850

Eckman, E. A., Adams, S. K., Troendle, F. J., Stodola, B. A., Kahn, M. A., Fauq, A. H., . . . Eckman, C. B. (2006). Regulation of steady-state beta-amyloid levels in the brain by neprilysin and endothelin-converting enzyme but not angiotensin-converting enzyme. *J Biol Chem, 281*(41), 30471-30478. doi:10.1074/jbc.M605827200

Ego-Stengel, V., & Wilson, M. A. (2010). Disruption of ripple-associated hippocampal activity during rest impairs spatial learning in the rat. *Hippocampus, 20*(1), 1-10. doi:10.1002/hipo.20707

Eimer, W. A., & Vassar, R. (2013). Neuron loss in the 5XFAD mouse model of Alzheimer's disease correlates with intraneuronal Aβ42 accumulation and Caspase-3 activation. *Mol Neurodegener, 8*, 2. doi:10.1186/1750-1326-8-2

El Khoury, J. B., Moore, K. J., Means, T. K., Leung, J., Terada, K., Toft, M., . . . Luster, A. D. (2003). CD36 mediates the innate host response to beta-amyloid. *J Exp Med, 197*(12), 1657-1666. doi:10.1084/jem.20021546

Ellenbogen, J. M., Hulbert, J. C., Stickgold, R., Dinges, D. F., & Thompson-Schill, S. L. (2006). Interfering with Theories of Sleep and Memory: Sleep, Declarative Memory, and Associative Interference. *Current Biology, 16*(13), 1290-1294. doi:https://doi.org/10.1016/j.cub.2006.05.024

Etter, G., van der Veldt, S., Manseau, F., Zarrinkoub, I., Trillaud-Doppia, E., & Williams, S. (2019). Optogenetic gamma stimulation rescues memory impairments in an Alzheimer's disease mouse model. *Nat Commun, 10*(1), 5322. doi:10.1038/s41467-019-13260-9

Fann, J. R., Ribe, A. R., Pedersen, H. S., Fenger-Grøn, M., Christensen, J., Benros, M. E., & Vestergaard, M. (2018). Long-term risk of dementia among people with traumatic brain injury in Denmark: a population-based observational cohort study. *Lancet Psychiatry, 5*(5), 424-431. doi:10.1016/s2215-0366(18)30065-8

Farrell, J. S., Hwaun, E., Dudok, B., & Soltesz, I. (2024). Neural and behavioural state switching during hippocampal dentate spikes. *Nature, 628*(8008), 590-595. doi:10.1038/s41586-024-07192-8

Fernandez, L. M., Vantomme, G., Osorio-Forero, A., Cardis, R., Béard, E., & Lüthi, A. (2018). Thalamic reticular control of local sleep in mouse sensory cortex. *Elife, 7*. doi:10.7554/eLife.39111

Fernandez, L. M. J., & Lüthi, A. (2020). Sleep Spindles: Mechanisms and Functions. *Physiological Reviews, 100*(2), 805-868. doi:10.1152/physrev.00042.2018

Fernández-Ruiz, A., Oliva, A., Fermino de Oliveira, E., Rocha-Almeida, F., Tingley, D., & Buzsáki, G. (2019). Long-duration hippocampal sharp wave ripples improve memory. *Science, 364*(6445), 1082-1086. doi:10.1126/science.aax0758

Fernández-Tomé, P., Brera, B., Arévalo, M. A., & de Ceballos, M. L. (2004). Beta-amyloid25-35 inhibits glutamate uptake in cultured neurons and astrocytes: modulation of uptake as a survival mechanism. *Neurobiol Dis, 15*(3), 580-589. doi:10.1016/j.nbd.2003.12.006

Ferrarelli, F., & Tononi, G. (2011). The thalamic reticular nucleus and schizophrenia. *Schizophr Bull, 37*(2), 306-315. doi:10.1093/schbul/sbq142
Feyissa, A. M., & Tatum, W. O. (2019). Adult EEG. *Handb Clin Neurol, 160*, 103-124. doi:10.1016/b978-0-444-64032-1.00007-2
Finger, C. E., Moreno-Gonzalez, I., Gutierrez, A., Moruno-Manchon, J. F., & McCullough, L. D. (2022). Age-related immune alterations and cerebrovascular inflammation. *Mol Psychiatry, 27*(2), 803-818. doi:10.1038/s41380-021-01361-1
Fisahn, A., Pike, F. G., Buhl, E. H., & Paulsen, O. (1998). Cholinergic induction of network oscillations at 40 Hz in the hippocampus in vitro. *Nature, 394*(6689), 186-189. doi:10.1038/28179
Flanigan, T. J., Xue, Y., Kishan Rao, S., Dhanushkodi, A., & McDonald, M. P. (2014). Abnormal vibrissa-related behavior and loss of barrel field inhibitory neurons in 5xFAD transgenics. *Genes Brain Behav, 13*(5), 488-500. doi:10.1111/gbb.12133
Fogel, S. M., & Smith, C. T. (2006). Learning-dependent changes in sleep spindles and Stage 2 sleep. *J Sleep Res, 15*(3), 250-255. doi:10.1111/j.1365-2869.2006.00522.x
Folch, J., Busquets, O., Ettcheto, M., Sánchez-López, E., Castro-Torres, R. D., Verdaguer, E., . . . Camins, A. (2018). Memantine for the Treatment of Dementia: A Review on its Current and Future Applications. *J Alzheimers Dis, 62*(3), 1223-1240. doi:10.3233/jad-170672
Fox, N. C., Warrington, E. K., Freeborough, P. A., Hartikainen, P., Kennedy, A. M., Stevens, J. M., & Rossor, M. N. (1996). Presymptomatic hippocampal atrophy in Alzheimer's disease. A longitudinal MRI study. *Brain, 119 (Pt 6)*, 2001-2007. doi:10.1093/brain/119.6.2001
Frackowiak, J., Wisniewski, H. M., Wegiel, J., Merz, G. S., Iqbal, K., & Wang, K. C. (1992). Ultrastructure of the microglia that phagocytose amyloid and the microglia that produce beta-amyloid fibrils. *Acta Neuropathol, 84*(3), 225-233. doi:10.1007/bf00227813
Fratiglioni, L., Launer, L. J., Andersen, K., Breteler, M. M., Copeland, J. R., Dartigues, J. F., . . . Hofman, A. (2000). Incidence of dementia and major subtypes in Europe: A collaborative study of population-based cohorts. Neurologic Diseases in the Elderly Research Group. *Neurology, 54*(11 Suppl 5), S10-15.
Fries, P. (2015). Rhythms for Cognition: Communication through Coherence. *Neuron, 88*(1), 220-235. doi:https://doi.org/10.1016/j.neuron.2015.09.034
Frinchi, M., Scaduto, P., Cappello, F., Belluardo, N., & Mudò, G. (2018). Heat shock protein (Hsp) regulation by muscarinic acetylcholine receptor (mAChR) activation in the rat hippocampus. *J Cell Physiol, 233*(8), 6107-6116. doi:10.1002/jcp.26454
Frotscher, M., & Léránth, C. (1985). Cholinergic innervation of the rat hippocampus as revealed by choline acetyltransferase immunocytochemistry: a combined light and electron microscopic study. *J Comp Neurol, 239*(2), 237-246. doi:10.1002/cne.902390210
Funane, T., Jun, H., Sutoko, S., Saido, T. C., Kandori, A., & Igarashi, K. M. (2022). Impaired sharp-wave ripple coordination between the medial entorhinal cortex and hippocampal CA1 of knock-in model of Alzheimer's disease. *Frontiers in Systems Neuroscience, 16*. doi:10.3389/fnsys.2022.955178
Furue, H., Katafuchi, T., & Yoshimura, M. (2007). In Vivo Patch-Clamp Technique. In W. Walz (Ed.), *Patch-Clamp Analysis: Advanced Techniques* (pp. 229-251). Totowa, NJ: Humana Press.
Gais, S., Mölle, M., Helms, K., & Born, J. (2002). Learning-dependent increases in sleep spindle density. *J Neurosci, 22*(15), 6830-6834. doi:10.1523/jneurosci.22-15-06830.2002
Gale, S. D., Baxter, L., & Thompson, J. (2016). Greater memory impairment in dementing females than males relative to sex-matched healthy controls. *Journal of Clinical and Experimental Neuropsychology, 38*(5), 527-533. doi:10.1080/13803395.2015.1132298
Games, D., Adams, D., Alessandrini, R., Barbour, R., Berthelette, P., Blackwell, C., . . . et al. (1995). Alzheimer-type neuropathology in transgenic mice overexpressing V717F beta-amyloid precursor protein. *Nature, 373*(6514), 523-527. doi:10.1038/373523a0

Gaykema, R. P., Luiten, P. G., Nyakas, C., & Traber, J. (1990). Cortical projection patterns of the medial septum-diagonal band complex. *J Comp Neurol, 293*(1), 103-124. doi:10.1002/cne.902930109
Giannoni, P., Arango-Lievano, M., Neves, I. D., Rousset, M. C., Baranger, K., Rivera, S., . . . Marchi, N. (2016). Cerebrovascular pathology during the progression of experimental Alzheimer's disease. *Neurobiol Dis, 88*, 107-117. doi:10.1016/j.nbd.2016.01.001
Girardeau, G., Benchenane, K., Wiener, S. I., Buzsáki, G., & Zugaro, M. B. (2009). Selective suppression of hippocampal ripples impairs spatial memory. *Nat Neurosci, 12*(10), 1222-1223. doi:10.1038/nn.2384
Girardeau, G., Cei, A., & Zugaro, M. (2014). Learning-induced plasticity regulates hippocampal sharp wave-ripple drive. *J Neurosci, 34*(15), 5176-5183. doi:10.1523/jneurosci.4288-13.2014
Girardeau, G., Inema, I., & Buzsáki, G. (2017). Reactivations of emotional memory in the hippocampus-amygdala system during sleep. *Nat Neurosci, 20*(11), 1634-1642. doi:10.1038/nn.4637
Glover, G. H. (2011). Overview of functional magnetic resonance imaging. *Neurosurg Clin N Am, 22*(2), 133-139, vii. doi:10.1016/j.nec.2010.11.001
Golub, J. S., Brickman, A. M., Ciarleglio, A. J., Schupf, N., & Luchsinger, J. A. (2020). Association of Subclinical Hearing Loss With Cognitive Performance. *JAMA Otolaryngol Head Neck Surg, 146*(1), 57-67. doi:10.1001/jamaoto.2019.3375
Gómez-Isla, T., Hollister, R., West, H., Mui, S., Growdon, J. H., Petersen, R. C., . . . Hyman, B. T. (1997). Neuronal loss correlates with but exceeds neurofibrillary tangles in Alzheimer's disease. *Ann Neurol, 41*(1), 17-24. doi:10.1002/ana.410410106
Gonzalez, C. E., Mak-McCully, R. A., Rosen, B. Q., Cash, S. S., Chauvel, P. Y., Bastuji, H., . . . Halgren, E. (2018). Theta Bursts Precede, and Spindles Follow, Cortical and Thalamic Downstates in Human NREM Sleep. *J Neurosci, 38*(46), 9989-10001. doi:10.1523/jneurosci.0476-18.2018
Gordon, E. B., & Sim, M. (1967). The E.E.G. in presenile dementia. *J Neurol Neurosurg Psychiatry, 30*(3), 285-291. doi:10.1136/jnnp.30.3.285
Gorgoni, M., Lauri, G., Truglia, I., Cordone, S., Sarasso, S., Scarpelli, S., . . . De Gennaro, L. (2016). Parietal Fast Sleep Spindle Density Decrease in Alzheimer's Disease and Amnesic Mild Cognitive Impairment. *Neural Plasticity, 2016*(1), 8376108. doi:https://doi.org/10.1155/2016/8376108
Gremer, L., Schölzel, D., Schenk, C., Reinartz, E., Labahn, J., Ravelli, R. B. G., . . . Schröder, G. F. (2017). Fibril structure of amyloid-β(1-42) by cryo-electron microscopy. *Science, 358*(6359), 116-119. doi:10.1126/science.aao2825
Griffiths, B. J., & Jensen, O. (2023). Gamma oscillations and episodic memory. *Trends in Neurosciences, 46*(10), 832-846. doi:https://doi.org/10.1016/j.tins.2023.07.003
Guo, J. L., Narasimhan, S., Changolkar, L., He, Z., Stieber, A., Zhang, B., . . . Lee, V. M. (2016). Unique pathological tau conformers from Alzheimer's brains transmit tau pathology in nontransgenic mice. *J Exp Med, 213*(12), 2635-2654. doi:10.1084/jem.20160833
Haass, C., & Selkoe, D. J. (2007). Soluble protein oligomers in neurodegeneration: lessons from the Alzheimer's amyloid beta-peptide. *Nat Rev Mol Cell Biol, 8*(2), 101-112. doi:10.1038/nrm2101
Hampel, H., Mesulam, M. M., Cuello, A. C., Farlow, M. R., Giacobini, E., Grossberg, G. T., . . . Khachaturian, Z. S. (2018). The cholinergic system in the pathophysiology and treatment of Alzheimer's disease. *Brain, 141*(7), 1917-1933. doi:10.1093/brain/awy132
Hanert, A., Schönfeld, R., Weber, F. D., Nowak, A., Döhring, J., Philippen, S., . . . Bartsch, T. (2024). Reduced overnight memory consolidation and associated alterations in sleep spindles and slow oscillations in early Alzheimer's disease. *Neurobiology of Disease, 190*, 106378. doi:https://doi.org/10.1016/j.nbd.2023.106378
Hardy, J. A., & Higgins, G. A. (1992). Alzheimer's disease: the amyloid cascade hypothesis. *Science, 256*(5054), 184-185. doi:10.1126/science.1566067
Harris, J. A., Devidze, N., Verret, L., Ho, K., Halabisky, B., Thwin, M. T., . . . Mucke, L. (2010). Transsynaptic Progression of Amyloid-β-Induced Neuronal Dysfunction

within the Entorhinal-Hippocampal Network. *Neuron, 68*(3), 428-441. doi:https://doi.org/10.1016/j.neuron.2010.10.020
Hasselmo, M. E. (2006). The role of acetylcholine in learning and memory. *Curr Opin Neurobiol, 16*(6), 710-715. doi:10.1016/j.conb.2006.09.002
Hasselmo, M. E., & McGaughy, J. (2004). High acetylcholine levels set circuit dynamics for attention and encoding and low acetylcholine levels set dynamics for consolidation. *Prog Brain Res, 145*, 207-231. doi:10.1016/s0079-6123(03)45015-2
Hasselmo, M. E., & Schnell, E. (1994). Laminar selectivity of the cholinergic suppression of synaptic transmission in rat hippocampal region CA1: computational modeling and brain slice physiology. *J Neurosci, 14*(6), 3898-3914. doi:10.1523/jneurosci.14-06-03898.1994
Hasselmo, M. E., Schnell, E., & Barkai, E. (1995). Dynamics of learning and recall at excitatory recurrent synapses and cholinergic modulation in rat hippocampal region CA3. *J Neurosci, 15*(7 Pt 2), 5249-5262. doi:10.1523/jneurosci.15-07-05249.1995
Hazel, J. R., & Williams, E. E. (1990). The role of alterations in membrane lipid composition in enabling physiological adaptation of organisms to their physical environment. *Prog Lipid Res, 29*(3), 167-227. doi:10.1016/0163-7827(90)90002-3
He, Q., Colon-Motas, K. M., Pybus, A. F., Piendel, L., Seppa, J. K., Walker, M. L., . . . Singer, A. C. (2021). A feasibility trial of gamma sensory flicker for patients with prodromal Alzheimer's disease. *Alzheimers Dement (N Y), 7*(1), e12178. doi:10.1002/trc2.12178
Helmchen, F. (2009). Frontiers in Neuroscience
Two-Photon Functional Imaging of Neuronal Activity. In R. D. Frostig (Ed.), *In Vivo Optical Imaging of Brain Function*. Boca Raton (FL): CRC Press/Taylor & Francis
Copyright © 2009, Taylor & Francis Group, LLC.
Herrmann, C. S. (2001). Human EEG responses to 1-100 Hz flicker: resonance phenomena in visual cortex and their potential correlation to cognitive phenomena. *Exp Brain Res, 137*(3-4), 346-353. doi:10.1007/s002210100682
Heurling, K., Leuzy, A., Jonasson, M., Frick, A., Zimmer, E. R., Nordberg, A., & Lubberink, M. (2017). Quantitative positron emission tomography in brain research. *Brain Res, 1670*, 220-234. doi:10.1016/j.brainres.2017.06.022
Hickman, S. E., Allison, E. K., & El Khoury, J. (2008). Microglial dysfunction and defective beta-amyloid clearance pathways in aging Alzheimer's disease mice. *J Neurosci, 28*(33), 8354-8360. doi:10.1523/jneurosci.0616-08.2008
Hill, N. J., Gupta, D., Brunner, P., Gunduz, A., Adamo, M. A., Ritaccio, A., & Schalk, G. (2012). Recording human electrocorticographic (ECoG) signals for neuroscientific research and real-time functional cortical mapping. *J Vis Exp*(64). doi:10.3791/3993
Holth, J., Patel, T., & Holtzman, D. M. (2017). Sleep in Alzheimer's Disease - Beyond Amyloid. *Neurobiol Sleep Circadian Rhythms, 2*, 4-14. doi:10.1016/j.nbscr.2016.08.002
Hounsgaard, J. (1978). Presynaptic inhibitory action of acetylcholine in area CA1 of the hippocampus. *Exp Neurol, 62*(3), 787-797. doi:10.1016/0014-4886(78)90284-4
Howard, M. W., Rizzuto, D. S., Caplan, J. B., Madsen, J. R., Lisman, J., Aschenbrenner-Scheibe, R., . . . Kahana, M. J. (2003). Gamma oscillations correlate with working memory load in humans. *Cereb Cortex, 13*(12), 1369-1374. doi:10.1093/cercor/bhg084
Hsiao, K., Chapman, P., Nilsen, S., Eckman, C., Harigaya, Y., Younkin, S., . . . Cole, G. (1996). Correlative memory deficits, Abeta elevation, and amyloid plaques in transgenic mice. *Science, 274*(5284), 99-102. doi:10.1126/science.274.5284.99
Hsieh, L. T., & Ranganath, C. (2014). Frontal midline theta oscillations during working memory maintenance and episodic encoding and retrieval. *Neuroimage, 85 Pt 2*(0 2), 721-729. doi:10.1016/j.neuroimage.2013.08.003
Hu, N., Yu, J. T., Tan, L., Wang, Y. L., Sun, L., & Tan, L. (2013). Nutrition and the risk of Alzheimer's disease. *Biomed Res Int, 2013*, 524820. doi:10.1155/2013/524820
Huan, T., Tran, T., Zheng, J., Sapkota, S., MacDonald, S. W., Camicioli, R., . . . Li, L. (2018). Metabolomics Analyses of Saliva Detect Novel Biomarkers of Alzheimer's Disease. *J Alzheimers Dis, 65*(4), 1401-1416. doi:10.3233/jad-180711

Huerta, P. T., & Lisman, J. E. (1993). Heightened synaptic plasticity of hippocampal CA1 neurons during a cholinergically induced rhythmic state. *Nature, 364*(6439), 723-725. doi:10.1038/364723a0

Iaccarino, H. F., Singer, A. C., Martorell, A. J., Rudenko, A., Gao, F., Gillingham, T. Z., . . . Tsai, L.-H. (2016). Gamma frequency entrainment attenuates amyloid load and modifies microglia. *Nature, 540*(7632), 230-235. doi:10.1038/nature20587

Ikonen, S., McMahan, R., Gallagher, M., Eichenbaum, H., & Tanila, H. (2002). Cholinergic system regulation of spatial representation by the hippocampus. *Hippocampus, 12*(3), 386-397. doi:10.1002/hipo.1109

Israel, L. L., Braubach, O., Shatalova, E. S., Chepurna, O., Sharma, S., Klymyshyn, D., . . . Black, K. L. (2023). Exposure to environmental airborne particulate matter caused wide-ranged transcriptional changes and accelerated Alzheimer's-related pathology: A mouse study. *Neurobiol Dis, 187*, 106307. doi:10.1016/j.nbd.2023.106307

Jack, C. R., Jr., Bennett, D. A., Blennow, K., Carrillo, M. C., Dunn, B., Haeberlein, S. B., . . . Sperling, R. (2018). NIA-AA Research Framework: Toward a biological definition of Alzheimer's disease. *Alzheimers Dement, 14*(4), 535-562. doi:10.1016/j.jalz.2018.02.018

Jack, C. R., Jr., Bennett, D. A., Blennow, K., Carrillo, M. C., Feldman, H. H., Frisoni, G. B., . . . Dubois, B. (2016). A/T/N: An unbiased descriptive classification scheme for Alzheimer disease biomarkers. *Neurology, 87*(5), 539-547. doi:10.1212/wnl.0000000000002923

Jacobs, E. G., Weiss, B. K., Makris, N., Whitfield-Gabrieli, S., Buka, S. L., Klibanski, A., & Goldstein, J. M. (2016). Impact of Sex and Menopausal Status on Episodic Memory Circuitry in Early Midlife. *J Neurosci, 36*(39), 10163-10173. doi:10.1523/jneurosci.0951-16.2016

Jang, S. H., Seo, W. S., & Kwon, H. G. (2016). Post-traumatic narcolepsy and injury of the ascending reticular activating system. *Sleep Medicine, 17*, 124-125. doi:https://doi.org/10.1016/j.sleep.2015.09.020

Jarmolowicz, A. I., Chen, H. Y., & Panegyres, P. K. (2015). The patterns of inheritance in early-onset dementia: Alzheimer's disease and frontotemporal dementia. *Am J Alzheimers Dis Other Demen, 30*(3), 299-306. doi:10.1177/1533317514545825

Jarrett, J. T., Berger, E. P., & Lansbury, P. T., Jr. (1993). The C-terminus of the beta protein is critical in amyloidogenesis. *Ann N Y Acad Sci, 695*, 144-148. doi:10.1111/j.1749-6632.1993.tb23043.x

Jenkins, J. G., & Dallenbach, K. M. (1924). Obliviscence during Sleep and Waking. *The American Journal of Psychology, 35*(4), 605-612. doi:10.2307/1414040

Jensen, O., Kaiser, J., & Lachaux, J. P. (2007). Human gamma-frequency oscillations associated with attention and memory. *Trends Neurosci, 30*(7), 317-324. doi:10.1016/j.tins.2007.05.001

Jeong, J., Kim, S. Y., & Han, S. H. (1998). Non-linear dynamical analysis of the EEG in Alzheimer's disease with optimal embedding dimension. *Electroencephalogr Clin Neurophysiol, 106*(3), 220-228. doi:10.1016/s0013-4694(97)00079-5

Ji, D., & Wilson, M. A. (2007). Coordinated memory replay in the visual cortex and hippocampus during sleep. *Nat Neurosci, 10*(1), 100-107. doi:10.1038/nn1825

Jiang, X., Gonzalez-Martinez, J., & Halgren, E. (2019). Coordination of Human Hippocampal Sharpwave Ripples during NREM Sleep with Cortical Theta Bursts, Spindles, Downstates, and Upstates. *J Neurosci, 39*(44), 8744-8761. doi:10.1523/jneurosci.2857-18.2019

Jiang, Y., Mullaney, K. A., Peterhoff, C. M., Che, S., Schmidt, S. D., Boyer-Boiteau, A., . . . Nixon, R. A. (2010). Alzheimer's-related endosome dysfunction in Down syndrome is Abeta-independent but requires APP and is reversed by BACE-1 inhibition. *Proc Natl Acad Sci U S A, 107*(4), 1630-1635. doi:10.1073/pnas.0908953107

Jiang, Y., Zhou, X., Ip, F. C., Chan, P., Chen, Y., Lai, N. C. H., . . . Ip, N. Y. (2022). Large-scale plasma proteomic profiling identifies a high-performance biomarker panel for Alzheimer's disease screening and staging. *Alzheimers Dement, 18*(1), 88-102. doi:10.1002/alz.12369

Jing, M., Li, Y., Zeng, J., Huang, P., Skirzewski, M., Kljakic, O., . . . Li, Y. (2020). An optimized acetylcholine sensor for monitoring in vivo cholinergic activity. *Nat Methods, 17*(11), 1139-1146. doi:10.1038/s41592-020-0953-2

Johnson, C. E., Duncan, M. J., & Murphy, M. P. (2024). Sex and Sleep Disruption as Contributing Factors in Alzheimer's Disease. *J Alzheimers Dis, 97*(1), 31-74. doi:10.3233/jad-230527

Johnson, V. E., Stewart, J. E., Begbie, F. D., Trojanowski, J. Q., Smith, D. H., & Stewart, W. (2013). Inflammation and white matter degeneration persist for years after a single traumatic brain injury. *Brain, 136*(Pt 1), 28-42. doi:10.1093/brain/aws322

Jones, M., McDermott, B., Oliveira, B. L., O'Brien, A., Coogan, D., Lang, M., . . . Shahzad, A. (2019). Gamma Band Light Stimulation in Human Case Studies: Groundwork for Potential Alzheimer's Disease Treatment. *J Alzheimers Dis, 70*(1), 171-185. doi:10.3233/jad-190299

Jordan, R. (2021). Optimized protocol for in vivo whole-cell recordings in head-fixed, awake behaving mice. *STAR Protoc, 2*(1), 100347. doi:10.1016/j.xpro.2021.100347

Jouvet, M. (1972). The role of monoamines and acetylcholine-containing neurons in the regulation of the sleep-waking cycle. *Ergeb Physiol, 64*, 166-307. doi:10.1007/3-540-05462-6_2

Ju, Y. E., McLeland, J. S., Toedebusch, C. D., Xiong, C., Fagan, A. M., Duntley, S. P., . . . Holtzman, D. M. (2013). Sleep quality and preclinical Alzheimer disease. *JAMA Neurol, 70*(5), 587-593. doi:10.1001/jamaneurol.2013.2334

Jucker, M., Beyreuther, K., Haass, C., Nitsch, R., & Christen, Y. (2006). *Alzheimer: 100 Years and Beyond*.

Jun, J. J., Steinmetz, N. A., Siegle, J. H., Denman, D. J., Bauza, M., Barbarits, B., . . . Harris, T. D. (2017). Fully integrated silicon probes for high-density recording of neural activity. *Nature, 551*(7679), 232-236. doi:10.1038/nature24636

Jura, B., Macrez, N., Meyrand, P., & Bem, T. (2019). Deficit in hippocampal ripples does not preclude spatial memory formation in APP/PS1 mice. *Scientific Reports, 9*(1), 20129. doi:10.1038/s41598-019-56582-w

Kagiampaki, Z., Rohner, V., Kiss, C., Curreli, S., Dieter, A., Wilhelm, M., . . . Patriarchi, T. (2023). Sensitive multicolor indicators for monitoring norepinephrine in vivo. *Nature Methods, 20*(9), 1426-1436. doi:10.1038/s41592-023-01959-z

Kam, K., Parekh, A., Sharma, R. A., Andrade, A., Lewin, M., Castillo, B., . . . Osorio, R. S. (2019). Sleep oscillation-specific associations with Alzheimer's disease CSF biomarkers: novel roles for sleep spindles and tau. *Mol Neurodegener, 14*(1), 10. doi:10.1186/s13024-019-0309-5

Kametani, H., & Kawamura, H. (1990). Alterations in acetylcholine release in the rat hippocampus during sleep-wakefulness detected by intracerebral dialysis. *Life Sci, 47*(5), 421-426. doi:10.1016/0024-3205(90)90300-g

Kanbayashi, T., Sugiyama, T., Aizawa, R., Saito, Y., Ogawa, Y., Kitajima, T., . . . Shimizu, T. (2002). Effects of donepezil (Aricept) on the rapid eye movement sleep of normal subjects. *Psychiatry Clin Neurosci, 56*(3), 307-308. doi:10.1046/j.1440-1819.2002.01008.x

Kang, J. E., Lim, M. M., Bateman, R. J., Lee, J. J., Smyth, L. P., Cirrito, J. R., . . . Holtzman, D. M. (2009). Amyloid-beta dynamics are regulated by orexin and the sleep-wake cycle. *Science, 326*(5955), 1005-1007. doi:10.1126/science.1180962

Karlsson, M. P., & Frank, L. M. (2008). Network dynamics underlying the formation of sparse, informative representations in the hippocampus. *J Neurosci, 28*(52), 14271-14281. doi:10.1523/jneurosci.4261-08.2008

Katzman, R. (1976). Editorial: The prevalence and malignancy of Alzheimer disease. A major killer. *Arch Neurol, 33*(4), 217-218. doi:10.1001/archneur.1976.00500040001001

Kent, B. A., Strittmatter, S. M., & Nygaard, H. B. (2018). Sleep and EEG Power Spectral Analysis in Three Transgenic Mouse Models of Alzheimer's Disease: APP/PS1, 3xTgAD, and Tg2576. *J Alzheimers Dis, 64*(4), 1325-1336. doi:10.3233/jad-180260

Kim, C. K., Yang, S. J., Pichamoorthy, N., Young, N. P., Kauvar, I., Jennings, J. H., . . . Deisseroth, K. (2016). Simultaneous fast measurement of circuit dynamics at

multiple sites across the mammalian brain. *Nature Methods, 13*(4), 325-328. doi:10.1038/nmeth.3770
Kim, D., Hwang, E., Lee, M., Sung, H., & Choi, J. H. (2015). Characterization of topographically specific sleep spindles in mice. *Sleep, 38*(1), 85-96. doi:10.5665/sleep.4330
Kim, S., Sato, Y., Mohan, P. S., Peterhoff, C., Pensalfini, A., Rigoglioso, A., . . . Nixon, R. A. (2016). Evidence that the rab5 effector APPL1 mediates APP-βCTF-induced dysfunction of endosomes in Down syndrome and Alzheimer's disease. *Mol Psychiatry, 21*(5), 707-716. doi:10.1038/mp.2015.97
Klink, R., & Alonso, A. (1997). Muscarinic modulation of the oscillatory and repetitive firing properties of entorhinal cortex layer II neurons. *J Neurophysiol, 77*(4), 1813-1828. doi:10.1152/jn.1997.77.4.1813
Knupp, A., Mishra, S., Martinez, R., Braggin, J. E., Szabo, M., Kinoshita, C., . . . Young, J. E. (2020). Depletion of the AD Risk Gene SORL1 Selectively Impairs Neuronal Endosomal Traffic Independent of Amyloidogenic APP Processing. *Cell Rep, 31*(9), 107719. doi:10.1016/j.celrep.2020.107719
Koch, G., Bonnì, S., Pellicciari, M. C., Casula, E. P., Mancini, M., Esposito, R., . . . Bozzali, M. (2018). Transcranial magnetic stimulation of the precuneus enhances memory and neural activity in prodromal Alzheimer's disease. *Neuroimage, 169*, 302-311. doi:https://doi.org/10.1016/j.neuroimage.2017.12.048
Koch, G., Casula, E. P., Bonnì, S., Borghi, I., Assogna, M., Minei, M., . . . Martorana, A. (2022). Precuneus magnetic stimulation for Alzheimer's disease: a randomized, sham-controlled trial. *Brain, 145*(11), 3776-3786. doi:10.1093/brain/awac285
Kondo, H., & Zaborszky, L. (2016). Topographic organization of the basal forebrain projections to the perirhinal, postrhinal, and entorhinal cortex in rats. *J Comp Neurol, 524*(12), 2503-2515. doi:10.1002/cne.23967
Konopacki, J., MacIver, M. B., Bland, B. H., & Roth, S. H. (1987). Carbachol-induced EEG 'theta' activity in hippocampal brain slices. *Brain Res, 405*(1), 196-198. doi:10.1016/0006-8993(87)91009-2
Kovács, K. A., O'Neill, J., Schoenenberger, P., Penttonen, M., Ranguel Guerrero, D. K., & Csicsvari, J. (2016). Optogenetically Blocking Sharp Wave Ripple Events in Sleep Does Not Interfere with the Formation of Stable Spatial Representation in the CA1 Area of the Hippocampus. *PLoS One, 11*(10), e0164675. doi:10.1371/journal.pone.0164675
Kowalska, A. (2003). Amyloid precursor protein gene mutations responsible for early-onset autosomal dominant Alzheimer's disease. *Folia Neuropathol, 41*(1), 35-40.
Kramis, R., Vanderwolf, C. H., & Bland, B. H. (1975). Two types of hippocampal rhythmical slow activity in both the rabbit and the rat: relations to behavior and effects of atropine, diethyl ether, urethane, and pentobarbital. *Exp Neurol, 49*(1 Pt 1), 58-85. doi:10.1016/0014-4886(75)90195-8
Kretner, B., Trambauer, J., Fukumori, A., Mielke, J., Kuhn, P. H., Kremmer, E., . . . Steiner, H. (2016). Generation and deposition of Aβ43 by the virtually inactive presenilin-1 L435F mutant contradicts the presenilin loss-of-function hypothesis of Alzheimer's disease. *EMBO Mol Med, 8*(5), 458-465. doi:10.15252/emmm.201505952
Krettek, J. E., & Price, J. L. (1978). Amygdaloid projections to subcortical structures within the basal forebrain and brainstem in the rat and cat. *J Comp Neurol, 178*(2), 225-254. doi:10.1002/cne.901780204
Kudrimoti, H. S., Barnes, C. A., & McNaughton, B. L. (1999). Reactivation of hippocampal cell assemblies: effects of behavioral state, experience, and EEG dynamics. *J Neurosci, 19*(10), 4090-4101. doi:10.1523/jneurosci.19-10-04090.1999
Kwart, D., Gregg, A., Scheckel, C., Murphy, E. A., Paquet, D., Duffield, M., . . . Tessier-Lavigne, M. (2019). A Large Panel of Isogenic APP and PSEN1 Mutant Human iPSC Neurons Reveals Shared Endosomal Abnormalities Mediated by APP β-CTFs, Not Aβ. *Neuron, 104*(2), 256-270.e255. doi:10.1016/j.neuron.2019.07.010
Lagarde, J., Olivieri, P., Caillé, F., Gervais, P., Baron, J. C., Bottlaender, M., & Sarazin, M. (2019). [(18)F]-AV-1451 tau PET imaging in Alzheimer's disease and suspected non-AD tauopathies using a late acquisition time window. *J Neurol, 266*(12), 3087-3097. doi:10.1007/s00415-019-09530-7

Lansink, C. S., Goltstein, P. M., Lankelma, J. V., McNaughton, B. L., & Pennartz, C. M. (2009). Hippocampus leads ventral striatum in replay of place-reward information. *PLoS Biol, 7*(8), e1000173. doi:10.1371/journal.pbio.1000173

Larsson, S. C., Traylor, M., Malik, R., Dichgans, M., Burgess, S., & Markus, H. S. (2017). Modifiable pathways in Alzheimer's disease: Mendelian randomisation analysis. *Bmj, 359*, j5375. doi:10.1136/bmj.j5375

Lasagna-Reeves, C. A., Castillo-Carranza, D. L., Sengupta, U., Guerrero-Munoz, M. J., Kiritoshi, T., Neugebauer, V., . . . Kayed, R. (2012). Alzheimer brain-derived tau oligomers propagate pathology from endogenous tau. *Sci Rep, 2*, 700. doi:10.1038/srep00700

Latreille, V., Carrier, J., Lafortune, M., Postuma, R. B., Bertrand, J. A., Panisset, M., . . . Gagnon, J. F. (2015). Sleep spindles in Parkinson's disease may predict the development of dementia. *Neurobiol Aging, 36*(2), 1083-1090. doi:10.1016/j.neurobiolaging.2014.09.009

Laws, K. R., Irvine, K., & Gale, T. M. (2018). Sex differences in Alzheimer's disease. *Current Opinion in Psychiatry, 31*(2), 133-139. doi:10.1097/yco.0000000000000401

Laxton, A. W., Tang-Wai, D. F., McAndrews, M. P., Zumsteg, D., Wennberg, R., Keren, R., . . . Lozano, A. M. (2010). A phase I trial of deep brain stimulation of memory circuits in Alzheimer's disease. *Ann Neurol, 68*(4), 521-534. doi:10.1002/ana.22089

Lee, A. T. C., Richards, M., Chan, W. C., Chiu, H. F. K., Lee, R. S. Y., & Lam, L. C. W. (2018). Association of Daily Intellectual Activities With Lower Risk of Incident Dementia Among Older Chinese Adults. *JAMA Psychiatry, 75*(7), 697-703. doi:10.1001/jamapsychiatry.2018.0657

Lee, L., Kosuri, P., & Arancio, O. (2014). Picomolar amyloid-β peptides enhance spontaneous astrocyte calcium transients. *J Alzheimers Dis, 38*(1), 49-62. doi:10.3233/jad-130740

Lee, S. F., Shah, S., Li, H., Yu, C., Han, W., & Yu, G. (2002). Mammalian APH-1 interacts with presenilin and nicastrin and is required for intramembrane proteolysis of amyloid-beta precursor protein and Notch. *J Biol Chem, 277*(47), 45013-45019. doi:10.1074/jbc.M208164200

Letemendia, F., & Pampiglione, G. (1958). Clinical and electroencephalographic observations in Alzheimer's disease. *J Neurol Neurosurg Psychiatry, 21*(3), 167-172. doi:10.1136/jnnp.21.3.167

Liao, Y. F., Wang, B. J., Cheng, H. T., Kuo, L. H., & Wolfe, M. S. (2004). Tumor necrosis factor-alpha, interleukin-1beta, and interferon-gamma stimulate gamma-secretase-mediated cleavage of amyloid precursor protein through a JNK-dependent MAPK pathway. *J Biol Chem, 279*(47), 49523-49532. doi:10.1074/jbc.M402034200

Lim, S., Shin, S., Sung, Y., Lee, H. E., Kim, K. H., Song, J. Y., . . . Kim, Y. K. (2023). Levosimendan inhibits disulfide tau oligomerization and ameliorates tau pathology in TauP301L-BiFC mice. *Experimental & Molecular Medicine, 55*(3), 612-627. doi:10.1038/s12276-023-00959-5

Lindwall, G., & Cole, R. D. (1984). Phosphorylation affects the ability of tau protein to promote microtubule assembly. *J Biol Chem, 259*(8), 5301-5305.

Lisman, J. E., & Jensen, O. (2013). The θ-γ neural code. *Neuron, 77*(6), 1002-1016. doi:10.1016/j.neuron.2013.03.007

Liu, A. A., Henin, S., Abbaspoor, S., Bragin, A., Buffalo, E. A., Farrell, J. S., . . . Buzsáki, G. (2022). A consensus statement on detection of hippocampal sharp wave ripples and differentiation from other fast oscillations. *Nat Commun, 13*(1), 6000. doi:10.1038/s41467-022-33536-x

Liu, C. C., Liu, C. C., Kanekiyo, T., Xu, H., & Bu, G. (2013). Apolipoprotein E and Alzheimer disease: risk, mechanisms and therapy. *Nat Rev Neurol, 9*(2), 106-118. doi:10.1038/nrneurol.2012.263

Liu, N., Wang, Y., An, A. Y., Banker, C., Qian, Y. H., & O'Donnell, J. M. (2020). Single housing-induced effects on cognitive impairment and depression-like behavior in male and female mice involve neuroplasticity-related signaling. *Eur J Neurosci, 52*(1), 2694-2704. doi:10.1111/ejn.14565

Liu, S., Pan, J., Tang, K., Lei, Q., He, L., Meng, Y., . . . Li, Z. (2020). Sleep spindles, K-complexes, limb movements and sleep stage proportions may be biomarkers for

amnestic mild cognitive impairment and Alzheimer's disease. *Sleep Breath, 24*(2), 637-651. doi:10.1007/s11325-019-01970-9
Livingston, G., Huntley, J., Sommerlad, A., Ames, D., Ballard, C., Banerjee, S., . . . Mukadam, N. (2020). Dementia prevention, intervention, and care: 2020 report of the Lancet Commission. *Lancet, 396*(10248), 413-446. doi:10.1016/s0140-6736(20)30367-6
Livingston, G., Sommerlad, A., Orgeta, V., Costafreda, S. G., Huntley, J., Ames, D., . . . Mukadam, N. (2017). Dementia prevention, intervention, and care. *Lancet, 390*(10113), 2673-2734. doi:10.1016/s0140-6736(17)31363-6
Lo, A. C., Evans, C. D., Mancini, M., Wang, H., Shcherbinin, S., Lu, M., . . . Willis, B. A. (2021). Phase II (NAVIGATE-AD study) Results of LY3202626 Effects on Patients with Mild Alzheimer's Disease Dementia. *J Alzheimers Dis Rep, 5*(1), 321-336. doi:10.3233/adr-210296
Locatelli, T., Cursi, M., Liberati, D., Franceschi, M., & Comi, G. (1998). EEG coherence in Alzheimer's disease. *Electroencephalogr Clin Neurophysiol, 106*(3), 229-237. doi:10.1016/s0013-4694(97)00129-6
Loomis, A. L., Harvey, E. N., & Hobart, G. (1935). POTENTIAL RHYTHMS OF THE CEREBRAL CORTEX DURING SLEEP. *Science, 81*(2111), 597-598. doi:10.1126/science.81.2111.597
Loughrey, D. G., Kelly, M. E., Kelley, G. A., Brennan, S., & Lawlor, B. A. (2018). Association of Age-Related Hearing Loss With Cognitive Function, Cognitive Impairment, and Dementia: A Systematic Review and Meta-analysis. *JAMA Otolaryngol Head Neck Surg, 144*(2), 115-126. doi:10.1001/jamaoto.2017.2513
Lowe, S. L., Duggan Evans, C., Shcherbinin, S., Cheng, Y. J., Willis, B. A., Gueorguieva, I., . . . Sims, J. R. (2021). Donanemab (LY3002813) Phase 1b Study in Alzheimer's Disease: Rapid and Sustained Reduction of Brain Amyloid Measured by Florbetapir F18 Imaging. *J Prev Alzheimers Dis, 8*(4), 414-424. doi:10.14283/jpad.2021.56
Lowe, S. L., Willis, B. A., Hawdon, A., Natanegara, F., Chua, L., Foster, J., . . . Sims, J. R. (2021). Donanemab (LY3002813) dose-escalation study in Alzheimer's disease. *Alzheimers Dement (N Y), 7*(1), e12112. doi:10.1002/trc2.12112
Lozano, A. M., Fosdick, L., Chakravarty, M. M., Leoutsakos, J. M., Munro, C., Oh, E., . . . Smith, G. S. (2016). A Phase II Study of Fornix Deep Brain Stimulation in Mild Alzheimer's Disease. *J Alzheimers Dis, 54*(2), 777-787. doi:10.3233/jad-160017
Lucey, B. P., Hicks, T. J., McLeland, J. S., Toedebusch, C. D., Boyd, J., Elbert, D. L., . . . Bateman, R. J. (2018). Effect of sleep on overnight cerebrospinal fluid amyloid β kinetics. *Ann Neurol, 83*(1), 197-204. doi:10.1002/ana.25117
Lueptow, L. M. (2017). Novel Object Recognition Test for the Investigation of Learning and Memory in Mice. *J Vis Exp*(126). doi:10.3791/55718
Lustenberger, C., Patel, Y. A., Alagapan, S., Page, J. M., Price, B., Boyle, M. R., & Fröhlich, F. (2018). High-density EEG characterization of brain responses to auditory rhythmic stimuli during wakefulness and NREM sleep. *Neuroimage, 169*, 57-68. doi:10.1016/j.neuroimage.2017.12.007
Lyman, M., Lloyd, D. G., Ji, X., Vizcaychipi, M. P., & Ma, D. (2014). Neuroinflammation: the role and consequences. *Neurosci Res, 79*, 1-12. doi:10.1016/j.neures.2013.10.004
Maezono, S. E. B., Kanuka, M., Tatsuzawa, C., Morita, M., Kawano, T., Kashiwagi, M., . . . Hayashi, Y. (2020). Progressive Changes in Sleep and Its Relations to Amyloid-β Distribution and Learning in Single App Knock-In Mice. *eNeuro, 7*(2). doi:10.1523/eneuro.0093-20.2020
Maingret, N., Girardeau, G., Todorova, R., Goutierre, M., & Zugaro, M. (2016). Hippocampo-cortical coupling mediates memory consolidation during sleep. *Nat Neurosci, 19*(7), 959-964. doi:10.1038/nn.4304
Malek, N., Baker, M. R., Mann, C., & Greene, J. (2017). Electroencephalographic markers in dementia. *Acta Neurol Scand, 135*(4), 388-393. doi:10.1111/ane.12638
Marighetto, A., Micheau, J., & Jaffard, R. (1993). Relationships between testing-induced alterations of hippocampal cholinergic activity and memory performance on two spatial tasks in mice. *Behav Brain Res, 56*(2), 133-144. doi:10.1016/0166-4328(93)90031-k

Marighetto, A., Micheau, J., & Jaffard, R. (1994). Effects of intraseptally injected glutamatergic drugs on hippocampal sodium-dependent high-affinity choline uptake in "naive" and "trained" mice. *Pharmacol Biochem Behav, 49*(3), 689-699. doi:10.1016/0091-3057(94)90089-2

Markowitz, J. S., Gutterman, E. M., Lilienfeld, S., & Papadopoulos, G. (2003). Sleep-related outcomes in persons with mild to moderate Alzheimer disease in a placebo-controlled trial of galantamine. *Sleep, 26*(5), 602-606. doi:10.1093/sleep/26.5.602

Marrosu, F., Portas, C., Mascia, M. S., Casu, M. A., Fà, M., Giagheddu, M., . . . Gessa, G. L. (1995). Microdialysis measurement of cortical and hippocampal acetylcholine release during sleep-wake cycle in freely moving cats. *Brain Res, 671*(2), 329-332. doi:10.1016/0006-8993(94)01399-3

Marshall, L., Helgadóttir, H., Mölle, M., & Born, J. (2006). Boosting slow oscillations during sleep potentiates memory. *Nature, 444*(7119), 610-613. doi:10.1038/nature05278

Martins, R. N., Turner, B. A., Carroll, R. T., Sweeney, D., Kim, K. S., Wisniewski, H. M., . . . Gandy, S. (1995). High levels of amyloid-beta protein from S182 (Glu246) familial Alzheimer's cells. *Neuroreport, 7*(1), 217-220.

Martorell, A. J., Paulson, A. L., Suk, H. J., Abdurrob, F., Drummond, G. T., Guan, W., . . . Tsai, L. H. (2019). Multi-sensory Gamma Stimulation Ameliorates Alzheimer's-Associated Pathology and Improves Cognition. *Cell, 177*(2), 256-271.e222. doi:10.1016/j.cell.2019.02.014

Massimini, M., Huber, R., Ferrarelli, F., Hill, S., & Tononi, G. (2004). The sleep slow oscillation as a traveling wave. *J Neurosci, 24*(31), 6862-6870. doi:10.1523/jneurosci.1318-04.2004

Mathis, A., Mamidanna, P., Cury, K. M., Abe, T., Murthy, V. N., Mathis, M. W., & Bethge, M. (2018). DeepLabCut: markerless pose estimation of user-defined body parts with deep learning. *Nature Neuroscience, 21*(9), 1281-1289. doi:10.1038/s41593-018-0209-y

Matsumoto, H., & Marsan, C. A. (1964). Cortical cellular phenomena in experimental epilepsy: Interictal manifestations. *Experimental Neurology, 9*(4), 286-304. doi:https://doi.org/10.1016/0014-4886(64)90025-1

Matsuo, E. S., Shin, R. W., Billingsley, M. L., Van deVoorde, A., O'Connor, M., Trojanowski, J. Q., & Lee, V. M. (1994). Biopsy-derived adult human brain tau is phosphorylated at many of the same sites as Alzheimer's disease paired helical filament tau. *Neuron, 13*(4), 989-1002. doi:10.1016/0896-6273(94)90264-x

Maurer, K., Volk, S., & Gerbaldo, H. (1997). Auguste D and Alzheimer's disease. *Lancet, 349*(9064), 1546-1549. doi:10.1016/s0140-6736(96)10203-8

McClelland, J. L., McNaughton, B. L., & O'Reilly, R. C. (1995). Why there are complementary learning systems in the hippocampus and neocortex: insights from the successes and failures of connectionist models of learning and memory. *Psychol Rev, 102*(3), 419-457. doi:10.1037/0033-295x.102.3.419

McDade, E., Voytyuk, I., Aisen, P., Bateman, R. J., Carrillo, M. C., De Strooper, B., . . . Lichtenthaler, S. F. (2021). The case for low-level BACE1 inhibition for the prevention of Alzheimer disease. *Nat Rev Neurol, 17*(11), 703-714. doi:10.1038/s41582-021-00545-1

McEwen, B. S. (2006). Sleep deprivation as a neurobiologic and physiologic stressor: Allostasis and allostatic load. *Metabolism, 55*(10 Suppl 2), S20-23. doi:10.1016/j.metabol.2006.07.008

McIntyre, C. K., Marriott, L. K., & Gold, P. E. (2003). Patterns of brain acetylcholine release predict individual differences in preferred learning strategies in rats. *Neurobiol Learn Mem, 79*(2), 177-183. doi:10.1016/s1074-7427(02)00014-x

McMillan, J. M., Mele, B. S., Hogan, D. B., & Leung, A. A. (2018). Impact of pharmacological treatment of diabetes mellitus on dementia risk: systematic review and meta-analysis. *BMJ Open Diabetes Res Care, 6*(1), e000563. doi:10.1136/bmjdrc-2018-000563

McShane, R., Westby, M. J., Roberts, E., Minakaran, N., Schneider, L., Farrimond, L. E., . . . Debarros, J. (2019). Memantine for dementia. *Cochrane Database Syst Rev, 3*(3), Cd003154. doi:10.1002/14651858.CD003154.pub6

Medori, R., Tritschler, H. J., LeBlanc, A., Villare, F., Manetto, V., Chen, H. Y., . . . et al. (1992). Fatal familial insomnia, a prion disease with a mutation at codon 178 of the prion protein gene. *N Engl J Med, 326*(7), 444-449. doi:10.1056/nejm199202133260704

Mendiola-Precoma, J., Berumen, L. C., Padilla, K., & Garcia-Alcocer, G. (2016). Therapies for Prevention and Treatment of Alzheimer's Disease. *Biomed Res Int, 2016*, 2589276. doi:10.1155/2016/2589276

Mesulam, M. M., & Mufson, E. J. (1984). Neural inputs into the nucleus basalis of the substantia innominata (Ch4) in the rhesus monkey. *Brain, 107 (Pt 1)*, 253-274. doi:10.1093/brain/107.1.253

Mesulam, M. M., Mufson, E. J., Levey, A. I., & Wainer, B. H. (1983). Cholinergic innervation of cortex by the basal forebrain: cytochemistry and cortical connections of the septal area, diagonal band nuclei, nucleus basalis (substantia innominata), and hypothalamus in the rhesus monkey. *J Comp Neurol, 214*(2), 170-197. doi:10.1002/cne.902140206

Miller, E. K., Lundqvist, M., & Bastos, A. M. (2018). Working Memory 2.0. *Neuron, 100*(2), 463-475. doi:10.1016/j.neuron.2018.09.023

Mintun, M. A., Lo, A. C., Duggan Evans, C., Wessels, A. M., Ardayfio, P. A., Andersen, S. W., . . . Skovronsky, D. M. (2021). Donanemab in Early Alzheimer's Disease. *N Engl J Med, 384*(18), 1691-1704. doi:10.1056/NEJMoa2100708

Miyamoto, D., Hirai, D., & Murayama, M. (2017). The Roles of Cortical Slow Waves in Synaptic Plasticity and Memory Consolidation. *Front Neural Circuits, 11*, 92. doi:10.3389/fncir.2017.00092

Mölle, M., Bergmann, T. O., Marshall, L., & Born, J. (2011). Fast and slow spindles during the sleep slow oscillation: disparate coalescence and engagement in memory processing. *Sleep, 34*(10), 1411-1421. doi:10.5665/sleep.1290

Mölle, M., Eschenko, O., Gais, S., Sara, S. J., & Born, J. (2009). The influence of learning on sleep slow oscillations and associated spindles and ripples in humans and rats. *European Journal of Neuroscience, 29*(5), 1071-1081. doi:https://doi.org/10.1111/j.1460-9568.2009.06654.x

Monmaur, P., Collet, A., Puma, C., Frankel-Kohn, L., & Sharif, A. (1997). Relations between acetylcholine release and electrophysiological characteristics of theta rhythm: a microdialysis study in the urethane-anesthetized rat hippocampus. *Brain Res Bull, 42*(2), 141-146. doi:10.1016/s0361-9230(96)00200-6

Montplaisir, J., Petit, D., Gauthier, S., Gaudreau, H., & Décary, A. (1998). Sleep disturbances and eeg slowing in alzheimer's disease. *Sleep Res Online, 1*(4), 147-151.

Moraes, W., Poyares, D., Sukys-Claudino, L., Guilleminault, C., & Tufik, S. (2008). Donepezil improves obstructive sleep apnea in Alzheimer disease: a double-blind, placebo-controlled study. *Chest, 133*(3), 677-683. doi:10.1378/chest.07-1446

Moraes Wdos, S., Poyares, D. R., Guilleminault, C., Ramos, L. R., Bertolucci, P. H., & Tufik, S. (2006). The effect of donepezil on sleep and REM sleep EEG in patients with Alzheimer disease: a double-blind placebo-controlled study. *Sleep, 29*(2), 199-205. doi:10.1093/sleep/29.2.199

Morinaga, A., Ono, K., Ikeda, T., Ikeda, Y., Shima, K., Noguchi-Shinohara, M., . . . Yamada, M. (2010). A comparison of the diagnostic sensitivity of MRI, CBF-SPECT, FDG-PET and cerebrospinal fluid biomarkers for detecting Alzheimer's disease in a memory clinic. *Dement Geriatr Cogn Disord, 30*(4), 285-292. doi:10.1159/000320265

Mullington, J. M., Haack, M., Toth, M., Serrador, J. M., & Meier-Ewert, H. K. (2009). Cardiovascular, inflammatory, and metabolic consequences of sleep deprivation. *Prog Cardiovasc Dis, 51*(4), 294-302. doi:10.1016/j.pcad.2008.10.003

Murray, P. S., Kirkwood, C. M., Gray, M. C., Ikonomovic, M. D., Paljug, W. R., Abrahamson, E. E., . . . Sweet, R. A. (2012). beta-Amyloid 42/40 ratio and kalirin expression in Alzheimer disease with psychosis. *Neurobiol Aging, 33*(12), 2807-2816. doi:10.1016/j.neurobiolaging.2012.02.015

Nadel, L., & Moscovitch, M. (1997). Memory consolidation, retrograde amnesia and the hippocampal complex. *Curr Opin Neurobiol, 7*(2), 217-227. doi:10.1016/s0959-4388(97)80010-4

Nail-Boucherie, K., Dourmap, N., Jaffard, R., & Costentin, J. (2000). Contextual fear conditioning is associated with an increase of acetylcholine release in the hippocampus of rat. *Brain Res Cogn Brain Res, 9*(2), 193-197. doi:10.1016/s0926-6410(99)00058-0

Nakai, J., Ohkura, M., & Imoto, K. (2001). A high signal-to-noise Ca(2+) probe composed of a single green fluorescent protein. *Nat Biotechnol, 19*(2), 137-141. doi:10.1038/84397

Nakashiba, T., Buhl, D. L., McHugh, T. J., & Tonegawa, S. (2009). Hippocampal CA3 output is crucial for ripple-associated reactivation and consolidation of memory. *Neuron, 62*(6), 781-787. doi:10.1016/j.neuron.2009.05.013

Nicolas, M., & Hassan, B. A. (2014). Amyloid precursor protein and neural development. *Development, 141*(13), 2543-2548. doi:10.1242/dev.108712

Nicole, O., Hadzibegovic, S., Gajda, J., Bontempi, B., Bem, T., & Meyrand, P. (2016). Soluble amyloid beta oligomers block the learning-induced increase in hippocampal sharp wave-ripple rate and impair spatial memory formation. *Scientific Reports, 6*(1), 22728. doi:10.1038/srep22728

Nicolelis, M. A., Ghazanfar, A. A., Faggin, B. M., Votaw, S., & Oliveira, L. M. (1997). Reconstructing the engram: simultaneous, multisite, many single neuron recordings. *Neuron, 18*(4), 529-537. doi:10.1016/s0896-6273(00)80295-0

Nieoullon, A., Bentué-Ferrer, D., Bordet, R., Tsolaki, M., & Förstl, H. (2008). Importance of circadian rhythmicity in the cholinergic treatment of Alzheimer's disease: focus on galantamine*. *Curr Med Res Opin, 24*(12), 3357-3367. doi:10.1185/03007990802522397

Nir, Y., Staba, R. J., Andrillon, T., Vyazovskiy, V. V., Cirelli, C., Fried, I., & Tononi, G. (2011). Regional slow waves and spindles in human sleep. *Neuron, 70*(1), 153-169. doi:10.1016/j.neuron.2011.02.043

Nordström, A., & Nordström, P. (2018). Traumatic brain injury and the risk of dementia diagnosis: A nationwide cohort study. *PLoS Med, 15*(1), e1002496. doi:10.1371/journal.pmed.1002496

Norton, S., Matthews, F. E., Barnes, D. E., Yaffe, K., & Brayne, C. (2014). Potential for primary prevention of Alzheimer's disease: an analysis of population-based data. *Lancet Neurol, 13*(8), 788-794. doi:10.1016/s1474-4422(14)70136-x

Novitskaya, Y., Sara, S. J., Logothetis, N. K., & Eschenko, O. (2016). Ripple-triggered stimulation of the locus coeruleus during post-learning sleep disrupts ripple/spindle coupling and impairs memory consolidation. *Learn Mem, 23*(5), 238-248. doi:10.1101/lm.040923.115

Nutu, M., Zetterberg, H., Londos, E., Minthon, L., Nagga, K., Blennow, K., . . . Ohrfelt, A. (2013). Evaluation of the cerebrospinal fluid amyloid-beta1-42/amyloid-beta1-40 ratio measured by alpha-LISA to distinguish Alzheimer's disease from other dementia disorders. *Dement Geriatr Cogn Disord, 36*(1-2), 99-110. doi:10.1159/000353442

O'Leary, T. P., Robertson, A., Chipman, P. H., Rafuse, V. F., & Brown, R. E. (2018). Motor function deficits in the 12 month-old female 5xFAD mouse model of Alzheimer's disease. *Behav Brain Res, 337*, 256-263. doi:10.1016/j.bbr.2017.09.009

O'Neill, J., Boccara, C. N., Stella, F., Schoenenberger, P., & Csicsvari, J. (2017). Superficial layers of the medial entorhinal cortex replay independently of the hippocampus. *Science, 355*(6321), 184-188. doi:10.1126/science.aag2787

O'Neill, J., Pleydell-Bouverie, B., Dupret, D., & Csicsvari, J. (2010). Play it again: reactivation of waking experience and memory. *Trends Neurosci, 33*(5), 220-229. doi:10.1016/j.tins.2010.01.006

O'Neill, J., Senior, T. J., Allen, K., Huxter, J. R., & Csicsvari, J. (2008). Reactivation of experience-dependent cell assembly patterns in the hippocampus. *Nature Neuroscience, 11*(2), 209-215. doi:10.1038/nn2037

Oakley, H., Cole, S. L., Logan, S., Maus, E., Shao, P., Craft, J., . . . Vassar, R. (2006). Intraneuronal beta-amyloid aggregates, neurodegeneration, and neuron loss in

transgenic mice with five familial Alzheimer's disease mutations: potential factors in amyloid plaque formation. *J Neurosci, 26*(40), 10129-10140. doi:10.1523/jneurosci.1202-06.2006

Obermayer, J., Verhoog, M. B., Luchicchi, A., & Mansvelder, H. D. (2017). Cholinergic Modulation of Cortical Microcircuits Is Layer-Specific: Evidence from Rodent, Monkey and Human Brain. *Front Neural Circuits, 11*, 100. doi:10.3389/fncir.2017.00100

Oblak, A. L., Lin, P. B., Kotredes, K. P., Pandey, R. S., Garceau, D., Williams, H. M., . . . Lamb, B. T. (2021). Comprehensive Evaluation of the 5XFAD Mouse Model for Preclinical Testing Applications: A MODEL-AD Study. *Frontiers in Aging Neuroscience, 13*. doi:10.3389/fnagi.2021.713726

Oddo, S., Caccamo, A., Shepherd, J. D., Murphy, M. P., Golde, T. E., Kayed, R., . . . LaFerla, F. M. (2003). Triple-transgenic model of Alzheimer's disease with plaques and tangles: intracellular Abeta and synaptic dysfunction. *Neuron, 39*(3), 409-421. doi:10.1016/s0896-6273(03)00434-3

Ogawa, S., Lee, T. M., Kay, A. R., & Tank, D. W. (1990). Brain magnetic resonance imaging with contrast dependent on blood oxygenation. *Proc Natl Acad Sci U S A, 87*(24), 9868-9872. doi:10.1073/pnas.87.24.9868

Okamura, N., Harada, R., Ishiki, A., Kikuchi, A., Nakamura, T., & Kudo, Y. (2018). The development and validation of tau PET tracers: current status and future directions. *Clin Transl Imaging, 6*(4), 305-316. doi:10.1007/s40336-018-0290-y

Olabarria, M., Noristani, H. N., Verkhratsky, A., & Rodríguez, J. J. (2010). Concomitant astroglial atrophy and astrogliosis in a triple transgenic animal model of Alzheimer's disease. *Glia, 58*(7), 831-838. doi:10.1002/glia.20967

Oliva, A., Fernández-Ruiz, A., Fermino de Oliveira, E., & Buzsáki, G. (2018). Origin of Gamma Frequency Power during Hippocampal Sharp-Wave Ripples. *Cell Reports, 25*(7), 1693-1700.e1694. doi:https://doi.org/10.1016/j.celrep.2018.10.066

Ooms, S., Overeem, S., Besse, K., Rikkert, M. O., Verbeek, M., & Claassen, J. A. (2014). Effect of 1 night of total sleep deprivation on cerebrospinal fluid β-amyloid 42 in healthy middle-aged men: a randomized clinical trial. *JAMA Neurol, 71*(8), 971-977. doi:10.1001/jamaneurol.2014.1173

Orlando, I. F., O'Callaghan, C., Lam, A., McKinnon, A. C., Tan, J. B. C., Michaelian, J. C., . . . Naismith, S. L. (2024). Sleep spindle architecture associated with distinct clinical phenotypes in older adults at risk for dementia. *Molecular Psychiatry, 29*(2), 402-411. doi:10.1038/s41380-023-02335-1

Osipova, D., Takashima, A., Oostenveld, R., Fernández, G., Maris, E., & Jensen, O. (2006). Theta and gamma oscillations predict encoding and retrieval of declarative memory. *J Neurosci, 26*(28), 7523-7531. doi:10.1523/jneurosci.1948-06.2006

Ossenkoppele, R., van der Kant, R., & Hansson, O. (2022). Tau biomarkers in Alzheimer's disease: towards implementation in clinical practice and trials. *Lancet Neurol, 21*(8), 726-734. doi:10.1016/s1474-4422(22)00168-5

Ou, Y. N., Xu, W., Li, J. Q., Guo, Y., Cui, M., Chen, K. L., . . . Yu, J. T. (2019). FDG-PET as an independent biomarker for Alzheimer's biological diagnosis: a longitudinal study. *Alzheimers Res Ther, 11*(1), 57. doi:10.1186/s13195-019-0512-1

Oudin, A., Forsberg, B., Adolfsson, A. N., Lind, N., Modig, L., Nordin, M., . . . Nilsson, L. G. (2016). Traffic-Related Air Pollution and Dementia Incidence in Northern Sweden: A Longitudinal Study. *Environ Health Perspect, 124*(3), 306-312. doi:10.1289/ehp.1408322

Oudin, A., Segersson, D., Adolfsson, R., & Forsberg, B. (2018). Association between air pollution from residential wood burning and dementia incidence in a longitudinal study in Northern Sweden. *PLoS One, 13*(6), e0198283. doi:10.1371/journal.pone.0198283

Pálhalmi, J., Paulsen, O., Freund, T. F., & Hájos, N. (2004). Distinct properties of carbachol- and DHPG-induced network oscillations in hippocampal slices. *Neuropharmacology, 47*(3), 381-389. doi:10.1016/j.neuropharm.2004.04.010

Palop, J. J., & Mucke, L. (2016). Network abnormalities and interneuron dysfunction in Alzheimer disease. *Nature Reviews Neuroscience, 17*(12), 777-792. doi:10.1038/nrn.2016.141

Paresce, D. M., Ghosh, R. N., & Maxfield, F. R. (1996). Microglial cells internalize aggregates of the Alzheimer's disease amyloid beta-protein via a scavenger receptor. *Neuron, 17*(3), 553-565. doi:10.1016/s0896-6273(00)80187-7

Parikh, V., Kozak, R., Martinez, V., & Sarter, M. (2007). Prefrontal acetylcholine release controls cue detection on multiple timescales. *Neuron, 56*(1), 141-154. doi:10.1016/j.neuron.2007.08.025

Parpura-Gill, A., Beitz, D., & Uemura, E. (1997). The inhibitory effects of beta-amyloid on glutamate and glucose uptakes by cultured astrocytes. *Brain Res, 754*(1-2), 65-71. doi:10.1016/s0006-8993(97)00043-7

Pastor, M. A., Artieda, J., Arbizu, J., Marti-Climent, J. M., Peñuelas, I., & Masdeu, J. C. (2002). Activation of human cerebral and cerebellar cortex by auditory stimulation at 40 Hz. *J Neurosci, 22*(23), 10501-10506. doi:10.1523/jneurosci.22-23-10501.2002

Pastor, M. A., Artieda, J., Arbizu, J., Valencia, M., & Masdeu, J. C. (2003). Human cerebral activation during steady-state visual-evoked responses. *J Neurosci, 23*(37), 11621-11627. doi:10.1523/jneurosci.23-37-11621.2003

Patel, A. A., McAlinden, N., Mathieson, K., & Sakata, S. (2020). Simultaneous Electrophysiology and Fiber Photometry in Freely Behaving Mice. *Front Neurosci, 14*, 148. doi:10.3389/fnins.2020.00148

Pensalfini, A., Kim, S., Subbanna, S., Bleiwas, C., Goulbourne, C. N., Stavrides, P. H., . . . Nixon, R. A. (2020). Endosomal Dysfunction Induced by Directly Overactivating Rab5 Recapitulates Prodromal and Neurodegenerative Features of Alzheimer's Disease. *Cell Rep, 33*(8), 108420. doi:10.1016/j.celrep.2020.108420

Peters, R., Ee, N., Peters, J., Booth, A., Mudway, I., & Anstey, K. J. (2019). Air Pollution and Dementia: A Systematic Review. *J Alzheimers Dis, 70*(s1), S145-s163. doi:10.3233/jad-180631

Petit, D., Gagnon, J. F., Fantini, M. L., Ferini-Strambi, L., & Montplaisir, J. (2004). Sleep and quantitative EEG in neurodegenerative disorders. *J Psychosom Res, 56*(5), 487-496. doi:10.1016/j.jpsychores.2004.02.001

Peyrache, A., Khamassi, M., Benchenane, K., Wiener, S. I., & Battaglia, F. P. (2009). Replay of rule-learning related neural patterns in the prefrontal cortex during sleep. *Nat Neurosci, 12*(7), 919-926. doi:10.1038/nn.2337

Phelps, M. E., & Mazziotta, J. C. (1985). Positron emission tomography: human brain function and biochemistry. *Science, 228*(4701), 799-809. doi:10.1126/science.2860723

Pisanello, F., Mandelbaum, G., Pisanello, M., Oldenburg, I. A., Sileo, L., Markowitz, J. E., . . . Sabatini, B. L. (2017). Dynamic illumination of spatially restricted or large brain volumes via a single tapered optical fiber. *Nat Neurosci, 20*(8), 1180-1188. doi:10.1038/nn.4591

Platt, B., Drever, B., Koss, D., Stoppelkamp, S., Jyoti, A., Plano, A., . . . Riedel, G. (2011). Abnormal cognition, sleep, EEG and brain metabolism in a novel knock-in Alzheimer mouse, PLB1. *PLoS One, 6*(11), e27068. doi:10.1371/journal.pone.0027068

Platt, B., & Riedel, G. (2011). The cholinergic system, EEG and sleep. *Behav Brain Res, 221*(2), 499-504. doi:10.1016/j.bbr.2011.01.017

Plucińska, K., Crouch, B., Koss, D., Robinson, L., Siebrecht, M., Riedel, G., & Platt, B. (2014). Knock-in of human BACE1 cleaves murine APP and reiterates Alzheimer-like phenotypes. *J Neurosci, 34*(32), 10710-10728. doi:10.1523/jneurosci.0433-14.2014

Prince, Paulson, Jeong, Zhang, Amigues, & Singer. (2021). Alzheimer's pathology causes impaired inhibitory connections and reactivation of spatial codes during spatial navigation. *Cell Rep, 35*(3), 109008. doi:10.1016/j.celrep.2021.109008

Prinz, P. N., Peskind, E. R., Vitaliano, P. P., Raskind, M. A., Eisdorfer, C., Zemcuznikov, N., & Gerber, C. J. (1982). Changes in the sleep and waking EEGs of nondemented and demented elderly subjects. *J Am Geriatr Soc, 30*(2), 86-93. doi:10.1111/j.1532-5415.1982.tb01279.x

Pulver, R. L., Kronberg, E., Medenblik, L. M., Kheyfets, V. O., Ramos, A. R., Holtzman, D. M., . . . McConnell, B. V. (2024). Mapping sleep's oscillatory events as a biomarker of Alzheimer's disease. *Alzheimer's & Dementia, 20*(1), 301-315. doi:https://doi.org/10.1002/alz.13420

Qiu, T., Liu, Q., Chen, Y. X., Zhao, Y. F., & Li, Y. M. (2015). Abeta42 and Abeta40: similarities and differences. *J Pept Sci, 21*(7), 522-529. doi:10.1002/psc.2789
Ragozzino, M. E., Pal, S. N., Unick, K., Stefani, M. R., & Gold, P. E. (1998). Modulation of hippocampal acetylcholine release and spontaneous alternation scores by intrahippocampal glucose injections. *J Neurosci, 18*(4), 1595-1601. doi:10.1523/jneurosci.18-04-01595.1998
Reitz, C., & Mayeux, R. (2014). Alzheimer disease: epidemiology, diagnostic criteria, risk factors and biomarkers. *Biochem Pharmacol, 88*(4), 640-651. doi:10.1016/j.bcp.2013.12.024
Ribary, U., Ioannides, A. A., Singh, K. D., Hasson, R., Bolton, J. P., Lado, F., . . . Llinás, R. (1991). Magnetic field tomography of coherent thalamocortical 40-Hz oscillations in humans. *Proc Natl Acad Sci U S A, 88*(24), 11037-11041. doi:10.1073/pnas.88.24.11037
Richard, B. C., Kurdakova, A., Baches, S., Bayer, T. A., Weggen, S., & Wirths, O. (2015). Gene Dosage Dependent Aggravation of the Neurological Phenotype in the 5XFAD Mouse Model of Alzheimer's Disease. *J Alzheimers Dis, 45*(4), 1223-1236. doi:10.3233/jad-143120
Robbe, D., Montgomery, S. M., Thome, A., Rueda-Orozco, P. E., McNaughton, B. L., & Buzsaki, G. (2006). Cannabinoids reveal importance of spike timing coordination in hippocampal function. *Nat Neurosci, 9*(12), 1526-1533. doi:10.1038/nn1801
Robles, T. F., & Carroll, J. E. (2011). Restorative biological processes and health. *Soc Personal Psychol Compass, 5*(8), 518-537. doi:10.1111/j.1751-9004.2011.00368.x
Rossini, P. M., Del Percio, C., Pasqualetti, P., Cassetta, E., Binetti, G., Dal Forno, G., . . . Babiloni, C. (2006). Conversion from mild cognitive impairment to Alzheimer's disease is predicted by sources and coherence of brain electroencephalography rhythms. *Neuroscience, 143*(3), 793-803. doi:10.1016/j.neuroscience.2006.08.049
Roth, F. C., Beyer, K. M., Both, M., Draguhn, A., & Egorov, A. V. (2016). Downstream effects of hippocampal sharp wave ripple oscillations on medial entorhinal cortex layer V neurons in vitro. *Hippocampus, 26*(12), 1493-1508. doi:https://doi.org/10.1002/hipo.22623
Rothman, S. M., & Olney, J. W. (1986). Glutamate and the pathophysiology of hypoxic--ischemic brain damage. *Ann Neurol, 19*(2), 105-111. doi:10.1002/ana.410190202
Roux, F., & Uhlhaas, P. J. (2014). Working memory and neural oscillations: α-γ versus θ-γ codes for distinct WM information? *Trends Cogn Sci, 18*(1), 16-25. doi:10.1016/j.tics.2013.10.010
Rowe, C. C., Ackerman, U., Browne, W., Mulligan, R., Pike, K. L., O'Keefe, G., . . . Villemagne, V. L. (2008). Imaging of amyloid beta in Alzheimer's disease with 18F-BAY94-9172, a novel PET tracer: proof of mechanism. *Lancet Neurol, 7*(2), 129-135. doi:10.1016/s1474-4422(08)70001-2
Russchen, F. T., Amaral, D. G., & Price, J. L. (1985). The afferent connections of the substantia innominata in the monkey, Macaca fascicularis. *J Comp Neurol, 242*(1), 1-27. doi:10.1002/cne.902420102
Sabia, S., Fayosse, A., Dumurgier, J., Schnitzler, A., Empana, J. P., Ebmeier, K. P., . . . Singh-Manoux, A. (2019). Association of ideal cardiovascular health at age 50 with incidence of dementia: 25 year follow-up of Whitehall II cohort study. *Bmj, 366*, l4414. doi:10.1136/bmj.l4414
Sadowski, J. H., Jones, M. W., & Mellor, J. R. (2016). Sharp-Wave Ripples Orchestrate the Induction of Synaptic Plasticity during Reactivation of Place Cell Firing Patterns in the Hippocampus. *Cell Rep, 14*(8), 1916-1929. doi:10.1016/j.celrep.2016.01.061
Saito, T., Matsuba, Y., Mihira, N., Takano, J., Nilsson, P., Itohara, S., . . . Saido, T. C. (2014). Single App knock-in mouse models of Alzheimer's disease. *Nat Neurosci, 17*(5), 661-663. doi:10.1038/nn.3697
Sanchez-Espinosa, M. P., Atienza, M., & Cantero, J. L. (2014). Sleep deficits in mild cognitive impairment are related to increased levels of plasma amyloid-β and cortical thinning. *Neuroimage, 98*, 395-404. doi:10.1016/j.neuroimage.2014.05.027
Sarter, M., & Lustig, C. (2020). Forebrain Cholinergic Signaling: Wired and Phasic, Not Tonic, and Causing Behavior. *J Neurosci, 40*(4), 712-719. doi:10.1523/jneurosci.1305-19.2019

Sawangjit, A., Oyanedel, C. N., Niethard, N., Salazar, C., Born, J., & Inostroza, M. (2018). The hippocampus is crucial for forming non-hippocampal long-term memory during sleep. *Nature, 564*(7734), 109-113. doi:10.1038/s41586-018-0716-8

Schliebs, R., & Arendt, T. (2006). The significance of the cholinergic system in the brain during aging and in Alzheimer's disease. *J Neural Transm (Vienna), 113*(11), 1625-1644. doi:10.1007/s00702-006-0579-2

Schmidt, R., Hofer, E., Bouwman, F. H., Buerger, K., Cordonnier, C., Fladby, T., . . . Sorbi, S. (2015). EFNS-ENS/EAN Guideline on concomitant use of cholinesterase inhibitors and memantine in moderate to severe Alzheimer's disease. *Eur J Neurol, 22*(6), 889-898. doi:10.1111/ene.12707

Schneider, F., Baldauf, K., Wetzel, W., & Reymann, K. G. (2014). Behavioral and EEG changes in male 5xFAD mice. *Physiology & Behavior, 135*, 25-33. doi:https://doi.org/10.1016/j.physbeh.2014.05.041

Schneider, L. (2020). A resurrection of aducanumab for Alzheimer's disease. *Lancet Neurol, 19*(2), 111-112. doi:10.1016/s1474-4422(19)30480-6

Sethi, M., Joshi, S. S., Webb, R. L., Beckett, T. L., Donohue, K. D., Murphy, M. P., . . . Duncan, M. J. (2015). Increased fragmentation of sleep-wake cycles in the 5XFAD mouse model of Alzheimer's disease. *Neuroscience, 290*, 80-89. doi:10.1016/j.neuroscience.2015.01.035

Sevigny, J., Chiao, P., Bussière, T., Weinreb, P. H., Williams, L., Maier, M., . . . Sandrock, A. (2016). The antibody aducanumab reduces Aβ plaques in Alzheimer's disease. *Nature, 537*(7618), 50-56. doi:10.1038/nature19323

Shimoda, S., Ozawa, T., Ichitani, Y., & Yamada, K. (2021). Long-term associative memory in rats: Effects of familiarization period in object-place-context recognition test. *PLoS One, 16*(7), e0254570. doi:10.1371/journal.pone.0254570

Shivamurthy, V. K., Tahari, A. K., Marcus, C., & Subramaniam, R. M. (2015). Brain FDG PET and the diagnosis of dementia. *AJR Am J Roentgenol, 204*(1), W76-85. doi:10.2214/ajr.13.12363

Shouse, M. N., & Siegel, J. M. (1992). Pontine regulation of REM sleep components in cats: integrity of the pedunculopontine tegmentum (PPT) is important for phasic events but unnecessary for atonia during REM sleep. *Brain Res, 571*(1), 50-63. doi:10.1016/0006-8993(92)90508-7

Siapas, A. G., & Wilson, M. A. (1998). Coordinated interactions between hippocampal ripples and cortical spindles during slow-wave sleep. *Neuron, 21*(5), 1123-1128. doi:10.1016/s0896-6273(00)80629-7

Siemers, E. R., Dean, R. A., Friedrich, S., Ferguson-Sells, L., Gonzales, C., Farlow, M. R., & May, P. C. (2007). Safety, tolerability, and effects on plasma and cerebrospinal fluid amyloid-beta after inhibition of gamma-secretase. *Clin Neuropharmacol, 30*(6), 317-325. doi:10.1097/WNF.0b013e31805b7660

Siemers, E. R., Quinn, J. F., Kaye, J., Farlow, M. R., Porsteinsson, A., Tariot, P., . . . May, P. C. (2006). Effects of a gamma-secretase inhibitor in a randomized study of patients with Alzheimer disease. *Neurology, 66*(4), 602-604. doi:10.1212/01.Wnl.0000198762.41312.E1

Simpson, E. H., Akam, T., Patriarchi, T., Blanco-Pozo, M., Burgeno, L. M., Mohebi, A., . . . Walton, M. E. (2024). Lights, fiber, action! A primer on in vivo fiber photometry. *Neuron, 112*(5), 718-739. doi:10.1016/j.neuron.2023.11.016

Sirota, A., Csicsvari, J., Buhl, D., & Buzsáki, G. (2003). Communication between neocortex and hippocampus during sleep in rodents. *Proceedings of the National Academy of Sciences, 100*(4), 2065-2069. doi:doi:10.1073/pnas.0437938100

Sloan, E. P., Fenton, G. W., Kennedy, N. S., & MacLennan, J. M. (1994). Neurophysiology and SPECT cerebral blood flow patterns in dementia. *Electroencephalogr Clin Neurophysiol, 91*(3), 163-170. doi:10.1016/0013-4694(94)90066-3

Smith, M. A., Rudnicka-Nawrot, M., Richey, P. L., Praprotnik, D., Mulvihill, P., Miller, C. A., . . . Perry, G. (1995). Carbonyl-related posttranslational modification of neurofilament protein in the neurofibrillary pathology of Alzheimer's disease. *J Neurochem, 64*(6), 2660-2666. doi:10.1046/j.1471-4159.1995.64062660.x

Sorg, C., Riedl, V., Mühlau, M., Calhoun, V. D., Eichele, T., Läer, L., . . . Wohlschläger, A. M. (2007). Selective changes of resting-state networks in individuals at risk for

Alzheimer's disease. *Proceedings of the National Academy of Sciences, 104*(47), 18760-18765. doi:10.1073/pnas.0708803104
Spencer, J. P., Middleton, L. J., & Davies, C. H. (2010). Investigation into the efficacy of the acetylcholinesterase inhibitor, donepezil, and novel procognitive agents to induce gamma oscillations in rat hippocampal slices. *Neuropharmacology, 59*(6), 437-443. doi:10.1016/j.neuropharm.2010.06.005
Spira, A. P., Gamaldo, A. A., An, Y., Wu, M. N., Simonsick, E. M., Bilgel, M., . . . Resnick, S. M. (2013). Self-reported sleep and β-amyloid deposition in community-dwelling older adults. *JAMA Neurol, 70*(12), 1537-1543. doi:10.1001/jamaneurol.2013.4258
Squire, L. R., & Alvarez, P. (1995). Retrograde amnesia and memory consolidation: a neurobiological perspective. *Current Opinion in Neurobiology, 5*(2), 169-177. doi:https://doi.org/10.1016/0959-4388(95)80023-9
Stam, C. J., van Cappellen van Walsum, A. M., Pijnenburg, Y. A., Berendse, H. W., de Munck, J. C., Scheltens, P., & van Dijk, B. W. (2002). Generalized synchronization of MEG recordings in Alzheimer's Disease: evidence for involvement of the gamma band. *J Clin Neurophysiol, 19*(6), 562-574. doi:10.1097/00004691-200212000-00010
Staresina, B. P., Bergmann, T. O., Bonnefond, M., van der Meij, R., Jensen, O., Deuker, L., . . . Fell, J. (2015). Hierarchical nesting of slow oscillations, spindles and ripples in the human hippocampus during sleep. *Nature Neuroscience, 18*(11), 1679-1686. doi:10.1038/nn.4119
Staresina, B. P., Niediek, J., Borger, V., Surges, R., & Mormann, F. (2023). How coupled slow oscillations, spindles and ripples coordinate neuronal processing and communication during human sleep. *Nature Neuroscience, 26*(8), 1429-1437. doi:10.1038/s41593-023-01381-w
Steadman, P. E., Xia, F., Ahmed, M., Mocle, A. J., Penning, A. R. A., Geraghty, A. C., . . . Frankland, P. W. (2020). Disruption of Oligodendrogenesis Impairs Memory Consolidation in Adult Mice. *Neuron, 105*(1), 150-164.e156. doi:10.1016/j.neuron.2019.10.013
Stedman, E., & Stedman, E. (1937). The mechanism of the biological synthesis of acetylcholine: The isolation of acetylcholine produced by brain tissue in vitro. *Biochem J, 31*(5), 817-827. doi:10.1042/bj0310817
Stefanacci, R. G. (2011). The costs of Alzheimer's disease and the value of effective therapies. *Am J Manag Care, 17 Suppl 13*, S356-362.
Steinmetz, N. A., Aydin, C., Lebedeva, A., Okun, M., Pachitariu, M., Bauza, M., . . . Harris, T. D. (2021). Neuropixels 2.0: A miniaturized high-density probe for stable, long-term brain recordings. *Science, 372*(6539). doi:10.1126/science.abf4588
Steriade, M. (2006). Grouping of brain rhythms in corticothalamic systems. *Neuroscience, 137*(4), 1087-1106. doi:10.1016/j.neuroscience.2005.10.029
Stewart, C. R., Stuart, L. M., Wilkinson, K., van Gils, J. M., Deng, J., Halle, A., . . . Moore, K. J. (2010). CD36 ligands promote sterile inflammation through assembly of a Toll-like receptor 4 and 6 heterodimer. *Nat Immunol, 11*(2), 155-161. doi:10.1038/ni.1836
Subedi, S., Sasidharan, S., Nag, N., Saudagar, P., & Tripathi, T. (2022). Amyloid Cross-Seeding: Mechanism, Implication, and Inhibition. *Molecules, 27*(6). doi:10.3390/molecules27061776
Sullivan, D., Csicsvari, J., Mizuseki, K., Montgomery, S., Diba, K., & Buzsáki, G. (2011). Relationships between hippocampal sharp waves, ripples, and fast gamma oscillation: influence of dentate and entorhinal cortical activity. *J Neurosci, 31*(23), 8605-8616. doi:10.1523/jneurosci.0294-11.2011
Sullivan, D., Mizuseki, K., Sorgi, A., & Buzsáki, G. (2014). Comparison of sleep spindles and theta oscillations in the hippocampus. *J Neurosci, 34*(2), 662-674. doi:10.1523/jneurosci.0552-13.2014
Sur, C., Kost, J., Scott, D., Adamczuk, K., Fox, N. C., Cummings, J. L., . . . Egan, M. F. (2020). BACE inhibition causes rapid, regional, and non-progressive volume reduction in Alzheimer's disease brain. *Brain, 143*(12), 3816-3826. doi:10.1093/brain/awaa332
Suzuki, S. S., & Smith, G. K. (1987). Spontaneous EEG spikes in the normal hippocampus. I. Behavioral correlates, laminar profiles and bilateral synchrony. *Electroencephalogr Clin Neurophysiol, 67*(4), 348-359. doi:10.1016/0013-4694(87)90123-4

Swanson, C. J., Zhang, Y., Dhadda, S., Wang, J., Kaplow, J., Lai, R. Y. K., . . . Cummings, J. L. (2021). A randomized, double-blind, phase 2b proof-of-concept clinical trial in early Alzheimer's disease with lecanemab, an anti-Aβ protofibril antibody. *Alzheimers Res Ther, 13*(1), 80. doi:10.1186/s13195-021-00813-8

Szczepańska, K., Bojarski, A. J., Popik, P., & Malikowska-Racia, N. (2023). Novel object recognition test as an alternative approach to assessing the pharmacological profile of sigma-1 receptor ligands. *Pharmacological Reports, 75*(5), 1291-1298. doi:10.1007/s43440-023-00516-x

Szelies, B., Grond, M., Herholz, K., Kessler, J., Wullen, T., & Heiss, W. D. (1992). Quantitative EEG mapping and PET in Alzheimer's disease. *J Neurol Sci, 110*(1-2), 46-56. doi:10.1016/0022-510x(92)90008-9

Szelies, B., Mielke, R., Herholz, K., & Heiss, W. D. (1994). Quantitative topographical EEG compared to FDG PET for classification of vascular and degenerative dementia. *Electroencephalogr Clin Neurophysiol, 91*(2), 131-139. doi:10.1016/0013-4694(94)90034-5

Szymusiak, R., & McGinty, D. (1986). Sleep suppression following kainic acid-induced lesions of the basal forebrain. *Exp Neurol, 94*(3), 598-614. doi:10.1016/0014-4886(86)90240-2

Taillard, J., Sagaspe, P., Berthomier, C., Brandewinder, M., Amieva, H., Dartigues, J. F., . . . Philip, P. (2019). Non-REM Sleep Characteristics Predict Early Cognitive Impairment in an Aging Population. *Front Neurol, 10*, 197. doi:10.3389/fneur.2019.00197

Tamminen, J., Payne, J. D., Stickgold, R., Wamsley, E. J., & Gaskell, M. G. (2010). Sleep spindle activity is associated with the integration of new memories and existing knowledge. *J Neurosci, 30*(43), 14356-14360. doi:10.1523/jneurosci.3028-10.2010

Tao, C., Zhang, G., Xiong, Y., & Zhou, Y. (2015). Functional dissection of synaptic circuits: in vivo patch-clamp recording in neuroscience. *Front Neural Circuits, 9*, 23. doi:10.3389/fncir.2015.00023

Teitelbaum, H., Lee, J. F., & Johannessen, J. N. (1975). Behaviorally evoked hippocampal theta waves: a cholinergic response. *Science, 188*(4193), 1114-1116. doi:10.1126/science.175440

Tensil, M., Hessler, J. B., Gutsmiedl, M., Riedl, L., Grimmer, T., & Diehl-Schmid, J. (2018). Sex Differences in Neuropsychological Test Performance in Alzheimer's Disease and the Influence of the ApoE Genotype. *Alzheimer Dis Assoc Disord, 32*(2), 145-149. doi:10.1097/wad.0000000000000229

Teplow, D. B. (1998). Structural and kinetic features of amyloid beta-protein fibrillogenesis. *Amyloid, 5*(2), 121-142. doi:10.3109/13506129808995290

Tolppanen, A. M., Taipale, H., & Hartikainen, S. (2017). Head or brain injuries and Alzheimer's disease: A nested case-control register study. *Alzheimers Dement, 13*(12), 1371-1379. doi:10.1016/j.jalz.2017.04.010

Tomlinson, B. E., Blessed, G., & Roth, M. (1968). Observations on the brains of non-demented old people. *J Neurol Sci, 7*(2), 331-356. doi:10.1016/0022-510x(68)90154-8

Tomlinson, B. E., Blessed, G., & Roth, M. (1970). Observations on the brains of demented old people. *J Neurol Sci, 11*(3), 205-242. doi:10.1016/0022-510x(70)90063-8

Traikapi, A., Kalli, I., Kyriakou, A., Stylianou, E., Symeou, R. T., Kardama, A., . . . Konstantinou, N. (2023). Episodic memory effects of gamma frequency precuneus transcranial magnetic stimulation in Alzheimer's disease: A randomized multiple baseline study. *J Neuropsychol, 17*(2), 279-301. doi:10.1111/jnp.12299

Tucker, H. M., Kihiko, M., Caldwell, J. N., Wright, S., Kawarabayashi, T., Price, D., . . . Estus, S. (2000). The plasmin system is induced by and degrades amyloid-beta aggregates. *J Neurosci, 20*(11), 3937-3946. doi:10.1523/jneurosci.20-11-03937.2000

Turgutalp, B., & Kizil, C. (2024). Multi-target drugs for Alzheimer's disease. *Trends in Pharmacological Sciences, 45*(7), 628-638. doi:https://doi.org/10.1016/j.tips.2024.05.005

Uchida, Y., Sugiura, S., Nishita, Y., Saji, N., Sone, M., & Ueda, H. (2019). Age-related hearing loss and cognitive decline - The potential mechanisms linking the two. *Auris Nasus Larynx, 46*(1), 1-9. doi:10.1016/j.anl.2018.08.010

Valero, M., Averkin, R. G., Fernandez-Lamo, I., Aguilar, J., Lopez-Pigozzi, D., Brotons-Mas, J. R., . . . Menendez de la Prida, L. (2017). Mechanisms for Selective Single-Cell Reactivation during Offline Sharp-Wave Ripples and Their Distortion by Fast Ripples. *Neuron, 94*(6), 1234-1247.e1237. doi:https://doi.org/10.1016/j.neuron.2017.05.032

Van Cauter, E., Leproult, R., & Plat, L. (2000). Age-related changes in slow wave sleep and REM sleep and relationship with growth hormone and cortisol levels in healthy men. *Jama, 284*(7), 861-868. doi:10.1001/jama.284.7.861

van Deursen, J. A., Vuurman, E. F., van Kranen-Mastenbroek, V. H., Verhey, F. R., & Riedel, W. J. (2011). 40-Hz steady state response in Alzheimer's disease and mild cognitive impairment. *Neurobiol Aging, 32*(1), 24-30. doi:10.1016/j.neurobiolaging.2009.01.002

van Dyck, C. H., Swanson, C. J., Aisen, P., Bateman, R. J., Chen, C., Gee, M., . . . Iwatsubo, T. (2023). Lecanemab in Early Alzheimer's Disease. *N Engl J Med, 388*(1), 9-21. doi:10.1056/NEJMoa2212948

Vandecasteele, M., Varga, V., Berényi, A., Papp, E., Barthó, P., Venance, L., . . . Buzsáki, G. (2014). Optogenetic activation of septal cholinergic neurons suppresses sharp wave ripples and enhances theta oscillations in the hippocampus. *Proc Natl Acad Sci U S A, 111*(37), 13535-13540. doi:10.1073/pnas.1411233111

Venegas, C., Kumar, S., Franklin, B. S., Dierkes, T., Brinkschulte, R., Tejera, D., . . . Heneka, M. T. (2017). Microglia-derived ASC specks cross-seed amyloid-β in Alzheimer's disease. *Nature, 552*(7685), 355-361. doi:10.1038/nature25158

Viña, J., & Lloret, A. (2010). Why women have more Alzheimer's disease than men: gender and mitochondrial toxicity of amyloid-beta peptide. *J Alzheimers Dis, 20 Suppl 2*, S527-533. doi:10.3233/jad-2010-100501

Vyazovskiy, V. V., Cirelli, C., Pfister-Genskow, M., Faraguna, U., & Tononi, G. (2008). Molecular and electrophysiological evidence for net synaptic potentiation in wake and depression in sleep. *Nat Neurosci, 11*(2), 200-208. doi:10.1038/nn2035

Wadman, M. (2012). US government sets out Alzheimer's plan. *Nature, 485*(7399), 426-427. doi:10.1038/485426a

Wang, D. V., Yau, H. J., Broker, C. J., Tsou, J. H., Bonci, A., & Ikemoto, S. (2015). Mesopontine median raphe regulates hippocampal ripple oscillation and memory consolidation. *Nat Neurosci, 18*(5), 728-735. doi:10.1038/nn.3998

Wang, J., Fang, Y., Wang, X., Yang, H., Yu, X., & Wang, H. (2017). Enhanced Gamma Activity and Cross-Frequency Interaction of Resting-State Electroencephalographic Oscillations in Patients with Alzheimer's Disease. *Front Aging Neurosci, 9*, 243. doi:10.3389/fnagi.2017.00243

Wang, Y., Gao, L., Chen, J., Li, Q., Huo, L., Wang, Y., . . . Du, J. (2021). Pharmacological Modulation of Nrf2/HO-1 Signaling Pathway as a Therapeutic Target of Parkinson's Disease. *Front Pharmacol, 12*, 757161. doi:10.3389/fphar.2021.757161

Wang, Y., Sun, Y., Wang, Y., Jia, S., Qiao, Y., Zhou, Z., . . . Peng, D. (2023). Urine metabolomics phenotyping and urinary biomarker exploratory in mild cognitive impairment and Alzheimer's disease. *Front Aging Neurosci, 15*, 1273807. doi:10.3389/fnagi.2023.1273807

Waragai, M., Yoshida, M., Mizoi, M., Saiki, R., Kashiwagi, K., Takagi, K., . . . Igarashi, K. (2012). Increased protein-conjugated acrolein and amyloid-beta40/42 ratio in plasma of patients with mild cognitive impairment and Alzheimer's disease. *J Alzheimers Dis, 32*(1), 33-41. doi:10.3233/JAD-2012-120253

Watamura, N., Sato, K., Shiihashi, G., Iwasaki, A., Kamano, N., Takahashi, M., . . . Sasaguri, H. (2022). An isogenic panel of App knock-in mouse models: Profiling β-secretase inhibition and endosomal abnormalities. *Science Advances, 8*(23), eabm6155. doi:doi:10.1126/sciadv.abm6155

Webster, H. H., & Jones, B. E. (1988). Neurotoxic lesions of the dorsolateral pontomesencephalic tegmentum-cholinergic cell area in the cat. II. Effects upon sleep-waking states. *Brain Res, 458*(2), 285-302. doi:10.1016/0006-8993(88)90471-4

Wei, P. P., Hunter, S. K., & Ross, R. G. (2017). Sleep Spindles and Auditory Sensory Gating: Two Measures of Cerebral Inhibition in Preschool-Aged Children are Strongly Correlated. *Colo J Psychiatry Psychol, 2*(1), 75-83.
Weiner, H., & Schuster, D. B. (1956). The electroencephalogram in dementia; some preliminary observations and correlations. *Electroencephalogr Clin Neurophysiol, 8*(3), 479-488. doi:10.1016/0013-4694(56)90014-1
Weingarten, M. D., Lockwood, A. H., Hwo, S. Y., & Kirschner, M. W. (1975). A protein factor essential for microtubule assembly. *Proc Natl Acad Sci U S A, 72*(5), 1858-1862. doi:10.1073/pnas.72.5.1858
Wessels, A. M., Lines, C., Stern, R. A., Kost, J., Voss, T., Mozley, L. H., . . . Egan, M. F. (2020). Cognitive outcomes in trials of two BACE inhibitors in Alzheimer's disease. *Alzheimers Dement, 16*(11), 1483-1492. doi:10.1002/alz.12164
West, M. J., Coleman, P. D., Flood, D. G., & Troncoso, J. C. (1994). Differences in the pattern of hippocampal neuronal loss in normal ageing and Alzheimer's disease. *Lancet, 344*(8925), 769-772. doi:10.1016/s0140-6736(94)92338-8
West, M. J., Kawas, C. H., Stewart, W. F., Rudow, G. L., & Troncoso, J. C. (2004). Hippocampal neurons in pre-clinical Alzheimer's disease. *Neurobiol Aging, 25*(9), 1205-1212. doi:10.1016/j.neurobiolaging.2003.12.005
Whitehouse, P. J., Price, D. L., Struble, R. G., Clark, A. W., Coyle, J. T., & Delon, M. R. (1982). Alzheimer's disease and senile dementia: loss of neurons in the basal forebrain. *Science, 215*(4537), 1237-1239. doi:10.1126/science.7058341
Wierzynski, C. M., Lubenov, E. V., Gu, M., & Siapas, A. G. (2009). State-dependent spike-timing relationships between hippocampal and prefrontal circuits during sleep. *Neuron, 61*(4), 587-596. doi:10.1016/j.neuron.2009.01.011
Wimmer, R. D., Astori, S., Bond, C. T., Rovó, Z., Chatton, J. Y., Adelman, J. P., . . . Lüthi, A. (2012). Sustaining sleep spindles through enhanced SK2-channel activity consolidates sleep and elevates arousal threshold. *J Neurosci, 32*(40), 13917-13928. doi:10.1523/jneurosci.2313-12.2012
Winer, J. R., Mander, B. A., Helfrich, R. F., Maass, A., Harrison, T. M., Baker, S. L., . . . Walker, M. P. (2019). Sleep as a Potential Biomarker of Tau and β-Amyloid Burden in the Human Brain. *J Neurosci, 39*(32), 6315-6324. doi:10.1523/jneurosci.0503-19.2019
Witton, J., Staniaszek, L. E., Bartsch, U., Randall, A. D., Jones, M. W., & Brown, J. T. (2016). Disrupted hippocampal sharp-wave ripple-associated spike dynamics in a transgenic mouse model of dementia. *J Physiol, 594*(16), 4615-4630. doi:10.1113/jphysiol.2014.282889
Woolf, N. J. (1991). Cholinergic systems in mammalian brain and spinal cord. *Prog Neurobiol, 37*(6), 475-524. doi:10.1016/0301-0082(91)90006-m
Woyshville, M. J., & Calabrese, J. R. (1994). Quantification of occipital EEG changes in Alzheimer's disease utilizing a new metric: the fractal dimension. *Biol Psychiatry, 35*(6), 381-387. doi:10.1016/0006-3223(94)90004-3
Wu, J., Ji, N., & Tsia, K. K. (2021). Speed scaling in multiphoton fluorescence microscopy. *Nature Photonics, 15*(11), 800-812. doi:10.1038/s41566-021-00881-0
Wyss-Coray, T., Loike, J. D., Brionne, T. C., Lu, E., Anankov, R., Yan, F., . . . Husemann, J. (2003). Adult mouse astrocytes degrade amyloid-beta in vitro and in situ. *Nat Med, 9*(4), 453-457. doi:10.1038/nm838
Xia, F., Yiu, A., Stone, S. S. D., Oh, S., Lozano, A. M., Josselyn, S. A., & Frankland, P. W. (2017). Entorhinal Cortical Deep Brain Stimulation Rescues Memory Deficits in Both Young and Old Mice Genetically Engineered to Model Alzheimer's Disease. *Neuropsychopharmacology, 42*(13), 2493-2503. doi:10.1038/npp.2017.100
Xiao, N. A., Zhang, J., Zhou, M., Wei, Z., Wu, X. L., Dai, X. M., . . . Chen, X. C. (2015). Reduction of Glucose Metabolism in Olfactory Bulb is an Earlier Alzheimer's Disease-related Biomarker in 5XFAD Mice. *Chin Med J (Engl), 128*(16), 2220-2227. doi:10.4103/0366-6999.162507
Xie, L., Kang, H., Xu, Q., Chen, M. J., Liao, Y., Thiyagarajan, M., . . . Nedergaard, M. (2013). Sleep drives metabolite clearance from the adult brain. *Science, 342*(6156), 373-377. doi:10.1126/science.1241224

Xu, H., Gouras, G. K., Greenfield, J. P., Vincent, B., Naslund, J., Mazzarelli, L., . . . Gandy, S. (1998). Estrogen reduces neuronal generation of Alzheimer beta-amyloid peptides. *Nat Med, 4*(4), 447-451. doi:10.1038/nm0498-447

Yamamoto, K., Tanei, Z. I., Hashimoto, T., Wakabayashi, T., Okuno, H., Naka, Y., . . . Iwatsubo, T. (2015). Chronic optogenetic activation augments aβ pathology in a mouse model of Alzheimer disease. *Cell Rep, 11*(6), 859-865. doi:10.1016/j.celrep.2015.04.017

Yang, H., & Jeong, Y. (2021). Correlation between Alteration of Sharp-wave Ripple Coupled Cortical Oscillation and Long-term Memory Deficit in Alzheimer Disease Model Mice. *Experimental Neurobiology, 30*(6), 430-440. doi:10.5607/en21046

Yang, H., & Jeong, Y. (2021). Correlation between Alteration of Sharp-wave Ripple Coupled Cortical Oscillation and Long-term Memory Deficit in Alzheimer Disease Model Mice. *Experimental Neurobiology, 30*(6), 430-440. doi:10.5607/en21046

Yang, Y., Gritton, H., Sarter, M., Aton, S. J., Booth, V., & Zochowski, M. (2021). Theta-gamma coupling emerges from spatially heterogeneous cholinergic neuromodulation. *PLoS Comput Biol, 17*(7), e1009235. doi:10.1371/journal.pcbi.1009235

Ylinen, A., Bragin, A., Nadasdy, Z., Jando, G., Szabo, I., Sik, A., & Buzsaki, G. (1995). Sharp wave-associated high-frequency oscillation (200 Hz) in the intact hippocampus: network and intracellular mechanisms. *The Journal of Neuroscience, 15*(1), 30-46. doi:10.1523/jneurosci.15-01-00030.1995

Yokoyama, M., Kobayashi, H., Tatsumi, L., & Tomita, T. (2022). Mouse Models of Alzheimer's Disease. *Front Mol Neurosci, 15*, 912995. doi:10.3389/fnmol.2022.912995

Yoon, S. S., & Jo, S. A. (2012). Mechanisms of Amyloid-β Peptide Clearance: Potential Therapeutic Targets for Alzheimer's Disease. *Biomolecules & therapeutics, 20*(3), 245-255. doi:10.4062/biomolther.2012.20.3.245

Yu, L., Edalji, R., Harlan, J. E., Holzman, T. F., Lopez, A. P., Labkovsky, B., . . . Olejniczak, E. T. (2009). Structural characterization of a soluble amyloid beta-peptide oligomer. *Biochemistry, 48*(9), 1870-1877. doi:10.1021/bi802046n

Yuan, Y., Gu, Z. X., & Wei, W. S. (2009). Fluorodeoxyglucose-positron-emission tomography, single-photon emission tomography, and structural MR imaging for prediction of rapid conversion to Alzheimer disease in patients with mild cognitive impairment: a meta-analysis. *AJNR Am J Neuroradiol, 30*(2), 404-410. doi:10.3174/ajnr.A1357

Zanier, E. R., Bertani, I., Sammali, E., Pischiutta, F., Chiaravalloti, M. A., Vegliante, G., . . . Chiesa, R. (2018). Induction of a transmissible tau pathology by traumatic brain injury. *Brain, 141*(9), 2685-2699. doi:10.1093/brain/awy193

Zhang, F., Zhong, R., Li, S., Fu, Z., Wang, R., Wang, T., . . . Le, W. (2019). Alteration in sleep architecture and electroencephalogram as an early sign of Alzheimer's disease preceding the disease pathology and cognitive decline. *Alzheimers Dement, 15*(4), 590-597. doi:10.1016/j.jalz.2018.12.004

Zhang, H., Fell, J., & Axmacher, N. (2018). Electrophysiological mechanisms of human memory consolidation. *Nat Commun, 9*(1), 4103. doi:10.1038/s41467-018-06553-y

Zhang, H., Geng, X., Wang, Y., Guo, Y., Gao, Y., Zhang, S., . . . Wang, L. (2021). The Significance of EEG Alpha Oscillation Spectral Power and Beta Oscillation Phase Synchronization for Diagnosing Probable Alzheimer Disease. *Front Aging Neurosci, 13*, 631587. doi:10.3389/fnagi.2021.631587

Zhang, M., Ganz, A. B., Rohde, S., Rozemuller, A. J. M., Bank, N. B., Reinders, M. J. T., . . . Holstege, H. (2023). Resilience and resistance to the accumulation of amyloid plaques and neurofibrillary tangles in centenarians: An age-continuous perspective. *Alzheimers Dement, 19*(7), 2831-2841. doi:10.1002/alz.12899

Zhang, R., Xue, G., Wang, S., Zhang, L., Shi, C., & Xie, X. (2012). Novel object recognition as a facile behavior test for evaluating drug effects in AβPP/PS1 Alzheimer's disease mouse model. *J Alzheimers Dis, 31*(4), 801-812. doi:10.3233/jad-2012-120151

Zhang, S., Iwata, K., Lachenmann, M. J., Peng, J. W., Li, S., Stimson, E. R., . . . Lee, J. P. (2000). The Alzheimer's peptide a beta adopts a collapsed coil structure in water. *J Struct Biol, 130*(2-3), 130-141. doi:10.1006/jsbi.2000.4288

Zhang, Y., Cao, L., Varga, V., Jing, M., Karadas, M., Li, Y., & Buzsáki, G. (2021). Cholinergic suppression of hippocampal sharp-wave ripples impairs working memory. *Proc Natl Acad Sci U S A, 118*(15). doi:10.1073/pnas.2016432118

Zhang, Y., Wang, Y., Shi, C., Shen, M., & Lu, F. (2021). Advances in retina imaging as potential biomarkers for early diagnosis of Alzheimer's disease. *Transl Neurodegener, 10*(1), 6. doi:10.1186/s40035-021-00230-9

Zhou, H., Li, H., Gowravaram, N., Quan, M., Kausar, N., & Gomperts, S. N. (2022). Disruption of hippocampal neuronal circuit function depends upon behavioral state in the APP/PS1 mouse model of Alzheimer's disease. *Scientific Reports, 12*(1), 21022. doi:10.1038/s41598-022-25364-2

Zhurakovskaya, E., Ishchenko, I., Gureviciene, I., Aliev, R., Gröhn, O., & Tanila, H. (2019). Impaired hippocampal-cortical coupling but preserved local synchrony during sleep in APP/PS1 mice modeling Alzheimer's disease. *Sci Rep, 9*(1), 5380. doi:10.1038/s41598-019-41851-5

Zong, W., Obenhaus, H. A., Skytøen, E. R., Eneqvist, H., de Jong, N. L., Vale, R., . . . Moser, E. I. (2022). Large-scale two-photon calcium imaging in freely moving mice. *Cell, 185*(7), 1240-1256.e1230. doi:10.1016/j.cell.2022.02.017